

# **For Reference**


---

**NOT TO BE TAKEN FROM THIS ROOM**



Ex libris  
UNIVERSITATIS  
ALBERTAENSIS





Digitized by the Internet Archive  
in 2023 with funding from  
University of Alberta Library

<https://archive.org/details/Dwight1980>













T H E   U N I V E R S I T Y   O F   A L B E R T A

RELEASE FORM

NAME OF AUTHOR ..... Stephen Kenneth Dwight .....

TITLE OF THESIS ..... The Chemistry of Binuclear Rhodium .....

..... Complexes with Small Molecules .....

DEGREE FOR WHICH THESIS WAS PRESENTED ..... Ph.D. ....

YEAR THIS DEGREE GRANTED ..... 1980 .....

Permission is hereby granted to THE UNIVERSITY OF ALBERTA LIBRARY to reproduce single copies of this thesis and to lend or sell such copies for private, scholarly or scientific research purposes only.

The author reserves other publication rights, and neither the thesis nor extensive extracts from it may be printed or otherwise reproduced without the author's written permission.







THE UNIVERSITY OF ALBERTA

THE CHEMISTRY OF BINUCLEAR RHODIUM COMPLEXES

WITH SMALL MOLECULES

by



STEPHEN KENNETH DWIGHT

A THESIS

SUBMITTED TO THE FACULTY OF GRADUATE STUDIES AND RESEARCH  
IN PARTIAL FULFILMENT OF THE REQUIREMENTS FOR THE DEGREE  
OF DOCTOR OF PHILOSOPHY

IN CHEMISTRY

EDMONTON, ALBERTA

FALL, 1980





THE UNIVERSITY OF ALBERTA  
FACULTY OF GRADUATE STUDIES AND RESEARCH

The undersigned certify that they have read, and  
recommend to the Faculty of Graduate Studies and Research,  
for acceptance, a thesis entitled The Chemistry of  
.....  
Binuclear Rhodium Complexes with Small Molecules ..... submitted  
by Stephen Kenneth Dwight ..... in partial fulfilment of the  
requirements for the degree of Doctor of Philosophy.





To my wife, Maureen.





## ABSTRACT

An X-ray structural determination of  $[\text{Rh}_2(\text{CO})_2(\mu\text{-Cl})(\text{DPM})_2][\text{BF}_4]$  ( $\text{DPM} = \text{Ph}_2\text{PCH}_2\text{PPh}_2$ ), has indicated that in this "A-frame" complex both the enclosed bridging site and exposed terminal sites are open to attack by small molecules. Whereas, in *trans*- $[\text{RhCl}(\text{CO})(\text{DPM})]_2$ , a structural determination has shown that the bridging site is effectively blocked by the equatorial ligands, in particular the chloro ligands are skewed into this site, leaving only the possibility of terminal attack.

Halide exchange reactions were carried out on *trans*- $[\text{RhCl}(\text{CO})(\text{DPM})]_2$  in an effort to prepare the bromo and iodo derivatives. Instead the complexes  $[\text{Rh}_2\text{Br}_2(\mu\text{-CO})(\text{DPM})_2]$ , which was structurally characterized, and  $[\text{Rh}_2\text{I}(\text{CO})(\mu\text{-CO})(\text{DPM})_2][\text{I}]$  were isolated as the final products. Iodide exchange on *trans*- $[\text{RhCl}(\text{CO})(\text{DAM})]_2$  ( $\text{DAM} = \text{Ph}_2\text{AsCH}_2\text{-AsPh}_2$ ) yields a mixture of *trans*- $[\text{RhI}(\text{CO})(\text{DAM})]_2$  and  $[\text{Rh}_2\text{I}(\text{CO})(\mu\text{-CO})(\text{DAM})_2][\text{I}]$ .

The chemistry of these binuclear rhodium species with  $\text{CO}$ ,  $\text{CS}_2$  and  $\text{SO}_2$  was investigated. The "A-frame" species  $[\text{Rh}_2(\text{CO})_2(\mu\text{-Cl})(\text{DPM})_2][\text{BPh}_4]$  undergoes a facile and reversible reaction with  $\text{SO}_2$  yielding  $[\text{Rh}_2(\text{CO})_2(\mu\text{-Cl})(\mu\text{-SO}_2)(\text{DPM})_2][\text{BPh}_4]$ . Spectroscopic studies indicate that attack by  $\text{SO}_2$  occurs directly at the bridging site. Treatment of this  $\text{SO}_2$  adduct with excess  $\text{SO}_2$  in the presence of chloride





ion or  $[\text{Rh}_2\text{Cl}_2(\text{CO})_2]^-$ , which functions as a chloride transfer agent, results in the isolation of a second product  $[\text{Rh}_2\text{Cl}_2(\mu\text{-SO}_2)(\text{DPM})_2]$  whose structure has been determined. Reaction of either *trans*- $[\text{RhCl}(\text{CO})(\text{DPM})]_2$  or  $[\text{Rh}_2\text{Cl}_2(\mu\text{-CO})(\text{DPM})_2]$  with  $\text{SO}_2$  results finally in the isolation of  $[\text{Rh}_2\text{Cl}_2(\mu\text{-SO}_2)(\text{DPM})_2]$  and reaction schemes are presented for both these reactions based on spectroscopic evidence. Treatment of  $[\text{Rh}_2\text{Cl}_2(\mu\text{-SO}_2)(\text{DPM})_2]$  with CO yields the tricarbonyl species  $[\text{Rh}_2(\text{CO})_2(\mu\text{-CO})(\mu\text{-Cl})(\text{DPM})_2][\text{Cl}]$ . Similarly the reaction of  $[\text{Rh}_2\text{Cl}_2(\mu\text{-CO})(\text{DPM})_2]$  with excess CO also yields this tricarbonyl species. However on slow stepwise addition of CO, *trans*- $[\text{RhCl}(\text{CO})(\text{DPM})]_2$  is isolated. Reaction of a mixture of *trans*- $[\text{RhI}(\text{CO})(\text{DAM})]_2$  and  $[\text{Rh}_2\text{I}(\text{CO})(\mu\text{-CO})(\text{DAM})_2][\text{I}]$  with CO or  $\text{SO}_2$  yield the products  $[\text{Rh}_2(\text{CO})_2(\mu\text{-L})(\mu\text{-I})(\text{DAM})_2][\text{I}]$  ( $\text{L} = \text{CO}, \text{SO}_2$ ).

Although  $\text{CS}_2$  does not react with  $[\text{Rh}_2(\text{CO})_2(\mu\text{-Cl})(\text{DPM})_2][\text{BPh}_4]$ , its reaction with either *trans*- $[\text{RhCl}(\text{CO})(\text{DPM})]_2$  or  $[\text{Rh}_2\text{Cl}_2(\mu\text{-CO})(\text{DPM})_2]$  yields as the final product  $[\text{Rh}_2\text{Cl}_2(\text{CO})(\text{C}_2\text{S}_4)(\text{DPM})_2]$ . A structural determination of this species has shown that two molecules of  $\text{CS}_2$  have condensed yielding a  $\text{C}_2\text{S}_4$  fragment which bridges the two rhodium centres such that a five membered  $\text{Rh}-\text{C}-\text{S}-\text{C}-\text{S}$  metallocycle and a four membered  $\text{Rh}-\text{C}-\text{S}-\text{Rh}$  metallocycle results. Reaction schemes for these reactions are presented based on spectroscopic data and analogies to  $\text{SO}_2$  and acetylene chemistry.



## ACKNOWLEDGEMENTS

The author wishes to express his gratitude and sincere appreciation to:

Professor M. Cowie for his expert guidance and friendly assistance during the course of this work.

Dr. A.R. Sanger for kindly supplying crystals of  $[\text{Rh}_2\text{Cl}_2(\mu\text{-SO}_2)(\text{DPM})_2]$ .

The group for their friendship and assistance.

The Natural Science and Engineering Research Council, Canada and the University of Alberta for their generous financial support.

Shirley Stawnychy for her expert preparation of this manuscript.

Maureen for her constant encouragement and companionship.





# TABLE OF CONTENTS

	Page
Dedication	iv
Abstract	v
Acknowledgements	vii
List of Tables	xiii
List of Figures	xvii
List of Abbreviations	xix
Chapter	
I Introduction	1
II The Structure of $[\text{Rh}_2(\text{CO})_2(\mu\text{-Cl})(\text{DPM})_2]\text{-}[\text{BF}_4]$ : A Binuclear "A-Frame" Complex	20
Introduction	20
Experimental	21
Preparation of $[\text{Rh}_2(\text{CO})_2(\mu\text{-Cl})(\text{DPM})_2]\text{-}[\text{BPh}_4]$	22
The Serendipitous Crystallization of $[\text{Rh}_2(\text{CO})_2(\mu\text{-Cl})(\text{DPM})_2][\text{BF}_4]$	22
Preparation of $[\text{Rh}_2(\text{CO})_2(\mu\text{-Cl})(\text{DPM})_2]\text{-}[\text{BF}_4]$	23
$^{31}\text{P}$ and $^{19}\text{F}$ NMR Results	23
Data Collection	24
Structure Solution and Refinement	28
Results	35
Description of Structure	47
Discussion	52



Chapter		Page
III	The Structure of <i>trans</i> -[RhCl(CO)(DPM)] <sub>2</sub>	54
	Introduction	54
	Experimental	56
	Crystallization of <i>trans</i> -[RhCl(CO)(DPM)] <sub>2</sub>	56
	Data Collection	56
	Solution of Structure	59
	Results	59
	Description of Structure	70
	Discussion	72
IV	The Chemistry of Binuclear Rhodium Complexes with Sulfur Dioxide and the Structure of [Rh <sub>2</sub> Cl <sub>2</sub> (μ-SO <sub>2</sub> )(DPM) <sub>2</sub> ]	75
	Introduction	75
	Experimental	77
	Preparation of [Rh <sub>2</sub> Cl <sub>2</sub> (μ-SO <sub>2</sub> )(DPM) <sub>2</sub> ]	77
	Method A	77
	Method B	78
	Method C	78
	Preparation of [Rh <sub>2</sub> (CO) <sub>2</sub> (μ-Cl)(DPM) <sub>2</sub> ][Cl], [Rh <sub>2</sub> (CO) <sub>2</sub> (μ-CO)(μ-Cl)(DPM) <sub>2</sub> ][Cl] and <i>cis</i> -[RhCl(CO)(DPM)] <sub>2</sub>	78
	Spectroscopic Studies on the Stepwise Reaction with SO <sub>2</sub>	81
	X-ray Data Collection	82
	Structure Solution and Refinement	82
	Results	85
	Discussion	96





Chapter		Page
	Description of Structure	96
	Transformation of $[\text{Rh}_2(\text{CO})_2(\mu\text{-SO}_2)(\mu\text{-Cl})\text{-(DPM)}_2]^+$ to $[\text{Rh}_2\text{Cl}_2(\mu\text{-SO}_2)(\text{DPM})_2]$	99
	Reaction of $[\text{Rh}_2\text{Cl}_2(\mu\text{-SO}_2)(\text{DPM})_2]$ with CO	103
	Reaction of <i>trans</i> - $[\text{RhCl}(\text{CO})(\text{DPM})]_2$ with $\text{SO}_2$	106
	Site of $\text{SO}_2$ Attack in $[\text{Rh}_2(\text{CO})_2(\mu\text{-Cl})\text{-(DPM)}_2]^+$	107
V	Unusual Structural and Chemical Trends Within a Series of Binuclear Rhodium Carbonyl Halide Complexes	110
	Introduction	110
	Experimental	110
	Preparation of $[\text{RhI}(\text{CO})(\mu\text{-CO})(\text{DPM})_2][\text{I}]$ , $[\text{Rh}_2\text{Br}_2(\mu\text{-CO})(\text{DPM})_2]$ and $[\text{Rh}_2\text{Cl}_2(\mu\text{-CO})\text{-(DPM)}_2]$	110
	Reactions with $\text{SO}_2$ and CO	111
	i) Dicarbonyl Species	111
	ii) Monocarbonyl Species	113
	Discussion	113
	Halide Exchange Reactions	113
	Reactions with CO	117
	i) Dicarbonyl Species	117
	ii) Monocarbonyl Species	120
	Reactions with $\text{SO}_2$	122
	i) Dicarbonyl Species	122
	ii) Monocarbonyl Species	124
	Summary	126



Chapter		Page
VI	The Structure of $[\text{Rh}_2\text{Br}_2(\mu\text{-CO})(\text{DPM})_2]$ : A Binuclear Rhodium Carbonyl Complex Having an Unusually Low Carbonyl Stretching Frequency	128
	Introduction	128
	Experimental	129
	Crystallization of $[\text{Rh}_2\text{Br}_2(\mu\text{-CO})(\text{DPM})_2]$	129
	Data Collection	129
	Structure Solution and Refinement	130
	Results	130
	Description of Structure	143
	Discussion	147
VII	Carbon Disulfide Chemistry and the Structure of $[\text{Rh}_2\text{Cl}_2(\text{CO})(\text{C}_2\text{S}_4)(\text{DPM})_2]$	150
	Introduction	150
	Experimental	151
	Preparation of $[\text{Rh}_2\text{Cl}_2(\text{CO})(\text{C}_2\text{S}_4)(\text{DPM})_2]$	152
	Spectroscopic Studies	152
	Crystallization of $[\text{Rh}_2\text{Cl}_2(\text{CO})(\text{C}_2\text{S}_4)\text{-(DPM)}_2]$	153
	X-ray Data Collection	153
	Solution of Structure	154
	Results	159
	Discussion	173
	Description of Structure	173
	Reaction of <i>trans</i> - $[\text{RhCl}(\text{CO})(\text{DPM})]_2$ and $[\text{Rh}_2\text{Cl}_2(\mu\text{-CO})(\text{DPM})_2]$ with $\text{CS}_2$	177
	Conclusions	181





Chapter		Page
VIII	Summary and Conclusions	182
	References and Footnotes	186
	Appendix 1: Programs Used in Crystal Structure Solution, Refinement and Analysis	201
	Appendix 2: Structure Factor Amplitudes for $[\text{Rh}_2(\text{CO})_2(\mu\text{-Cl})(\text{DPM})_2][\text{BF}_4]$ , <i>trans</i> - $[\text{RhCl}(\text{CO})(\text{DPM})]_2$ , $[\text{Rh}_2\text{Cl}_2(\mu\text{-SO}_2)(\text{DPM})_2]$ , $[\text{Rh}_2\text{Br}_2(\mu\text{-CO})(\text{DPM})_2]$ and $[\text{Rh}_2\text{Cl}_2(\text{CO})\text{-}$ $(\text{C}_2\text{S}_4)(\text{DPM})_2]$	204



# LIST OF TABLES

Table		Page
1	Summary of Crystal Data and Intensity Collection for $[\text{Rh}_2\text{Cl}_2(\text{CO})(\text{C}_2\text{S}_4)(\text{DPM})_2]$	25
2	Derivation of the Rh-Rh Vectors for the Space Group $\text{P}\bar{1}$	29
3	Assignment of the Most Intense Patterson Map Vectors	30
4	Positional and Thermal Parameters for the Nongroup Atoms of $[\text{Rh}_2(\text{CO})_2(\mu\text{-Cl})(\text{DPM})_2]\text{-}[\text{BF}_4]$	37
5	Derived Parameters for the Rigid Group Atoms of $[\text{Rh}_2(\text{CO})_2(\mu\text{-Cl})(\text{DPM})_2][\text{BF}_4]$	38
6	Idealized Positional and Thermal Parameters for the Hydrogen Atoms of $[\text{Rh}_2(\text{CO})_2(\mu\text{-Cl})(\text{DPM})_2][\text{BF}_4]$	39
7	Least-Squares Plane Calculations	40
8	Selected Distances ( $\text{\AA}$ ) in $[\text{Rh}_2(\text{CO})_2(\mu\text{-Cl})(\text{DPM})_2][\text{BF}_4]$	41
9	Selected Angles (deg) in $[\text{Rh}_2(\text{CO})_2(\mu\text{-Cl})(\text{DPM})_2][\text{BF}_4]$	42
10	Summary of Crystal Data and Intensity Collection for <i>trans</i> - $[\text{RhCl}(\text{CO})(\text{DPM})]_2$	57
11	Positional and Thermal Parameters for the Nongroup Atoms of <i>trans</i> - $[\text{RhCl}(\text{CO})(\text{DAM})]_2$	61





Table		Page
12	Derived Parameters for the Rigid Group Atoms of <i>trans</i> -[RhCl(CO)(DPM)] <sub>2</sub>	62
13	Idealized Positional and Thermal Parameters for the Hydrogen Atoms of <i>trans</i> -[RhCl(CO)(DPM)] <sub>2</sub>	63
14	Least-Squares Plane Calculations	64
15	Selected Distances (Å) in <i>trans</i> -[RhCl(CO)(DPM)] <sub>2</sub>	65
16	Selected Angles (deg) in <i>trans</i> -[RhCl(CO)(DPM)] <sub>2</sub>	66
17	Analytical Data on Complexes	79
18	Spectral and Conductivity Data on the Complexes	80
19	Summary of Crystal Data and Intensity Collection for [Rh <sub>2</sub> Cl <sub>2</sub> (μ-SO <sub>2</sub> )(DPM) <sub>2</sub> ]	83
20	Positional and Thermal Parameters for the Nongroup Atoms of [Rh <sub>2</sub> Cl <sub>2</sub> (μ-SO <sub>2</sub> )(DPM) <sub>2</sub> ]	87
21	Derived Parameters for the Rigid Group Atoms of [Rh <sub>2</sub> Cl <sub>2</sub> (μ-SO <sub>2</sub> )(DPM) <sub>2</sub> ]	88
22	Idealized Positional and Thermal Parameters for the Hydrogen Atoms of [Rh <sub>2</sub> Cl <sub>2</sub> (μ-SO <sub>2</sub> )(DPM) <sub>2</sub> ]	89
23	Least-Squares Plane Calculations	90



Table		Page
24	Selected Distances ( $\text{\AA}$ ) in $[\text{Rh}_2\text{Cl}_2(\mu\text{-SO}_2)(\text{DPM})_2]$	91
25	Selected Angles (deg) in $[\text{Rh}_2\text{Cl}_2(\mu\text{-SO}_2)(\text{DPM})_2]$	92
26	Spectral Data for the Complexes	112
27	Summary of Crystal Data and Intensity Collection for $[\text{Rh}_2\text{Br}_2(\mu\text{-CO})(\text{DPM})_2]$	131
28	Positional and Thermal Parameters for the Nongroup Atoms of $[\text{Rh}_2\text{Br}_2(\mu\text{-CO})(\text{DPM})_2]$	134
29	Derived Parameters for the Rigid Group Atoms of $[\text{Rh}_2\text{Br}_2(\mu\text{-CO})(\text{DPM})_2]$	135
30	Idealized Positional and Thermal Parameters for the Hydrogen Atoms of $[\text{Rh}_2\text{Br}_2(\mu\text{-CO})(\text{DPM})_2]$	136
31	Least-Squares Plane Calculations	137
32	Selected Distances ( $\text{\AA}$ ) in $[\text{Rh}_2\text{Br}_2(\mu\text{-CO})(\text{DPM})_2]$	138
33	Selected Angles (deg) in $[\text{Rh}_2\text{Br}_2(\mu\text{-CO})(\text{DPM})_2]$	139
34	Summary of Crystal Data and Intensity Collection for $[\text{Rh}_2\text{Cl}_2(\text{CO})(\text{C}_2\text{S}_4)(\text{DPM})_2]$	155
35	Positional and Thermal Parameters for the Nongroup Atoms of $[\text{Rh}_2\text{Cl}_2(\text{CO})(\text{C}_2\text{S}_4)(\text{DPM})_2]$	161



Table		Page
36	Derived Parameters for the Rigid Group Atoms of $[\text{Rh}_2\text{Cl}_2(\text{CO})(\text{C}_2\text{S}_4)(\text{DPM})_2]$	162
37	Idealized Positional and Thermal Parameters for the Hydrogen Atoms of $[\text{Rh}_2\text{Cl}_2(\text{CO})(\text{C}_2\text{S}_4)(\text{DPM})_2]$	164
38	Least-Squares Plane Calculations	165
39	Selected Distances (Å) in $[\text{Rh}_2\text{Cl}_2(\text{CO})(\text{C}_2\text{S}_4)(\text{DPM})_2]$	166
40	Selected Angles (deg) in $[\text{Rh}_2\text{Cl}_2(\text{CO})(\text{C}_2\text{S}_4)(\text{DPM})_2]$	167
41	$10 \times (F_{\text{obs}} \text{ vs. } F_{\text{cal}})$ for $[\text{Rh}_2(\text{CO})_2(\mu\text{-Cl})(\text{DPM})_2][\text{BF}_4]$	*
42	$10 \times (F_{\text{obs}} \text{ vs. } F_{\text{cal}})$ for <i>trans</i> - $[\text{RhCl}(\text{CO})(\text{DPM})]_2$	*
43	$10 \times (F_{\text{obs}} \text{ vs. } F_{\text{cal}})$ for $[\text{Rh}_2\text{Cl}_2(\mu\text{-SO}_2)(\text{DPM})]_2$	*
44	$10 \times (F_{\text{obs}} \text{ vs. } F_{\text{cal}})$ for $[\text{Rh}_2\text{Br}_2(\mu\text{-CO})(\text{DPM})_2]$	*
45	$10 \times (F_{\text{obs}} \text{ vs. } F_{\text{cal}})$ for $[\text{Rh}_2\text{Cl}_2(\text{CO})(\text{C}_2\text{S}_4)(\text{DPM})_2]$	*

\*On Microfiche in Back Pocket.





# LIST OF FIGURES

Figure		Page
1	Coordination Modes of the Carbonyl Ligand	6
2	Structurally Characterized Coordination Modes of Carbon Disulfide	10
3	Coordination Modes of Sulfur Dioxide with Transition Metals	12
4	Cell Packing Diagram of $[\text{Rh}_2(\text{CO})_2(\mu\text{-Cl})(\text{DPM})_2][\text{BF}_4]$	43
5	A Perspective View of the $[\text{Rh}_2(\text{CO})_2(\mu\text{-Cl})(\text{DPM})_2]^+$ Cation	44
6	The Inner Coordination Sphere of $[\text{Rh}_2(\text{CO})_2(\mu\text{-Cl})(\text{DPM})_2]^+$ Cation	45
7	The Two Independent Tetrafluoroborate Anions	46
8	Cell Packing Diagram of <i>trans</i> - $[\text{RhCl}(\text{CO})(\text{DPM})]_2$	67
9	A Perspective View of <i>trans</i> - $[\text{RhCl}(\text{CO})(\text{DPM})]_2$	68
10	The Inner Coordination Sphere of <i>trans</i> - $[\text{RhCl}(\text{CO})(\text{DPM})]_2$	69
11	Reaction Scheme of $[\text{Rh}_2(\text{CO})_2(\mu\text{-Cl})(\text{DPM})_2][\text{BPh}_4]$ with CO and SO <sub>2</sub>	76
12	Cell Packing Diagram of $[\text{Rh}_2\text{Cl}_2(\mu\text{-SO}_2)(\text{DPM})_2]$	93



Figure		Page
13	A Perspective View of $[\text{Rh}_2\text{Cl}_2(\mu\text{-SO}_2)(\text{DPM})_2]$	94
14	The Inner Coordination Sphere of $[\text{Rh}_2\text{Cl}_2(\mu\text{-SO}_2)(\text{DPM})_2]$	95
15	A Reaction Scheme for Binuclear Rh-DPM Complexes with CO and SO <sub>2</sub>	104
16	The $^{31}\text{P}\{^1\text{H}\}$ NMR Spectra at 223°K of a) $\text{Rh}_2\text{I}(\text{CO})(\mu\text{-CO})(\text{DPM})_2[\text{I}]$ and b) $[\text{Rh}_2\text{-Br}_2(\mu\text{-CO})(\text{DPM})_2]$	115
17	A Scheme for the Reaction of $[\text{Rh}_2\text{Cl}_2(\mu\text{-CO})(\text{DPM})_2]$ with CO	121
18	A Possible Reaction Sequence for the Reaction of $[\text{Rh}_2\text{Br}_2(\mu\text{-CO})(\text{DPM})_2]$ with SO <sub>2</sub>	125
19	Cell Packing Diagram of $[\text{Rh}_2\text{Br}_2(\mu\text{-CO})(\text{DPM})_2]$	140
20	A Perspective View of $[\text{Rh}_2\text{Br}_2(\mu\text{-CO})(\text{DPM})_2]$	141
21	The Inner Coordination Sphere of $[\text{Rh}_2\text{Br}_2(\mu\text{-CO})(\text{DPM})_2]$	142
22	Stereoviews for Molecules A and B of $[\text{Rh}_2\text{Cl}_2(\text{CO})(\text{C}_2\text{S}_4)(\text{DPM})_2]$	170
23	A Perspective View for Dimers A and B of $[\text{Rh}_2\text{Cl}_2(\text{CO})(\text{C}_2\text{S}_4)(\text{DPM})_2]$	171
24	The Equatorial Planes of Dimers A and B of $[\text{Rh}_2\text{Cl}_2(\text{CO})(\text{C}_2\text{S}_4)(\text{DPM})_2]$	172
25	Proposed Scheme for the Reaction of <i>trans</i> - $[\text{RhCl}(\text{CO})(\text{DPM})]_2$ with CS <sub>2</sub>	179



## LIST OF ABBREVIATIONS

Me	=	methyl
Et	=	ethyl
n-Pr	=	n-propyl
i-Pr	=	iso-propyl
n-Bu	=	n-butyl
t-Bu	=	tert-butyl
COD	=	1,5 cyclooctadiene
THF	=	tetrahydrofuran
HFB	=	hexafluoro-2-butyne
DMA	=	dimethylacetylenedicarboxylate
DPM	=	bis(diphenylphosphino)methane
DAM	=	bis(diphenylarsino)methane





## CHAPTER I.

### INTRODUCTION

Homogeneous catalysis by transition metal complexes is currently, and has been for two decades, an area of considerable interest.<sup>1-4</sup> Several important successes have been achieved in this area translating homogeneously catalyzed reactions into viable commercial processes. Included among these are the Wacker process for olefin oxidation based on a palladium catalyst,<sup>5,6</sup> the hydroformylation process using a rhodium (I) phosphine complex<sup>7</sup> and the carbonylation of methanol to acetic acid employing a rhodium carbonyl iodide species.<sup>8,9</sup>

Many approaches have been used in catalytic studies, however it remains of fundamental importance to obtain an understanding of the chemical processes which occur at the metal centre during the catalytic reaction. Such information is required if one hopes intelligently to modify the catalyst's properties to achieve the results desired. With this objective in mind it becomes convenient to break the catalytic reaction down into three steps:<sup>10</sup> 1) substrate coordination and activation; 2) substrate transformation into product or product precursor; and 3) product elimination. If catalyst regeneration has not occurred a fourth step, that of catalyst regeneration, must also be added.

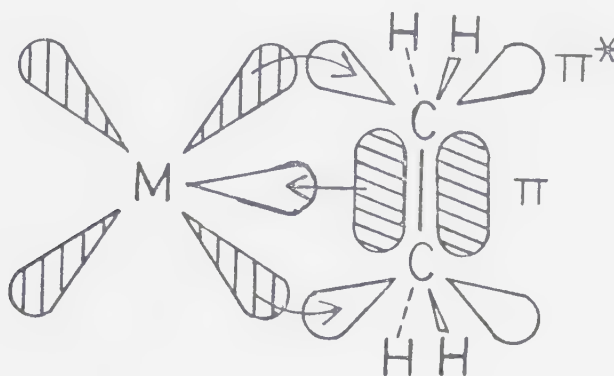


In catalytic reactions direct information about any of the above steps is, by the very nature of the catalytic process, limited. However, one approach which has proven useful, involves model system studies utilizing complexes which are similar to a given catalyst but which are not themselves catalysts.<sup>10-12</sup> By this approach useful analogies can be made between the model system and the related catalyst. It is obvious, therefore, that small molecule coordination in transition metal complexes and the activation of the small molecule by the metal centre are of interest in that these topics pertain to the first step in the above breakdown of catalytic reactions. It is on this theme, i.e. the coordination and activation of small molecules in transition metal complexes, that this thesis will concentrate.

In studies of small molecule coordination and activation, the initial step involves the coordination of the small molecule to a coordinately unsaturated metal centre. Here it is important to have a knowledge of how the small molecule coordinates in order to understand the resulting chemistry. Concurrent with coordination is activation of the small molecule, making it more reactive than it was prior to coordination. Activation results from a net change in the electron density distribution within the coordinated molecule. In molecular orbital terms this corresponds to electron donation from the substrate bonding



orbitals to the metal centre followed by back donation from the metal centre into orbitals which are antibonding in terms of the substrate bonds. The well known Dewar, Chatt, Duncanson<sup>13,14</sup> model for ethylene coordination to metals, which is diagrammed below, is a familiar example of this.



The bonding here is considered to consist of two interdependent components: 1) donation of  $\pi$ -electron density from the olefin to a  $\sigma$ -type acceptor orbital on the metal atom; and 2) back donation of electron density from filled metal  $dxz$  or other  $d\pi-p\pi$  hybrid orbitals into antibonding  $\pi^*$  orbitals of the olefin. Both components are synergically related, that is an increase in one component tends to promote an increase in the other and further both tend to decrease the bond order of the olefinic linkage. The structural results of this ethylene activation are well documented,<sup>15,16</sup> showing a lengthening of the C-C bond and a bending back of the hydrogen atoms away from the metal



centre. Clearly, a thorough understanding of this first important step in catalytic processes, that of substrate coordination and activation, is extremely important for a better understanding of these reactions.

In this thesis the small molecules whose transition metal chemistry will be pursued are carbon monoxide, carbon disulfide and sulfur dioxide. Each of these molecules has important relevance to catalysis. The catalyzed activation of carbon monoxide, for example, is of importance since the conversion of coal<sup>17</sup> to substitute natural gas, hydrocarbons and organic chemicals is based on the metal catalyzed reduction of carbon monoxide via methanation reactions and the Fischer-Tropsch synthesis.<sup>18-21</sup> Carbon disulfide activation, on the other hand, may serve as a useful model for the activation of the less reactive carbon dioxide molecule, which is an abundant potential feedstock for hydrocarbon production.<sup>10</sup> And with the increased utilization of coal, the deleterious effects of sulfur dioxide on the environment encourage efforts aimed at its removal. The use of transition metal catalysts for SO<sub>2</sub> removal from flue gases has proven useful in this regard.<sup>22-26</sup>

Furthermore, the three small molecules of interest are particularly germane to studies of small molecule coordination and activation since they each display a rich variety of coordination modes in metal complexes. Their study promises to yield valuable information relating these coordination modes to properties of the metal complexes, and





therefore promises to increase our understanding of factors affecting small molecule coordination and activation.

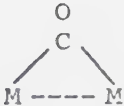
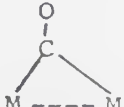
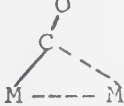
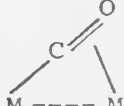
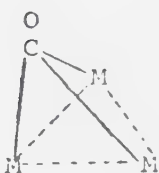
Insertion reactions of these small molecules other than into metal-metal bonds, although potentially important models for catalytic processes such as the Fischer-Tropsch synthesis,<sup>20,21</sup> the catalytic carbonylation of methanol to acetic acid,<sup>8</sup> and hydroformylation reactions,<sup>27,28</sup> will not be discussed here.

The carbonyl group, which has been extensively studied,<sup>10,29</sup> is found to be a tremendously versatile ligand displaying a wide variety of coordination modes. These modes, together with examples of each are presented in Figure 1. The first and most common bonding mode is that of the terminal carbonyl ligand. In this geometry the carbonyl group is associated with only one metal centre, is bound through the carbon atom and has an essentially linear M-C-O linkage.

The second class is that of the doubly bridging carbonyl group in which the carbonyl ligand is associated simultaneously with two metal centres. In this case classification is somewhat more complex than in the terminal class, since now the carbonyl ligand can display a significant range in coordination geometries. For the sake of convenience however, these ligands can be grouped into three classes; symmetrical, asymmetrical and semibridging. One method of distinguishing these three, somewhat arbitrary classes is based on metal-carbonyl bond distances. For the



Figure 1. Coordination Modes of the Carbonyl Ligand

Mode		Example	Reference
terminal	M-C-O	<i>trans</i> -[IrCl(CO) <sub>2</sub> (PPh <sub>3</sub> ) <sub>2</sub> ] <i>trans</i> -[RhCl(CO)(DAM)] <sub>2</sub>	30 31
symmetrical-μ <sub>2</sub>		[Pd <sub>2</sub> Cl <sub>2</sub> (μ-CO)(DAM) <sub>2</sub> ] [Fe <sub>2</sub> (CO) <sub>6</sub> (μ-CO)(DPM)]	32 33
asymmetrical-μ <sub>2</sub>		[Rh(CO)(μ-CO)(PPh <sub>3</sub> ) <sub>2</sub> ] <sub>2</sub> [Rh <sub>2</sub> (CO) <sub>2</sub> (μ-CO)(μ-Cl)(DPM) <sub>2</sub> ] <sup>+</sup>	34 35
semibridging-μ <sub>2</sub>		[Fe <sub>2</sub> (CO) <sub>5</sub> (μ-CO)(PhCCPh)]	36
linear-μ <sub>2</sub>		[Mn <sub>2</sub> (CO) <sub>4</sub> (μ-CO)(DPM) <sub>2</sub> ]	37
triply-bridging		[Co <sub>6</sub> (CO) <sub>14</sub> ] <sup>4-</sup>	38



symmetrical species the metal-carbonyl distances differ by less than  $3\sigma$  where,  $\sigma = \sqrt{\sigma_a^2 + \sigma_b^2}$  and  $\sigma_a$  and  $\sigma_b$  are the standard deviations in the two metal-carbonyl bond lengths. The species within the semibridging group, on the other hand, are arbitrarily defined as having metal-carbonyl distances, which differ by greater than  $0.3 \text{ \AA}$ , and the third class, containing the asymmetrical species, between the two above extremes. In addition, a further distinction between these differing doubly bridging carbonyl geometries can be made based on the carbonyl C-O vector. In the symmetrical bridging mode the C-O vector is perpendicular to the M-M axis whereas in the asymmetrical and semibridging groups the C-O vector tends away from normality. Therefore, the closer the carbonyl geometry approaches the semibridging limit, the closer the M-C-O linkage is to being colinear with respect to the more strongly bound metal.

Another bridging carbonyl geometry, that of the linear- $\mu_2$ -bridging carbonyl mode, might be considered as a further extreme of the semibridging mode. In this carbonyl bonding mode the carbonyl ligand is  $\sigma$ -bound to one metal centre, resulting in an approximately linear M-C-O linkage and is simultaneously  $\pi$ -bound to a second metal centre. Unlike all previous carbonyl bonding modes, however, which function as two electron donors, this linear- $\mu_2$ -bridging ligand acts as a four electron donor.

The carbonyl ligand can also function as a triply bridging ligand having the carbonyl group simultaneously





associated with three metal centres. As with the doubly bridging carbonyl ligands, the triply bridging carbonyl group can be either symmetrical or asymmetrical.

Until recently it was a well established dogma of transition metal carbonyl chemistry that bridging carbonyl groups were always accompanied by a metal-metal bond.<sup>39,40</sup> However, the recent structural characterizations of  $[\text{Pd}_2\text{Cl}_2(\mu\text{-CO})(\text{DAM})_2]$ ,<sup>32</sup>  $[\text{Pt}_2\text{Cl}_2(\mu\text{-CO})(\text{DAM})_2]$ <sup>41</sup> and  $[\text{Rh}_2\text{Cl}_2(\mu\text{-CO})(\mu\text{-DMA})(\text{DPM})_2]$ <sup>42</sup> have shown that this is not the case. In each of the three complexes the metal-metal separation (ranging from  $3.162(4)\text{\AA}$  to  $3.354(1)\text{\AA}$ ) is too long for a direct metal-metal interaction and the metal-carbonyl-metal angles are *ca.*  $120^\circ$ , contrasting with conventional bridging carbonyl ligands where angles between  $62^\circ$  and  $90^\circ$  are common.<sup>29</sup> The drawings in Figure 1, therefore, show dotted lines between the metal atoms to avoid implications regarding the presence or absence of a metal-metal bond.

The differentiation between the above carbonyl bonding modes can in general be conveniently carried out using infrared spectroscopy, since the carbonyl stretching frequencies for terminal carbonyl ligands are usually higher than those of doubly bridging carbonyl groups which are in turn higher than those for the triply bridging mode. However, differentiation between the types of doubly bridging modes presents a problem, since no obvious trend in their carbonyl stretching frequencies is observed. Thus, in



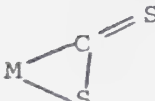
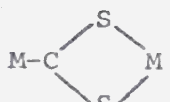
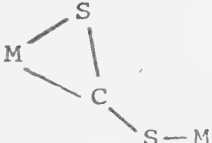
$[\text{Pt}_2\text{Cl}_2(\mu\text{-CO})(\text{DAM})_2]$ ,<sup>41</sup> which contains a symmetrical carbonyl ligand, the carbonyl frequency ( $1638\text{ cm}^{-1}$ ) is significantly different than that observed in the analogous palladium complex,  $[\text{Pd}_2\text{Cl}_2(\mu\text{-CO})(\text{DAM})_2]$  ( $1704\text{ cm}^{-1}$ ) but compares well with that of  $[\text{Mn}_2(\text{CO})_4(\mu\text{-CO})(\text{DPM})_2]$  ( $1645\text{ cm}^{-1}$ ),<sup>37</sup> which contains a linear- $\mu_2$ -bridging carbonyl group. It is relevant to discussions of carbonyl activation that the carbonyl stretching frequencies indicate an increase in activation (i.e. a decrease in C-O bond order) as the number of metal atoms associated with the ligand increases.

The carbon disulfide molecule also displays a variety of coordination modes, both in mononuclear and polynuclear species. Yet this small molecule has received relatively little attention with only a few species having been structurally characterized.<sup>43,44</sup> The three modes of carbon disulfide coordination which were structurally characterized at the time this research was undertaken are summarized in Figure 2. In the  $\text{C,S-}\eta^2$  coordination geometry the carbon disulfide molecule is associated with only one metal centre, coordinating in a side-on manner via one of the sulfur atoms and the carbon atom. This is perhaps the commonest mode of  $\text{CS}_2$  coordination. In addition, two bridging geometries have been observed for the carbon disulfide ligand, shown in Figure 2 as modes A and B. Mode A has the carbon atom bound to one metal centre and the two sulfur atoms coordinated to the second metal centre;



Figure 2. Structurally Characterized Coordination

## Modes of Carbon Disulfide

	Mode	Example	Reference
$C, S-\eta^2$		$[Pt(PPh_3)_2(CS_2)]$	45
bridging A		$[Pt_2Cl(CS_2)(PPh_3)_4]^+$	46
bridging B		$(PhMe_2P)_2(CO)_2Fe(CS_2)Mn(CO)_2Cp$	47



whereas mode B, has the  $\text{CS}_2$  ligand coordinated in an  $\text{C}, \text{S}-\eta^2$  fashion to one metal centre and via the second sulfur atom to the other metal centre.

Two other  $\text{CS}_2$  bonding modes have been proposed although these have not been structurally characterized. Coordination of  $\text{CS}_2$  through the sulfur atom ( $\text{M}-\text{S}=\text{C}=\text{S}$ ) has been suggested,<sup>48</sup> however these species tend to be poorly characterized. Condensation of the carbon disulfide molecules yielding a  $\text{C}_2\text{S}_5$  fragment has also been proposed in  $[\text{RhCl}(\text{PPh}_3)_2(\text{C}_2\text{S}_5)]$ <sup>49</sup> but characterization is again incomplete. In addition to these proposed coordination modes two others are possible based on analogies with  $\text{CO}_2$  chemistry. These involve either a  $\text{C}_2\text{S}_4$  fragment, resulting from the condensation of two  $\text{CS}_2$  molecules, analogous to the  $\text{C}_2\text{O}_4$  fragment observed in  $[\text{IrCl}(\text{C}_2\text{O}_4)(\text{PPh}_3)_2]$ ,<sup>50</sup> or an  $\eta^1$  carbon-bound species analogous to that proposed for  $\text{CO}_2$  coordination in  $[\text{Ni}(\text{CO}_2)(\text{P}(\text{n-Bu})_3)_3]$ .<sup>51</sup>

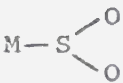
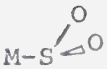

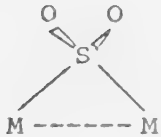
Correlations between the coordination mode of carbon disulfide and the infrared stretching frequencies have not been reported to date due to the limited structural data available. But again a significant drop in  $\text{CS}_2$  stretching frequencies is observed on coordination implying activation of this molecule.

The sulfur dioxide ligand also displays a variety of coordination geometries in transition metal complexes.<sup>52,53</sup> Those geometries which have been structurally characterized are shown in Figure 3. When associated with a single metal





Figure 3. Coordination Modes of Sulfur Dioxide  
with Transition Metals

Mode		Example	Reference
coplanar- $\eta^1$		$[\text{Ni}(\text{SO}_2)(\text{PPh}_3)_3]$ $[\text{CpRh}(\text{C}_2\text{H}_4)(\text{SO}_2)]$	54 55
pyramidal- $\eta^1$		$[\text{IrCl}(\text{CO})(\text{SO}_2)(\text{PPh}_3)_2]$ $[\text{RhCl}(\text{SO}_2)(\text{PPh}_3)_2]_2$	56 57
$\text{O}, \text{S}-\eta^2$		$[\text{Rh}(\text{NO})(\eta^2-\text{SO}_2)(\text{PPh}_3)_2]$ $[\text{RuCl}(\text{NO})(\eta^2-\text{SO}_2)(\text{PPh}_3)_2]$	58 59
bridging- $\mu_2$		$[\text{Ir}_2(\text{CO})_4\text{H}_2(\text{SO}_2)(\text{PPh}_3)_2]$ $[\text{Ir}_2(\text{CO})_2\text{I}_4(\text{SO}_2)(\text{PPh}_3)_2]$	60 61
$\eta^1\text{-O}$	$\text{M}-\text{O}-\text{S}-\text{O}$	$[\text{SbF}_5\text{OSO}]^a$	62

<sup>a</sup>Although Sb is not a transition metal, this represents a potential coordination mode in transition metal complexes.



centre sulfur dioxide can exhibit the following coordination modes: the coplanar geometry, in which the  $M-SO_2$  framework is approximately planar; the pyramidal geometry, with the  $SO_2$  plane inclined to the  $M-S$  vector;  $O,S-\eta^2$  coordination with the sulfur atom and one of the oxygen atoms coordinated to the metal in a side-on manner; and terminal  $\eta^1-O$  coordination, in which the sulfur dioxide ligand is bound through one of the oxygen atoms. The coplanar and pyramidal coordination modes are often compared to the linear and bent geometries observed with the more extensively studied nitrosyl ligand.<sup>63</sup>

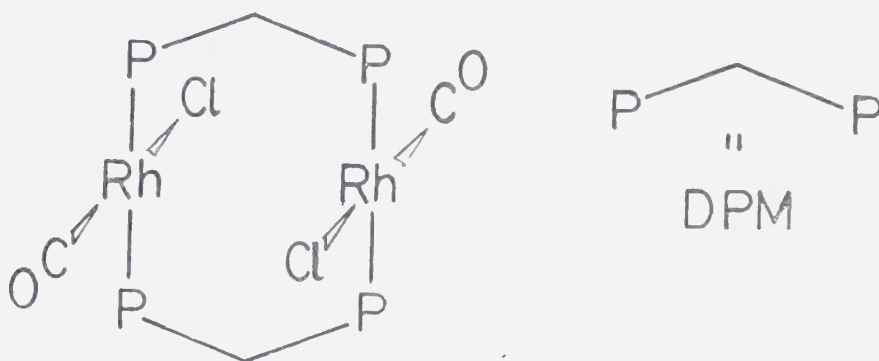
Sulfur dioxide has also been observed to bridge two metal centres in a symmetrical fashion. As now appears to be the case with the carbonyl ligand, a metal-metal bond is not a prerequisite to having a bridging  $SO_2$  group. Therefore, in  $[(Cp)_2Fe_2(CO)_4(\mu-SO_2)]$ <sup>64</sup> the  $SO_2$  ligand is bridging and unsupported, whereas in  $[Ir_2(CO)_4H_2(PPh_3)_2-(\mu-SO_2)]$ <sup>60</sup> the bridging  $SO_2$  ligand is accompanied by a metal-metal bond. Sulfur dioxide coordination to a terminal halogen in a pyramidal fashion is also known, as for example in  $[Pt(Me)(I-SO_2)(PPh_3)_2]$ .<sup>65</sup>

Spectroscopic identification of the sulfur dioxide coordination mode is not without difficulty. Although the various coordination geometries have associated ranges of  $\nu(SO)$ , large regions of overlap exist, especially between the bridging and pyramidal modes where the regions



are essentially superimposed.<sup>53</sup> Thus unambiguous identification of the coordination geometry using infrared techniques, is in some cases difficult.

The chemistry of the above small molecules will be limited, in this thesis, to that involving binuclear diphosphine and diarsine bridged complexes of rhodium, similar to that shown below for *trans*-[RhCl(CO)(DPM)]<sub>2</sub>:<sup>66</sup>



These binuclear complexes are closely related to group VIII mononuclear, four coordinate phosphine complexes such as Vallarino's compound, [RhCl(CO)(PPh<sub>3</sub>)<sub>2</sub>]<sup>67</sup> and Vaska's compound, [IrCl(CO)(PPh<sub>3</sub>)<sub>2</sub>].<sup>68</sup> These mononuclear compounds have received a great deal of attention in the last twenty years and have been found to display a wide variety of small molecule addition and oxidative addition reactions.<sup>69,70</sup> The analogous binuclear complexes, of the type shown above, have on the other hand received much less attention and very little small molecule chemistry has been reported



for them. In these binuclear complexes the metal atoms are held in close proximity by the bridging DPM or DAM ligands and, although chemistry similar to the related mononuclear complexes might be expected, one might also anticipate differences in their chemistries owing to the effects of metal proximity, in the binuclear case. In these species, the metal centres can react independently of each other reacting essentially as two monomeric units, or one metal centre can perturb the other thereby altering its chemistry significantly relative to the related mononuclear complex. Balch and Tulyathan<sup>71</sup> have carried out studies in this regard, relating the chemistry at the metal centres to the distance between them, utilizing diphosphines and other bidentate ligands of varying bite size to bridge two square planar Rh(I) centres. In one example, involving complexes of the type  $[\text{RhCl}(\text{CO})(\text{L-L})]_2$ , where  $\text{L-L} = \text{Ph}_2\text{P}(\text{CH}_2)_n\text{PPh}_2$  ( $n=3,4$ ),  $\text{SO}_2$  attack was observed at only one rhodium site. It was therefore concluded that the normal reactivity of the rhodium site is diminished in these dimeric complexes and it was suggested that this lack of reactivity resulted from the inability of the unreactive rhodium site to readjust its coordination geometry to the arrangement necessary to bind a second substrate molecule.

The close proximity of the metals in binuclear species also suggests that they may serve as useful models for multi-centered metal catalysis.<sup>11</sup>





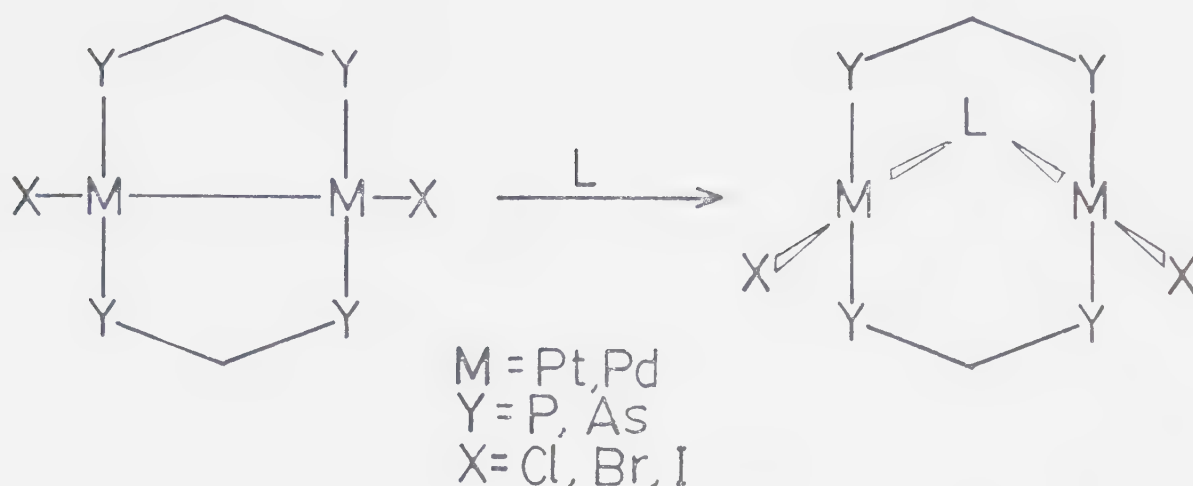
Although binuclear transition metal species have been reported for several bidentate diphosphine and diarsine ligands including  $R_2PPR_2$  ( $R = Me, Et, Ph$ ),<sup>72</sup>  $Me_2AsAsMe_2$ ,<sup>73</sup>  $Me_2XYXMe_2$  ( $X = P, As$ ;  $Y = O, S$ ),<sup>73,74</sup>  $Me_2P(CH_2)_2PMe_2$ ,<sup>75</sup>  $Ph_2P(CH_2)_2AsPh_2$ ,<sup>76</sup>  $(t-Bu)_2P(CH_2)_nP(t-Bu)_2$  ( $n = 10, 12$ ),<sup>77</sup>  $Ph_2PCC(PPh_2)(CF_2)_n$  ( $n = 2, 3, 4$ )<sup>78,79</sup> and  $Me_2AsCC(AsMe_2)(CF_2)_n$  ( $n = 2, 3$ ),<sup>78,79</sup> no reports on the chemistry of binuclear species containing these ligands with the small molecules of interest have appeared.

With the ligand of specific interest, bis(diphenylphosphino)methane (DPM) and bis(diphenylarsino)methane (DAM), several binuclear transition metal complexes are known, including:  $[Mn_2(CO)_8(DPM)]$ ,<sup>80</sup>  $[Mn_2(CO)_6(DPM)_2]$ ,<sup>80</sup>  $[Mn_2(CO)_4-(\mu-CO)(DPM)_2]$ ,<sup>37,80</sup>  $[Mn_2(CO)_5(\text{para-CH}_3C_6H_4NC)(DPM)_2]$ ,<sup>81</sup>  $[Mn(CO)_4(\mu\text{-para-CH}_3C_6H_4NC)(DPM)_2]$ ,<sup>81</sup>  $[Fe_2(CO)_6(\mu-CO)-(DPM)_2]$ ,<sup>33</sup> and  $[IrCl(CO)(DPM)]_2$ .<sup>82</sup> Again the reactivity of these complexes towards small molecules has not been reported.

Some small molecule chemistry has been reported for binuclear DPM and DAM species of Pt, Pd and Rh. The Pt(I)<sup>83</sup> and Pd(I)<sup>32,84</sup> species of the type  $[MX(L-L)]_2$  ( $M = Pd, Pt$ ;  $X = Cl, Br$ ;  $L-L = DPM, DAM$ ), for example, undergo facile reactions with several small molecules including CO,<sup>32,41,84</sup> SO<sub>2</sub>,<sup>85</sup>  $PhN_2^+$ ,<sup>86</sup> CNR ( $R = CH_3, C_6H_{11}, C_6H_5, \text{para-CH}_3-C_6H_4$ ),<sup>84</sup> acetylenes,<sup>87</sup> olefins,<sup>87</sup> N<sub>2</sub>CH<sub>2</sub> (which yields a methylene species)<sup>88</sup> and S<sub>8</sub> (which yields a sulfido species)<sup>85b</sup> as



shown below, by inserting into the metal-metal bond.



The carbonyl adduct,  $[\text{Pd}_2\text{Cl}_2(\mu\text{-CO})(\text{DAM})_2]$ ,<sup>32</sup> represented the first structural characterization of a carbonyl ligand bridging two nonbonded metal centres. In addition, the insertions of CO and  $\text{SO}_2$  in these systems were shown to be reversible. Kubiak and Eisenberg<sup>89</sup> have aptly dubbed these species "A-frame" complexes owing to the configuration of the equatorial ligands which roughly describes a letter A having the ligand L at the apex.

In addition, DPM-bridged Pd species are reported to undergo two other reactions. The first involves insertion of  $\text{SnCl}_2$  into the Pd-Cl bonds of  $[\text{PdCl}(\text{DPM})]_2$  yielding  $[\text{Pd}_2\text{Cl}(\text{SnCl}_3)(\text{DPM})_2]$  and  $[\text{Pd}(\text{SnCl}_3)(\text{DPM})]_2$ .<sup>90</sup> The second involves halide displacement from  $[\text{Pd}_2\text{Cl}_2(\mu\text{-CNR})(\text{DPM})_2]$  in the presence of excess isocyanide to reversibly yield the dicationic species  $[\text{Pd}_2(\text{CNR})_2(\mu\text{-CNR})(\text{DPM})_2]^{2+}$ .<sup>84</sup>



Some small molecule chemistry of DPM-bridged rhodium complexes has also been reported. The reaction of the rhodium dicarbonyl "A-frame" species,  $[\text{Rh}_2(\text{CO})_2(\mu\text{-Cl})(\text{DPM})_2][\text{BPh}_4]$  with CO produces the tricarbonyl complex  $[\text{Rh}_2(\text{CO})_2(\mu\text{-CO})(\mu\text{-Cl})(\text{DPM})_2][\text{BPh}_4]$ .<sup>35,91</sup> However in contrast to the Pd and Pt species (vide supra) where insertion into a metal-metal bond occurs, carbon monoxide addition here occurs with the formation of a Rh-Rh bond. This tricarbonyl species verifies that small molecules can coordinate in the open bridging site of these "A-frame" complexes as was originally suggested by Eisenberg and Kubiak.<sup>89</sup> The analogous sulfido bridged "A-frame" species,  $[\text{Rh}_2(\text{CO})_2(\mu\text{-S})(\text{DPM})_2]$  has been treated with MeI, EtI, or LiI followed by CO addition resulting in a species postulated as  $[\text{RhI}(\text{CO})(\mu\text{-CO})(\text{DPM})]_2$ .<sup>89</sup> However, based on the spectral data presented, this species is probably more correctly assigned as an iodo-bridged tricarbonyl complex, analogous to the cationic chloro-bridged species noted above. In addition, the reaction of the sulfido-bridged complex with HCl yields the species *trans*- $[\text{RhCl}(\text{CO})(\text{DPM})]_2$ .<sup>89</sup> Both  $[\text{Rh}_2(\text{CO})_2(\mu\text{-S})(\text{DPM})_2]$ <sup>89</sup> and *trans*- $[\text{RhCl}(\text{CO})(\text{DPM})]_2$ <sup>71</sup> have been reported to react with  $\text{SO}_2$ , however the formulations for the products are unknown. Finally *trans*- $[\text{RhCl}(\text{CO})(\text{DPM})]_2$  has been observed to react with iodine yielding the novel Rh(II) species  $[\text{RhClI}(\text{CO})(\text{DPM})]_2$ .<sup>71</sup>

Owing to the lack of small molecule chemistry with binuclear Rh species and because of the potential relevance of



such studies to catalytically interesting systems, as mentioned previously, an investigation into the chemistry of  $\text{trans-}[\text{RhCl}(\text{CO})(\text{DPM})]_2$  and  $[\text{Rh}_2(\text{CO})_2(\mu\text{-Cl})(\text{DPM})_2]^+$  with  $\text{CO}$ ,  $\text{CS}_2$  and  $\text{SO}_2$  was undertaken.

Since it is difficult on the basis of analytical and spectral data to unambiguously assign the mode of small molecule coordination, the technique of X-ray diffraction was used extensively throughout this study. The reader is referred to several standard texts for detailed discussions of the theoretical and experimental considerations of X-ray diffraction.<sup>92-95</sup>





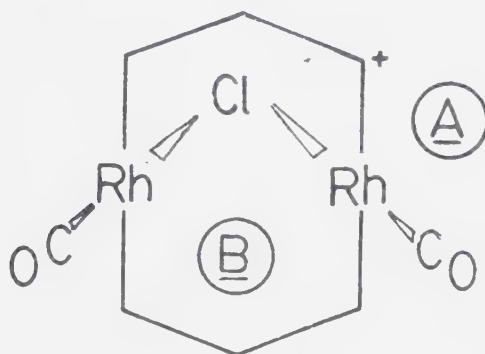
## CHAPTER II.

### The Structure of $[\text{Rh}_2(\text{CO})_2(\mu\text{-Cl})(\text{DPM})_2][\text{BF}_4]$ :

#### A Binuclear "A-frame" Complex

#### INTRODUCTION

The cationic complex,  $[\text{Rh}_2(\text{CO})_2(\mu\text{-Cl})(\text{DPM})_2]^+$  (1), was assumed to be an "A-frame" type species, as shown below, based on spectral data, on the structural characterization of its carbonyl adduct,<sup>35,91</sup>  $[\text{Rh}_2(\text{CO})_2(\mu\text{-CO})(\mu\text{-Cl})(\text{DPM})_2]^+$  (2) and on analogies with the sulfido-bridged species,<sup>89</sup>  $[\text{Rh}_2(\text{CO})_2(\mu\text{-S})(\text{DPM})_2]$  (3).



1

Complex 1 reacts reversibly with  $\text{CO}$ <sup>35,91</sup> and  $\text{SO}_2$ <sup>96</sup> (see Chapter IV) and undergoes facile reactions with several other small molecules, including  $\text{NO}$ <sup>97</sup> and tetracyanoethylene.<sup>98</sup> The reactions of 1 with  $\text{CO}$  and  $\text{SO}_2$  contrast the two possible modes of attack on this species by small molecules.



Whereas CO attacks the open terminal coordination site A, remote from the bridging site B and results in one of the originally coordinated carbonyl ligands swinging into the bridging site,<sup>91</sup> SO<sub>2</sub> seems to attack directly at the bridging site yielding  $[\text{Rh}_2(\text{CO})_2(\mu\text{-Cl})(\mu\text{-SO}_2)(\text{DPM})_2]^+$ .<sup>96</sup>

The structural determination of the closely related, sulfido bridged "A-frame" complex 3,<sup>89</sup> indicated that the bridging site was blocked, at least in the solid state, by four of the DPM phenyl groups. In particular, two rings were found to severely obstruct this site. Although the details of the chemistry of 3 with small molecules are not known to us, other "A-frame" species, having their bridging sites obstructed in the same way, show chemistry consistent with terminal ligand attack as opposed to attack at the bridging site (see Chapter IV). Since 1 seems to allow attack at both the bridging and terminal sites, it was of interest to obtain precise structural information on this "A-frame" species with hopes of establishing possible structure-reactivity correlations.

### EXPERIMENTAL

All solvents used throughout this study were dried and degassed prior to use and all reactions were performed under Schlenk conditions using an atmosphere of dinitrogen or the reactant gas. RhCl<sub>3</sub>·3H<sub>2</sub>O was purchased from Research Organic/Inorganic Chemical Corporation and DPM and



DAM were purchased from Strem Chemicals. All other chemicals were reagent grade and used as received. Infrared spectra were recorded on either a Perkin Elmer Model 467 spectrometer or a Nicolet 7199 F.T. interferometer using Nujol mulls on KBr plates. NMR spectra were recorded on a Bruker HFX-90 NMR spectrometer. Conductivity measurements were obtained on a Yellow Springs Instruments Model 31 Conductivity bridge using approximately 1.0 mM solutions in acetone.

#### Preparation of $[\text{Rh}_2(\text{CO})_2(\mu\text{-Cl})(\text{DPM})_2][\text{BPh}_4]$

Treatment of a solution of 0.100 g (0.202 mmol) of  $[\text{RhCl}(\text{COD})]_2$ <sup>99</sup> in 20 mL of  $\text{CH}_2\text{Cl}_2$  with 0.103 g (0.269 mmol) of DPM dissolved in 5 mL of toluene under a carbon monoxide atmosphere yielded  $[\text{Rh}_2(\text{CO})_2(\mu\text{-CO})(\mu\text{-Cl})(\text{DPM})_2][\text{RhCl}_2(\text{CO})_2]$ . Addition of 0.458 g (1.34 mmol) of  $\text{NaBPh}_4$ , followed by 40 mL of  $\text{Et}_2\text{O}$  resulted in the precipitation of the cationic tricarbonyl species as the  $\text{BPh}_4^-$  salt in 90% yield. Slow concentration of this solution of  $[\text{Rh}_2(\text{CO})_2(\mu\text{-CO})(\mu\text{-Cl})(\text{DPM})_2]^+[\text{BPh}_4]^-$  under a dinitrogen flow yielded the dicarbonyl species,  $[\text{Rh}_2(\text{CO})_2(\mu\text{-Cl})(\text{DPM})_2][\text{BPh}_4]$ , as a yellow-orange microcrystalline solid.

#### The serendipitous crystallization of $[\text{Rh}_2(\text{CO})_2(\mu\text{-Cl})(\text{DPM})_2][\text{BF}_4]$

To a solution of 0.100 g (0.072 mmol) of  $[\text{Rh}_2(\text{CO})_2(\mu\text{-Cl})(\text{DPM})_2][\text{BPh}_4]$  in 8 mL of acetone was added 0.020 g (0.080 mmol) of  $[\text{PhN}_2][\text{PF}_6]$ . Slow diffusion of  $\text{Et}_2\text{O}$  into the reaction mixture yielded yellow-orange prismatic crys-



tals. Although too few of the yellow-orange crystals were obtained for elemental analysis or a  $^{31}\text{P}$  NMR spectrum, an infrared spectrum of the complex ( $\nu(\text{CO})$  1995(s), 1978(vs)  $\text{cm}^{-1}$ ;  $\nu(\text{BF})$  1060 (m,br)  $\text{cm}^{-1}$ ) indicated that they were  $[\text{Rh}_2(\text{CO})_2(\mu\text{-Cl})(\text{DPM})_2][\text{BF}_4]$ .

#### Preparation of $[\text{Rh}_2(\text{CO})_2(\mu\text{-Cl})(\text{DPM})_2][\text{BF}_4]$

To a solution of 0.100 g (0.075 mmol) of  $[\text{Rh}_2(\text{CO})_2(\mu\text{-Cl})(\text{DPM})_2][\text{RhCl}_2(\text{CO})_2]$  in 10 mL of  $\text{CH}_2\text{Cl}_2$  was added 0.017 g (0.150 mmol) of  $\text{NaBF}_4$ . Slow concentration of this solution under a dinitrogen stream yielded yellow-orange crystals of  $[\text{Rh}_2(\text{CO})_2(\mu\text{-Cl})(\text{DPM})_2][\text{BF}_4]$ . The infrared spectrum of this compound was identical to that of the crystals initially obtained, one of which was used in the structure determination (vide infra).

#### $^{31}\text{P}$ and $^{19}\text{F}$ NMR Results

A solution was prepared in  $d^6$ -acetone containing 0.050 g (0.036 mmol) of  $[\text{Rh}_2(\text{CO})_2(\mu\text{-Cl})(\text{DPM})_2][\text{BPh}_4]$  and 0.010 g (0.040 mmol) of  $[\text{PhN}_2][\text{PF}_6]$ . The  $^{19}\text{F}$  and  $^{31}\text{P}\{^1\text{H}\}$  NMR were recorded immediately after preparation and again after approximately two weeks. The initial spectra showed that the only fluorine containing species was the  $\text{PF}_6^-$  anion ( $^{19}\text{F}$  NMR  $\delta = 71.7$  ppm,  $^{100}$  doublet,  $|J_{\text{P-F}}| = 707$  Hz;  $^{31}\text{P}\{^1\text{H}\}$  NMR  $\delta = 144.0$  ppm,  $^{101}$  septet,  $J_{\text{P-F}} = 708$  Hz). The spectra of the aged sample showed the presence of the  $\text{PF}_6^-$  anion as well as resonances in the  $^{19}\text{F}$  NMR at  $\delta = 130.8$  ppm





(heptet,  $|J_{F-H}| = 6.3$  Hz, possibly  $\text{Me}_2\text{SiF}_2$ );  $\delta = 150.0$  ppm (singlet) and  $\delta = 150.1$  ppm (br singlet,  $\text{BF}_4^-$ ). In both  $^{31}\text{P}\{^1\text{H}\}$  NMR spectra (new and two week old samples) the resonance due to the cation  $[\text{Rh}_2(\text{CO})_2(\mu\text{-Cl})(\text{DPM})_2]^+$  was observed. No other rhodium-DPM species was detected.

### Data Collection

A crystal of the title compound was mounted and sealed in a glass capillary. Preliminary film data showed  $\bar{1}$  Laué symmetry and no systematic absences, consistent with the space groups  $P1$  and  $P\bar{1}$ . The centrosymmetric space group  $P\bar{1}$  was chosen and later verified by; (1) the successful refinement of the structure with acceptable positional parameters, thermal parameters and agreement indices, and (2) the location of all hydrogen atoms in electron density difference maps. Accurate cell parameters were obtained by a least-squares analysis of the setting angles of 12 carefully centered reflections chosen from diverse regions of reciprocal space ( $50^\circ < 2\theta < 70^\circ$ ,  $\text{CuK}\alpha$  radiation) and obtained by using a narrow X-ray source (see Table I for pertinent crystal data). A cell reduction<sup>102</sup> failed to show the presence of higher symmetry. The reduced cell is reported.

Intensity data were collected on a Picker four-circle automated diffractometer equipped with a scintillation counter and pulse-height analyzer, tuned to accept 90% of the  $\text{CuK}\alpha$  peak. Background counts were measured at both ends of the scan range with crystal and counter stationary.



Table 1. Summary of Crystal Data and Intensity Collection  
for  $[\text{Rh}_2(\text{CO})_2(\mu\text{-Cl})(\text{DPM})_2][\text{BF}_4]$

Compound	[Rh <sub>2</sub> (CO) <sub>2</sub> (μ-Cl)(DPM) <sub>2</sub> ][BF <sub>4</sub> ]																																												
Formula	C <sub>52</sub> H <sub>44</sub> B <sub>1</sub> Cl <sub>1</sub> F <sub>4</sub> O <sub>2</sub> P <sub>4</sub> Rh <sub>2</sub>																																												
Formula Weight	1152.89 amu																																												
Reduced Cell Parameters																																													
a	13.044 (1) Å																																												
b	14.962 (1) Å																																												
c	12.800 (1) Å																																												
α	96.20 (1) °																																												
β	92.56 (1) °																																												
γ	86.42 (1) °																																												
V	2476.8 Å <sup>3</sup>																																												
Z	2																																												
Density	1.545 g·cm <sup>-3</sup> (calc'd.) 1.547(5) g·cm <sup>-3</sup> (expt'l. by flotation)																																												
Space Group	C <sub>i</sub> <sup>1</sup> - P $\bar{1}$																																												
Crystal Dimensions	0.345 x 0.303 x 0.147 mm																																												
Crystal Volume	0.0129 mm <sup>3</sup>																																												
Crystal Faces (and distances from an arbitrary origin within the crystal (mm))	<table><tr><td>1</td><td>1</td><td>0</td><td>(0.145)</td></tr><tr><td>1</td><td><math>\bar{1}</math></td><td>0</td><td>(0.145)</td></tr><tr><td><math>\bar{1}</math></td><td>1</td><td>0</td><td>(0.155)</td></tr><tr><td><math>\bar{1}</math></td><td><math>\bar{1}</math></td><td>0</td><td>(0.195)</td></tr><tr><td>0</td><td>0</td><td>1</td><td>(0.075)</td></tr><tr><td>0</td><td>0</td><td><math>\bar{1}</math></td><td>(0.071)</td></tr><tr><td>0</td><td><math>\bar{1}</math></td><td>0</td><td>(0.222)</td></tr><tr><td>0</td><td>1</td><td><math>\bar{1}</math></td><td>(0.122)</td></tr><tr><td>0</td><td><math>\bar{1}</math></td><td>1</td><td>(0.162)</td></tr><tr><td><math>\bar{1}</math></td><td>0</td><td>1</td><td>(0.122)</td></tr><tr><td><math>\bar{1}</math></td><td>0</td><td>0</td><td>(0.208)</td></tr></table>	1	1	0	(0.145)	1	$\bar{1}$	0	(0.145)	$\bar{1}$	1	0	(0.155)	$\bar{1}$	$\bar{1}$	0	(0.195)	0	0	1	(0.075)	0	0	$\bar{1}$	(0.071)	0	$\bar{1}$	0	(0.222)	0	1	$\bar{1}$	(0.122)	0	$\bar{1}$	1	(0.162)	$\bar{1}$	0	1	(0.122)	$\bar{1}$	0	0	(0.208)
1	1	0	(0.145)																																										
1	$\bar{1}$	0	(0.145)																																										
$\bar{1}$	1	0	(0.155)																																										
$\bar{1}$	$\bar{1}$	0	(0.195)																																										
0	0	1	(0.075)																																										
0	0	$\bar{1}$	(0.071)																																										
0	$\bar{1}$	0	(0.222)																																										
0	1	$\bar{1}$	(0.122)																																										
0	$\bar{1}$	1	(0.162)																																										
$\bar{1}$	0	1	(0.122)																																										
$\bar{1}$	0	0	(0.208)																																										
Temperature	20 °C																																												
Radiation	CuKα (λ=1.540562 Å) filtered with 0.5 mil thick nickel foil																																												
μ	77.256 cm <sup>-1</sup>																																												
Range in Absorption	0.156 - 0.403																																												
Correction Factors																																													



Table 1, continued

Takeoff Angle	2.90°
Scan Speed	2° in 2θ/min
Scan Range	0.80° below $K_{\alpha 1}$ to 0.80° above $K_{\alpha 2}$
Background Counting Time	10s ( $3^\circ < 2\theta < 75^\circ$ ); 20s ( $75^\circ < 2\theta \leq 104^\circ$ ); 40s ( $104^\circ < 2\theta \leq 120^\circ$ )
2θ limits	$3^\circ < 2\theta \leq 120^\circ$
2θ units for centred reflections	$50^\circ < 2\theta \leq 70^\circ$
Final number of variables	298
Unique Data Collected	7416
Unique Data Used ( $F_o^2 \geq 3\sigma(F_o^2)$ )	5729
Error in observation of unit weight	1.792
R	0.046
$R_w$	0.064



Assuming approximate linearity of background, the intensity of the peak (I) is given by:

$$I = PK - (B_1 + B_2) t_p / t_B \quad (2)$$

where PK = peak count,  $t_p$  = peak scan time,  $t_B$  = the sum of the two background collection times and  $B_1$  and  $B_2$  are the background counts. Standard deviations in the intensity were computed from the relationship:

$$\sigma(I) = (PK + t^2 B_T + p^2 I^2)^{1/2} \quad (3)$$

where  $B_T = B_1 + B_2$ ,  $t = t_p / t_B$  and  $p$  is an ignorance factor used to account for machine uncertainty and to prevent unreasonably high weighting being applied to reflections of high intensity (a value of 0.05 was used for  $p$ ).<sup>103</sup> The intensities of three standard reflections were measured automatically every 100 reflections and four additional standards were measured three times a day in order to check crystal stability and centering. All standards remained constant to within 1.5% of the mean throughout the data collection.

The intensities of 7416 unique reflections ( $3^\circ \leq 2\theta \leq 120^\circ$ ) were measured using  $\text{CuK}\alpha$  radiation. Of these, 5729 were considered significantly above background ( $F^2 / \sigma(F^2) \geq 3.0$ , see Table 1) and were used in subsequent calculations. These observed data were reduced to structure factor amplitudes and standard deviations in the structure factors,  $\sigma(F)$ , by correction for Lorentz, polarization and absorption





effects.<sup>92-95</sup> Similar procedures of data collection and reduction were followed on all subsequent structures.

### Structure Solution and Refinement

A Patterson map<sup>104,105</sup> was computed between the limits  $0 \leq u \leq 1.0$ ,  $0 \leq v \leq 1.0$  and  $0 \leq w \leq 0.5$ . The Rh-Rh vectors are derived for two independent rhodium atoms in the space group  $P\bar{1}$  in Table 2. The origin peak corresponds to the sum of the vectors between every atom and itself, in the unit cell. Therefore the magnitude of the origin vector is roughly proportional to:  $\sum_i z_i^2$ , summed over the contents of the unit cell,  $= (4 \times 45^2 + 2 \times 17^2 + 8 \times 15^2 + 8 \times 9^2 + 4 \times 8^2 + 104 \times 6^2 + 2 \times 5^2 + 88 \times 1^2) = 15264$ . In the Fourier program used to calculate the vector map, the origin peak is normalized to 1000. Therefore assuming comparable thermal parameters for all atoms one expects the Rh(1)-Rh(2) vectors which are doubly weighted (see Table 2) to have an approximate, normalized value of 265 (ie.  $\frac{2 \times 45^2}{15264} \times 1000$ ), and the Rh(1)-Rh(1) and Rh(2)-Rh(2) vectors, which are singly weighted to have an intensity of 133 above background. Viewing the Patterson map, the nine most intense peaks of which, are summarized in Table 3, it is obvious that three vectors, instead of the anticipated two, are observed with weights comparable to those expected for the Rh(1)-Rh(2) vectors. One of these three, the second peak listed, is actually a result of Rh-P vector build-up. Generally the DPM ligands are mutually trans



Table 2. Derivation of the Rh-Rh Vectors for the Space Group  $p\bar{1}$ 

	$x_1, y_1, z_1^a$	$\bar{x}_1, \bar{y}_1, \bar{z}_1$	$x_2, y_2, z_2$	$\bar{x}_2, \bar{y}_2, \bar{z}_2$
$x_1, y_1, z_1$	$0, 0, 0$	$2\bar{x}_1, 2\bar{y}_1, 2\bar{z}_1$	$-(x_1 - x_2)$ $-(y_1 - y_2)$ $-(z_1 - z_2)$	$-(x_1 + x_2)$ $-(y_1 + y_2)$ $-(z_1 + z_2)$
$\bar{x}_1, \bar{y}_1, \bar{z}_1$	$2x_1, 2y_1, 2z_1$	$0, 0, 0$	$x_1 + x_2$ $y_1 + y_2$ $z_1 + z_2$	$x_1 - x_2$ $y_1 - y_2$ $z_1 - z_2$
$x_2, y_2, z_2$	$x_1 - x_2$ $y_1 - y_2$ $z_1 - z_2$	$-(x_1 + x_2)$ $-(y_1 + y_2)$ $-(z_1 + z_2)$	$0, 0, 0$	$2\bar{x}_2, 2\bar{y}_2, 2\bar{z}_2$
$\bar{x}_2, \bar{y}_2, \bar{z}_2$	$x_1 + x_2$ $y_1 + y_2$ $z_1 + z_2$	$-(x_1 - x_2)$ $-(y_1 - y_2)$ $-(z_1 - z_2)$	$2x_2, 2y_2, 2z_2$	$0, 0, 0$

Vector	Weight
$0, 0, 0$	4
$x_1 + x_2, y_1 + y_2, z_1 + z_2$	2
$-(x_1 + x_2), -(y_1 + y_2), -(z_1 + z_2)$	2
$x_1 - x_2, y_1 - y_2, z_1 - z_2$	2
$-(x_1 - x_2), -(y_1 - y_2), -(z_1 - z_2)$	2
$2\bar{x}_1, 2\bar{y}_1, 2\bar{z}_1$	1
$2x_1, 2y_1, 2z_1$	1
$2x_2, 2y_2, 2z_2$	1
$2\bar{x}_2, 2\bar{y}_2, 2\bar{z}_2$	1

<sup>a</sup> $(x_1, y_1, z_1)$  and  $(x_2, y_2, z_2)$  are the coordinates of Rh(1) and Rh(2) respectively.

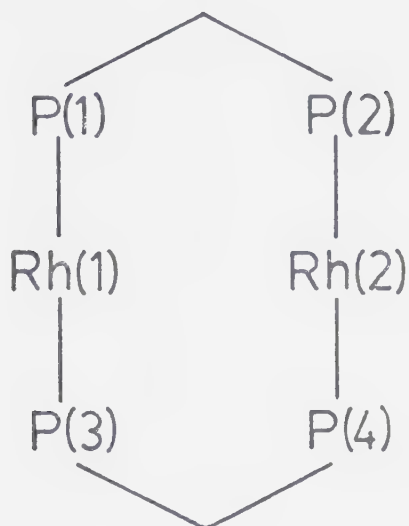


Table 3: Assignment of the Most Intense Patterson  
Map Vectors

No.	u	v	w	Relative Weight	Assignment
1	0.640	0.420	0.192	357	$(x_1+x_2, y_1+y_2, z_1+z_2)$
2	0.960	0.030	0.192	339	Rh-P vector build-up
3	0.160	0.120	0.064	290	$(x_1-x_2, y_1-y_2, z_1-z_2)$
4	0.120	0.150	0.224	190	Rh-P vector build-up
5	0.680	0.390	0.032	187	Rh-P vector build-up
6	0.800	0.540	0.256	180	$(2x_1, 2y_1, 2z_1)$
7	0.600	0.420	0.384	175	Rh-P vector build-up
8	0.000	0.180	0.000	152	Rh(1)-Cl and Rh(1)-O
9	0.480	0.270	0.160	148	$(2x_2, 2y_2, 2z_2)$



and the Rh-P framework is approximately planar as shown below:



The Rh(1)-P(1), Rh(2)-P(2), P(3)-Rh(1) and P(4)-Rh(2) vectors are therefore almost coincident, yielding a Rh-P vector build-up of approximate weight 353 ( $\frac{2 \times 4 \times 15 \times 45}{15264} \times 1000$ ). Similarly other vector build-ups may also occur. This complication in solving the Patterson maps continued throughout this study, however it is readily overcome by using image seeking techniques and comparing vector lengths. Typically Rh-P vectors are *ca.* 2.35 Å whereas the Rh(1)-Rh(2) vectors are in the range 2.7 - 3.4 Å. Applying these methods it became obvious that the first peak was associated with the Rh(1)-Rh(2) vector,  $(x_1+x_2, y_1+y_2, z_1+z_2)$  and the third peak with the Rh(1)-Rh(2) vector  $(x_1-x_2, y_1-y_2, z_1-z_2)$  with the latter having a distance from the origin of *ca.* 2.87 Å (the approximate metal-metal separation in the





dimer). The second peak which is approximately  $2.52 \text{ \AA}$  from the (1.0,0.0,0.0) origin is due to Rh-P vector build-up. The positions of the rhodium atoms are then calculated as Rh(1) (0.40,0.27,0.13) and Rh(2) (0.23,0.14,0.07). The sixth peak then corresponds to the  $(2x_1, 2y_1, 2z_1)$  vector and the ninth peak to the  $(2x_2, 2y_2, 2z_2)$  vector, with the intervening peaks resulting from vector build-up as indicated in Table 3.

A full-matrix, least-squares refinement based on the two rhodium atom positions converged in two cycles to  $R=0.46$  and  $R_w=0.56$ . These  $R$  factors as calculated in the least-squares program are defined as:

$$R = \Sigma ||F_O| - |F_C|| / \Sigma |F_O| \quad (4)$$

and

$$R_w = \{ \Sigma w (|F_O| - |F_C|)^2 / \Sigma w |F_O|^2 \}^{1/2} \quad (5)$$

where  $|F_O|$  and  $|F_C|$  are the observed and calculated structure amplitudes, respectively, and  $w$ , the weighting factor, is defined as  $w = 1/\sigma^2(F)$ . The function minimized during the least square refinement was  $\Sigma w (|F_O| - |F_C|)^2$ . Structure factors were calculated using the atomic scattering factors taken from Cromer and Waber's<sup>106</sup> tabulation for all atoms except hydrogen for which the values of Stewart *et al.*<sup>107</sup> were used. Anomalous dispersion corrections,<sup>108</sup> both real and imaginary<sup>109</sup> were applied to  $F_C$ .



An electron density difference map, phased on the two rhodium atom positions, yielded the location of the phosphorus and chlorine atoms. A subsequent least-squares refinement and electron density difference map calculated using the rhodium, phosphorus and chlorine atom positions, revealed the location of all other non-hydrogen atoms within the cation. The carbon atoms of the phenyl rings were refined in all least-squares calculations as rigid groups having  $D_{6h}$  symmetry and C-C distances of  $1.392 \text{ \AA}$ .

Although the infrared spectrum indicated that the present complex had crystallized as the  $\text{BF}_4^-$  salt, our initial unwillingness to accept the apparent transformation of  $\text{PF}_6^-$  and  $\text{BPh}_4^-$  into  $\text{BF}_4^-$  together with the pseudo octahedral coordination about the central atom in the electron density difference map, led us to attempt refinement of the electron density about the l(c) and l(f) inversion centres as  $\text{PF}_6^-$  anions. However, these refinement attempts proved unsuccessful, even considering disorder of the groups. The thermal parameters for both phosphorus atoms exceeded  $30 \text{ \AA}^2$  and chemically unreasonable P-F distances resulted. A closer inspection of the electron density difference map revealed that there were eight peaks about both sets of inversion centres and not just the six originally located. The placement of these eight peaks corresponded to superimposed, inversion related, tetrahedral  $\text{BF}_4^-$  groups. Furthermore, the central peaks were more consistent with boron than phosphorus, having intensities in the electron density dif-



ference map ( $4.7$  and  $3.3 \text{ e}/\text{\AA}^3$ ) comparable to the half-weighted fluorine peaks ( $3.7$ - $1.8 \text{ e}/\text{\AA}^3$ ). Refinement of this model as inversion disordered  $\text{BF}_4^-$  groups proceeded well, resulting in reasonable bond lengths, thermal parameters and well defined tetrahedral geometries about the central boron atom.

The data were corrected for the effects of absorption by Gaussian integration. All non-group atoms excluding hydrogen were refined with anisotropic thermal parameters, where the form of the thermal ellipsoid used was  $\exp[-(\beta_{11}h^2 + \beta_{22}k^2 + \beta_{33}l^2 + 2\beta_{12}hk + 2\beta_{13}hl + 2\beta_{23}kl)]$ .

An electron density difference map at this stage revealed the location of all hydrogen atoms in the structure. These atoms were included as fixed contributions in calculating the structure factors and were not refined. Their idealized positions were calculated from the geometries of their attached carbon atoms by using C-H distances of  $0.95 \text{ \AA}$ . Hydrogen atoms were assigned isotropic thermal parameters of  $1 \text{ \AA}^2$  greater than those of their attached carbon atom or  $1 \text{ \AA}^2$  greater than the equivalent isotropic B when the carbon atom was refined anisotropically. Throughout this study hydrogen atoms were always handled in a similar manner.

The final model with 298 parameters varied converged to  $R = 0.046$  and  $R_w = 0.064$ . In the final electron density difference map all of the highest 20 peaks were in the vicinity of the phenyl rings ( $0.66$ - $0.41 \text{ e}/\text{\AA}^3$ ), with smaller



residuals in the areas of the  $\text{BF}_4^-$  anions. A typical carbon atom on an earlier difference map had an electron density of about  $5.0 \text{ e}/\text{\AA}^3$ .

The programs used in the solution and refinement of structure and presentation of data are listed briefly in Appendix I.

## Results

The final positional and thermal parameters for the nongroup and group atoms are given in Tables 4 and 5, respectively. The idealized positional and thermal parameters for the hydrogen atoms are given in Table 6. Least-squares plane calculations are recorded in Table 7 and selected bond lengths and angles are shown in Tables 8 and 9, respectively. A listing of the observed and calculated structure amplitudes is available.<sup>110</sup>

The unit cell of  $[\text{Rh}_2(\text{CO})_2(\mu\text{-Cl})(\text{DPM})_2][\text{BF}_4]$  is shown in Figure 4. The crystallographic *b* axis is horizontal to the right, the *c* axis runs from top to bottom and the *a* axis goes into the page. With the exception of the methylene hydrogen atoms, which are drawn artificially small for clarity of the drawing, 20% thermal ellipsoids are used on this and all subsequent drawings unless noted otherwise. Only one set of the inversion disordered F atoms for each  $\text{BF}_4^-$  group is included. Figure 5 presents a perspective view of the  $[\text{Rh}_2(\text{CO})_2(\mu\text{-Cl})(\text{DPM})_2]^+$  cation, including the numbering scheme. The numbering of the phenyl carbon atoms





starts at the carbon bound to the phosphorus atom and increases sequentially around the ring. The inner coordination sphere of the  $[\text{Rh}_2(\text{CO})_2(\mu\text{-Cl})(\text{DPM})_2]^+$  cation is shown in Figure 6 along with some relevant bond lengths. In this figure 50% thermal ellipsoids are used. The two independent tetrafluoroborate anions are shown in Figure 7; again only one of each of the disorder sets of F atoms is included.



TABLE 4. Positional and Thermal Parameters For The Nongroup Atoms of  $[\text{Rh}_2(\text{CO})_2(\mu\text{-Cl})(\text{DPM})_2][\text{BF}_4]$ .

Atom	a			b			z	U11	U22	U33	U12	U13	U23
	x	y											
Rh(1)	0.40834(4)	0.26969(3)	0.12814(3)	4.39(3)	3.55(3)	2.97(2)	-0.60(2)	0.40(2)	0.16(2)				
Rh(2)	0.22036(3)	0.13772(3)	0.07315(3)	3.50(3)	4.48(3)	2.83(2)	-0.32(2)	0.20(2)	0.02(2)				
C1	0.4043(1)	0.1092(1)	0.1290(1)	4.06(8)	3.84(8)	4.00(7)	0.05(6)	-0.07(6)	0.38(6)				
P(1)	0.3529(1)	0.2916(1)	0.2999(1)	4.30(9)	3.56(8)	2.98(7)	-0.28(7)	0.24(6)	0.20(6)				
P(2)	0.1855(1)	0.1546(1)	0.2482(1)	3.84(8)	3.97(9)	3.02(7)	-0.31(7)	0.19(6)	0.37(6)				
P(3)	0.4513(1)	0.2486(1)	-0.0471(1)	3.76(8)	4.04(9)	3.41(8)	-0.14(7)	0.54(6)	0.41(7)				
P(4)	0.2316(1)	0.1132(1)	-0.0994(1)	3.56(8)	4.34(9)	3.03(7)	-0.08(7)	0.31(6)	-0.02(6)				
O(1)	0.1525(5)	0.4614(4)	0.1349(5)	12.0(5)	4.9(3)	7.0(4)	-2.7(3)	1.0(4)	0.4(3)				
O(2)	0.0117(4)	0.1436(5)	0.0009(5)	3.3(3)	16.0(7)	6.7(4)	-0.9(3)	-0.5(3)	0.4(4)				
C(1)	0.4330(6)	0.3875(5)	0.1318(5)	6.8(5)	4.8(4)	3.5(3)	-1.4(4)	1.0(3)	-0.2(3)				
C(2)	0.0363(5)	0.1438(6)	0.0295(5)	4.6(4)	9.5(6)	3.1(3)	-0.5(4)	1.1(3)	0.1(4)				
C(3)	0.2026(5)	0.1943(4)	0.3379(4)	4.3(3)	3.3(3)	2.7(3)	-0.6(3)	0.2(3)	0.3(2)				
C(4)	0.4151(5)	0.1398(4)	-0.1155(5)	3.9(3)	4.4(4)	3.1(3)	-0.5(3)	0.4(3)	0.1(3)				
P(1)	1/2	0	1/2	8(1)	6(1)	24(4)	1(1)	-5(2)	5(2)				
P(2)	0	1/2	0	5.5(8)	8(1)	4.4(6)	-3.8(7)	1.8(6)	-1.4(6)				
F(1)	0.4693(8)	0.0401(7)	0.400(1)	7.8(7)	7.0(7)	16(1)	1.2(6)	0.5(8)	3.8(7)				
F(2)	0.416(1)	-0.0482(9)	0.518(1)	11(1)	9.2(9)	15(1)	-0.1(8)	-1.5(9)	4.1(8)				
F(3)	0.585(1)	-0.057(2)	0.471(2)	7.4(9)	20(2)	25(2)	1(1)	-2(1)	10(2)				
F(4)	0.504(3)	0.071(2)	0.590(2)	26(3)	34(4)	26(4)	-11(3)	-8(3)	21(3)				
F(5)	-0.021(3)	0.516(2)	0.101(1)	17(2)	21(2)	7(1)	4(2)	2(1)	1(1)				
F(6)	-0.101(1)	0.543(2)	-0.036(1)	10(1)	28(2)	10(1)	4(1)	-0.3(9)	2(1)				
F(7)	-0.015(3)	0.420(2)	-0.032(3)	24(3)	30(3)	22(3)	-13(3)	11(2)	-11(3)				
F(8)	0.062(2)	0.536(4)	-0.036(4)	14(2)	40(5)	23(3)	-11(3)	5(3)	8(4)				

a Estimated standard deviations in the least significant figure(s) are given in parentheses in this and all subsequent tables.

b The form of the thermal ellipsoid is:  $\exp[-2\pi^2(a^*U_{11}h^2+b^*U_{22}k^2+c^*U_{33}l^2+2a^*b^*U_{12}hk+2a^*c^*U_{13}hl+2b^*c^*U_{23}kl)]$ . The quantities given in the table are the thermal coefficients  $\times 10^3$ .



TABLE 5. Derived Parameters For the Rigid Group Atoms of [Rh2(CO)2(mu-C1)(DPM)2][BF4].

Atom	X	Y	Z	B(A <sup>2</sup> )	Atom	X	Y	Z	B(A <sup>2</sup> )
C(11)	0.4583(4)	0.3097(3)	0.3990(3)	3.2(1)	C(51)	0.3953(4)	0.3319(3)	-0.1297(5)	3.1(1)
C(12)	0.5109(4)	0.3878(3)	0.3988(4)	5.1(2)	C(52)	0.3195(4)	0.3956(3)	-0.0927(3)	3.7(1)
C(13)	0.5950(4)	0.4031(3)	0.4678(4)	6.1(2)	C(53)	0.2792(3)	0.4599(3)	-0.1566(4)	4.7(2)
C(14)	0.6266(4)	0.3403(3)	0.5370(3)	5.2(2)	C(54)	0.3146(4)	0.4603(3)	-0.2575(5)	4.8(2)
C(15)	0.5740(4)	0.2622(3)	0.5373(4)	4.7(2)	C(55)	0.3904(4)	0.3966(3)	-0.2945(3)	4.9(2)
C(16)	0.4893(4)	0.2463(3)	0.4683(4)	4.0(1)	C(56)	0.4308(3)	0.3324(3)	-0.2306(4)	4.1(1)
C(21)	0.2626(4)	0.3859(3)	0.3353(5)	3.1(1)	C(61)	0.5878(3)	0.2488(4)	-0.0706(3)	3.4(1)
C(22)	0.2239(4)	0.3376(3)	0.4394(5)	4.0(1)	C(62)	0.6338(4)	0.3306(3)	-0.0484(4)	5.0(2)
C(23)	0.1575(5)	0.4677(3)	0.4596(3)	4.9(2)	C(63)	0.7376(4)	0.3360(3)	-0.0662(4)	5.8(2)
C(24)	0.1193(4)	0.5260(3)	0.3974(5)	5.3(2)	C(64)	0.7955(3)	0.2596(4)	-0.1063(3)	6.3(2)
C(25)	0.1537(4)	0.5143(3)	0.2949(5)	5.4(2)	C(65)	0.7495(4)	0.1778(3)	-0.1285(4)	7.5(2)
C(26)	0.2251(5)	0.4443(3)	0.2647(3)	4.4(1)	C(66)	0.6457(4)	0.1725(3)	-0.1106(4)	5.5(2)
C(31)	0.1530(4)	0.0436(3)	0.2949(4)	3.1(1)	C(71)	0.2819(4)	-0.0054(3)	-0.1488(5)	3.6(1)
C(32)	0.0703(4)	0.0085(3)	0.2509(4)	4.7(2)	C(72)	0.3512(4)	-0.0443(3)	-0.2225(3)	4.9(2)
C(33)	0.0407(3)	-0.0706(3)	0.2858(3)	5.5(2)	C(73)	0.3497(4)	-0.1357(4)	-0.2571(3)	6.4(2)
C(34)	0.0985(4)	-0.1097(3)	0.3647(4)	6.7(2)	C(74)	0.2789(4)	-0.1882(3)	-0.2180(5)	6.5(2)
C(35)	0.1852(4)	-0.0696(3)	0.4087(4)	6.5(2)	C(75)	0.2096(4)	-0.1493(3)	-0.1443(3)	6.9(2)
C(36)	0.2159(3)	0.0095(3)	0.3738(3)	4.6(2)	C(76)	0.2110(4)	-0.0579(4)	-0.1097(3)	5.3(2)
C(41)	0.0735(5)	0.2272(3)	0.2846(3)	3.2(1)	C(81)	0.2112(4)	0.1735(3)	-0.1989(3)	3.2(1)
C(42)	0.0435(6)	0.2979(3)	0.2256(3)	4.2(1)	C(82)	0.2215(4)	0.1442(3)	-0.3051(5)	4.5(1)
C(43)	-0.0436(4)	0.3531(3)	0.2515(5)	5.2(2)	C(83)	0.1700(5)	0.1919(3)	-0.3811(3)	5.5(2)
C(44)	-0.4006(5)	0.3375(3)	0.3364(3)	5.4(2)	C(84)	0.1082(4)	0.2687(3)	-0.3509(3)	5.5(2)
C(45)	-0.0705(6)	0.2668(3)	0.3954(3)	5.0(2)	C(85)	0.0979(4)	0.2979(3)	-0.2447(5)	5.2(2)
C(46)	0.0165(4)	0.2116(3)	0.3695(5)	4.0(1)	C(86)	0.1494(5)	0.2503(3)	-0.1687(3)	4.1(1)

## Rigid Group Parameters

	a		b	
	Xc	Yc	Zc	
Ring1	0.5425(2)	0.3250(2)	0.4680(3)	Delta
Ring2	0.1913(2)	0.4560(2)	0.3671(3)	0.449(3)
Ring3	0.1283(3)	-0.0306(2)	0.3298(3)	2.443(3)
Ring4	-0.0135(2)	0.2823(2)	0.3105(2)	3.671(3)
Ring5	0.3550(2)	0.3961(2)	-0.1936(2)	-0.699(3)
Ring6	0.6916(3)	0.2542(3)	-0.0884(3)	2.424(3)
Ring7	0.2804(3)	-0.0968(2)	-0.1834(3)	3.350(4)
Ring8	0.1597(2)	0.2211(2)	-0.2749(3)	3.311(3)
a				-0.653(3)
				1.719(4)
				6.049(3)
				1.338(4)
				2.445(4)
				0.826(4)
				1.212(4)
				0.241(3)
				0.726(4)
				3.792(3)

a Xc, Yc and Zc are the fractional coordinates of the centroid of the rigid group.

b The rigid group orientation angles Delta, Epsilon and Eta (radians) are the angles by which the rigid body is rotated with respect to a set of axes X, Y and Z. The origin is the centre of the ring; X is parallel to a\*, Z is parallel to c and Y is parallel to the line defined by the intersection of the plane containing a\* and b\* with the plane containing b and c.



TABLE 6. Idealized Positional and Thermal Parameters For the Hydrogen Atoms of [Rh2(CO)2(mu-Cl)(DPM)2][BF4].

Atom	x	y	z	B(A <sup>2</sup> )	Atom	x	y	z	B(A <sup>2</sup> )
H(1C3)	0.2662	0.2099	0.4060	3.70	H(45)	-0.1094	0.2562	0.4534	6.03
H(2C3)	0.3434	0.1462	0.3411	3.70	H(46)	0.0370	0.1634	0.4098	5.02
H(1C4)	0.4592	0.0936	-0.0895	4.04	H(52)	0.2953	0.3953	-0.0238	4.72
H(2C4)	0.4253	0.1405	-0.1884	4.04	H(53)	0.2274	0.5034	-0.1313	5.71
H(12)	0.4893	0.4308	0.3517	6.07	H(54)	0.2871	0.5042	-0.3011	5.83
H(13)	0.6308	0.4565	0.4678	7.09	H(55)	0.4145	0.3970	-0.3634	5.88
H(14)	0.6840	0.3508	0.5842	6.22	H(56)	0.4824	0.2889	-0.2559	5.08
H(15)	0.5955	0.2193	0.5846	5.75	H(62)	0.5944	0.3827	-0.0213	6.05
H(16)	0.4540	0.1936	0.4685	4.97	H(63)	0.7691	0.3917	-0.0512	6.79
H(22)	0.2545	0.3578	0.4887	4.97	H(64)	0.8664	0.2632	-0.1184	7.32
H(23)	0.1345	0.4757	0.5395	5.86	H(65)	0.7890	0.1257	-0.1558	8.52
H(24)	0.0712	0.5738	0.4180	6.34	H(66)	0.6144	0.1166	-0.1258	6.53
H(25)	0.1281	0.5541	0.2456	6.44	H(72)	0.3994	-0.0084	-0.2493	5.92
H(26)	0.2482	0.4362	0.1947	5.42	H(73)	0.3970	-0.1621	-0.3075	7.40
H(32)	0.0208	0.0352	0.1970	5.72	H(74)	0.2779	-0.2505	-0.2417	7.47
H(33)	-0.0193	-0.0978	0.2558	6.52	H(75)	0.1613	-0.1851	-0.1176	7.87
H(34)	0.0781	-0.1635	0.3887	7.65	H(76)	0.1638	-0.0314	-0.0594	6.34
H(35)	0.2255	-0.0962	0.4628	7.53	H(82)	0.2636	0.0918	-0.3257	5.54
H(36)	0.2756	0.0368	0.4040	5.62	H(83)	0.1769	0.1720	-0.4536	6.50
H(42)	0.0824	0.3085	0.1676	5.19	H(84)	0.0729	0.3013	-0.4027	6.52
H(43)	-0.0640	0.4013	0.2112	6.24	H(85)	0.0556	0.3504	-0.2240	6.16
H(44)	-0.1600	0.3751	0.3541	6.39	H(86)	0.1424	0.2702	-0.0962	5.09





Table 7. Least-Squares Plane Calculations

Plane no.		Equation <sup>a</sup>				
1		$-0.9474X+0.0789Y-0.3102Z+5.4077 = 0.0$				
2		$-0.2057X-0.9781Y-0.0322Z+2.5719 = 0.0$				
3		$-0.5694X+0.7959Y-0.2055Z+0.3962 = 0.0$				
4		$-0.5653X+0.7961Y-0.2159Z+0.3913 = 0.0$				
5		$0.2996Z-0.0306Y-0.9536Z+0.0220 = 0.0$				

Atom		Deviations from the Planes (Å) <sup>a</sup>				
		Plane no.				
		1	2	3	4	5
Rh(1)		-0.0093(5)				
Rh(2)			-0.0077(5)	-0.0058(5)	-0.0043(5)	-0.0002(4)
Cl		-0.0092(14)	0.0042(14)	0.0057(5)	0.0042(5)	-0.0001(4)
P(1)		0.0668(16)				0.0012(14)
P(2)			0.0384(16)	.0696(15)		
P(3)				- .0691(15)		
P(4)		0.0684(15)				
O(1)		-0.522(7) <sup>b</sup>	0.0393(16)		0.0519(16)	0.056(6) <sup>b</sup>
O(2)			0.417(8) <sup>b</sup>		-0.0517(16)	0.031(6) <sup>b</sup>
C(1)		-0.293(7)				0.031(6)
C(2)			0.214(8)	-0.708(6) <sup>b</sup>		0.014(6)
C(3)					-0.678(6) <sup>b</sup>	
C(4)						

Dihedral Angle Between Planes		
Plane A	Plane B	Angle(deg)
1	2	82.66
3	5	89.95
4	5	89.31

<sup>a</sup>X, Y, and Z are the orthogonal coordinates (Å) with X along the a axis, Y in the (a-b) plane and Z along c\*-axis.

<sup>b</sup>Not included in least squares plane calculation.



Table 8: Selected Distances (Å) in  $[\text{Rh}_2(\text{CO})_2(\mu\text{-Cl})(\text{DPM})_2][\text{BF}_4]$ 

Bond Distances					
Rh(1)-Cl	2.406(2)		P(1)-C(11)	1.832(4)	1.822(5)
Rh(2)-Cl	2.380(2)		P(1)-C(21)	1.825(3)	
Rh(1)-C(1)	1.807(7)		P(2)-C(31)	1.821(4)	
Rh(2)-C(2)	1.799(7)		P(2)-C(41)	1.823(3)	
Rh(1)-P(1)	2.324(2)	2.321(2) <sup>a</sup>	P(3)-C(51)	1.819(3)	
Rh(1)-P(3)	2.320(2)		P(3)-C(61)	1.819(4)	
Rh(2)-P(2)	2.319(2)		P(4)-C(71)	1.818(4)	
Rh(2)-P(4)	2.322(2)		P(4)-C(81)	1.822(4)	
C(1)-O(1)	1.184(8)		B(1)-F(1)	1.49(1)	1.38(10)
C(2)-O(2)	1.202(9)		B(1)-F(2)	1.39(1)	
P(1)-C(3)	1.825(6)	1.836(8)	B(1)-F(3)	1.39(2)	
P(2)-C(3)	1.843(6)		B(1)-F(4)	1.47(4)	
P(3)-C(4)	1.841(6)		B(2)-F(5)	1.33(2)	
P(4)-C(4)	1.836(6)		B(2)-F(6)	1.51(1)	
			B(2)-F(7)	1.25(3)	
			B(2)-F(8)	1.24(3)	

## Nonbonded Distances

Rh(1)-Rh(2)	3.1520(8)	Cl-H1C4	2.90
P(1)-P(2)	3.088(2)	C(1)-H(52)	2.63
P(3)-P(4)	3.097(2)	C(2)-H(86)	2.72
O(1)-H(26)	2.86	F(1)-H(16)	2.37
O(1)-H(12)	2.87	F(1)-H(2)	2.37
O(1)-H(62)	2.89	F(3)-H(16)	2.35
O(2)-H(75)	2.76	F(3)-H(36)	2.38
C(1)-H(26)	2.61	H(36)-H(2)	2.15
Cl-H2C3	2.85	H(66)-H(3)	2.15

<sup>a</sup>For averaged quantities, the estimated standard deviation is the larger of an individual standard deviation or the standard deviation of a single observation as calculated from the mean.



Table 9: Selected Angles (Deg) in  $[\text{Rh}_2(\text{CO})_2(\mu\text{-Cl})(\text{DPM})_2][\text{BF}_4]$ 

## Bond Angles

Cl-Rh(1)-C(1)	170.9(2)	C(11)-P(1)-C(21)	102.2(2)
Cl-Rh(1)-P(1)	90.44(5)	C(31)-P(2)-C(41)	102.4(2)
Cl-Rh(1)-P(3)	89.68(5)	C(51)-P(3)-C(61)	102.6(2)
C(1)-Rh(1)-P(1)	91.0(2)	C(71)-P(4)-C(81)	105.8(2)
C(1)-Rh(1)-P(3)	89.5(2)	P(1)-C(3)-P(2)	114.7(3)
P(1)-Rh(1)-P(3)	176.20(6)	P(3)-C(4)-P(4)	114.7(3)
Cl-Rh(2)-C(2)	172.6(3)	P(1)-C(11)-C(12)	117.0(3)
Cl-Rh(2)-P(2)	88.59(5)	P(1)-C(11)-C(16)	122.8(3)
Cl-Rh(2)-P(4)	88.28(5)	P(1)-C(21)-C(22)	118.5(2)
C(2)-Rh(2)-P(2)	91.7(2)	P(1)-C(21)-C(26)	121.5(2)
C(2)-Rh(2)-P(4)	91.1(2)	P(2)-C(31)-C(32)	116.5(3)
P(2)-Rh(2)-P(4)	176.12(6)	P(2)-C(31)-C(36)	123.4(3)
Rh(1)-Cl-Rh(2)	82.38(5)	P(2)-C(41)-C(42)	119.4(2)
Rh(1)-C(1)-O(1)	177.4(7)	P(2)-C(41)-C(46)	120.6(2)
Rh(2)-C(2)-O(2)	177.0(8)	P(3)-C(51)-C(52)	121.0(2)
Rh(1)-P(1)-C(3)	112.6(2)	P(3)-C(51)-C(56)	119.0(2)
Rh(2)-P(2)-C(3)	112.8(2)	P(3)-C(61)-C(62)	116.9(3)
Rh(1)-P(3)-C(4)	113.6(2)	P(3)-C(61)-C(66)	123.0(3)
Rh(2)-P(4)-C(4)	113.8(2)	P(4)-C(71)-C(72)	121.9(3)
Rh(1)-P(1)-C(11)	113.9(2)	P(4)-C(71)-C(76)	118.1(3)
Rh(1)-P(1)-C(21)	118.7(1)	P(4)-C(81)-C(82)	120.1(3)
Rh(2)-P(2)-C(31)	112.6(2)	P(4)-C(86)-C(86)	119.9(3)
Rh(2)-P(2)-C(41)	117.8(1)	F(1)-B(1)-F(2)	103.5(7)
Rh(1)-P(3)-C(51)	115.9(1)	F(1)-B(1)-F(3)	102.8(9)
Rh(1)-P(3)-C(61)	115.5(2)	F(1)-B(1)-F(4)	111 (1)
Rh(2)-P(4)-C(71)	111.5(2)	F(2)-B(1)-F(3)	111.6(9)
Rh(2)-P(4)-C(81)	118.8(2)	F(2)-B(1)-F(4)	105 (1)
C(3)-P(1)-C(11)	103.9(2)	F(3)-B(1)-F(4)	122 (1)
C(3)-P(1)-C(21)	103.8(2)	F(5)-B(2)-F(6)	93 (2)
C(3)-P(2)-C(31)	103.5(2)	F(5)-B(2)-F(7)	110 (1)
C(3)-P(2)-C(41)	106.2(2)	F(5)-B(2)-F(8)	122 (2)
C(4)-P(3)-C(51)	104.5(2)	F(6)-B(2)-F(7)	99 (2)
C(4)-P(3)-C(61)	103.0(2)	F(6)-B(2)-F(8)	106 (2)
C(4)-P(4)-C(71)	102.5(3)	F(7)-B(2)-F(8)	120 (2)
C(4)-P(4)-C(81)	102.8(2)		

## Torsion Angles

P(1)-Rh(1)-Rh(2)-P(2)	3.70(5)	C(2)-Rh(2)-P(4)-C(71)	85.3(3)
P(1)-Rh(1)-Rh(2)-P(4)	179.84(6)	C(2)-Rh(2)-P(4)-C(81)	-38.1(3)
P(2)-Rh(2)-Rh(1)-P(3)	-178.90(6)	C(11)-P(1)-P(2)-C(31)	8.5(3)
P(3)-Rh(1)-Rh(2)-P(4)	-2.76(6)	C(11)-P(1)-P(3)-C(61)	-1.4(2)
C(1)-Rh(1)-P(1)-C(11)	72.9(3)	C(21)-P(1)-P(2)-C(41)	3.0(2)
C(1)-Rh(1)-P(1)-C(21)	-47.6(3)	C(21)-P(1)-P(3)-C(51)	-1.8(2)
C(1)-Rh(1)-P(3)-C(51)	45.9(3)	C(31)-P(2)-P(4)-C(71)	1.2(2)
C(1)-Rh(1)-P(3)-C(61)	-74.2(3)	C(41)-P(2)-P(4)-C(81)	-3.4(3)
C(2)-Rh(2)-P(2)-C(31)	-84.0(3)	C(51)-P(3)-P(4)-C(81)	-5.6(2)
C(2)-Rh(2)-P(2)-C(41)	34.9(3)	C(61)-P(3)-P(4)-C(71)	-11.3(4)



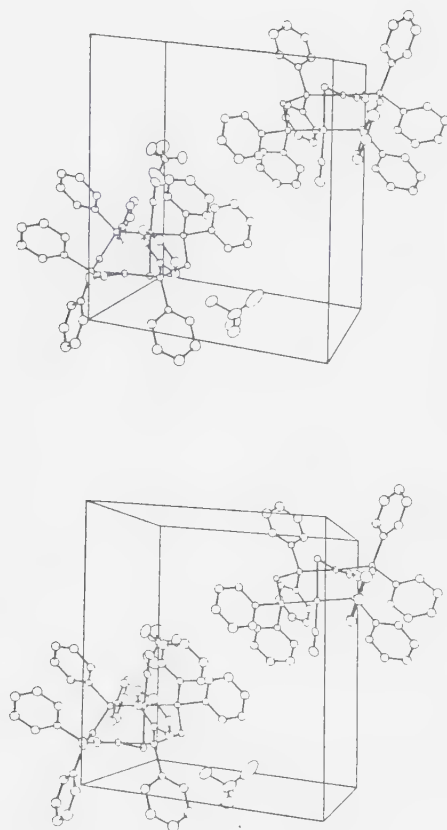


Figure 4. Cell Packing Diagram of  $[\text{Rh}_2(\text{CO})_2(\mu\text{-Cl})(\text{DPM})_2]\cdot[\text{BF}_4]_4$ .





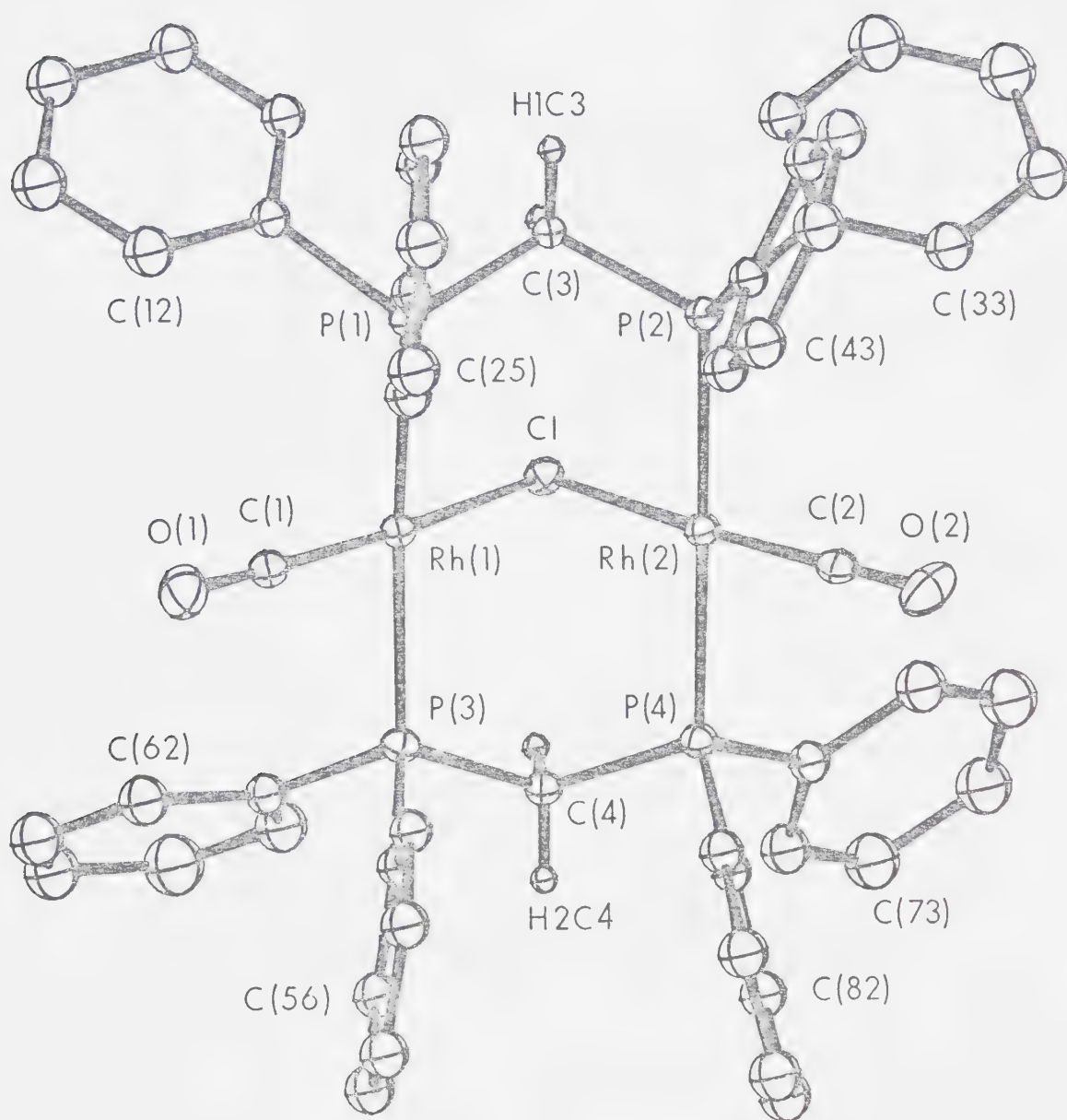


Figure 5. A Perspective View of the  $[\text{Rh}_2(\text{CO})_2(\mu\text{-Cl})(\text{DPM})_2]^+$  Cation.



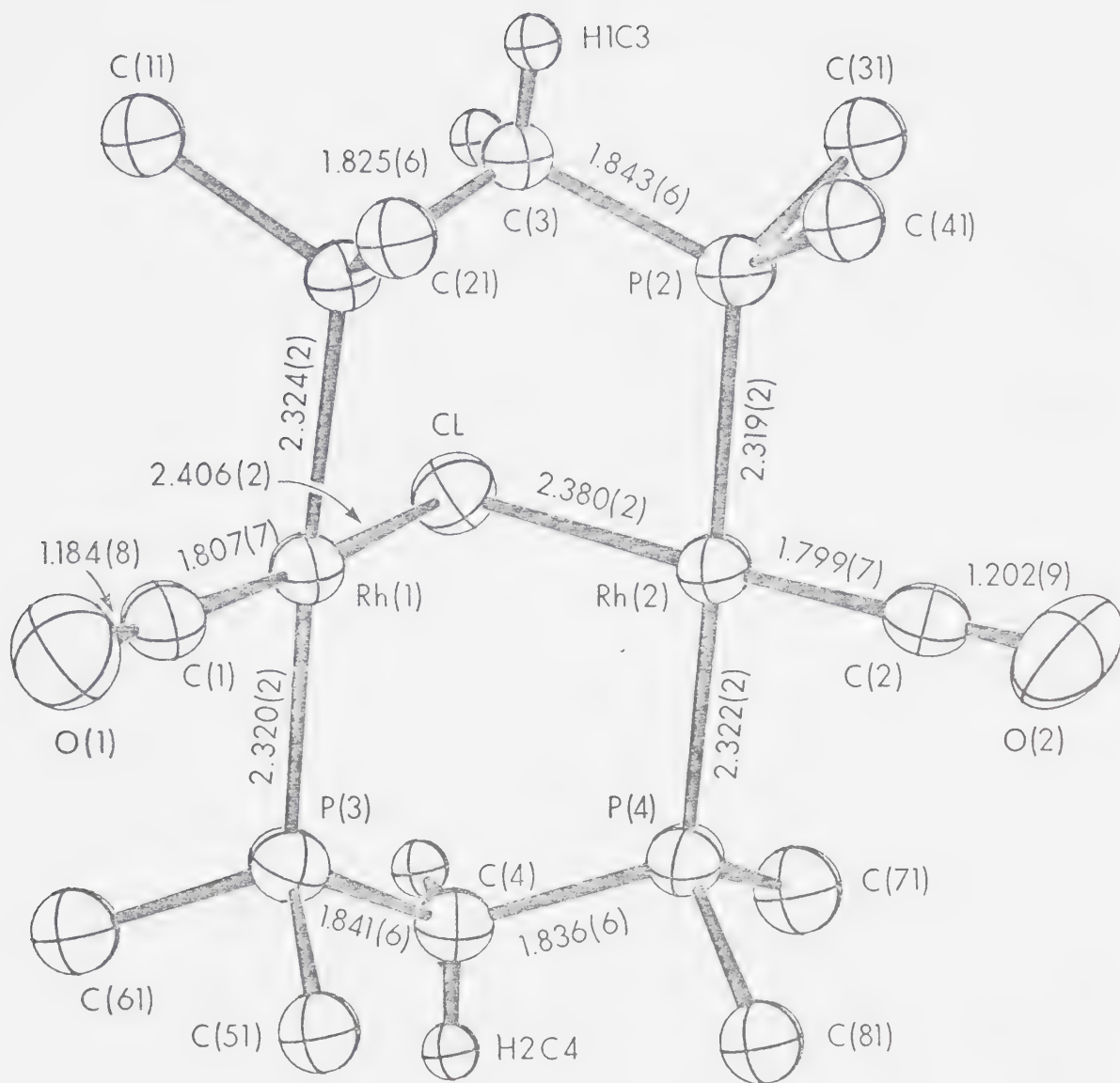


Figure 6. The Inner Coordination Sphere of  $[\text{Rh}_2(\text{CO})_2(\mu\text{-Cl})(\text{DPM})_2]^+$  Cation.



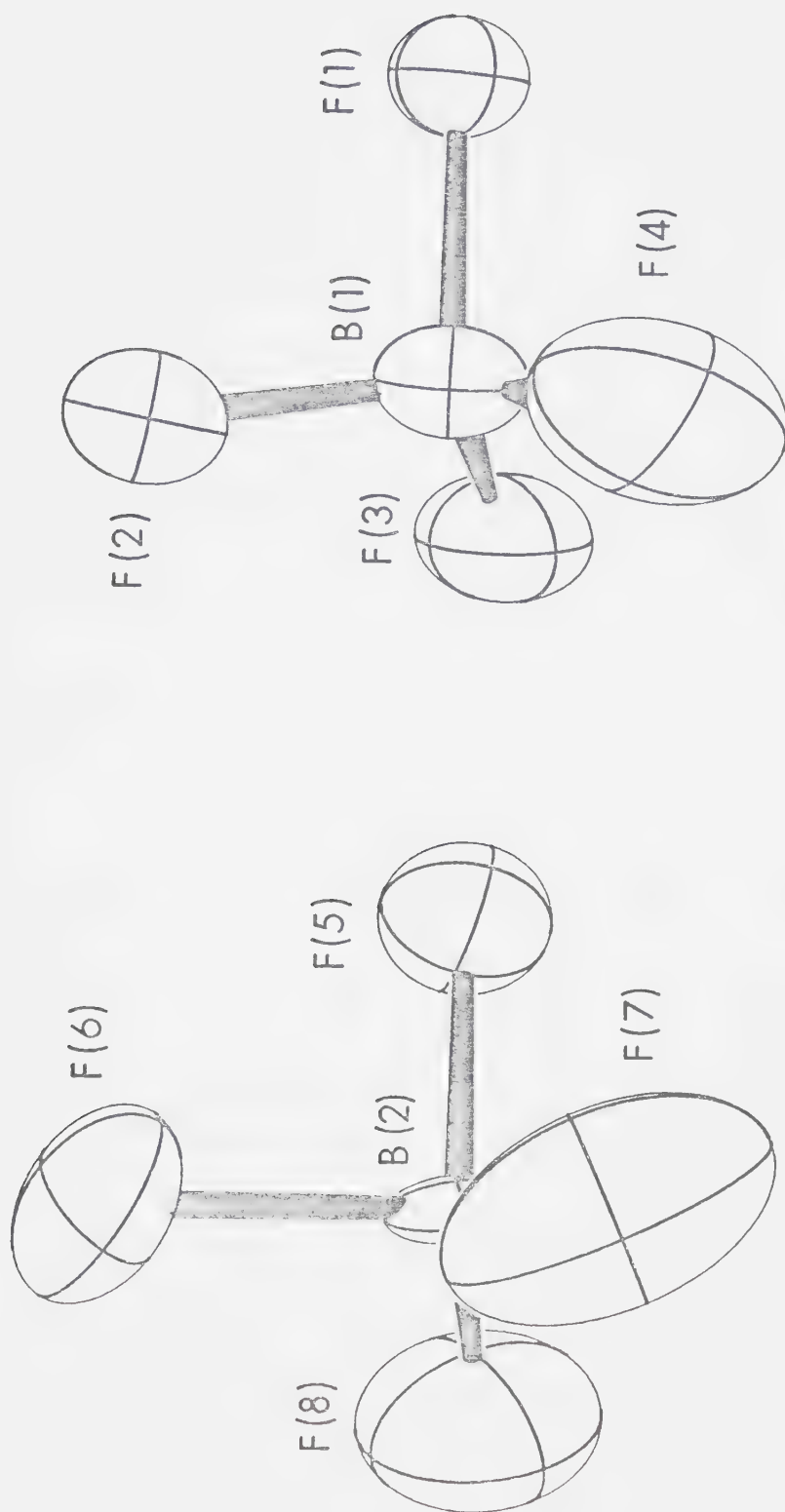


Figure 7. The Two Independent Tetrafluoroborate Anions.



## DESCRIPTION OF STRUCTURE

The two independent  $\text{BF}_4^-$  anions, although inversion disordered and undergoing a large amount of thermal vibration, show reasonable tetrahedral geometries (see Figure 4). The range in the B-F distances (1.24(3)-1.51(1) $\overset{\circ}{\text{\AA}}$ ) and the F-B-F angles (93(2)-122(2) $^\circ$ ) are not unreasonable considering the observed disorder and thermal motion, suggesting that the refined model is acceptable. These values are in reasonable agreement with other structural determinations involving  $\text{BF}_4^-$  salts.<sup>111</sup> The only significant nonbonded contacts involving the  $\text{BF}_4^-$  anion are between the fluorine atoms and the phenyl hydrogen atoms (see Table 8). These distances (2.35-2.38  $\overset{\circ}{\text{\AA}}$ ) are somewhat shorter than the sum of their van der Waal's radii (2.57)<sup>112</sup> and may explain the orientations of the phenyl rings and the relatively open bridging site, between the two rhodium centres (vide infra).

The  $[\text{Rh}_2(\text{CO})_2(\mu\text{-Cl})(\text{DPM})_2]^+$  cation displays the expected "A-frame" geometry in which the rhodium atoms are bridged by two DPM ligands which are mutually trans. The chloro ligand bridges the two metal centres in the equatorial plane perpendicular to the Rh-P vectors, and the carbonyl ligands, also lying in this plane, are bonded to each Rh atom trans to the bridging Cl atom. Both Rh atoms display slightly distorted square-planar geometries, whose least-square planes are inclined to each other by 82.66 $^\circ$ .





The distortions from square planar geometry seem to result from close nonbonded contacts between the carbonyl ligands and the hydrogen atoms of the endo phenyl groups which enclose the bridging site. Indeed the larger distortion, about Rh(1), is accompanied by the shortest nonbonded contacts, involving C(1) and O(1) (see Table 8).

The relatively long Rh...Rh separation of  $3.1520(8)\text{\AA}$  is consistent with no formal Rh-Rh bond. This distance is significantly longer than the Rh-Rh distance of  $2.8415(7)\text{\AA}$  observed in the carbonyl adduct  $[\text{Rh}_2(\text{CO})_2(\mu\text{-CO})(\mu\text{-Cl})(\text{DPM})_2] \cdot [\text{BPh}_4] (2)$ ,<sup>35</sup> where all evidence suggests the presence of a formal Rh-Rh single bond. The absence of a formal Rh-Rh bond in the present complex is substantiated by the following structural parameters: i) the Rh-Rh separation is significantly greater than the intraligand P...P separations of  $3.088(2)$  and  $3.097(2)\text{\AA}$ , (when the metals are mutually bonded the converse is true);<sup>35b</sup> ii) the Rh(1)-Cl-Rh(2) angle of  $82.38(5)^\circ$  compares well with values typically observed when no formal metal-metal bond is present (range  $80\text{--}95^\circ$ )<sup>113-116</sup> and contrasts to the value of  $66.51(4)^\circ$  observed in the Rh-Rh bonded carbonyl adduct 2. In addition, the absence of a formal metal-metal bond is required to explain the observed diamagnetism and to give each rhodium atom a 16-electron configuration.

The Rh-Cl distances of  $2.406(2)$  and  $2.380(2)\text{\AA}$  are in the range typically observed in other chloro-bridged dimer



systems (*ca.* 2.30-2.45 Å)<sup>113-116</sup> and are significantly shorter than those observed in the carbonyl adduct **2** (2.575(2) and 2.607(2) Å).<sup>35</sup> The observed asymmetry in these parameters involving the chloro ligand presumably results as a consequence of nonbonded contacts, since there is no *a priori* reason to expect a chemical difference in the two rhodium centres. In support of this argument, the shortest nonbonded contacts involving the chloro ligands are H2C3-Cl and H1C4-Cl (2.80-2.90 Å, respectively). These interactions act in such a way as to force the bridging chloro ligand out of the symmetrical position towards Rh(2). This chloride asymmetry is reflected in the parameters of the carbonyl groups which are trans to the Cl atom. Although not statistically significant, the trend in the carbonyl parameters is consistent with the chloro ligand acting as a weaker  $\pi$ -donor to Rh(1) than to Rh(2) with the concomitant result that C(1)O(1) has a weaker  $\pi$ -accepting ability compared to C(2)O(2) (Rh(1)-C(1) = 1.807(7) Å, C(1)-O(1) = 1.184(8) Å, Rh(2)-C(2) = 1.799(7) Å, C(2)-O(2) = 1.202(9) Å). No other short contacts are observed that would readily explain the observed asymmetry in the chloro ligand. The slight bend in both carbonyl ligands (Rh-C-O(av) = 177.2(8)°) is not unusual and is probably also steric in origin.

Within the Rh-DPM framework the parameters are not unusual. The Rh-P distances (average 2.321(2) Å) compare well with other Rh-DPM<sup>35,88-90,96</sup> systems and are typical for Rh(1)-phosphine distances when trans to another phos-



phine ligand (e.g., 2.322(4) and 2.338(4) Å in red and orange Wilkinson's catalyst).<sup>117</sup> The P-C distances (both methylene and phenyl) are quite ordinary and the P-C-P angles (average 114.7(3)°) are close to the expected tetrahedral value as is typical when the DPM ligand bridges two metals.

The methylene groups of the DPM ligands are folded in a cis configuration, with both groups inclined towards the bridging chloro ligand. Therefore, C(3) is 0.708(6) Å out of the Rh(1)-P(1)-P(2)-Rh(2) plane and C(4) is 0.678(6) Å out of the Rh(1)-P(3)-P(4)-Rh(2) plane. This cis methylene orientation is quite typical of most analogous DPM and DAM bridged species.<sup>32,35,41,81,85,89</sup> In general the methylene groups bend towards the more sterically encumbered site; so for example when two bridging equatorial ligands are present, the folding is towards the more bulky of these bridging ligands. By folding in this manner the non-bonded contacts between the more bulky phenyl groups and the equatorial ligands are minimized. Further, in the present structure the cis methylene configuration results in a phenyl ring orientation which allows relatively free access to the bridging site, between the Rh atoms and opposite the chloro ligand. The trans configuration of the methylene groups has been observed<sup>31,32,83b,118</sup> when there is no steric preference for one side of the Rh-phosphine framework over the other.



Viewed along the Rh-Rh axis the Rh-P vectors on adjacent rhodium atoms are close to eclipsed as is evidenced by the small P-Rh(1)-Rh(2)-P torsion angles (0.16(6) to 3.70(5)°, see Table 9). This presents an interesting contrast to that observed in the analogous sulfido bridged species,  $[\text{Rh}_2(\text{CO})_2(\mu\text{-S})(\text{DPM})_2]^{89}$  (3), which appears to be severely twisted about the Rh-Rh axis. Model building has shown that this twist about the Rh-Rh axis in "A-frame" complexes results in two of the endo phenyl rings moving into the bridging site, thereby effectively blocking this site, as was observed in the sulfido bridged species. The orientation of the phenyl rings in the present species, however is such that the bridging site is more accessible than in the sulfido complex. It is difficult, however, in the present case to draw analogies between the solution chemistries and the solid state structures since the observed differences in phosphine twists between 1 and 3 may be a result of crystal packing. Indeed in the present complex the  $\text{BF}_4^-$  anion at the 1(c) inversion centre sits directly above the bridging site (see Figure 4) and displays non-bonded contacts with the hydrogen atoms of the surrounding phenyl rings which are shorter than van der Waal's distances<sup>112</sup> (vide supra). It is expected that the  $\text{BF}_4^-$  anion, in this position, exerts considerable influence on the orientations of these phenyl groups and hence on the crowding of the bridging site. Certainly there is no obvious chemical reason to explain the twist difference in the two otherwise similar compounds.





## DISCUSSION

The crystallization of 1 as the  $\text{BF}_4^-$  salt was somewhat of a surprise, considering that the anions initially present were  $\text{PF}_6^-$  and  $\text{BPh}_4^-$ . There are two obvious sources of this  $\text{BF}_4^-$  anion. The first is through fluorination of  $\text{BPh}_4^-$  anion by HF, which is known to be present in acetone solutions of  $\text{PF}_6^-$ , and the second is through leaching of boron from the borosilicate glass by HF. On the basis of  $^{31}\text{P}$  and  $^{19}\text{F}$  NMR studies, it seems that the latter is more likely. When complex 1 and  $[\text{N}_2\text{Ph}][\text{PF}_6]$  are reacted in acetone and the mixture left for several weeks the NMR spectra indicated that the  $\text{PF}_6^-$  concentration is greatly diminished, and shows the presence of fluorosilanes,  $\text{BF}_4^-$  and other unidentified species. Furthermore, the NMR tubes and glassware used in the crystallizations were found to be etched, suggesting that significant leaching of the glass had occurred. In any case the well formed crystals were a pleasant surprise since all known previous attempts to obtain suitable single crystals of complex 1 with other anions had failed.<sup>119</sup>

Although the present structure seems significantly different than that of the sulfido bridged analogue 3 with respect to crowding of the bridging site, it is believed that this is a consequence more of solid-state effects than of chemical differences. Any differences in the chemistries of these two species that might occur are more likely a conse-



quence of the difference in bridging ligands ( $S^{2-}$  and  $Cl^{-}$ ) and the overall charge of the species. In this regard it will be of obvious interest to compare the chemistries of these species.

The present structure verifies that the bridging site in DPM-bridged species is accessible to small molecules and therefore it is not unexpected that some small molecules, such as  $SO_2$ , are capable of attack at this site, as the experimental evidence suggests (Chapter IV). It is however, not obvious, based on this structure determination, why some small molecules attack at the bridging site and others attack at the terminal site.

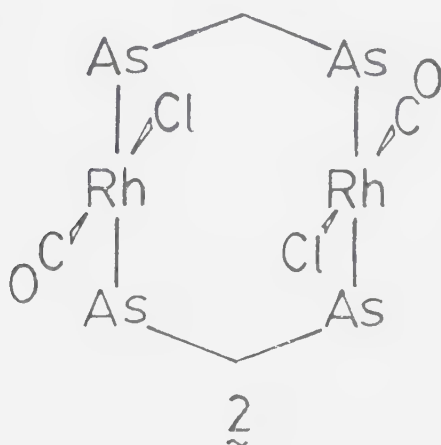


### CHAPTER III.

#### The Structure of *trans*-[RhCl(CO)(DPM)]<sub>2</sub>

##### INTRODUCTION

The reactions of *trans*-[RhCl(CO)(DPM)]<sub>2</sub> (1) with small molecules were investigated as part of our studies into the chemistry of DPM-bridged binuclear rhodium complexes.<sup>35,96</sup> Although the structure of compound 1 had not been determined, it was believed, on the basis of X-ray powder diffraction studies,<sup>66</sup> to be the same as the DAM-bridged analogue, *trans*-[RhCl(CO)(DAM)]<sub>2</sub> (2),<sup>31</sup> whose structure is known and whose framework is sketched below:



Unlike the "A-frame" species (see Chapter II),<sup>120</sup> only the terminal sites above the square planar metal atoms in 1 and 2 are open to attack since the sites between the metals are blocked by the chloro and carbonyl ligands.



In spite of the proposed structural analogies in compounds 1 and 2,<sup>66</sup> however, significant differences in their chemistries led us to question the extent of their similarities. It had been noted, for example, that "ketonic" carbonyl complexes of Pt and Pd were more stable with DAM than with DPM,<sup>32,41,84</sup> whereas our work tended to indicate that the opposite was true with rhodium. In species containing unsupported bridging ligands, such as the "ketonic" carbonyl ligand, we anticipated that the metal-metal separation might be an important factor in determining the stability of the unsupported ligand complex. Since the obvious difference in the DPM and DAM ligands lies in their ligand bites, due to the greater size of As compared to P, and since the DAM ligand would therefore tend to prefer larger metal-metal separations than DPM, it was deemed important to obtain structural information on the DPM complex 1 in order to compare the metal-metal separations and the subsequent effects on ligand orientations in the two compounds 1 and 2.

Furthermore, we prepared an isomer of 1,<sup>96</sup> which appears to be the cis-dichlorodicarbonyl species (see Chapter IV). This isomer has a greatly differing solubility and chemistry with CO compared to the trans isomer 1 so structural comparisons of the two species seemed in order. Therefore, when reaction of 1 (of which suitable, single crystals had never been obtained by us) with CS<sub>2</sub> resulted in the serendipitous crystallization of well formed rhombs of complex 1, it was decided to undertake its structural





determination.

## EXPERIMENTAL

### Crystallization of *trans*-[RhCl(CO)(DPM)]<sub>2</sub>

To a suspension of 0.100 g (0.091 mmol) of *trans*-[RhCl(CO)(DPM)]<sub>2</sub><sup>66</sup> in 15 mL of CH<sub>2</sub>Cl<sub>2</sub> was added 15 mL of CS<sub>2</sub>. After one hour diethyl ether was added to the clear red solution to induce crystallization. The red solid obtained was then redissolved in 15 mL of CH<sub>2</sub>Cl<sub>2</sub> from which well formed yellow crystals were obtained by diethyl ether diffusion. Chemical and spectral analysis showed that the crystals were the starting material, complex 1.

### Data Collection

A clear yellow plate of *trans*-[RhCl(CO)(DPM)]<sub>2</sub> was mounted on a glass fiber. Preliminary film data showed  $\bar{1}$  Laué symmetry and no systematic absences, consistent with the space groups P1 or  $P\bar{1}$ . The centrosymmetric space group was chosen and later verified by the successful refinement of the structure with acceptable positional parameters, thermal parameters and agreement indices and the location of all hydrogen atoms in the electron density difference maps. A cell reduction<sup>102</sup> failed to show the presence of higher symmetry. The reduced cell is reported and is presented together with the pertinent crystal data and details of data collection are in Table 10. Otherwise data collection proceeded as described in Chapter II.







Table 10, continued

Takeoff Angle	4.1°
Scan Speed	2° in 2θ/min
Scan Range	1.00 below $K_{\alpha 1}$ to 1.00 above $K_{\alpha 2}$
Background Counting Time	10s ( $3^\circ < 2\theta < 60^\circ$ ) 20s ( $60^\circ < 2\theta \leq 120^\circ$ )
2θ limits	$3.0^\circ \leq 2\theta \leq 120.0^\circ$
2θ limits for centered reflections	$60^\circ \leq 2\theta \leq 70^\circ$
Final number of variables	113
Unique Data Collected	3505
Unique Data Used ( $F_O^2 \geq 3\sigma(F_O^2)$ )	3368
Error in observation of unit weight	1.866
R	0.037
$R_w$	0.069



## Solution of Structure

The independent Rh atom position was obtained from a sharpened Patterson map. Subsequent least-squares calculations and electron density difference maps led to the location of all other atoms. Anomalous dispersion terms<sup>108</sup> for Rh, P and Cl were included in  $F_C$ . The carbon atoms of the phenyl rings were refined as rigid groups. Hydrogen atoms were included as fixed contributions and not refined. All nongroup atoms were refined individually with anisotropic thermal parameters (for a more detailed discussion of structure solution and rigid group treatment see Chapter II).

The final model with 115 parameters varied converged to  $R=0.037$  and  $R_w=0.069$ .<sup>121</sup> In the final electron density difference map all of the highest 20 peaks were in the vicinities of the phenyl rings ( $0.91$ - $0.54$   $e/\text{\AA}^3$ ). A typical carbon atom on an earlier electron density difference map had an electron density of  $7.7$   $e/\text{\AA}^3$ .

## Results

The final positional and thermal parameters for the nongroup and group atoms are given in Tables 11 and 12, respectively. The idealized positional and thermal parameters for the hydrogen atoms are given in Table 13. Least squares plane calculations are presented in Table 14 and selected bond distances and angles are given in Tables 15 and 16, respectively. A listing of observed and calculated structure amplitudes is available.<sup>110</sup> The unit cell of





*trans*-[RhCl(CO)(DPM)]<sub>2</sub> is shown in Figure 8. Four adjacent molecules are drawn in order to show some of the packing interactions. The crystallographic *b* axis runs from bottom to top of the page, the *c* axis is horizontal to the right and the *a* axis runs into the page. Figure 9 presents a perspective view of the compound, including the numbering scheme (phenyl hydrogens have the same number as their attached carbon atom). The inner coordination sphere of *trans*-[RhCl(CO)(DPM)]<sub>2</sub> is shown in Figure 10, along with some relevant bond lengths, 50% thermal ellipsoids are drawn.



Table 11. Positional and Thermal Parameters For the Nongroup Atoms of Trans-[RhCl(CO)(DPM)]<sub>2</sub>.

Atom	a			z	b			U12	U13	U23
	x	y			U11	U22	U33			
Rh	0.02710(2)	-0.04223(2)	0.15345(2)	0.15345(2)	2.36(2)	2.13(2)	2.83(2)	-0.68(1)	1.26(1)	0.09(1)
Cl	0.18334(9)	0.06132(8)	0.2207(1)	0.2207(1)	3.63(5)	3.77(5)	4.22(5)	-1.76(4)	1.70(4)	-0.16(4)
P(1)	-0.22241(9)	0.20635(7)	-0.13917(9)	-0.13917(9)	2.63(5)	2.20(4)	3.00(5)	-0.64(3)	1.32(4)	0.24(3)
P(2)	-0.17744(9)	0.12221(7)	0.15280(9)	0.15280(9)	2.48(4)	2.34(4)	2.90(5)	-0.69(3)	1.32(4)	-0.01(3)
O(1)	-0.1297(4)	-0.1852(3)	0.1355(4)	0.1355(4)	7.1(2)	4.4(2)	10.3(3)	-2.9(2)	5.8(2)	-0.9(2)
C(1)	-0.0725(4)	-0.1309(3)	0.1376(5)	0.1376(5)	3.4(2)	3.4(2)	5.6(3)	-1.0(2)	2.4(2)	-1.2(2)
C(2)	-0.2019(3)	0.1785(3)	-0.0309(4)	-0.0309(4)	2.6(2)	2.7(2)	2.9(2)	-0.7(1)	1.5(1)	-0.2(1)

a

Estimated standard deviations in the least significant figure(s) are given in parentheses in this and all subsequent tables.

b

The form of the thermal ellipsoid is:  $z = (a^*U_{11}h^2 + b^*U_{22}k^2 + c^*U_{33}l^2 + 2a^*b^*U_{12}hk + 2a^*c^*U_{13}hl + 2b^*c^*U_{23}kl)]$ . The quantities given in the table are the coefficients  $\times 10^3$ .



TABLE 12. Derived Parameters For the Rigid Group Atoms of Trans-[RhCl(CO)(DPM)]2.

Atom	x	y	z	B(A <sup>2</sup> )	Atom	x	y	z	B(A <sup>2</sup> )
C(11)	-0.2018(3)	0.3442(2)	-0.0656(3)	2.48(6)	C(31)	-0.1562(3)	0.2475(2)	0.2675(3)	2.43(6)
C(12)	-0.3189(2)	0.4518(2)	-0.1109(2)	3.66(8)	C(32)	-0.0330(3)	0.2239(2)	0.3966(2)	3.61(8)
C(13)	-0.3039(2)	0.5548(2)	-0.0460(2)	4.71(9)	C(33)	-0.0182(4)	0.3131(3)	0.4952(2)	4.9(1)
C(14)	-0.1719(3)	0.5503(2)	0.0641(3)	4.9(1)	C(34)	-0.1265(3)	0.4259(2)	0.4648(3)	4.64(9)
C(15)	-0.0519(2)	0.4428(2)	0.1094(2)	4.34(9)	C(35)	-0.2496(3)	0.4495(2)	0.3357(2)	4.57(9)
C(16)	-0.0698(2)	0.3397(2)	0.0445(2)	3.09(7)	C(36)	-0.2645(4)	0.3603(3)	0.2371(2)	3.33(7)
C(21)	-0.3759(6)	0.2513(2)	-0.3145(2)	2.51(6)	C(41)	-0.2962(4)	0.0928(3)	0.2113(6)	2.25(6)
C(22)	-0.5019(5)	0.2311(3)	-0.3546(5)	3.10(7)	C(42)	-0.4395(5)	0.1074(2)	0.1225(4)	2.86(6)
C(23)	-0.6134(4)	0.2652(3)	-0.4909(3)	3.92(8)	C(43)	-0.5214(2)	0.0819(2)	0.1747(2)	3.29(7)
C(24)	-0.5989(6)	0.3194(2)	-0.5870(2)	4.30(9)	C(44)	-0.4600(4)	0.0420(3)	0.3157(6)	3.29(7)
C(25)	-0.4728(5)	0.3396(3)	-0.5469(5)	4.55(9)	C(45)	-0.3166(5)	0.0274(2)	0.4045(4)	3.83(8)
C(26)	-0.3614(4)	0.3055(3)	-0.4107(3)	3.67(8)	C(46)	-0.2347(2)	0.0529(2)	0.3524(2)	3.40(7)

Rigid Group Parameters

a				b			
Xc				Delta			
Yc				Epsilon			
Zc				Eta			
Ring1	-0.1869(2)	0.4473(2)	-0.0007(2) <sup>a</sup>	-0.231(2)	2.822(2)	4.892(1)	
Ring2	-0.4874(2)	0.2854(2)	-0.4508(2)	0.916(2)	2.384(3)	3.127(3)	
Ring3	-0.1413(2)	0.3367(2)	0.3662(2)	2.683(2)	2.597(2)	1.198(2)	
Ring4	-0.3781(2)	0.0674(1)	0.2635(2)	4.237(2)	2.366(3)	4.823(3)	

<sup>a</sup> Xc,Yc and Zc are the fractional coordinates of the centroid of the rigid group.

<sup>b</sup> The rigid group orientation angles Delta,Epsilon and Eta(radians) are the angles by which the rigid body is rotated with respect to a set of axes X,Y and Z. The origin is the centre of the ring; X is parallel to a\*, Z is parallel to c and Y is parallel to the line defined by the intersection of the plane containing a\* and b\* with the plane containing b and c.



TABLE 13. Idealized Positional and Thermal Parameters For the Hydrogen Atoms of Trans-[RhCl(CO)(DPM)]<sub>2</sub>.

Atom	x	y	z	B(A <sup>2</sup> )	Atom	x	y	z	B(A <sup>2</sup> )
H(1)	-0.3433	0.1229	-0.0808	3.22	H(26)	-0.2751	0.3186	-0.3835	4.70
H(2)	-0.3770	0.2501	-0.0251	3.22	H(32)	0.0412	0.1466	0.4177	4.62
H(12)	-0.4090	0.4550	-0.1858	4.50	H(33)	0.0663	0.2969	0.5833	5.89
H(13)	-0.3839	0.6284	-0.0766	5.52	H(34)	-0.1158	0.4867	0.5319	5.64
H(14)	-0.1618	0.6209	0.1085	5.81	H(35)	-0.3232	0.5262	0.3150	5.49
H(15)	0.0353	0.4400	0.1845	5.39	H(36)	-0.3484	0.3759	0.1493	4.38
H(16)	0.0102	0.2666	0.0753	4.18	H(42)	-0.4814	0.1353	0.0266	3.85
H(22)	-0.5127	0.1947	-0.2891	3.99	C(43)	-0.6192	0.0921	0.1140	4.33
H(23)	-0.7000	0.2520	-0.5185	4.85	H(44)	-0.5159	0.0245	0.3511	4.40
H(24)	-0.6749	0.3426	-0.6803	5.19	H(45)	-0.2748	0.0001	0.5008	4.74
H(25)	-0.4625	0.3759	-0.6128	5.46	H(46)	-0.1370	0.0433	0.4134	4.31





Table 14. Least-Squares Plane Calculations

Plane no.	Equation
1	$-0.7174X - 0.5092Y - 0.4755Z + 0.0 = 0.0^a$
2	$0.1832X + 0.1661Y - 0.9689Z + 1.5689 = 0.0$

Deviations from the Planes ( $\text{\AA}$ )

Plane no.	Atom				
	Rh	P(1)	P(2)	P(2)'	Cl
1	-0.0047(2)	-0.040(1)	0.040(1)		
2	-0.0021(2)	0.0637(9)		0.0608(9)	-0.0492(9)
					-0.302(4)
					-0.553(4)
					0.720(4) <sup>b</sup>

Angle between Rh-Rh vector and plane 2 =  $75.9^\circ$

<sup>a</sup>X, Y, and Z are orthogonal coordinates ( $\text{\AA}$ ) with X along the a axis  
Y in the a-b plane and Z along the C\*-axis.

<sup>b</sup>Not included in least squares plane calculation.



Table 15. Selected Distances ( $\text{\AA}$ ) in *trans*-[RhCl(CO)(DPM)]<sub>2</sub>

<u>Bonded</u>			
Rh-Cl	2.3875 (9)	P(1)-C(11)	1.833 (2)
Rh-P(1)	2.3141 (9)	P(1)-C(21)	1.831 (2)
Rh-P(2) <sup>a</sup>	2.3315 (9)	P(2)-C(31)	1.834 (2)
Rh-C(1)	1.814 (4)	P(2)-C(41)	1.842 (2)
P(1)-C(2)	1.840 (3)	C(1)-O	1.102 (5)
P(2)-C(2)	1.835 (3)		

<u>Nonbonded</u>			
Rh-Rh <sup>1</sup>	3.2386 (5)	O-H(14) <sup>c</sup>	2.56
Rh-Cl <sup>1</sup>	3.569 (1)	C(1)-H(16) <sup>1</sup>	2.69
P(1)-P(2)	3.130 (1)	C(2)-H(42)	2.57
Cl-H(16)	2.69	C(2)-H(22)	2.64
Cl-H(45) <sup>b</sup>	2.73		

<sup>a</sup>Primed atoms related to unprimed atoms by a center of inversion in this and all subsequent tables.

<sup>b</sup>Atom located at  $\bar{x}$ ,  $\bar{y}$ ,  $1-z$ .

<sup>c</sup>Atom located at  $x$ ,  $y-1$ ,  $z$ .



Table 16. Selected Angles (deg) in *trans*-[RhCl(CO)(DPM)]<sub>2</sub>Bond Angles

Cl-Rh-P(1)	86.20(3)	C(2)-P(1)-C(11)	102.7(1)
Cl-Rh-P(2)'	95.33(3)	C(2)-P(1)-C(21)	103.2(1)
Cl-Rh-C(1)	169.1(1)	C(2)-P(2)-C(31)	107.8(1)
C(1)-Rh-P(1)	91.6(1)	C(2)-P(2)-C(41)	101.8(1)
C(1)-Rh-P(2)'	87.5(1)	C(11)-P(1)-C(21)	103.1(1)
P(1)-Rh-P(2)'	176.50(2)	C(31)-P(2)-C(41)	99.5(1)
Rh-C(1)-O	176.3(4)	P(1)-C(11)-C(12)	121.0(1)
P(1)-C(2)-P(2)	116.8(2)	P(1)-C(11)-C(16)	118.9(1)
Rh-P(1)-C(2)	112.2(1)	P(1)-C(21)-C(22)	122.8(1)
Rh-P(2)'-C(2)'	110.9(1)	P(1)-C(21)-C(26)	117.1(1)
Rh-P(1)-C(11)	121.22(8)	P(2)-C(31)-C(32)	117.3(1)
Rh-P(1)-C(21)	112.39(9)	P(2)-C(31)-C(36)	122.4(1)
Rh-P(2)'-C(31)'	120.35(8)	P(2)-C(41)-C(42)	123.6(1)
Rh-P(2)'-C(41)'	114.53(9)	P(2)-C(41)-C(46)	116.4(1)

Torsion Angles

P(1)-Rh-Rh'-P(2)	2.19(3)	C(1)-Rh-P(1)-C(2)	140.6(2)
Cl-Rh-P(1)-C(2)	-50.1(1)	C(1)-Rh-P(1)-C(11)	18.9(2)
Cl-Rh-P(1)-C(11)	-171.7(1)	C(1)-Rh-P(1)-C(21)	-103.5(2)
Cl-Rh-P(1)-C(21)	65.74(9)	C(1)-Rh-P(2)'-C(2)'	-90.8(2)
Cl-Rh-P(2)'-C(2)'	99.7(1)	C(1)-Rh-P(2)'-C(31)'	142.2(2)
Cl-Rh-P(2)'-C(31)'	-27.2(1)	C(1)-Rh-P(2)'-C(41)'	23.7(2)
Cl-Rh-P(2)'-C(41)'	-145.73(9)		

Vector-Plane Normal Angles

Rh-Rh', Rh-Cl-P(1)	12.98(2)
Rh-Rh', Rh-C(1)-P(2)'	23.6(1)



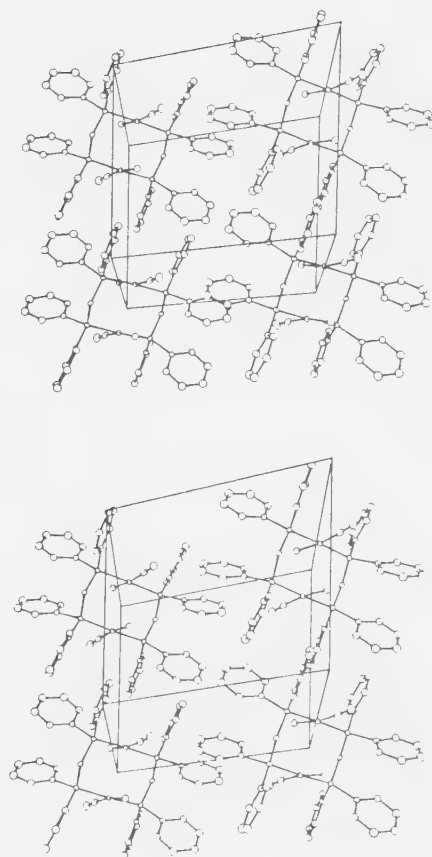


Figure 8. Cell Packing Diagram of  $\text{trans-}[\text{RhCl}(\text{CO})(\text{DPM})]_2 \cdot$ .





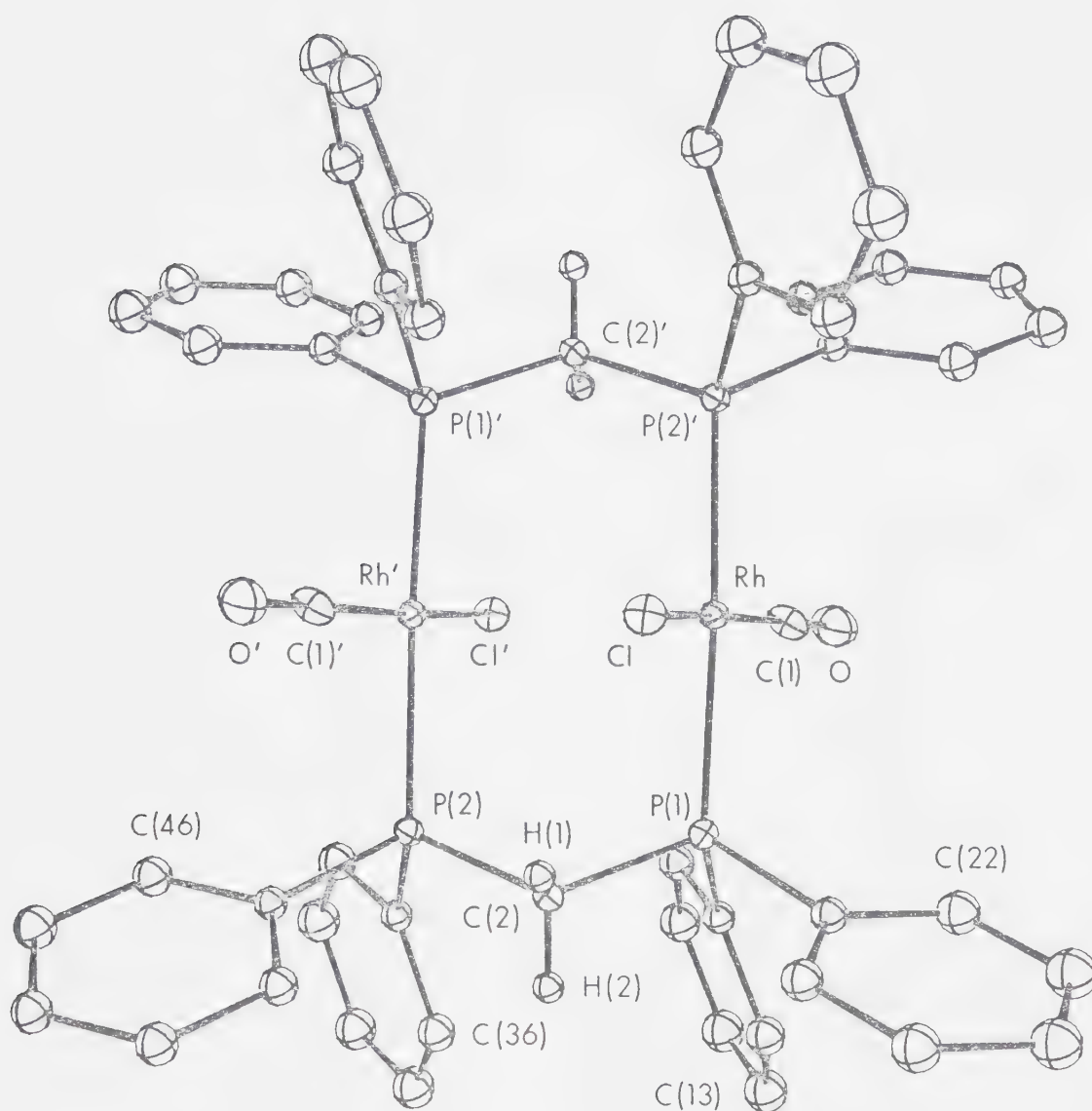


Figure 9. A Perspective View of *trans*-[RhCl(CO)(DPM)]<sub>2</sub>.



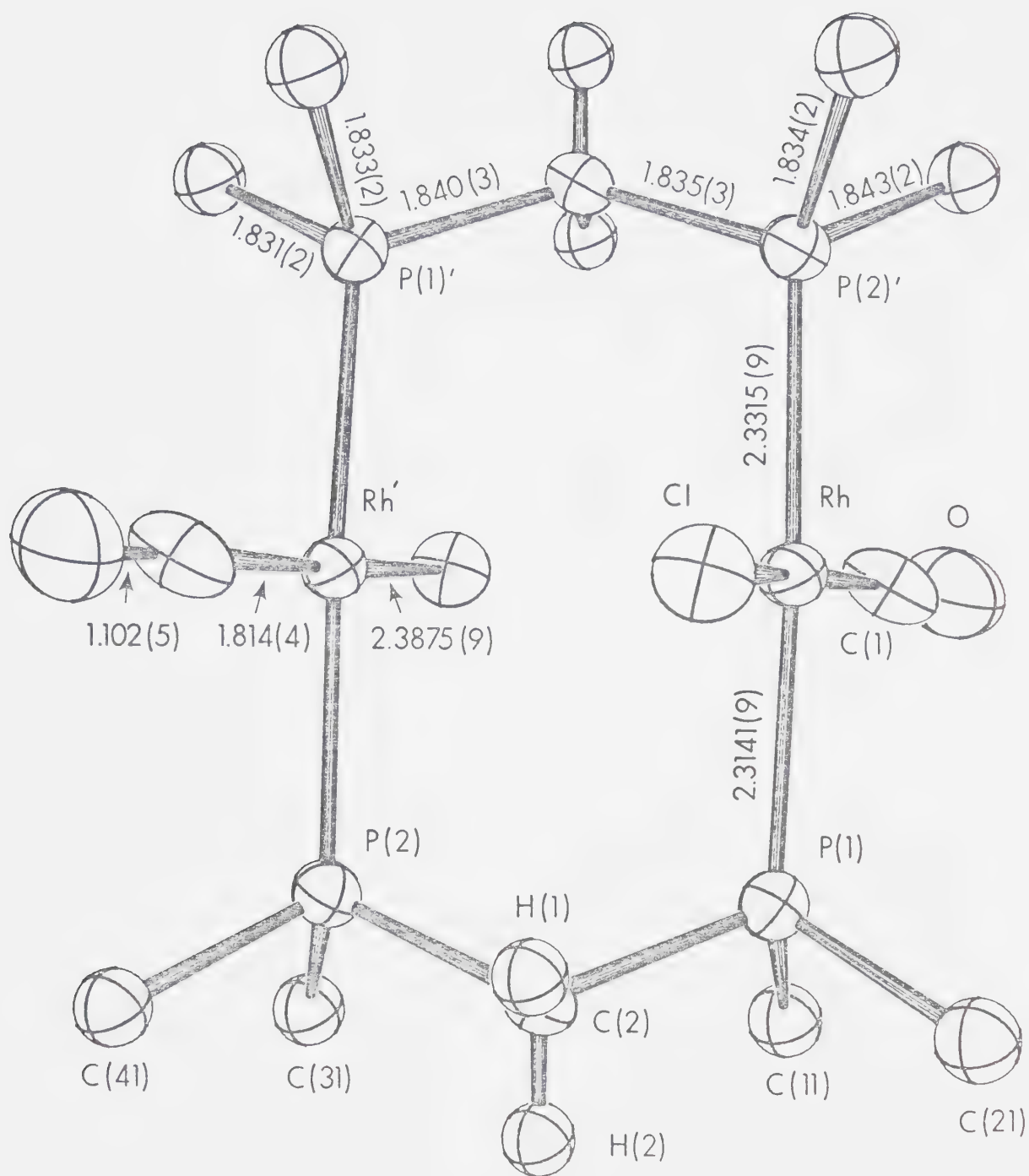


Figure 10. The Inner Coordination Sphere of  $trans\text{-}[\text{RhCl}(\text{CO})\text{-(DPM)}]_2$ .



## DESCRIPTION OF STRUCTURE

The structure of *trans*-[RhCl(CO)(DPM)]<sub>2</sub> (1) consists of a discrete dimeric unit located on the inversion centre at the origin; thus the molecule possesses crystallographically imposed  $\bar{1}$  symmetry. The coordination about each Rh atom is effectively square planar with trans geometry about each metal, much like Vallarino's compound<sup>66</sup> and its analogues.<sup>122</sup> Slight tetrahedral distortions of the square plane are evident as was observed in the red and orange forms of Wilkinson's compound.<sup>117,123</sup> Therefore the two phosphorus atoms are folded towards each other in the direction of the Rh-Rh vector whereas the Cl and CO ligands are folded in the opposite direction (Table 14). The dimeric unit is composed of two of these parallel square planes in an eclipsed conformation and bridged by the diphosphine ligands. These planes are arranged such that the chloro ligands on adjacent rhodium atoms are mutually trans, as are the carbonyl ligands. Significantly, the square planes are not perpendicular to the Rh-Rh vector but are inclined to it by *ca.* 75.9° (Table 14) with the chloro ligands folded in towards the bridging sites between the metal centers. This same twist of the Rh square planes is also observed in *trans*-[RhCl(CO)(DAM)]<sub>2</sub>, although it was not noted in the original report on this compound.<sup>31</sup> The skewing of these planes seems to result from an attempt to minimize the non-bonded contacts between the equatorial chloro and carbonyl ligands and the phenyl rings. So in the observed



conformation the Rh-Cl and Rh-CO vectors are staggered with respect to the P-C vectors (Table 16).

Within the Rh-DPM framework the parameters are essentially as observed in other similar DPM-bridged complexes.<sup>35,37,84,85,89</sup> The two independent Rh-P distances (2.3141(9) and 2.3315(9) Å) are significantly different, however no chemical significance is attached to this difference. More likely the difference is a consequence of packing considerations (vide infra). Unlike most other DPM-bridged species which have a cis methylene arrangement, the methylene groups in the present compound are folded in a trans configuration with the methylene carbon atoms displaced by 0.720(4) Å from the best intraligand Rh-P-P-Rh planes. The folding of the methylene carbon atoms out of these planes occurs such that the phenyl groups avoid the equatorial ligands.

The parameters involving the chloro- and carbonyl ligands are not unusual, being typical for Rh(I) phosphino complexes.<sup>31,35,89,120,122</sup>

The relatively long Rh...Rh separation of 3.2386(5) Å is consistent with no formal metal-metal bond, and is in fact significantly longer than the non-bonded Rh...Rh separations of 3.1520(8) Å and 3.155(4) Å observed in  $[\text{Rh}_2(\text{CO})_2(\mu\text{-Cl})(\text{DPM})_2][\text{BF}_4]$ <sup>120</sup> (Chapter II) and  $[\text{Rh}_2(\text{CO})_2(\mu\text{-S})(\text{DPM})_2]$ ,<sup>89</sup> respectively. In these two "A-frame" species the metal centres are held closer than in the present structure owing to the constraints of the bridging





chloro and sulfido ligands, respectively, in the former two species. As in previous determinations in which no metal-metal bond was present the intraligand P...P separation ( $3.130(1)\text{\AA}$ ) is significantly less than the Rh...Rh separation. However the Rh...Rh separation is still considerably less than that observed in the DAM analogue ( $3.396(1)\text{\AA}$ ),<sup>31</sup> reflecting the differences in bite size of the two ligands. A further indication that the Rh-Rh interaction, in the present compound, is repulsive is seen in a comparison of the P-C-P ( $116.8(2)^\circ$ ) and As-C-As ( $113.5(4)^\circ$ ) angles in the DPM and DAM<sup>31</sup> complexes, respectively. The larger P-C-P angle reflects the strain on the DPM ligand as the metal centres are tending apart.

A comparison of the metrical parameters of the DPM and DAM ligands in the present complex and in *trans*-[RhCl(CO)-(DAM)]<sub>2</sub>,<sup>31</sup> respectively, shows the expected trend resulting from the larger covalent radius of As compared to P. Therefore the average P-C<sub>methylene</sub> ( $1.838(4)\text{\AA}$ ),<sup>124</sup> P-C<sub>phenyl</sub> ( $1.835(5)\text{\AA}$ ) and Rh-P ( $2.32(1)\text{\AA}$ ) distances are all significantly less than the corresponding As-C<sub>methylene</sub> ( $1.97(2)\text{\AA}$ ), As-C<sub>phenyl</sub> ( $1.936(9)\text{\AA}$ ) and Rh-As ( $2.407(4)\text{\AA}$ ) distances.

### DISCUSSION

The primary reason for undertaking the structural determination of *trans*-[RhCl(CO)(DPM)]<sub>2</sub> was to permit comparisons between it and the analogous DAM complex<sup>31</sup> in order to gain an understanding of the differences in their



solubilities and chemistries. Based on the packing of the complex, shown in Figure 5, it is not difficult to understand the insolubility of the DPM complex. All the phenyl rings in the lattice have one of essentially two orientations allowing extremely efficient packing of the molecules and efficient stacking of the parallel phenyl rings. However, since the DPM complex turns out to be essentially isostructural with the DAM analogue we find the solubility differences somewhat surprising. It is therefore assumed that the subtle differences resulting from the larger Rh(DAM) framework (vide supra) result in less efficient packing than in the DPM complex. The effect of the larger molecular framework is obvious in the cell parameters which result in unit cell volume of the DAM complex being *ca.* 4% larger than that of the DPM complex.

As had been expected, the Rh...Rh separation in the DPM complex is significantly shorter than that in the DAM complex. This arises because of the smaller bite of the DPM ligand which holds the metals closer together. It is anticipated that these different ligand bites will have significant effects on the stability of species containing bridging ligands, especially unsupported ligands such as "ketonic" carbonyls. Certainly studies to date do indicate a difference in stability between DPM and DAM "ketonic" carbonyl species. The present structure and that of complex 2 conclusively establish the significantly different effects that the DPM and DAM ligands have in establishing



metal-metal separations, in analogous structures. However, it must be noted that the present structure and that of 2 as determined by Mague<sup>31</sup> reflect only the preferred metal-metal separations of the two ligands under similar conditions. These ligands have extremely flexible bites which are rather easily changed. Therefore, a redetermination of the structure of *trans*-[RhCl(CO)(DAM)]<sub>2</sub>,<sup>125</sup> as the CH<sub>2</sub>Cl<sub>2</sub> solvate, indicates a Rh-Rh separation of only 3.236(2)Å. This is of course comparable to that in the present DPM compound and much less than that observed in the identical unsolvated complex. The difference (0.160(2)Å) is due presumably to packing considerations. At the other extreme, the largest metal-metal separation of 3.492(1)Å, has been observed in [Pd<sub>2</sub>Cl<sub>2</sub>(μ-HFB)(DPM)<sub>2</sub>],<sup>87</sup> indicating just how far the metals can be forced apart. Notwithstanding, the minimum and maximum metal-metal separations allowed should occur in DPM and DAM, respectively, as is the case for the two essentially isostructural compounds 1 and 2.



## CHAPTER IV.

### The Chemistry of Binuclear Rhodium Complexes with Sulfur Dioxide and the Structure of $[\text{Rh}_2\text{Cl}_2(\mu\text{-SO}_2)(\text{DPM})_2]$

#### INTRODUCTION

The cationic "A-frame" species  $[\text{Rh}_2(\text{CO})_2(\mu\text{-Cl})(\text{DPM})_2]^+$  (1) has been shown to undergo facile and often reversible reactions with small molecules.<sup>35a,91,96a</sup> An X-ray structural determination of 1 as the  $\text{BF}_4^-$  salt has indicated that both the enclosed bridging site, between the metal centres, and the terminal exposed sites, remote from the bridging site, are open to attack by small molecules<sup>120</sup> (Chapter II). The accessibility of these sites has been confirmed by experiments which have shown that CO attacks at the terminal site,<sup>91</sup> yielding  $[\text{Rh}_2(\text{CO})_2(\mu\text{-CO})(\mu\text{-Cl})(\text{DPM})_2]^+$  (2) (see Figure 11), whereas preliminary studies indicated that attack by  $\text{SO}_2$  seems to occur directly at the bridging site.<sup>96a</sup> Therefore a detailed study of the chemistry of  $[\text{Rh}_2(\text{CO})_2(\mu\text{-Cl})(\text{DPM})_2]^+$  with  $\text{SO}_2$  was undertaken to gain a better understanding of the modes of  $\text{SO}_2$  attack and coordination.

It was also observed that on prolonged treatment of the initially formed adduct  $[\text{Rh}_2(\text{CO})_2(\mu\text{-Cl})(\mu\text{-SO}_2)(\text{DPM})_2]^+$  (3) with  $\text{SO}_2$ , a disproportionation reaction seemed to occur yielding a neutral carbonyl free species containing  $\text{SO}_2$ , which was formulated as  $[\text{Rh}_2\text{Cl}_2(\mu\text{-SO}_2)(\text{DPM})_2]$  (4), and at





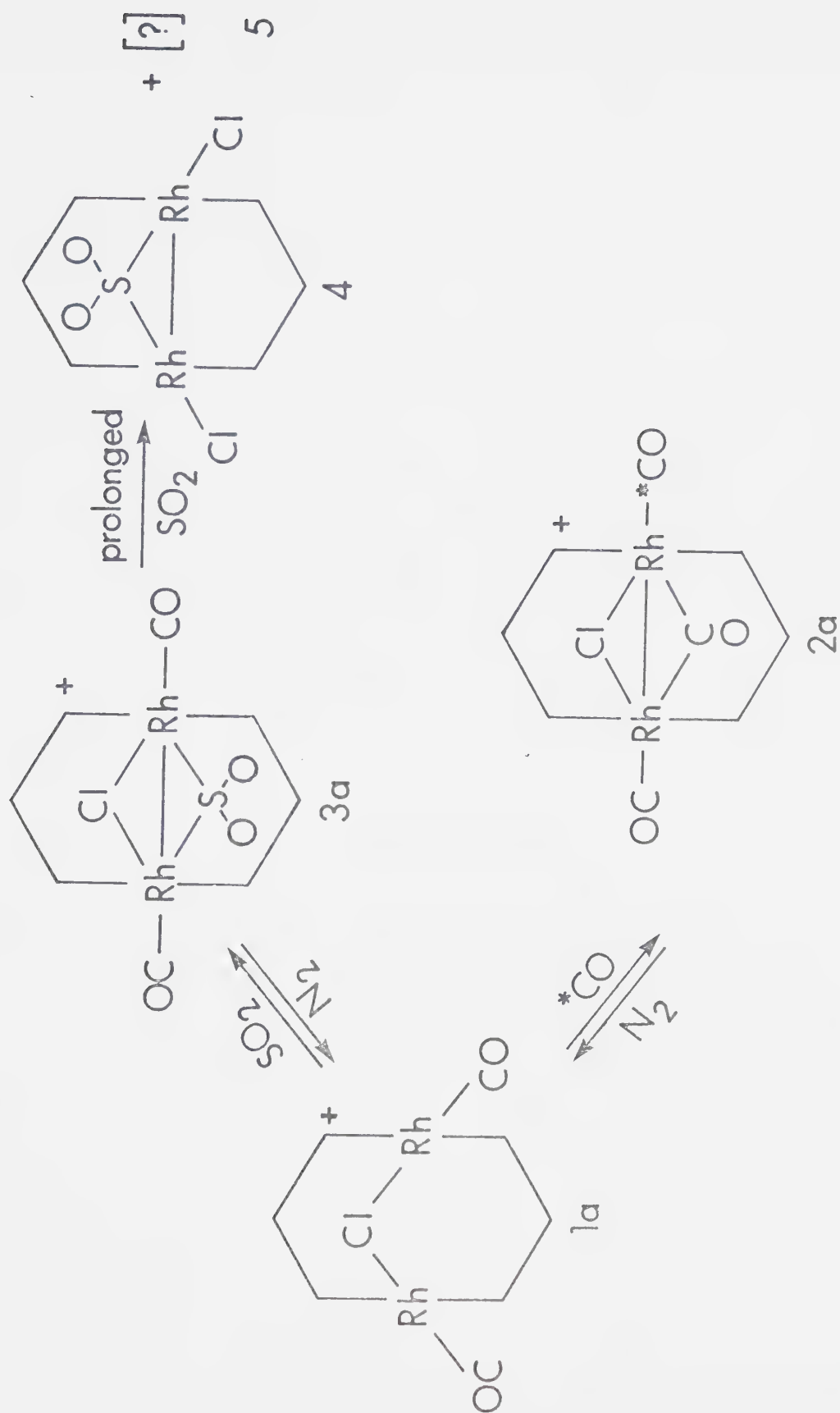


Figure 11. Reaction Scheme of  $[\text{Rh}_2(\text{CO})_2(\mu\text{-Cl})(\text{DPM})_2][\text{BPh}_4]$  with  $\text{CO}$  and  $\text{SO}_2$ .



least one other unidentified species (5).<sup>96a</sup> The structural characterization of this new SO<sub>2</sub> complex was undertaken to establish unambiguously its identity and a detailed investigation of the chemistry yielding the species was undertaken to establish the nature of this "disproportionation" reaction.

In addition the chemistry of another binuclear complex, *trans*-[RhCl(CO)(DPM)]<sub>2</sub>, with SO<sub>2</sub> was investigated to offer comparisons with the chemistry of the "A-frame" species (1). In the dichlorodicarbonyl species only terminal attack is possible, since the positions between the metal centres are blocked by the equatorial ligands<sup>126</sup> (Chapter III). Therefore, interesting comparisons in the chemistries of this species with that of the "A-frame" complex (1) were anticipated.

### EXPERIMENTAL

#### Preparation of [Rh<sub>2</sub>Cl<sub>2</sub>(μ-SO<sub>2</sub>)(DPM)<sub>2</sub>], Method A

A solution of 0.100 g (0.072 mmol) of [Rh<sub>2</sub>(CO)<sub>2</sub>(μ-Cl)(DPM)<sub>2</sub>][BPh<sub>4</sub>] in 10 mL of THF was treated with SO<sub>2</sub> for 10 min and then crystallization was induced by addition of diethyl ether saturated with SO<sub>2</sub>. The resulting red orange crystals, analyzed as [Rh<sub>2</sub>(CO)<sub>2</sub>(μ-Cl)(μ-SO<sub>2</sub>)(DPM)<sub>2</sub>][BPh<sub>4</sub>] (3a) and were obtained in 90-95% yield. This solid was redissolved in THF and slow concentration under a stream of SO<sub>2</sub> yielded the final product, [Rh<sub>2</sub>Cl<sub>2</sub>(μ-SO<sub>2</sub>)(DPM)<sub>2</sub>], 4, as well formed red-orange crystals. The remaining solution



was yellow. The yield of this second  $\text{SO}_2$  complex varied between 0 and 50%, depending on the batch of  $\text{Rh}_2(\text{CO})_2(\mu\text{-Cl})\text{-(DPM)}_2$  [BPh<sub>4</sub>] used (vide infra). Elemental analyses for all complexes are shown in Table 17 and the spectroscopic data and conductivity measurements are given in Table 18.

#### Method B

A suspension of 0.200 g (0.182 mmol) of *trans*- $[\text{RhCl}(\text{CO})(\text{DPM})]_2$ <sup>66</sup> in 20 mL of  $\text{CH}_2\text{Cl}_2$  was treated with  $\text{SO}_2$  for approximately 2 h. Slow concentration, under a stream of  $\text{SO}_2$ , yielded the desired crystalline product in 95% yield.

#### Method C

To a solution of 0.100 g (0.202 mmol) of  $[\text{RhCl}(\text{COD})]_2$ <sup>99</sup> in 20 mL of  $\text{CH}_2\text{Cl}_2$  was added 0.156 g (0.405 mmol) of DPM dissolved in 5 mL of benzene. Immediate treatment with  $\text{SO}_2$  and concentration of the solution by evaporation under  $\text{SO}_2$  yielded the crystalline product  $[\text{Rh}_2\text{Cl}_2(\mu\text{-SO}_2)(\text{DPM})_2]$  in 90% yield.

Preparation of  $[\text{Rh}_2(\text{CO})_2(\mu\text{-Cl})(\text{DPM})_2][\text{Cl}]$ ,  $[\text{Rh}_2(\text{CO})_2(\mu\text{-CO})(\mu\text{-Cl})(\text{DPM})_2][\text{Cl}]$  and *cis*- $[\text{RhCl}(\text{CO})(\text{DPM})]_2$

Treatment of a solution of 0.100 g (0.085 mmol) of  $[\text{Rh}_2\text{Cl}_2(\text{SO}_2)(\text{DPM})_2]$  in 10 mL of  $\text{CH}_2\text{Cl}_2$  with CO and concentration under a CO stream yielded quantitatively the product  $[\text{Rh}_2(\text{CO})_2(\mu\text{-CO})(\mu\text{-Cl})(\text{DPM})_2][\text{Cl}]$  (2b) as an orange microcrystalline solid. Pumping on this solid under vacuum resulted in the total conversion of 2b to  $[\text{Rh}_2(\text{CO})_2(\mu\text{-Cl})\text{-(DPM)}_2]$



Table 17. Analytical Data on Complexes

No.	Complex	Found	Calculated
2b.	$[\text{Rh}_2(\text{CO})_2(\mu\text{-CO})(\mu\text{-Cl})(\text{DPM})_2][\text{Cl}]$	C, 56.39; H, 4.25; Cl, 6.43	C, 56.36; H, 3.93, Cl, 6.28
3a.	$[\text{Rh}_2(\text{CO})_2(\mu\text{-Cl})(\mu\text{-SO}_2)(\text{DPM})_2][\text{BPh}_4]$	C, 62.85; H, 4.44	C, 62.98; H, 4.45
3b.	$[\text{Rh}_2(\text{CO})_2(\mu\text{-Cl})(\mu\text{-SO}_2)(\text{DPM})_2][\text{Cl}]$	C, 53.01, H, 4.09	C, 53.58; H, 3.80
4.	$[\text{Rh}_2\text{Cl}_2(\mu\text{-SO}_2)(\text{DPM})_2]$	C, 54.6; H, 3.80	C, 54.12; H, 4.00
6.	$\text{cis-}[\text{Rh}_2\text{Cl}_2(\text{CO})_2(\text{DPM})_2]$	C, 57.37; H, 4.55; Cl, 6.46	C, 56.70; H, 4.03; Cl, 6.44





Table 18. Spectral and Conductivity Data on the Complexes

No.	Complex	Infrared Absorption Maxima <sup>a</sup>	Assignment	<sup>31</sup> P{ <sup>1</sup> H}nmr Chemical Shifts <sup>b</sup>	Conductivity <sup>c</sup> (ohm <sup>-1</sup> cm <sup>2</sup> mole <sup>-1</sup> )
1a.	[Rh <sub>2</sub> (CO) <sub>2</sub> (μ-Cl)(DPM) <sub>2</sub> ][BPh <sub>4</sub> ] <sup>d</sup>	1997(s), 1978(vs)	ν <sub>CO</sub>	16.1 (113.3 Hz)	99.0
1b.	[Rh <sub>2</sub> (CO) <sub>2</sub> (μ-Cl)(DPM) <sub>2</sub> ][Cl]	1994(s), 1972(vs)	ν <sub>CO</sub>	--	--
2a.	[Rh <sub>2</sub> (CO) <sub>2</sub> (μ-CO)(μ-Cl)(DPM) <sub>2</sub> ][BPh <sub>4</sub> ] <sup>d</sup>	1992(s), 1977(vs), 1863(s)	ν <sub>CO</sub>	29.6 (94.2 Hz)	94.0
2b.	[Rh <sub>2</sub> (CO) <sub>2</sub> (μ-CO)(μ-Cl)(DPM) <sub>2</sub> ][Cl]	2004(s), 1960(vs), 1868(s)	ν <sub>CO</sub>	29.8 (94.0 Hz)	115.0 (acetone) 49.6 (CH <sub>2</sub> Cl <sub>2</sub> )
3a.	[Rh <sub>2</sub> (CO) <sub>2</sub> (μ-Cl)(μ-SO <sub>2</sub> )(DPM) <sub>2</sub> ][BPh <sub>4</sub> ]	2015(s), 1985(ssh)	ν <sub>CO</sub>	24.6 (91.3 Hz)	90.0
		1229(m), 1070(m)	ν <sub>SO<sub>2</sub></sub>		
3b.	[Rh <sub>2</sub> (CO) <sub>2</sub> (μ-Cl)(μ-SO <sub>2</sub> )(DPM) <sub>2</sub> ][Cl]	2010(s), 1985(ssh)	ν <sub>CO</sub>	24.5 (91.6 Hz)	65.0
		1230(m), 1071(m)	ν <sub>SO<sub>2</sub></sub>		
4.	[Rh <sub>2</sub> Cl <sub>2</sub> (μ-SO <sub>2</sub> )(DPM) <sub>2</sub> ]	1191(m), 1063(m)	ν <sub>SO<sub>2</sub></sub>	19.6 (115.0 Hz)	0
5.	<i>cis</i> -[Rh <sub>2</sub> Cl <sub>2</sub> (CO) <sub>2</sub> (DPM) <sub>2</sub> ]	1971(s)	ν <sub>CO</sub>	19.6 (113.5 Hz)	0
7.	<i>trans</i> -[Rh <sub>2</sub> Cl <sub>2</sub> (CO) <sub>2</sub> (DPM) <sub>2</sub> ] <sup>e</sup>	1968(s)	ν <sub>CO</sub>		0

<sup>a</sup>Infrared spectra were run as Nujol Mulls on KBr Plates; vs, very strong; s, strong; m, medium; w, weak; sh, shoulder.

<sup>b</sup><sup>31</sup>P{<sup>1</sup>H} nmr chemical shifts are relative to H<sub>3</sub>PO<sub>4</sub> (down field positive), coupling constants (<sup>1</sup>J<sub>Rh-P</sub> + x J<sub>Rh-P</sub>|)

<sup>c</sup>Solvent is acetone unless noted otherwise.

<sup>d</sup>References 35 and 91.

<sup>e</sup>Reference 66.



(DPM)<sub>2</sub>][Cl] (1b). Bubbling dinitrogen through the solution of 2b followed by slow concentration under dinitrogen yielded "*cis*-[RhCl(CO)(DPM)]<sub>2</sub>" 6 as a yellow crystalline solid.

#### Spectroscopic Studies on the Stepwise Reactions with SO<sub>2</sub>

A solution was prepared by dissolving 0.100 g (0.072 mmol) of 1a in 3 mL of CD<sub>2</sub>Cl<sub>2</sub> in a 10 mm NMR tube. This was cooled in a 2-propanol/dry ice bath and approximately 0.5 mL of gaseous SO<sub>2</sub> was admitted. The <sup>31</sup>P{<sup>1</sup>H} NMR spectrum was recorded immediately at 223 K. This procedure was repeated measuring the NMR spectrum after each addition of SO<sub>2</sub> until nearly all of 1a had been converted to 3a. Throughout the experiment only resonances assignable to 1a or 3a were detected.

Infrared spectra were recorded in an analogous manner, by recording the infrared spectrum after each stepwise addition of 0.5 ml of SO<sub>2</sub> (at atmospheric pressure) to a CH<sub>2</sub>Cl<sub>2</sub> solution of 1a (0.500 g (0.361 mmol) in 30 mL). Only bands assignable to complexes 1a, 3a and free SO<sub>2</sub> were detected. The stepwise addition of SO<sub>2</sub> to *trans*-[RhCl(CO)(DPM)]<sub>2</sub> was similarly monitored by infrared spectroscopy; however, in this case infrared bands at 1740(m), 1995(sh) and 2020(s) cm<sup>-1</sup> were observed at intermediate times in the experiment. After all of the *trans*-dichlorodicarbonyl complex had reacted, only bands attributable to 3b and free SO<sub>2</sub> were observed (Table 18). The NMR and infrared studies on both complexes indicated



that several additions of  $\text{SO}_2$  were required before any evidence of a reaction was detected.

A  $^{31}\text{P}\{^1\text{H}\}$  NMR spectrum of a sample of  $\underline{3a}$  that had "disproportionated" showed bands assignable to  $\underline{3a}$  and  $\underline{4}$  as well as bands at  $\delta = 8.05$  ppm (singlet),  $^{101} \delta = 5.90$  ppm (doublet, 70 Hz) and  $\delta = -13.4$  ppm (doublet, 120 Hz). The sum of the integrated intensities of the last three peaks was approximately equal to that of  $\underline{4}$ .

### X-ray Data Collection

Red crystals of  $[\text{Rh}_2\text{Cl}_2(\mu\text{-SO}_2)(\text{DPM})_2]$  suitable for single-crystal X-ray diffraction studies, were supplied by Dr. A.R. Sanger of the Alberta Research Council. Preliminary film data showed that the crystals belonged to the monoclinic system with extinctions ( $h0l$ ,  $l$  odd;  $0k0$ ,  $k$  odd) characteristic of the centrosymmetric space group  $\text{P}2_1/\text{c}$ . See Table 19 for pertinent crystal data and intensity collection information and Chapter II for a more complete discussion of data collection.

### Structure Solution and Refinement

The structure was solved by using a sharpened Patterson map to locate the two independent Rh atoms. Subsequent refinements and electron density difference maps led to the location of all remaining atoms. Anomalous dispersion terms<sup>108</sup> for Rh, P, Cl and S were included in  $F_c$ . The phenyl rings were refined as rigid groups and the hydrogen atoms were included as fixed contributions and not refined.



Table 19. Summary of Crystal Data and Intensity Collection  
for  $[\text{Rh}_2\text{Cl}_2(\mu\text{-SO}_2)(\text{DPM})_2]$

Compound	[Rh <sub>2</sub> Cl <sub>2</sub> (μ-SO <sub>2</sub> )(DPM) <sub>2</sub> ]																																
Formula	C <sub>50</sub> H <sub>44</sub> Cl <sub>2</sub> O <sub>2</sub> P <sub>4</sub> Rh <sub>2</sub> S																																
Formula Weight	1109.58 amu																																
Cell Parameters																																	
a	18.228(1) Å																																
b	13.526(1) Å																																
c	19.632(2) Å																																
β	104.72(1)°																																
V	4681.6 Å <sup>3</sup>																																
Z	4																																
Density	1.574 g·cm <sup>-3</sup> (calc'd.) 1.59(2) g·cm <sup>-3</sup> (expt'l. by flotation)																																
Space Group	C <sub>2h</sub> <sup>5</sup> - P2 <sub>1</sub> /c																																
Crystal Dimensions	0.31 x 0.21 x 0.06 mm																																
Crystal Volume	0.0025 mm <sup>3</sup>																																
Crystal Faces (and distances from an arbitrary origin within the crystal (mm))	<table><tr><td><math>\bar{1}</math></td><td>0</td><td>0</td><td>(0.0213)</td></tr><tr><td><math>\bar{1}</math></td><td>0</td><td>0</td><td>(0.0194)</td></tr><tr><td>0</td><td>0</td><td><math>\bar{1}</math></td><td>(0.1470)</td></tr><tr><td>0</td><td>0</td><td><math>\bar{1}</math></td><td>(0.1460)</td></tr><tr><td><math>\bar{1}</math></td><td>1</td><td>0</td><td>(0.0913)</td></tr><tr><td><math>\bar{1}</math></td><td><math>\bar{1}</math></td><td>0</td><td>(0.0810)</td></tr><tr><td><math>\bar{1}</math></td><td><math>\bar{1}</math></td><td>0</td><td>(0.0790)</td></tr><tr><td><math>\bar{1}</math></td><td><math>\bar{1}</math></td><td>0</td><td>(0.0940)</td></tr></table>	$\bar{1}$	0	0	(0.0213)	$\bar{1}$	0	0	(0.0194)	0	0	$\bar{1}$	(0.1470)	0	0	$\bar{1}$	(0.1460)	$\bar{1}$	1	0	(0.0913)	$\bar{1}$	$\bar{1}$	0	(0.0810)	$\bar{1}$	$\bar{1}$	0	(0.0790)	$\bar{1}$	$\bar{1}$	0	(0.0940)
$\bar{1}$	0	0	(0.0213)																														
$\bar{1}$	0	0	(0.0194)																														
0	0	$\bar{1}$	(0.1470)																														
0	0	$\bar{1}$	(0.1460)																														
$\bar{1}$	1	0	(0.0913)																														
$\bar{1}$	$\bar{1}$	0	(0.0810)																														
$\bar{1}$	$\bar{1}$	0	(0.0790)																														
$\bar{1}$	$\bar{1}$	0	(0.0940)																														
Temperature	20°C																																
Radiation	CuKα (λ=1.540562 Å) filtered with 0.5mil thick nickel foil																																
μ	89.55 cm <sup>-1</sup>																																
Range in Absorption	0.229 - 0.700																																
Correction Factors																																	
Receiving Aperture	3x3 mm, 30 cm from the crystal																																
Takeoff Angle	2.6°																																





Table 19, continued

Scan Speed	2° in 2θ/min ( $3^\circ < 2\theta < 100^\circ$ )
Scan Range	1° in 2θ/min ( $100^\circ < 2\theta < 123^\circ$ ) 0.75° below $K_{\alpha 1}$ to 0.75° above $K_{\alpha 2}$
Background Counting Time	10s ( $3^\circ < 2\theta < 76^\circ$ ) 20s ( $76^\circ < 2\theta < 100^\circ$ ) 40s ( $100^\circ < 2\theta < 123^\circ$ )
2θ limits	$3^\circ \leq 2\theta \leq 123^\circ$
2θ units for centred reflections	$50^\circ \leq 2\theta \leq 70^\circ$
Final number of variables	216
Unique Data Collected	7690
Unique Data Used ( $F_O^2 \geq 3\sigma(F_O^2)$ )	5207
Error in observation of unit weight	2.199
R	0.058
$R_w$	0.067



All nongroup atoms were refined individually with anisotropic thermal parameters. An isotropic secondary extinction parameter was included and refined since several intense low angle reflections systematically showed  $F_{\text{obs}}$  significantly less than  $F_{\text{cal}}$ .<sup>92</sup> (For a more detailed discussion of the techniques used in solution of the structure see Chapter II.)

The final model with 216 parameters varied converged to  $R = 0.058$  and  $R_w = 0.067$ .<sup>121</sup> In the final electron density difference map all of the 20 highest residuals were in the vicinities of the phenyl groups ( $0.99$ - $0.55$   $\text{e}/\text{\AA}^3$ ). A typical carbon atom on an earlier synthesis had an electron density of about  $3.9$   $\text{e}/\text{\AA}^3$ .

On the basis of the high thermal parameters of some of these group atoms and the residuals about the phenyl groups, it seems that an anisotropic refinement of the phenyl carbon atoms would have been more suitable. However this was not attempted due to the very high cost and the feeling that no significant change would result in the parameters of interest.

## Results

The positional and thermal parameters for the individual anisotropic atoms, rigid group atoms and idealized hydrogen atoms are given in Tables 20, 21 and 22, respectively. Least-squares plane calculations are shown in Table 23 and selected bond lengths and angles are given in Tables 24



and 25, respectively. A listing of the observed and calculated structure amplitudes is available.<sup>110</sup>

A stereoview of the unit cell is shown in Figure 12. The crystallographic *a* axis is horizontal to the right, the *c* axis runs from top to bottom and the *b* axis goes into the page. Figure 13 presents a perspective view of the compound including the numbering scheme (phenyl hydrogen atoms have the same number as their attached carbon atom). The inner coordination sphere is shown in Figure 14 along with some relevant bond lengths, 50% thermal ellipsoids are drawn.



TABLE 20. Positional and Thermal Parameters For The Nongroup Atoms of [Rh<sub>2</sub>C<sub>12</sub>(μ-SO<sub>2</sub>)(DPM)<sub>2</sub>].

Atom	a			b			U11	U22	U33	U12	U13	U23
	x	y	z	x	y	z						
Rh(1)	0.27944(3)	0.33834(5)	0.51141(3)	3.61(4)	3.37(4)	3.52(4)	-0.11(3)	1.37(3)	0.04(3)			
Rh(2)	0.21069(3)	0.16337(5)	0.45320(3)	3.41(4)	3.65(4)	2.77(4)	0.05(3)	0.86(3)	-0.10(3)			
P(1)	0.1677(1)	0.4272(2)	0.5018(1)	4.1(1)	3.8(1)	3.7(1)	0.2(1)	1.6(1)	0.2(1)			
P(2)	0.0937(1)	0.2442(2)	0.4266(1)	3.3(1)	4.2(1)	3.2(1)	-0.1(1)	1.07(9)	0.0(1)			
P(3)	0.3957(1)	0.2738(2)	0.5056(1)	3.7(1)	4.0(1)	4.8(1)	-0.1(1)	1.6(1)	0.1(1)			
P(4)	0.3232(1)	0.0771(2)	0.4579(1)	4.2(1)	4.1(1)	3.9(1)	0.9(1)	0.6(1)	-0.4(1)			
Cl(1)	0.3413(1)	0.4912(2)	0.5333(2)	5.2(1)	4.0(1)	8.2(2)	-0.7(1)	1.3(1)	-0.3(1)			
Cl(2)	0.1495(1)	0.0353(2)	0.3805(1)	4.8(1)	4.8(1)	4.3(1)	-1.0(1)	1.2(1)	-1.1(1)			
S	0.2441(1)	0.2110(2)	0.5622(1)	4.1(1)	3.8(1)	2.8(1)	-0.11(9)	1.10(9)	0.09(9)			
O(1)	0.3057(4)	0.1574(5)	0.6091(3)	5.2(4)	5.3(4)	3.2(3)	0.7(3)	0.4(3)	0.9(3)			
O(2)	0.1805(3)	0.2256(5)	0.5932(3)	4.9(4)	5.6(4)	3.4(3)	0.3(3)	2.4(3)	0.7(3)			
C(1)	0.0830(5)	0.3497(6)	0.4814(5)	3.5(4)	4.2(5)	3.9(5)	0.4(4)	1.3(4)	0.4(4)			
C(2)	0.4077(5)	0.1385(6)	0.5106(5)	4.1(5)	4.5(5)	4.4(6)	0.3(4)	1.0(4)	0.2(4)			

<sup>a</sup>

Estimated standard deviations in the least significant figure(s) are given in parentheses in this and all subsequent tables.

<sup>b</sup>The form of the thermal ellipsoid is:  $\exp[-2\pi^2(a^{*2}U_{11}h^2+b^{*2}U_{22}k^2+c^{*2}U_{33}l^2+2a^{*}b^{*}U_{12}hk+2a^{*}c^{*}U_{13}hl+2b^{*}c^{*}U_{23}kl)]$ . The quantities given in the table are the thermal coefficients  $\times 10^2$ .





TABLE 21. Derived Parameters For the Rigid Group Atoms of [Rh2C12( $\mu$ -S02)(DPM)2].

Atom	X	Y	Z	B(A <sup>2</sup> )	Atom	X	Y	Z	B(A <sup>2</sup> )
C(11)	0.1471(6)	0.5213(5)	0.4326(5)	3.4(2)	C(51)	0.4781(9)	0.3152(7)	0.5723(4)	3.7(2)
C(12)	0.1927(5)	0.5318(5)	0.3860(4)	4.7(2)	C(52)	0.531(1)	0.3813(7)	0.5592(7)	7.0(3)
C(13)	0.1763(7)	0.6044(6)	0.3341(4)	6.1(3)	C(53)	0.5924(6)	0.4107(5)	0.6138(8)	8.1(4)
C(14)	0.1142(6)	0.6666(5)	0.3288(5)	6.3(3)	C(54)	0.6001(9)	0.3740(7)	0.6815(4)	7.3(3)
C(15)	0.0686(5)	0.6561(5)	0.3755(4)	7.9(4)	C(55)	0.547(1)	0.3079(7)	0.6946(7)	12.3(6)
C(16)	0.0850(7)	0.5835(6)	0.4274(4)	6.6(3)	C(56)	0.4857(6)	0.2785(5)	0.6400(8)	9.7(5)
C(21)	0.1620(5)	0.4948(5)	0.5809(3)	3.7(2)	C(61)	0.408(2)	0.3061(6)	0.419(1)	4.3(2)
C(22)	0.1879(5)	0.5919(5)	0.5907(3)	5.9(3)	C(62)	0.478(1)	0.3022(5)	0.4032(9)	8.3(4)
C(23)	0.1933(4)	0.6390(4)	0.6548(4)	6.3(3)	C(63)	0.483(2)	0.3235(6)	0.4032(9)	10.2(5)
C(24)	0.1726(5)	0.5892(5)	0.7091(3)	6.1(3)	C(64)	0.419(2)	0.3488(6)	0.335(1)	7.8(4)
C(25)	0.1467(5)	0.4921(5)	0.6994(3)	5.6(3)	C(65)	0.348(1)	0.3527(5)	0.2994(9)	6.3(3)
C(26)	0.1413(4)	0.4450(4)	0.6353(4)	4.5(2)	C(66)	0.343(2)	0.3314(6)	0.367(1)	4.5(2)
C(31)	0.0039(4)	0.1740(4)	0.429(1)	3.1(2)	C(71)	0.349(1)	0.0554(7)	0.3747(5)	4.6(2)
C(32)	-0.0037(9)	0.1526(6)	0.4941(6)	5.9(3)	C(72)	0.4136(9)	0.0005(6)	0.3759(8)	11.5(6)
C(33)	-0.069(1)	0.1015(6)	0.4982(6)	7.6(4)	C(73)	0.4372(5)	-0.0123(6)	0.3144(9)	14.8(7)
C(34)	-0.1211(4)	0.0718(4)	0.437(1)	5.8(3)	C(74)	0.396(1)	0.0298(7)	0.2516(5)	8.7(4)
C(35)	-0.1086(9)	0.0932(6)	0.3715(6)	6.0(3)	C(75)	0.3309(9)	0.0846(6)	0.2504(8)	6.0(3)
C(36)	-0.044(1)	0.1443(6)	0.3673(6)	5.4(3)	C(76)	0.3073(5)	0.0974(6)	0.3119(9)	4.6(2)
C(41)	0.0776(6)	0.2969(5)	0.3383(5)	3.1(2)	C(81)	0.3265(5)	-0.0469(5)	0.4969(5)	4.0(2)
C(42)	0.0170(5)	0.3601(5)	0.3109(4)	5.0(2)	C(82)	0.3470(5)	-0.0588(5)	0.5698(5)	5.6(3)
C(43)	0.0079(4)	0.4008(4)	0.2441(6)	6.0(3)	C(83)	0.3457(5)	-0.1523(7)	0.5990(3)	6.7(3)
C(44)	0.0594(6)	0.3784(5)	0.2048(5)	5.2(2)	C(84)	0.3238(5)	-0.2340(5)	0.5553(5)	6.5(3)
C(45)	0.1200(5)	0.3152(5)	0.2322(4)	5.2(2)	C(85)	0.3033(5)	-0.2220(5)	0.4825(5)	9.0(4)
C(46)	0.1291(4)	0.2745(4)	0.2990(6)	4.1(2)	C(86)	0.3046(5)	-0.1285(7)	0.4533(3)	8.6(4)

## Rigid Group Parameters

	<sup>a</sup> Xc			<sup>b</sup> Delta			Epsilon			Eta		
	Xc	Yc	Zc	Delta	Epsilon	Eta	Xc	Yc	Zc	Delta	Epsilon	Eta
Ring1	0.1306(3)	0.5939(4)	0.3807(3)	-0.703(4)	0.864(7)	4.322(6)						
Ring2	0.1673(2)	0.5420(4)	0.6450(3)	0.339(5)	1.464(5)	5.775(5)						
Ring3	-0.0561(3)	0.1229(3)	0.4328(3)	1.049(4)	1.79(1)	1.48(1)						
Ring4	0.0685(3)	0.3376(3)	0.2715(3)	2.242(4)	1.124(7)	2.452(7)						
Ring5	0.5391(3)	0.3446(4)	0.6269(3)	0.872(6)	2.146(8)	5.824(9)						
Ring6	0.4133(3)	0.3274(3)	0.3513(3)	-1.303(5)	0.62(2)	4.04(2)						
Ring7	0.3722(3)	0.0426(4)	0.3132(4)	-0.980(6)	1.45(1)	2.92(1)						
Ring8	0.3252(3)	-0.1404(4)	0.5261(3)	0.144(5)	1.853(5)	1.165(5)						

<sup>a</sup><sup>b</sup> Xc, Yc and Zc are the fractional coordinates of the centroid of the rigid group.

The rigid group orientation angles Delta, Epsilon and Eta (radians) are the angles by which the rigid body is rotated with respect to a set of axes X, Y and Z. The origin is the centre of the ring; X is parallel to a\*, Z is parallel to c and Y is parallel to the line defined by the intersection of the plane containing a\* and b\* with the plane containing b and c.



TABLE 22. Idealized Positional and Thermal Parameters For the Hydrogen Atoms of [Rh<sub>2</sub>C12(mu-SO<sub>2</sub>)(DPM)<sub>2</sub>].

Atom	x	y	z	B(A <sup>2</sup> )	Atom	x	y	z	B(A <sup>2</sup> )
H(1C1)	0.0409	0.3882	0.4571	3.99	H(45)	0.1552	0.2998	0.2054	6.20
H(2C1)	0.0739	0.3262	0.5241	3.99	H(46)	0.1705	0.2313	0.3177	5.09
H(1C2)	0.4163	0.1179	0.5583	4.43	H(52)	0.5261	0.4064	0.5129	7.98
H(2C2)	0.4502	0.1205	0.4937	4.43	H(53)	0.6288	0.4559	0.6048	9.09
H(12)	0.2351	0.4894	0.3896	5.72	H(54)	0.6416	0.3941	0.7187	8.29
H(13)	0.2075	0.6116	0.3023	7.13	H(55)	0.5519	0.2829	0.7407	13.27
H(14)	0.1030	0.7161	0.2934	7.33	H(56)	0.4493	0.2334	0.6489	10.73
H(15)	0.0262	0.6985	0.3718	8.93	H(62)	0.5221	0.2846	0.4387	9.35
H(16)	0.0538	0.5763	0.4591	7.59	H(63)	0.5311	0.3206	0.3245	11.11
H(22)	0.2020	0.6259	0.5536	6.84	H(64)	0.4222	0.3633	0.2371	8.82
H(23)	0.2110	0.7052	0.6615	7.20	H(65)	0.3043	0.3701	0.2640	7.29
H(24)	0.1763	0.6212	0.7529	7.10	H(66)	0.2953	0.3341	0.3783	5.52
H(25)	0.1326	0.4579	0.7364	6.60	H(72)	0.4417	-0.0280	0.4190	12.62
H(26)	0.1236	0.3786	0.6286	5.55	H(73)	0.4815	-0.0497	0.3155	15.60
H(32)	0.0321	0.1729	0.5359	6.91	H(74)	0.4121	0.0209	0.2099	9.66
H(33)	-0.0773	0.0869	0.5428	8.60	H(75)	0.3028	0.1133	0.2076	7.05
H(34)	-0.1655	0.0370	0.4397	6.77	H(76)	0.2629	0.1350	0.3110	5.64
H(35)	-0.1442	0.0730	0.3296	6.98	H(82)	0.3620	-0.0030	0.5996	6.57
H(36)	-0.0349	0.1590	0.3226	6.43	H(83)	0.3597	-0.1604	0.6487	7.68
H(42)	-0.0181	0.3754	0.3377	6.03	H(84)	0.3229	-0.2977	0.5753	7.51
H(43)	-0.0334	0.4439	0.2254	6.96	H(85)	0.2883	-0.2775	0.4527	10.05
H(44)	0.0533	0.4061	0.1593	6.20	H(86)	0.2906	-0.1201	0.4037	9.60



Table 23. Least-Squares Plane Calculations

Plane No.	Equation <sup>a</sup>
1	$0.2235 X + 0.3314 Y - 0.9166 Z + 6.7751 = 0.0$
2	$-0.9043 X + 0.4149 Y - 0.1006 Z + 1.3775 = 0.0$
3	$-0.3075 X - 0.8651 Y - 0.3962 Z + 7.2045 = 0.0$

## Deviation from Planes (Å)

Atom

Plane No.	Rh(1)	Rh(2)	P(1)	P(2)	P(3)	P(4)	C(1)	C(2)	S	O(1)	O(2)
1	-0.0407(6)	-0.0272(6)	0.081(2)	0.352(2)	0.250(2)	0.250(2)	-0.234(9) <sup>b</sup>	-0.400(9) <sup>b</sup>			
2	0.0	0.0							0.0		
3									0.0	0.0	0.0

Dihedral Angle Between Planes 2 and 3 = 92.35°

<sup>a</sup>X, Y, Z are the orthogonal coordinates (Å) with X along the a axis, Y in the a-b plane and Z along the c\* axis.<sup>b</sup>Not included in least squares plane calculations.



Table 24. Selected Distances ( $\text{\AA}$ ) in  $\text{Rh}_2\text{Cl}_2(\mu\text{-SO}_2)(\text{DPM})_2$ 

Bond Distances			
Rh(1)-Rh(2)	2.7838(8)	P(1)-C(1)	1.824(9)
Rh(1)-S	2.169(2)	P(2)-C(1)	1.827(9)
Rh(2)-S	2.169(2)	P(3)-C(2)	1.843(9)
Rh(1)-Cl(1)	2.342(2)	P(4)-C(2)	1.822(9)
Rh(2)-Cl(2)	2.341(2)	P(1)-C(11)	1.830(6)
Rh(1)-P(1)	2.330(2)	P(1)-C(21)	1.830(6)
Rh(1)-P(3)	2.320(2)	P(2)-C(31)	1.824(5)
Rh(2)-P(2)	2.334(2)	P(2)-C(41)	1.827(5)
Rh(2)-P(4)	2.341(2)	P(3)-C(51)	1.812(7)
S-O(1)	1.452(6)	P(3)-C(61)	1.820(7)
S-O(2)	1.452(6)	P(4)-C(71)	1.832(7)
		P(4)-C(81)	1.839(6)

1.829(9)

1.827(8)

## Nonbonded Distances

P(1)-P(2)	3.018(3)	O(1)-H1C2	2.52
P(3)-P(4)	3.012(3)	O(2)-H(45) <sup>b</sup>	2.39
Rh(1)-H(66)	2.70	O(2)-H2C1	2.48
Rh(2)-H(46)	2.73	O(2)-H(26)	2.49
C(52)-H(62)	2.67	H2C1-H(26)	2.15
C(62)-H(52)	2.54	H1C2-H(82)	2.17
O(1)-H(82)	2.43	H(46)-H(76)	2.16
		H(52)-H(62)	2.19

<sup>a</sup>For averaged quantities, the estimated standard deviation is the larger of an individual standard deviation or the standard deviation of a single observation as calculated from the mean.

<sup>b</sup>H(45) is associated with the molecule at the general equivalent position  $x, 1/2 - y, 1/2 + z$ .





Table 25. Selected Angles (deg) in  $\text{Rh}_2\text{Cl}_2(\mu\text{-SO}_2)(\text{DPM})_2$ 

## Bond Angles

Rh(2)-Rh(1)-Cl(1)	166.28(8)	Rh(1)-P(3)-C(51)	116.6(3)
Rh(2)-Rh(1)-P(1)	96.43(6)	Rh(1)-P(3)-C(61)	106.6(3)
Rh(2)-Rh(1)-P(3)	88.94(6)	Rh(2)-P(4)-C(71)	117.6(3)
Rh(2)-Rh(1)-S	50.07(6)	Rh(2)-P(4)-C(81)	114.0(3)
Cl(1)-Rh(1)-S	143.33(9)	C(1)-P(1)-C(11)	103.5(4)
Cl(1)-Rh(1)-P(1)	85.98(9)	C(1)-P(1)-C(21)	104.3(4)
Cl(1)-Rh(1)-P(3)	86.45(9)	C(1)-P(2)-C(31)	100.1(4)
P(1)-Rh(1)-P(3)	168.46(9)	C(1)-P(2)-C(41)	103.8(3)
P(1)-Rh(1)-S	95.23(8)	C(2)-P(3)-C(51)	101.7(4)
P(3)-Rh(1)-S	96.04(8)	C(2)-P(3)-C(61)	103.4(4)
Rh(1)-Rh(2)-Cl(2)	167.17(6)	C(2)-P(4)-C(71)	102.2(4)
Rh(1)-Rh(2)-P(2)	89.10(6)	C(2)-P(4)-C(81)	102.2(4)
Rh(1)-Rh(2)-P(4)	96.25(6)	C(11)-P(1)-C(21)	103.7(3)
Rh(1)-Rh(2)-S	50.08(6)	C(31)-P(2)-C(41)	106.9(3)
Cl(2)-Rh(2)-S	142.44(8)	C(51)-P(3)-C(61)	108.9(4)
Cl(2)-Rh(2)-P(2)	86.75(7)	C(71)-P(4)-C(81)	103.7(4)
Cl(2)-Rh(2)-P(4)	86.11(8)	P(1)-C(11)-C(12)	120.9(4)
P(2)-Rh(2)-P(4)	169.59(9)	P(1)-C(11)-C(16)	119.0(4)
P(2)-Rh(2)-S	95.37(8)	P(1)-C(21)-C(22)	119.9(4)
P(4)-Rh(2)-S	94.91(8)	P(1)-C(21)-C(26)	119.6(4)
Rh(1)-S-Rh(2)	79.84(7)	P(2)-C(31)-C(32)	117.9(4)
O(1)-S-O(2)	111.9(4)	P(2)-C(31)-C(36)	122.1(4)
Rh(1)-S-O(1)	114.6(3)	P(2)-C(41)-C(42)	121.8(4)
Rh(1)-S-O(2)	116.5(3)	P(2)-C(41)-C(46)	118.2(4)
Rh(2)-S-O(1)	117.1(3)	P(3)-C(51)-C(52)	123.7(6)
Rh(2)-S-O(2)	113.6(3)	P(3)-C(51)-C(56)	116.3(6)
Rh(1)-P(1)-C(1)	113.3(3)	P(3)-C(61)-C(62)	122.6(5)
Rh(2)-P(2)-C(1)	117.5(3)	P(3)-C(61)-C(66)	117.3(5)
Rh(1)-P(3)-C(2)	117.9(3)	P(4)-C(71)-C(72)	118.5(6)
Rh(2)-P(4)-C(2)	113.6(3)	P(4)-C(71)-C(76)	121.4(6)
Rh(1)-P(1)-C(11)	115.5(2)	P(4)-C(81)-C(82)	120.4(5)
Rh(1)-P(1)-C(21)	115.2(2)	P(4)-C(81)-C(86)	119.6(5)
Rh(2)-P(2)-C(31)	118.9(2)	P(1)-C(1)-P(2)	111.6(4)
Rh(2)-P(2)-C(41)	108.2(2)	P(3)-C(2)-P(4)	110.5(5)

## Torsion Angles

P(1)-Rh(1)-Rh(2)-P(2)	6.31(8)	C(21)-P(1)-P(2)-C(31)	18.3(5)
P(3)-Rh(1)-Rh(2)-P(4)	7.60(9)	C(51)-P(3)-P(4)-C(81)	20.5(6)
P(1)-Rh(1)-Rh(2)-P(4)	177.36(9)	C(61)-P(3)-P(4)-C(71)	17.1(4)
P(3)-Rh(1)-Rh(2)-P(2)	163.45(8)	C(11)-P(1)-Rh(1)-Cl(1)	60.1(3)
C(1)-P(1)-P(3)-C(2)	16.2(5)	C(21)-P(1)-Rh(2)-Cl(2)	60.9(3)
C(1)-P(2)-P(4)-C(2)	15.3(5)	C(31)-P(2)-Rh(2)-Cl(2)	44.8(3)
C(11)-P(1)-P(3)-C(61)	18.2(4)	C(41)-P(2)-Rh(2)-Cl(2)	77.3(3)
C(21)-P(1)-P(3)-C(51)	17.9(4)	C(51)-P(3)-Rh(1)-Cl(1)	43.2(3)
C(31)-P(2)-P(4)-C(81)	17.4(4)	C(61)-P(3)-Rh(1)-Cl(1)	78.5(3)
C(41)-P(2)-P(4)-C(71)	17.2(4)	C(71)-P(4)-Rh(2)-Cl(2)	60.0(3)
C(11)-P(1)-P(2)-C(41)	12.2(3)	C(81)-P(4)-Rh(2)-Cl(2)	61.6(3)



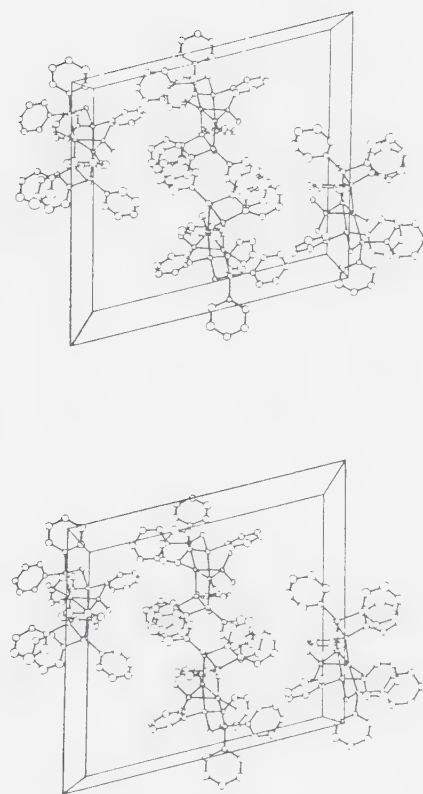


Figure 12. Cell Packing Diagram of  $[\text{Rh}_2\text{Cl}_2(\mu\text{-SO}_2)(\text{DPM})_2]$ .



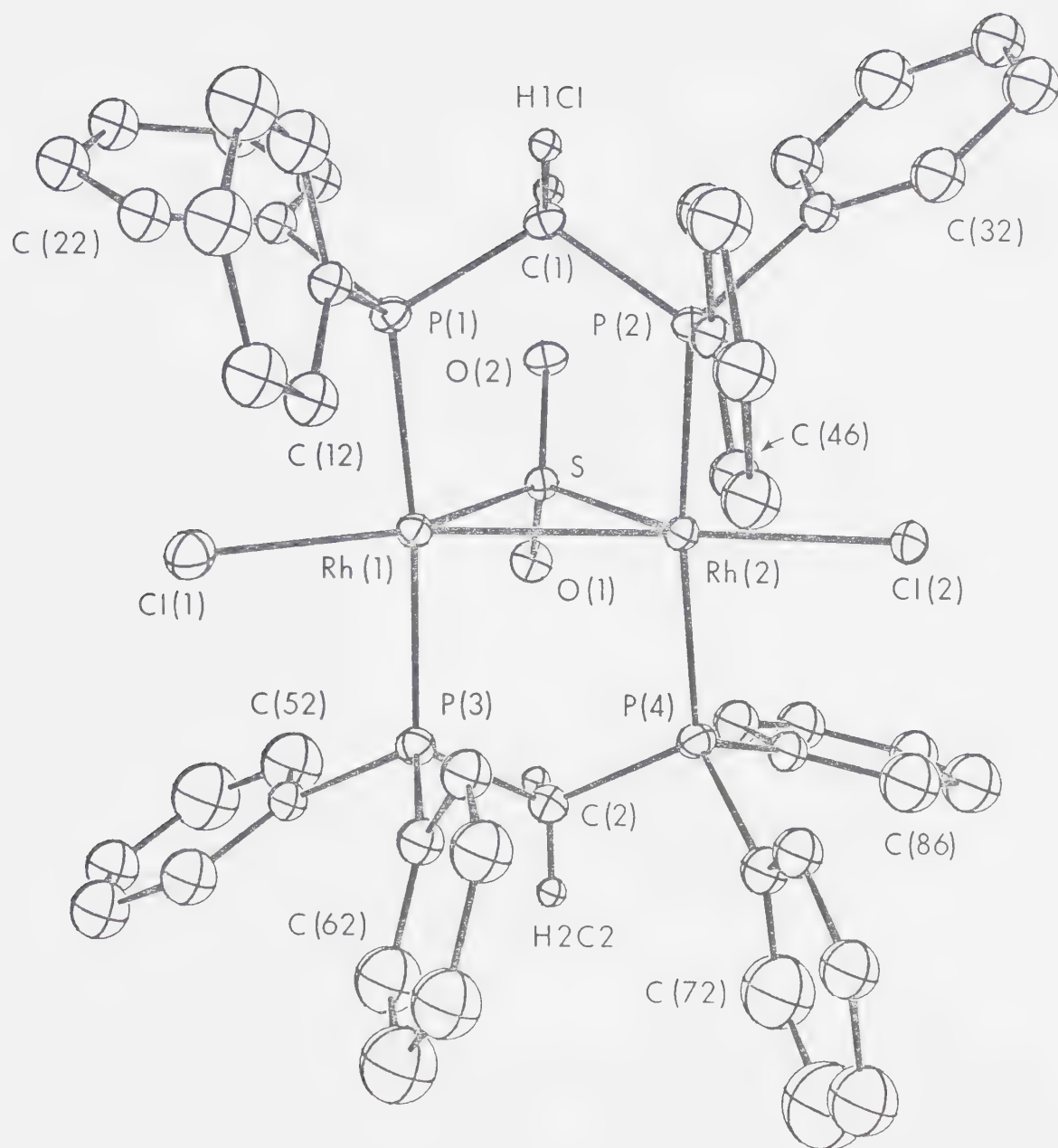


Figure 13. A Perspective View of  $[\text{Rh}_2\text{Cl}_2(\mu\text{-SO}_2)(\text{DPM})_2]$ .



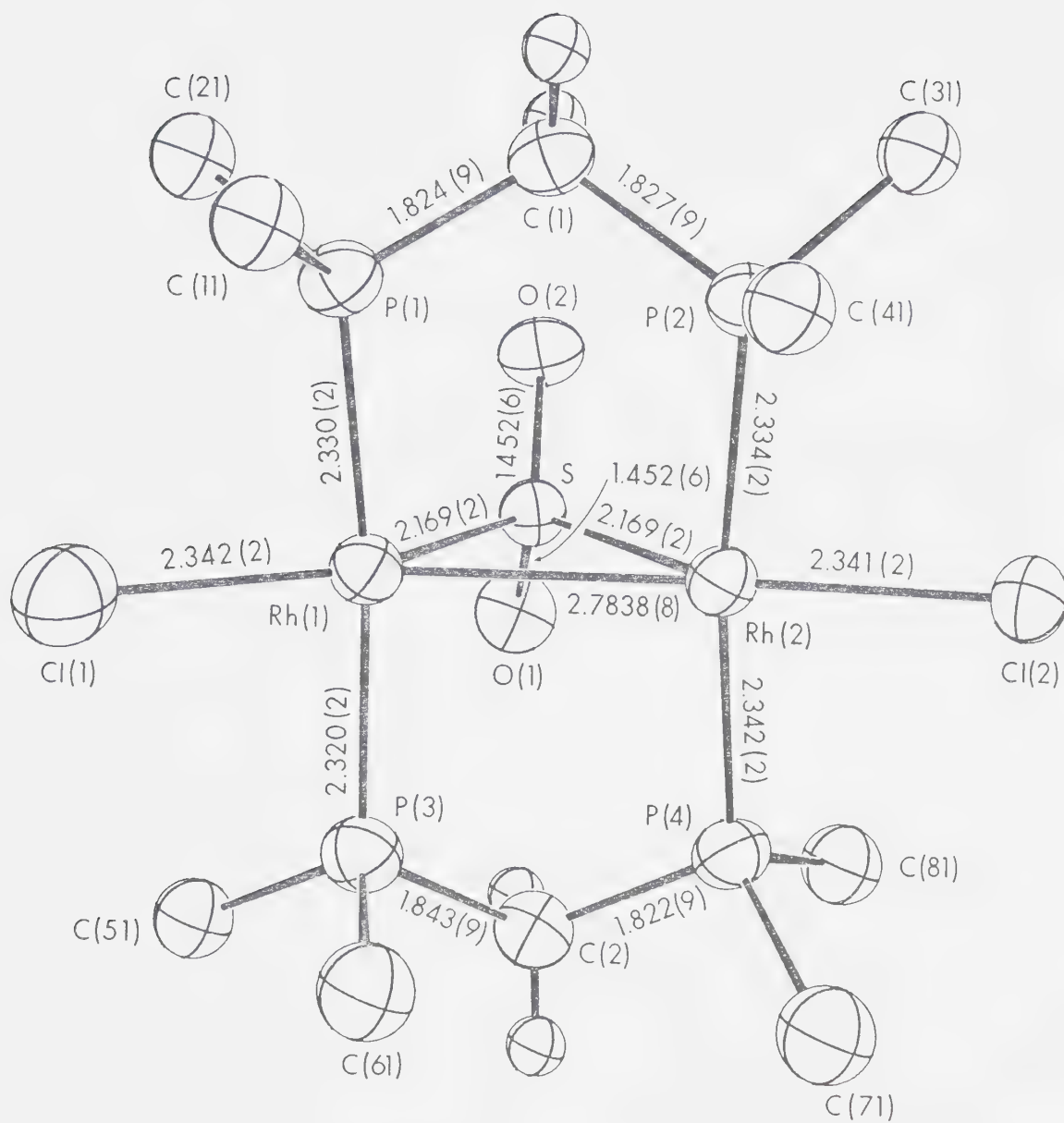


Figure 14. The Inner Coordination Sphere of  $[\text{Rh}_2\text{Cl}_2-(\mu\text{-SO}_2)(\text{DPM})_2]$ .





## DISCUSSION

### Description of Structure

The complex,  $[\text{Rh}_2\text{Cl}_2(\mu\text{-SO}_2)(\text{DPM})_2]$ , displays a distorted "A-frame" geometry, similar to that displayed by the palladium analogue  $[\text{Pd}_2\text{Cl}_2(\mu\text{-SO}_2)(\text{DPM})_2]$ <sup>85</sup> (apart from the metal-metal bond in the present species). The "A" configuration is described by the chloro and sulfur dioxide ligands in the equatorial plane, with the apical position occupied by the bridging  $\text{SO}_2$  ligand. Both rhodium centres are bridged by two DPM ligands, which are mutually trans and approximately perpendicular to the equatorial plane. The distortion from the idealized "A-frame" structure which would have the terminal Cl ligands trans to the bridging  $\text{SO}_2$  ligand results both from close nonbonded contacts between the chloro ligands and the phenyl rings and from the presence of the Rh-Rh bond (see Figure 13 and Table 24). Therefore, unlike other "A-frame" complexes which have approximately square planar coordination at the metals, the present complex exhibits a highly distorted trigonal-bipyramidal metal environment with the average S-Rh-Rh, S-Rh-Cl and Cl-Rh-Rh angles (50.07(6), 142.9(5) and 166.7(5)°, respectively, see Table 25) deviating significantly from the idealized 120° value.

The Rh-Rh distance of 2.7838(9) Å is consistent with a normal Rh-Rh single bond, falling within the range previously reported for such distances (2.617(3)-2.8415(7) Å).<sup>35,126-133</sup>



The present value can be compared to that observed in the related Rh-Rh bonded tricarbonyl species  $[\text{Rh}_2(\text{CO})_2(\mu\text{-CO})-(\mu\text{-Cl})(\text{DPM})_2]^+$   $(2.8415(7)\text{\AA})^{35}$  and can be contrasted to the distances of  $3.1520(8)$  and  $3.155(4)\text{\AA}$ , respectively, for  $[\text{Rh}_2(\text{CO})_2(\mu\text{-Cl})(\text{DPM})_2]^+$   $^{120}$  and  $[\text{Rh}_2(\text{CO})_2(\mu\text{-S})(\text{DPM})_2]$ ,  $^{89}$  in which no Rh-Rh bond is present.

The geometry of the bridging  $\text{SO}_2$  ligand is consistent with a Rh-Rh bonded system. Thus the acute Rh-S-Rh angle of  $79.84(7)^\circ$  indicates compression along the Rh-Rh axis and is comparable to other such values obtained when  $\text{SO}_2$  bridges a metal-metal bond ( $72.6(1) - 75.6(2)^\circ$ )  $^{60,134-136}$  but is significantly smaller than the range in M-S-M angles observed ( $91.2(2) - 118.0(2)^\circ$ )  $^{64,85,137}$  when  $\text{SO}_2$  bridges two metal atoms which are not bonded to each other. The bonding in this  $\text{SO}_2$  ligand is symmetrical (Rh(1)-S = Rh(2) - S =  $2.169(2)\text{\AA}$ ) and these Rh-S distances are significantly shorter than the metal-sulfur distances observed in other sulfur dioxide bridged complexes of the second and third row platinum metals ( $[\text{Pd}_2\text{Cl}_2(\mu\text{-SO}_2)(\text{DPM})_2]$ , Pd-S =  $2.234(3)$  and  $2.240(3)\text{\AA}$ ;  $^{85}$   $[\text{IrH}(\text{CO})_2(\text{PPh}_3)_2]\text{SO}_2$ , Ir-S =  $2.313\text{\AA}$ ;  $^{60}$   $[\text{Pd}_3(\text{SO}_2)_2(t\text{-BuNC})_5]$ , Pd-S (av.) =  $2.261(9)\text{\AA}$ ;  $^{138}$  and  $[\text{Pt}_3(\text{SO}_2)_3(\text{PPh}_3)_3]$ , Pt-S(av.) =  $2.275(5)\text{\AA}$ ).  $^{136}$  The S-O distances of  $1.452(6)\text{\AA}$  and the O-S-O angle of  $111.9(4)^\circ$  compare well with other determinations in which  $\text{SO}_2$  acts as either a bridging or a terminal ligand  $^{52,134-138}$  and can be compared to the analogous parameters in free  $\text{SO}_2$



(1.431(1) Å and 119.0(5)°, respectively).<sup>139</sup> The differences between free and coordinated SO<sub>2</sub> can be attributed to back donation into SO<sub>2</sub> orbitals which are slightly bonding with respect to the O-O interaction and antibonding with respect to the S-O interactions.<sup>52</sup> However, more simply they reflect the change from sp<sup>2</sup> to sp<sup>3</sup> hybridization about the sulfur atom. The Rh-S-O angles are also close to the expected tetrahedral values.

The Rh-Cl distances of 2.342(2) and 2.341(2) Å are not unusual; however they are somewhat shorter than those typically observed (range 2.355(2) - 2.386(3) Å)<sup>31,122,123,140</sup> for rhodium (I) phosphine complexes.

Within the Rh-DPM framework most parameters are usual. The Rh-P distances (average 2.331(9) Å)<sup>124</sup> are within the range normally observed when phosphine ligands are mutually trans,<sup>35,85,89,117,120</sup> and the P-C distances (both methylene and phenyl) compare well with other determinations.<sup>35,85,89,120</sup> The methylene carbon atoms of the bridging DPM ligand are folded in a cis configuration towards the sulfur dioxide ligand (see Table 23 and Figure 13). This orientation of the methylene groups allows the phenyl groups to stagger themselves with respect to the terminal chloro ligands in the equatorial plane (see Cl-Rh-P phenyl torsion angles, Table 25) and also places four of the eight phenyl rings in the open positions around the bridging site. Viewed down the Rh-Rh axis the Rh-P vectors are slightly staggered with



respect to one another as can be seen from the P-Rh-Rh-P torsion angles of  $6.31(8)^\circ$  and  $7.60(9)^\circ$ . This observed twist in the Rh-DPM framework thrusts rings 4 and 6 further into the enclosed bridging site, effectively blocking this site and resulting in short Rh-H nonbonded contacts ( $\text{Rh}(1) - \text{H}(66) = 2.70 \text{ \AA}$  and  $\text{Rh}(2) - \text{H}(46) = 2.73 \text{ \AA}$ ). Although the enclosed site is effectively blocked by these phenyl rings, the exposed terminal sites are conspicuously vacant and open to attack by small molecules.

Transformation of  $[\text{Rh}_2(\text{CO})_2(\mu\text{-Cl})(\mu\text{-SO}_2)(\text{DPM})_2]^+$  to  $[\text{Rh}_2\text{Cl}_2(\mu\text{-SO}_2)(\text{DPM})_2]$

The reaction of the parent "A-frame" complex, as the  $\text{BPh}_4^-$  salt, 1a, with sulfur dioxide yields initially the sulfur dioxide adduct  $[\text{Rh}_2(\text{CO})_2(\mu\text{-SO}_2)(\mu\text{-Cl})(\text{DPM})_2][\text{BPh}_4]$  3a (see Figure 11). The assignment of this structure is based on (1) the infrared spectrum which is similar to that of the carbonyl adduct 2a, which has been characterized by an X-ray structural determination;<sup>35</sup> (2) the  $\text{SO}_2$  bands in the infrared spectrum at  $1230$  and  $1070 \text{ cm}^{-1}$  which are in the region observed for other  $\text{SO}_2$  ligands bridging metal-metal bonded centres;<sup>60,138</sup> (3) the  $^{31}\text{P}\{^1\text{H}\}$  NMR spectrum which displays only one phosphorus environment; (4) satisfactory elemental analysis; and (5) treatment of a solution of 3a with dinitrogen which leads to  $\text{SO}_2$  loss and isolation of the parent species 1a.





Prolonged treatment of a solution of  $\underline{3a}$  with  $\text{SO}_2$  resulted in an apparent disproportionation reaction yielding  $[\text{Rh}_2\text{Cl}_2(\mu\text{-SO}_2)(\text{DPM})_2]$  ( $\underline{4}$ ) as a brown microcrystalline solid and a yellow solution containing the other unidentified disproportionation product(s). Subsequent attempts to repeat the above reaction have shown that it is not a simple disproportionation reaction. When the reaction was repeated using the pure parent "A-frame", which had been recrystallized several times, it was found that the reaction stopped at the sulfur dioxide adduct  $\underline{3a}$ . Whereas when  $\underline{1a}$  was purified by only a single crystallization or if the reaction was carried out in situ without purification of  $\underline{1a}$ , the transformation of compound  $\underline{3a}$  to  $\underline{4}$  proceeded to completion in about 4 h. This suggested the involvement of an impurity in the reaction yielding compound  $\underline{4}$ .

Since  $[\text{RhHCl}(\text{DPM})_2][\text{BPh}_4]$  was known to be an impurity in some preparations of  $\underline{1a}$ ,<sup>141</sup> this species was added to solutions of  $\underline{3a}$  to assess its effect on the above reaction. It was found however, that even when present in equimolar amounts this hydrido complex had no apparent effect on the reaction rate.

Another potential impurity is the  $[\text{RhCl}_2(\text{CO})_2]^-$  anion, which is generated as the counter ion in the initial preparation of  $[\text{Rh}_2(\text{CO})_2(\mu\text{-Cl})(\text{DPM})_2]^+$  (see Chapter II). An ion exchange was then performed to replace this anion with  $\text{BPh}_4^-$ . However, if exchange is incomplete, trace amounts



of  $[\text{Rh}(\text{Cl})_2(\text{CO})_2]^-$  may be present. To test the possible involvement of the  $[\text{RhCl}_2(\text{CO})_2]^-$  anion, we treated the complex  $[\text{Rh}_2(\text{CO})_2(\mu\text{-Cl})(\text{DPM})_2][\text{RhCl}_2(\text{CO})_2]$ , 1c, with  $\text{SO}_2$ . Regardless of solvent, the transformation of 3 to 4 proceeded to completion in every case within 3 h. When traces of 1c were added to pure 1a, this reaction again occurred much more readily than with only pure 1a, suggesting the involvement of the  $[\text{RhCl}_2(\text{CO})_2]^-$  anion as a chloride transfer agent in the reaction. It has already been shown by Balch and co-workers<sup>142</sup> that the dimer  $[\text{RhCl}(\text{CO})_2]_2$  abstracts chloride anion from *trans*- $[\text{RhCl}(\text{CO})(\text{DAM})]_2$  to give  $[\text{Rh}_2(\text{CO})_2(\mu\text{-Cl})(\text{DAM})_2]^+$  and  $[\text{RhCl}_2(\text{CO})_2]^-$ . It is not unreasonable to expect therefore that a similar process is occurring in the transformation of 3 to 4. In fact a model of  $[\text{Rh}_2(\text{CO})_2(\mu\text{-CO})(\mu\text{-Cl})(\text{DPM})_2][\text{RhCl}_2(\text{CO})_2]$ , constructed from data made available to us by Professor Balch,<sup>142,143</sup> shows that the anion approaches the tricarbonyl cationic species (which we assume is structurally similar to complex 3a), in such an orientation that chloride transfer from the anion to the cation is very feasible. We believe that the species resulting from  $\text{Cl}^-$  transfer by  $[\text{RhCl}_2(\text{CO})_2]^-$ , i.e.,  $[\text{RhCl}(\text{CO})_2]$  or the dimer  $[\text{RhCl}(\text{CO})_2]_2$ , then abstracts a chloride ion from another cationic species 3a to restart the process, resulting in a net chloride transfer reaction. The rhodium-DPM species produced is presumably a neutral dichlorodicarbonyl, sulfur



dioxide bridged species,  $[\text{Rh}_2\text{Cl}_2(\text{CO})_2(\mu\text{-SO}_2)(\text{DPM})_2]$ , which then loses CO to yield complex 4.

It is not surprising that the relatively small species  $[\text{RhCl}_2(\text{CO})_2]^-$  is accomplishing the chloride transfer as opposed to any species containing the bulky DPM ligand. Of course when the chloride ion is added directly to a solution of 3a, evaporation of this solution under a  $\text{SO}_2$  atmosphere results in quantitative conversion of 3a to 4. Therefore the conversion of complex 3a into 4 occurs in the presence of any chloride ion source. It is also of interest at this stage to note the differences between  $\text{SO}_2$  and CO in these systems. In the presence of a chloride ion source the  $\text{SO}_2$  adduct 3a is unstable, yielding complex 4, whereas the analogous tricarbonyl species  $[\text{Rh}_2(\text{CO})_2(\mu\text{-CO})(\mu\text{-Cl})(\text{DPM})_2][\text{X}]$ ,  $\text{X} = \text{Cl}^-$  (vide infra) or  $[\text{RhCl}_2(\text{CO})_2]^-$ ,<sup>142</sup> are stable and readily isolated. Two possible reasons are suggested for this difference. The bridging  $\text{SO}_2$ , we believe withdraws more electron density from the metals than the bridging CO ligands. This favours nucleophilic  $\text{Cl}^-$  attack on the  $\text{SO}_2$  adduct. Another significant difference lies in the orientation of the methylene carbon atoms of the DPM ligands. Structural studies have shown that the methylene groups fold towards the more bulky bridging equatorial group. In the carbonyl adduct this is the Cl ligand, whereas in the  $\text{SO}_2$  adduct the bulkier group is the  $\text{SO}_2$  ligand. Thus, methylene orientation in the  $\text{SO}_2$  adduct may



lead to a more favourable orientation of the phenyl rings allowing easier access of the chloride donor to the metal center.

Efforts at characterizing the other so-called disproportionation products have met with little success. On the basis of  $^{31}\text{P}\{^1\text{H}\}$  NMR spectra of the products in this reaction, we find, in addition to resonances due to  $\tilde{4}$ , that at least three other unidentified resonances occur. The sum of their integrated intensities is approximately equal to that of complex  $\tilde{4}$ . It seems therefore that the second product in the reaction, species  $\tilde{5}$ , is unstable and is reacting further to yield the species observed in the NMR experiment. This is consistent with the fact that the relative intensities of the bands in the infrared spectra of the yellow product changed from sample to sample. However, it was noted that no carbonyl species was ever observed in the infrared spectra of the final yellow product.

#### Reaction of $[\text{Rh}_2\text{Cl}_2(\mu\text{-SO}_2)(\text{DPM})_2]$ with CO

Reaction of  $\tilde{4}$  with CO, was initially believed to yield the tricarbonyl species *cis*- $[\text{Rh}_2\text{Cl}_2(\text{CO})_2(\mu\text{-CO})(\text{DPM})_2]$ .<sup>96a</sup> However further investigations have shown that this tricarbonyl species is actually  $[\text{Rh}_2(\text{CO})_2(\mu\text{-CO})(\mu\text{-Cl})(\text{DPM})_2]\text{-}[\text{Cl}]$ ,  $\tilde{2b}$ , (see Figure 15). It is a 1:1 electrolyte in acetone and dichloromethane solutions, its  $^{31}\text{P}\{^1\text{H}\}$  NMR spectrum is identical to that of the  $\text{BPh}_4^-$  salt, whose structure has been determined,<sup>35</sup> and its infrared spectrum is





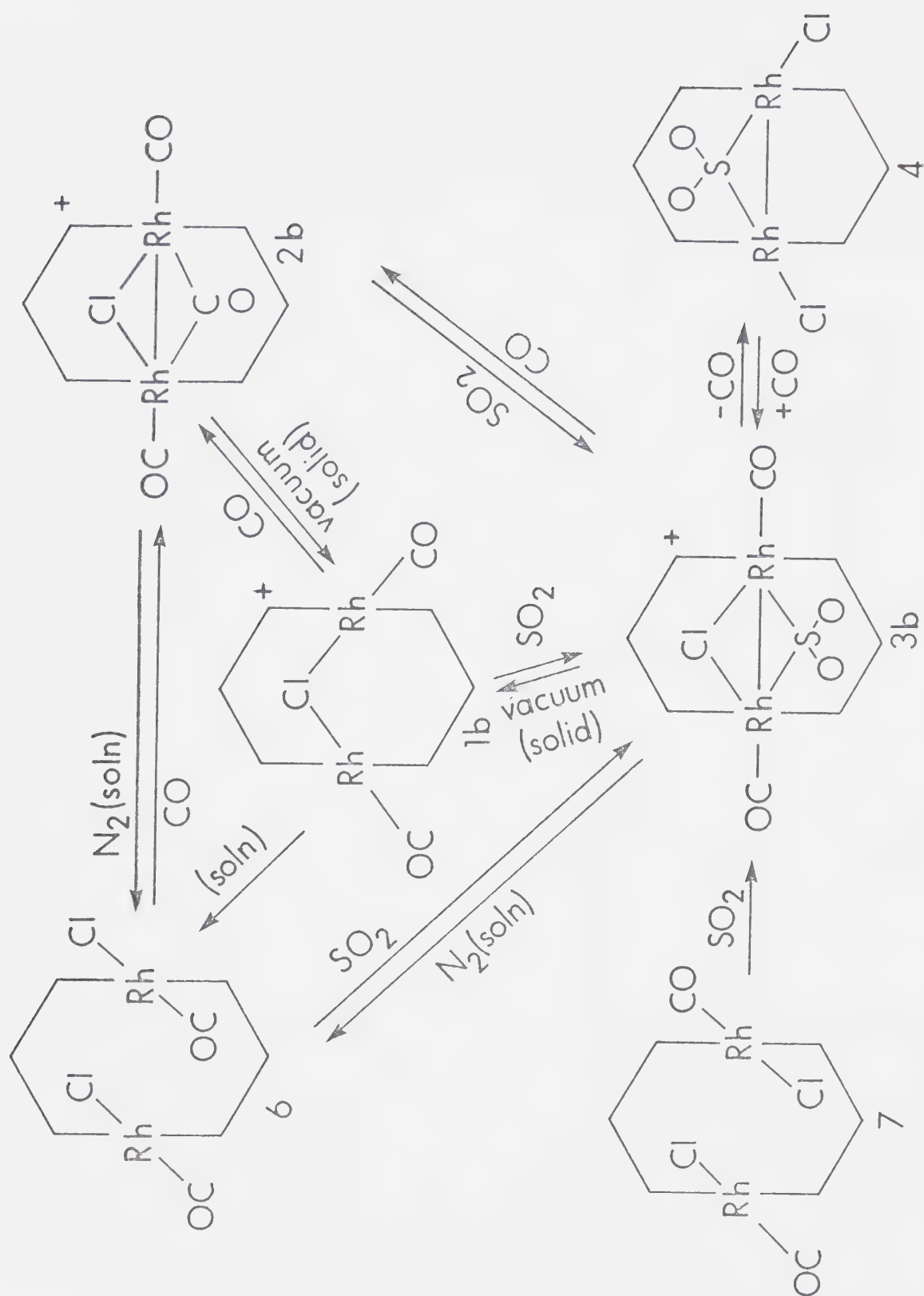


Figure 15. A Reaction Scheme for Binuclear Rh-DPM Complexes with CO and SO<sub>2</sub>.



also similar to that of the  $\text{BPh}_4^-$  salt. Under vacuum, a solid sample of  $\underline{2b}$  loses the bridging carbonyl ligand as indicated by its infrared spectrum, which is essentially identical with that of  $\underline{1a}$  (see Table 18). This species can therefore be formulated as  $[\text{Rh}_2(\text{CO})_2(\mu\text{-Cl})(\text{DPM})_2][\text{Cl}]$  ( $\underline{1b}$ ). A solution of  $\underline{1b}$ , however is a nonelectrolyte, and it is believed that recoordination of the chloride ion occurs such that the species present in solution is actually *cis*- $[\text{RhCl}(\text{CO})(\text{DPM})]_2$  ( $\underline{6}$ , see Figure 15). Complex  $\underline{6}$  can also be obtained directly by bubbling  $\text{N}_2$  through a solution of  $\underline{2b}$ . The infrared spectra of  $\underline{6}$  and  $\underline{1b}$  are markedly different and furthermore the  $^{31}\text{P}\{^1\text{H}\}$  NMR spectrum of  $\underline{6}$  is not similar to that of the  $\text{BPh}_4^-$  "A-frame" complex  $\underline{1a}$ . This together with the conductivity differences between  $\underline{1a}$  and  $\underline{6}$  supports our assignment of this species as *cis*- $[\text{RhCl}(\text{CO})(\text{DPM})]_2$ . In addition, the infrared spectrum and elemental analysis of  $\underline{6}$  are essentially identical with those of the trans analogue  $\underline{7}$ . Our formulation of  $\underline{6}$  as the cis species instead of the trans isomer is based on chemical differences. Complex  $\underline{6}$  is soluble in  $\text{CH}_2\text{Cl}_2$  and acetone whereas the trans analogue  $\underline{7}$  is extremely insoluble. Furthermore,  $\underline{6}$  reacts readily and reversibly with CO in  $\text{CH}_2\text{Cl}_2$  to give  $\underline{2b}$ , whereas  $\underline{7}$  does not react even after extended periods of time. However, unambiguous assignment of complex  $\underline{6}$  as the cis species must await a structural determination. The *trans*-DAM analogue, *trans*- $[\text{RhCl}(\text{CO})(\text{DAM})]_2$ , has been observed to crystallize in different



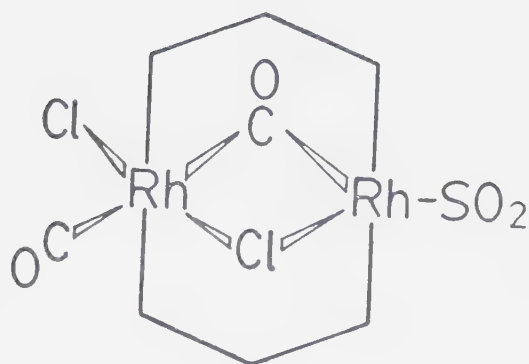
forms,<sup>31,125</sup> therefore  $\tilde{6}$  may be another crystalline modification of  $\tilde{7}$ .

Both the cis and trans species ( $\tilde{6}$  and  $\tilde{7}$ , respectively) react with  $\text{SO}_2$  to yield the species  $[\text{Rh}_2(\text{CO})_2(\mu\text{-Cl})(\mu\text{-SO}_2)(\text{DPM})_2][\text{Cl}]$ ,  $\tilde{3b}$ , which is assigned this structure on the basis of its conductivity (1:1 electrolyte) and its  $^{31}\text{P}\{^1\text{H}\}$  NMR spectrum which shows only one phosphorus environment and which is identical with that of its  $\text{BPh}_4^-$  analogue  $\tilde{3a}$  (vide supra). In addition, when solutions of  $\tilde{6}$  and  $\tilde{7}$  are treated for prolonged periods of time with  $\text{SO}_2$ , complex  $\tilde{4}$  is obtained (see Figure 15).

#### Reaction of *trans*- $[\text{RhCl}(\text{CO})(\text{DPM})]_2$ with $\text{SO}_2$

The reaction of the trans species ( $\tilde{7}$ ) with  $\text{SO}_2$  has been studied by monitoring, using infrared spectroscopy, the slow stepwise addition of  $\text{SO}_2$ . Initially species are observed which contain bridging carbonyl ligands ( $\nu_{\text{CO}} = 1740 \text{ cm}^{-1}$ ). Upon completion of the reaction none of these species is observed; instead only the symmetric  $\text{SO}_2$ -bridged species  $\tilde{3b}$  remains. In addition a solution containing the initially formed product of the  $\text{SO}_2$  reaction with  $\tilde{7}$  is nonconducting for several minutes (although on the basis of spectral and colour changes it is obvious that a reaction has occurred) after which it becomes a 1:1 electrolyte. The above data are consistent with terminal attack of  $\text{SO}_2$  and formation of an intermediate species of the form:





This species is then believed to lose  $\text{Cl}^-$  and to rearrange to the final product  $\underline{3b}$ , having a bridging  $\text{SO}_2$  ligand. The possibility that the carbonyl vibration at  $1740\text{ cm}^{-1}$  is due to the monocarbonyl species  $[\text{Rh}_2\text{Cl}_2(\mu\text{-CO})(\text{DPM})_2]$  (see Chapter V), which was observed in the analogous reaction with  $\text{CS}_2$  at intermediate times, is ruled out since this species is never detected in the  $^{31}\text{P}$  NMR spectra of this reaction.

#### Site of $\text{SO}_2$ attack in $[\text{Rh}_2(\text{CO})_2(\mu\text{-Cl})(\text{DPM})_2]^+$

In these "A-frame" species, there are two potential sites of attack, either directly at the enclosed site, bridging the metal centres, or at a terminal, exposed position remote from the bridging site. It has been shown that CO attacks  $\underline{1a}$  terminally, forcing one of the previously coordinated ligands into the bridging site.<sup>35,91</sup> Likewise CO appears to attack the  $\text{SO}_2$  "A-frame" complex  $\underline{4}$  terminally since no evidence is obtained for attack at





the bridging site. In contrast,  $\text{SO}_2$  appears to attack complex 1 directly at the bridging site, which has been shown by the structural determination of  $[\text{Rh}_2(\text{CO})_2(\mu\text{-Cl})\text{-(DPM)}_2][\text{BF}_4]$  to be open<sup>120</sup> (see Chapter II). Spectroscopic evidence supports  $\text{SO}_2$  attack at the bridging site. The infrared spectra obtained during the slow stepwise addition of  $\text{SO}_2$  to 1a displayed no bands assignable to bridging carbonyl species. On the basis of the analogous reaction of 1 with CO and of the reaction of the *trans*-dichloro-dicarbonyl species 7 with  $\text{SO}_2$  (vide supra), both of which occur by terminal attack, we would have anticipated observing species with bridging CO bands in the infrared spectra, if attack of  $\text{SO}_2$  on 1 were also terminal. Furthermore even at  $-50^\circ\text{C}$  when the reaction is monitored by  $^{31}\text{P}\{^1\text{H}\}$  NMR techniques the only resonances observed are assignable to the symmetric species 1a and 3a. If attack were terminal, it is anticipated that resonances assignable to an asymmetrical species would be observed. We believe therefore that, on the basis of the above data, terminal attack of 1 with  $\text{SO}_2$  can be ruled out, since no asymmetric species were detected. Furthermore we feel that it is unlikely that a facile rearrangement is operating since no simple rearrangement mechanism can be devised that would readily yield the symmetric bridged species 3a from terminal attack. The reasons for the varying modes of CO and  $\text{SO}_2$  in complex 1 is at the present time not obvious, although



attack by the better  $\pi$ -acid ( $\text{SO}_2$ ) would be favoured at the bridging site since in this site both electron rich metals can donate electron density to this ligand.



## CHAPTER V.

### Unusual Structural and Chemical Trends Within a Series of Binuclear Rhodium Carbonyl Halide Complexes

#### INTRODUCTION

The reaction of  $\text{SO}_2$  with *trans*- $[\text{RhCl}(\text{CO})(\text{DPM})]_2$  (1) and *trans*- $[\text{RhCl}(\text{CO})(\text{DAM})]_2$  (2) is believed to proceed through an intermediate of the form  $[\text{Rh}_2\text{Cl}(\text{CO})(\text{SO}_2)(\mu\text{-Cl})(\mu\text{-CO})(\text{L-L})_2]$  ( $\text{L-L} = \text{DPM or DAM}$ )<sup>96</sup> (Chapter IV). However, this intermediate is short lived in the case of DPM and is not observed in the case of DAM, making definitive characterization impossible. Since the stabilities of these intermediates appear to change on going from DPM to DAM as the bridging ligand, it was felt that by changing halides, it might have been possible to isolate this intermediate, as a result of the increased steric bulk of the bromo and iodo ligands slowing the rearrangement process. Therefore the preparation of the previously unreported *trans*- dibromo and *trans*-diiodo, DPM complexes and the *trans*-diiodo, DAM complex was attempted.

#### EXPERIMENTAL

Preparation of  $[\text{Rh}_2\text{I}(\text{CO})(\mu\text{-CO})(\text{DPM})_2][\text{I}]$ ,  $[\text{Rh}_2\text{Br}_2(\mu\text{-CO})(\text{DPM})_2]$  and  $[\text{Rh}_2\text{Cl}_2(\mu\text{-CO})(\text{DPM})_2]$

Typically 0.100 g of *trans*- $[\text{RhCl}(\text{CO})(\text{DPM})]_2$ <sup>66</sup> was suspended in 15 mL of  $\text{CH}_2\text{Cl}_2$  and to this a five fold excess of



the halide salt (NaBr, KI), in a minimum volume of methanol, was added. After *ca.* 12 h the solution was concentrated to about 15 mL then precipitated with diethyl ether and dried in vacuum, yielding  $[\text{Rh}_2\text{X}(\text{CO})(\mu\text{-CO})(\text{DPM})_2][\text{X}]$  ( $\text{X} = \text{Br}, \text{I}$ ). However in solution the bromo species undergoes CO loss at room temperature over a period of 24 h, or on refluxing in  $\text{CH}_2\text{Cl}_2$  for 2 h yielding  $[\text{Rh}_2\text{Br}_2(\mu\text{-CO})(\text{DPM})_2]$ . The analogous chloro complex,  $[\text{Rh}_2\text{Cl}_2(\mu\text{-CO})(\text{DPM})_2]$  was obtained as a red-brown species in solution on refluxing a toluene suspension of *trans*- $[\text{RhCl}(\text{CO})(\text{DPM})]_2$  for 12 h. Recrystallization of all species was from methylene chloride and diethyl ether. Typical yields were from 70 to 90%. Elemental analyses:  $[\text{Rh}_2\text{Br}_2(\mu\text{-CO})(\text{DPM})_2]$ :  $\text{C}_{51}\text{H}_{44}\text{Br}_2\text{O}_1\text{P}_4\text{Rh}_2$ ; calc. C, 52.70; H, 3.81; Br, 13.7: Found C, 52.3; H, 3.70; Br, 13.0:  $[\text{Rh}_2\text{I}(\text{CO})(\mu\text{-CO})(\text{DPM})_2][\text{I}]$ :  $\text{C}_{52}\text{H}_{44}\text{I}_2\text{O}_2\text{P}_4\text{Rh}_2$ ; calc. C, 48.62; H, 3.45: Found C, 48.25; H, 3.51. See Table 26 for spectral data.

### Reactions with $\text{SO}_2$ and $\text{CO}$

#### (a) Dicarbonyl Species

Typically 0.100 g of  $[\text{RhX}(\text{CO})(\text{DPM})]_2$  or  $[\text{RhX}(\text{CO})(\text{DAM})]_2$  ( $\text{X} = \text{Cl}, \text{Br}, \text{I}$ ) in 15 mL of  $\text{CH}_2\text{Cl}_2$  was treated with  $\text{SO}_2$  or  $\text{CO}$  for 10 min, the volume was reduced under a stream of the reactant gas to about 7 mL and then the products were precipitated with diethyl ether saturated with the reactant





Table 26. Spectral Data for the Complexes

No.	Complex	Infrared Absorption Maxima (cm <sup>-1</sup> ) <sup>a</sup>	<sup>31</sup> P{ <sup>1</sup> H}nmr Chemical Shifts (ppm) <sup>b</sup>
3	[Rh <sub>2</sub> Br(μ-CO)(CO)(DPM) <sub>2</sub> ][Br]	1958(s), 1800(m)	25.0 (multiplet)
4a	[Rh <sub>2</sub> Cl <sub>2</sub> (μ-CO)(DPM) <sub>2</sub> ]	1745(s)	19.7 (115.9 Hz)
4b	[Rh <sub>2</sub> Br <sub>2</sub> (μ-CO)(DPM) <sub>2</sub> ]	1745(s)	19.4 (114.7 Hz)
5	[Rh <sub>2</sub> I(μ-CO)(CO)(DPM) <sub>2</sub> ][I]	1955(s), 1810(m)	21.5 (multiplet)
6,7	[Rh <sub>2</sub> I <sub>2</sub> (CO) <sub>2</sub> (DAM) <sub>2</sub> ]	1965(sh), 1940(s), 1820(m)	-
9a	[Rh <sub>2</sub> (CO) <sub>2</sub> (μ-CO)(μ-Cl)(DPM) <sub>2</sub> ][Cl]	2004(m), 1960(s), 1868(m)	29.8 (94.0)
9b	[Rh <sub>2</sub> (CO) <sub>2</sub> (μ-CO)(μ-Br)(DPM) <sub>2</sub> ][Br]	2005(m), 1968(s), 1865(m)	28.7 (93.8)
9c	[Rh <sub>2</sub> (CO) <sub>2</sub> (μ-CO)(μ-I)(DPM) <sub>2</sub> ][I]	1990(sh), 1970(s), 1860(m)	26.6 (92.7)
10a	[Rh <sub>2</sub> (CO) <sub>2</sub> (μ-SO <sub>2</sub> )(μ-Cl)(DPM) <sub>2</sub> ][Cl]	2010(s), 1980(sh), 1230(m), 1070(m)	24.5 (91.6)
10b	[Rh <sub>2</sub> (CO) <sub>2</sub> (μ-SO <sub>2</sub> )(μ-Br)(DPM) <sub>2</sub> ][Br]	2005(s), 1970(sh), 1230(m), 1085(m)	27.0 (90.6)
10c	[Rh <sub>2</sub> (μ-SO <sub>2</sub> )(μ-I)(CO) <sub>2</sub> (DPM) <sub>2</sub> ][I]	2005(m), 1990(s), 1210(m), 1065(m)	26.0 (90.3)
11	[Rh <sub>2</sub> (CO) <sub>2</sub> (μ-CO)(μ-I)(DAM) <sub>2</sub> ][I]	2005(m), 1958(s), 1860(m)	-
12	[Rh <sub>2</sub> (CO) <sub>2</sub> (μ-SO <sub>2</sub> )(μ-I)(DAM) <sub>2</sub> ][I]	1985(s), 1205(m), 1065(m)	-
13a	[Rh <sub>2</sub> Cl <sub>2</sub> (μ-SO <sub>2</sub> )(DPM) <sub>2</sub> ]	1191(m), 1063(s)	19.6 (113.5)
13b	[Rh <sub>2</sub> Br <sub>2</sub> (μ-SO <sub>2</sub> )(DPM) <sub>2</sub> ]	1190(m), 1060(s)	21.1 (113.6)

<sup>a</sup>Infrared spectra were run as nujol mulls on KBr plates; s, strong; m, medium; w, weak; sh, shoulder.

<sup>b</sup><sup>31</sup>P{<sup>1</sup>H}nmr chemical shifts are relative to H<sub>3</sub>PO<sub>4</sub> (downfield positive), coupling constants (<sup>1</sup>J<sub>Rh-P</sub> + <sup>x</sup>J<sub>Rh-P</sub>) are given in parentheses. The solvent used was CD<sub>2</sub>Cl<sub>2</sub>.



gas. Yields of the expected products,  $[\text{Rh}_2(\text{CO})_2(\mu\text{-L})(\mu\text{-X})(\text{DPM})_2][\text{X}]$  ( $\text{L} = \text{CO}, \text{SO}_2$ ;  $\text{X} = \text{Cl}, \text{Br}, \text{I}$ ) averaged *ca.* 75%. The reversibility of the  $\text{CO}$  and  $\text{SO}_2$  reactions were studied by dissolving the products of these reactions in  $\text{CH}_2\text{Cl}_2$  and bubbling  $\text{N}_2$  through the solution for up to 48 h.

### (b) Monocarbonyl Species

Typically 200 mg of sample was dissolved in 2 mL of  $\text{CD}_2\text{Cl}_2$  and the reactant gas introduced a bubble at a time. The  $^{31}\text{P}\{^1\text{H}\}$  NMR spectra were recorded, at  $-50^\circ\text{C}$ . After each addition of gas until no significant changes were observed. The infrared spectra were recorded in an analogous manner using 200 mg of sample in 20 mL of  $\text{CH}_2\text{Cl}_2$ .

## DISCUSSION

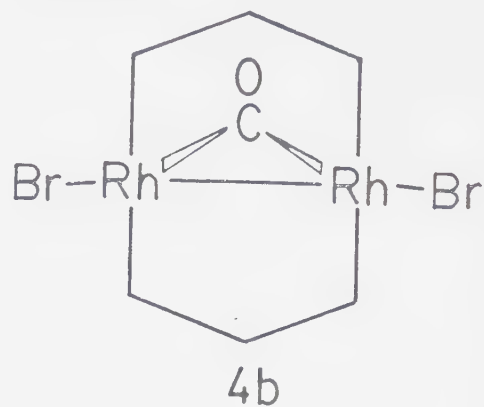
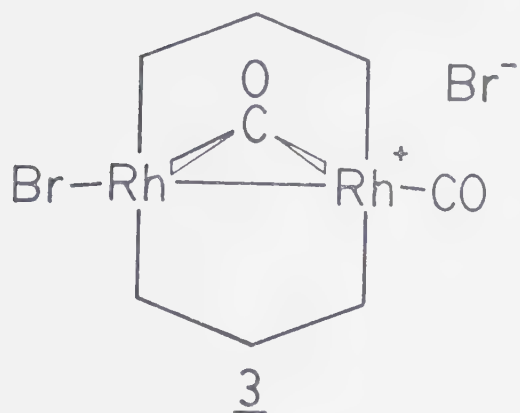
### Halide Exchange Reactions

The products of the halide exchange reactions show interesting chemical and structural trends which seem to depend on the steric bulk of the halide ligands and also on the crowding at the two metal centres as governed by the bridging DPM and DAM groups.

The reaction of *trans*- $[\text{RhCl}(\text{CO})(\text{DPM})]_2$  (1), with NaBr yields initially  $[\text{Rh}_2\text{Br}(\text{CO})(\mu\text{-CO})(\text{DPM})_2][\text{Br}]$  (3), a species with bands in the infrared spectrum at 1958 and 1800  $\text{cm}^{-1}$ , consistent with terminal and bridging carbonyl ligands. This species is a 1:1 electrolyte in acetone (70  $\text{ohm}^{-1} \text{cm}^{-2} \text{mole}^{-1}$ ) and its  $^{31}\text{P}\{^1\text{H}\}$  NMR spectrum, which is similar to the iodo species,



shown in Figure 16, (vide infra) indicates an asymmetric structure. This evidence coupled with elemental analysis leads to the formulation of 3 as shown below



In solution complex 3 recoordinates  $\text{Br}^-$  and undergoes CO loss, over a period of several hours, to yield  $[\text{Rh}_2\text{Br}_2(\mu\text{-CO})(\text{DPM})_2]$  (4b), which has been characterized by an X-ray structure determination<sup>144</sup> (see Chapter VI). The  $^{31}\text{P}\{^1\text{H}\}$  NMR spectrum of this species is shown in Figure 16 and is consistent with the symmetric structure observed in the solid state. All  $^{31}\text{P}\{^1\text{H}\}$  NMR parameters (Table 26) are in excellent agreement with those of the analogous species  $[\text{Rh}_2\text{X}_2(\mu\text{-SO}_2)(\text{DPM})_2]$  ( $\text{X} = \text{Cl}, \text{Br}$ ).<sup>96</sup> A solution of 4b is non conducting. The analogous chloro complex,  $[\text{Rh}_2\text{Cl}_2(\mu\text{-CO})(\text{DPM})_2]$  (4a) is obtained on refluxing a suspension of the *trans*-dichloro dicarbonyl species 1. This reaction has also been observed by Professor Balch and coworkers,<sup>143</sup> although it is not clear whether the species isolated by



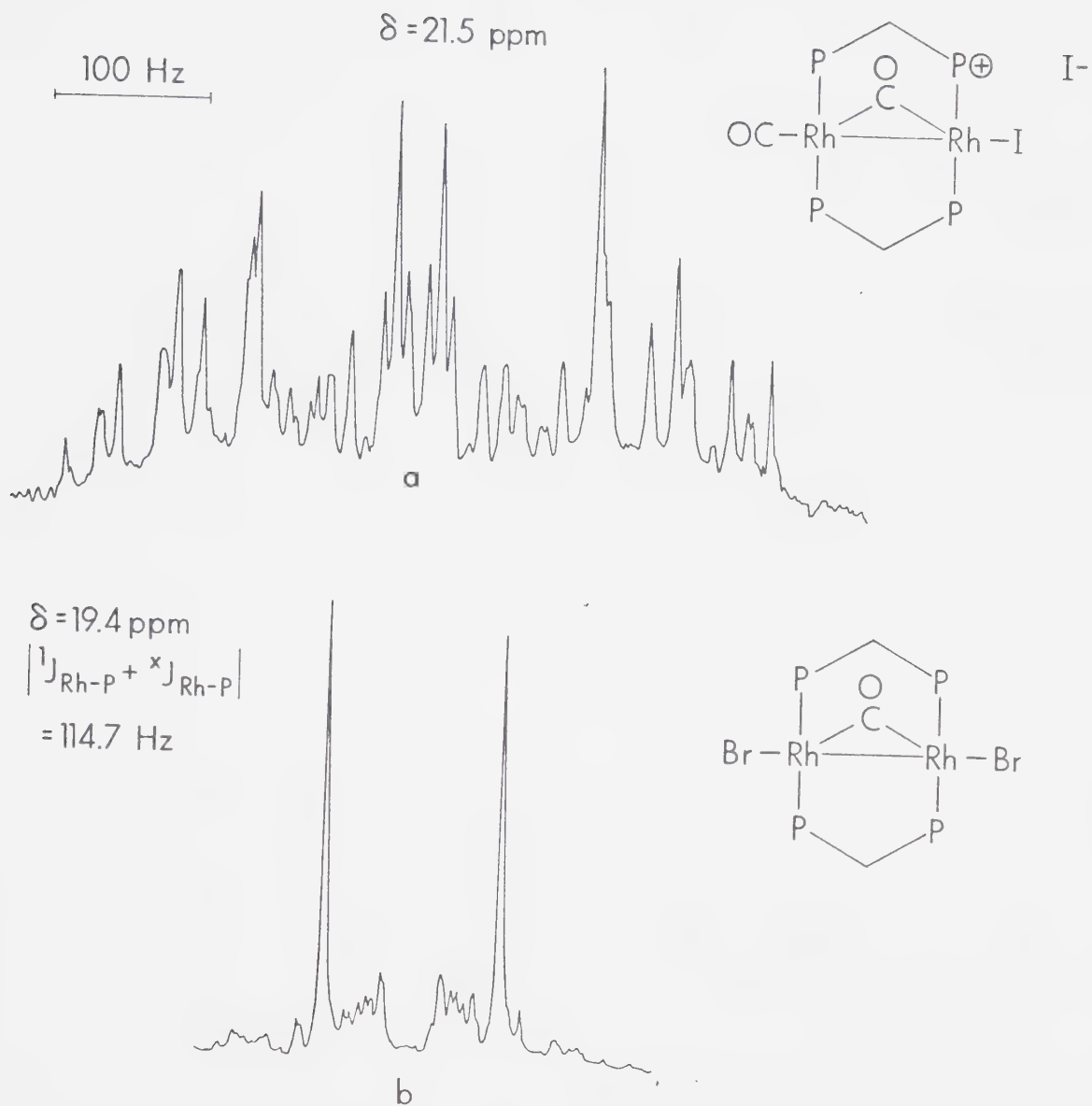


Figure 16. The  $^{31}\text{P}\{^1\text{H}\}$  NMR Spectra at 223 K of a)  $[\text{Rh}_2\text{I}(\text{CO})(\mu\text{-CO})(\text{DPM})_2]^+ [\text{I}]^-$  and b)  $[\text{Rh}_2\text{Br}_2(\mu\text{-CO})(\text{DPM})_2]$ .





these workers is identical to the one which we observe.

The reaction of 1 with KI yields  $[\text{Rh}_2\text{I}(\text{CO})(\mu\text{-CO})(\text{DPM})_2][\text{I}]$  (5), analogous to complex 3. The carbonyl bands in the infrared spectrum are observed at 1955 and 1810  $\text{cm}^{-1}$  and the  $^{31}\text{P}\{^1\text{H}\}$  NMR spectrum (Figure 16) is consistent with the asymmetric structure proposed. Complex 5 is a 1:1 electrolyte in solution. Unlike complex 3 however, complex 5 is stable under  $\text{N}_2$  in solution and does not undergo CO loss.

The bromo DAM species, *trans*- $[\text{RhBr}(\text{CO})(\text{DAM})]_2$ , is known and is probably structurally similar to *trans*-dichloro-dicarbonyl DAM species (2).<sup>66</sup> Iodide exchange on complex 2 yields a species which infrared studies and elemental analysis indicate is probably a mixture of the *trans*-diiodo-dicarbonyl complex, *trans*- $[\text{RhI}(\text{CO})(\text{DAM})]_2$  (6) and an asymmetric species  $[\text{Rh}_2\text{I}(\text{CO})(\mu\text{-CO})(\text{DAM})_2][\text{I}]$  (7), which is probably similar to the DPM species 5. The asymmetric species comprises about 75% of the product.

The structural trends observed in the above series of DPM and DAM halides is therefore consistent with steric bulk arguments indicating that the *trans* configuration of equatorial ligands, as observed in the dichloro species 1 and 2, and in *trans*- $[\text{RhBr}(\text{CO})(\text{DAM})]_2$ , is destabilized with bulkier halide ligands. The larger steric bulk of the bromo ligand, compared to the chloro ligand, does not favour simultaneous coordination of both bromo and both carbonyl ligands in the DPM complex and the asymmetric, ionic species



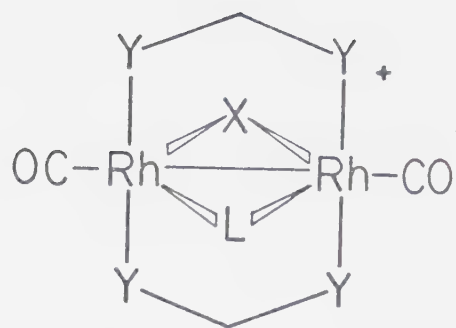
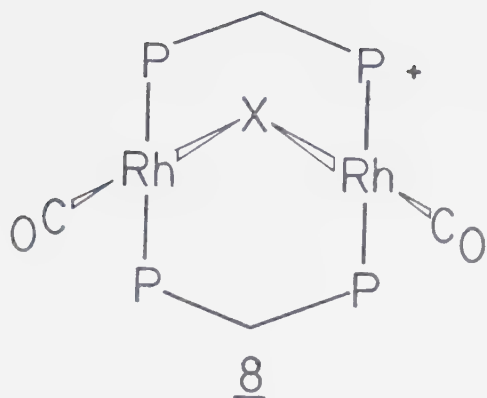
is formed initially. When bromide recoordination does occur it is accompanied by CO loss to give the monocarbonyl species 4b. With the DPM ligand, the stable iodo species is the asymmetric complex 5, again because simultaneous coordination of all iodo and carbonyl ligands is not favoured due to steric crowding. Furthermore, the large size of  $I^-$  does not favour its recoordination and CO loss is not observed in this species. The effect of the large DAM ligand is seen in the dibromo DAM species which still exists as the trans complex  $[RhBr(CO)(DAM)]_2$ , unlike its DPM analogue. The DAM ligand presumably allows more room to accommodate the larger bromo ligand. Even with the bulkier iodo ligand some *trans*- $[RhI(CO)(DAM)]_2$  6 is observed together with the asymmetric species 7.

#### Reactions with CO

##### i) Dicarbonyl Species

It is interesting that no evidence is seen for the symmetric "A-frame" species 8 ( $X = Br, I$ ), even though the reaction of 3 and 5 with CO and  $SO_2$  yield species 9 and 10, respectively, which are analogous to the products obtained (9a and 10a) by the reaction of 8a ( $X = Cl$ ) with these small molecules.<sup>35,91,96</sup> The  $^{31}P\{^1H\}$  NMR spectra of the tricarbonyl species 9b and 9c ( $X = Br, I$ , respectively,  $L = CO$ ) show one phosphine environment and are extremely similar to that of the chloro analogue,  $[Rh_2(CO)_2(\mu-CO)(\mu-Cl)(DPM)_2]^+$  9a, whose structure has been determined.<sup>35,142</sup> These DPM





9 L=CO, Y=P

10 L=SO<sub>2</sub>, Y=P

11 L=CO, Y=As, X=I

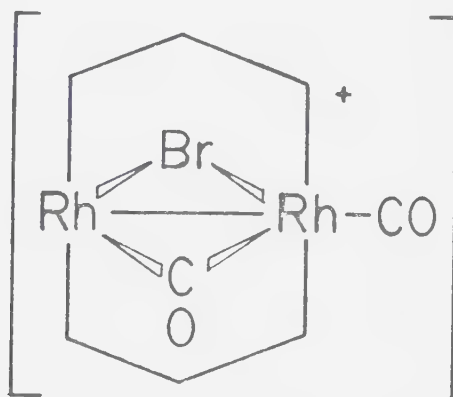
12 L=SO<sub>2</sub>, Y=As, X=I

tricarbonyl complexes show an interesting trend in  $^{31}\text{P}$  shifts and coupling constants (Cl, Br, I;  $\delta = 29.6, 28.7, 26.6$  ppm;  $|\text{}^1J_{\text{Rh-P}} + \text{}^xJ_{\text{Rh-P}}| = 94.2, 93.8, 92.7$  Hz, respectively). Furthermore, the infrared data for compounds 9a, 9b and 9c are all closely comparable. The complexes, *trans*-[RhX(CO)-(DAM)]<sub>2</sub> (X=Cl, Br), like their DPM chloro analogue, 1 show no reaction with CO under our conditions. Reaction of the mixture of iodo-DAM species 6 and 7 with CO however results in the isolation of a tricarbonyl species 11, which appears from its infrared spectrum, to be analogous to 9b and 9c.

An investigation of the ease of decarbonylation of complexes 9 shows a notable trend. The chloro complex 9a readily loses CO in solution under an N<sub>2</sub> stream or in the solid state under vacuum,<sup>35,91</sup> the bromo species 9b on the



other hand does not lose CO in the solid state under vacuum even after 72 h but loses it slowly in solution to give complex 3 and subsequently complex 4b. The iodo species 9c does not lose CO in either the solid state or in solution. The DAM-iodo species 11 undergoes CO loss slowly in solution under an N<sub>2</sub> stream. On decarbonylation of the bromo tricarbonyl species 9b, the complex initially produced is the asymmetric species 3. This is consistent with the findings of Mague and coworkers<sup>35,91</sup> which indicate that in the chlorotricarbonyl complex 9a, it is initially a terminal carbonyl group which is lost with the bridging carbonyl ligand then moving to the terminal site. Assuming the same mechanism for the bromo analogue, the intermediate species after carbonyl loss would then be:



Because of the large size of the bromo ligand it is this ligand which moves to the less sterically encumbered terminal site yielding species 3, whereas in the chloro





species migration of the carbonyl ligand is favoured, presumably for electronic reasons.

## ii) Monocarbonyl Species

Reaction of  $[\text{Rh}_2\text{X}_2(\mu\text{-CO})(\text{DPM})_2]$  ( $\text{X} = \text{Cl}$ ,  $\underline{4a}$ ;  $\text{X} = \text{Br}$ ,  $\underline{4b}$ ) with excess CO results in the formation of the tricarbonyl species  $\underline{9a}$  and  $\underline{9b}$ . When slow stepwise reaction of  $\underline{4b}$  with CO is monitored by  $^{31}\text{P}\{^1\text{H}\}$  NMR spectroscopy, resonances are observed which are assignable to the asymmetric dicarbonyl species  $\underline{3}$  and to the tricarbonyl complex  $\underline{9b}$ . Complex  $\underline{3}$  is observed throughout the reaction but only in trace amounts. In contrast, the monocarbonyl species is found in significant quantities until completion of the reaction. It seems therefore that CO reacts preferentially with  $\underline{3}$  compared to  $\underline{4b}$ .

If instead of reacting  $\underline{4a}$  with excess CO, the CO is added slowly, *trans*- $[\text{RhCl}(\text{CO})(\text{DPM})]_2$  ( $\underline{1}$ ) precipitates from solution (see Figure 17). The observation of two products ( $\underline{1}$  and  $\underline{9a}$ ) from slow and rapid addition, respectively, of CO suggests the presence of an intermediate dicarbonyl species,  $[\text{Rh}_2\text{Cl}(\text{CO})(\mu\text{-CO})(\text{DPM})_2][\text{Cl}]$   $\underline{3a}$ , analogous to the bromo species  $\underline{3}$ . We postulate that on slow CO addition attack of this intermediate by  $\text{Cl}^-$  occurs giving complex  $\underline{1}$ , whereas in the presence of excess CO (ie. during rapid CO addition), attack by CO predominates yielding instead the tricarbonyl species  $\underline{9a}$ . Based on our other work with related "A-frame" species<sup>96b,144</sup> and on a consideration of



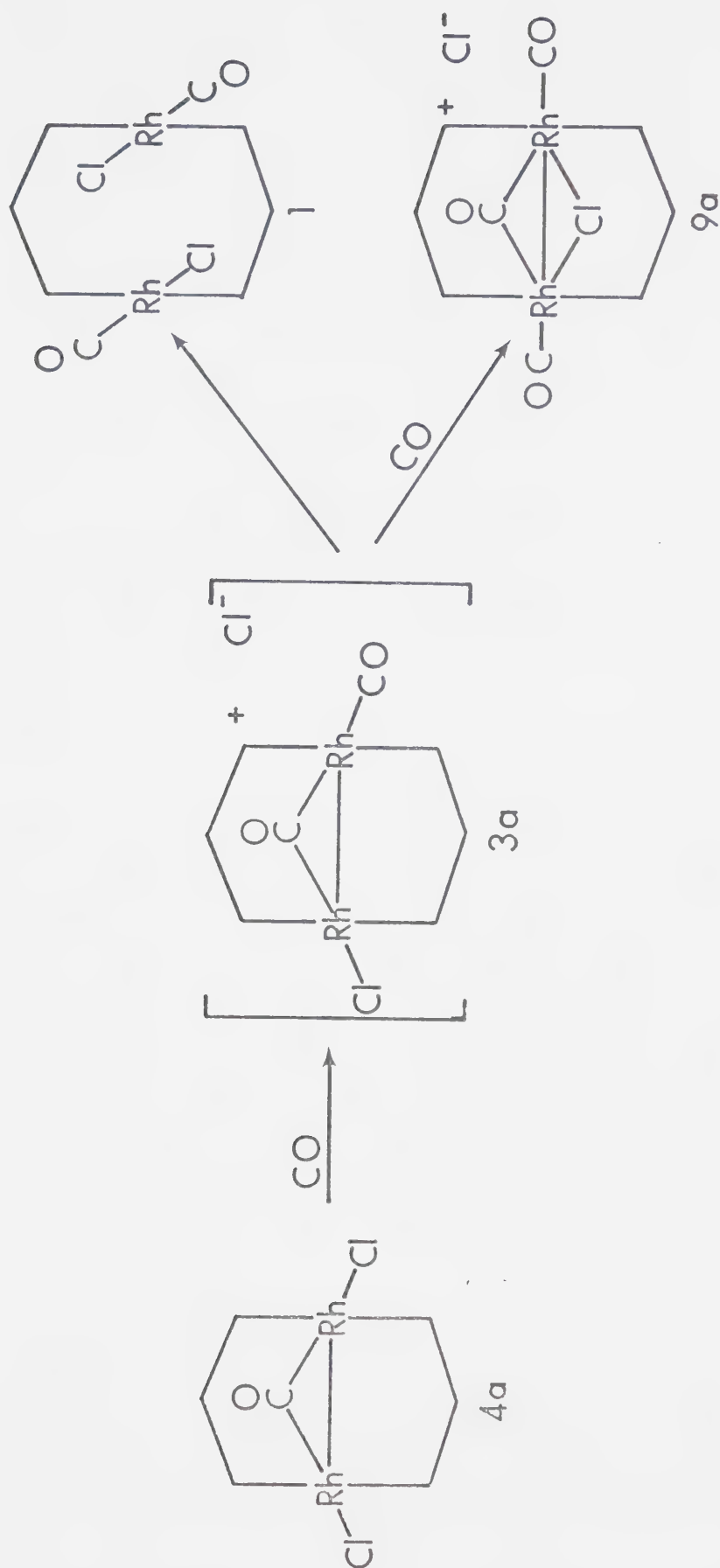
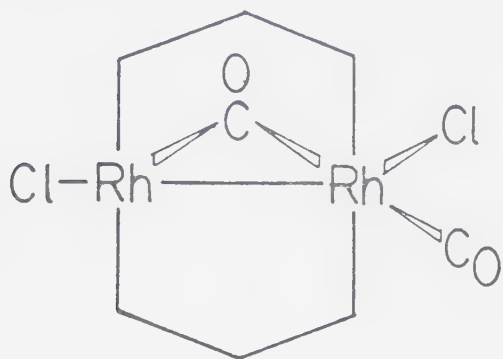


Figure 17. A Scheme for the Reaction of  $[\text{Rh}_2\text{Cl}_2(\mu\text{-CO})(\text{DPM})_2]$  with CO.



the electronic preference of each metal we would predict that  $\text{Cl}^-$  attack on species 3a (Figure 17) occurs at the metal site between the bridging and terminal CO ligands yielding a species as shown below, which could then rearrange to the *trans*-dichlorodicarbonyl species (1).



Support of this postulated intermediate comes from the structural determination<sup>145</sup> of an analogous species which has  $(\text{MeO})_2\text{PN}(\text{Et})\text{P}(\text{OMe})_2$  instead of the DPM ligands and adopts this asymmetric geometry. Similarly if CO attacks species 3a between the bridging carbonyl and chloro ligand, as we believe it does, complex 9a is obtained by a facile shift of the chloro ligand into the bridging position.

#### Reactions with $\text{SO}_2$ --

##### i) Dicarbonyl Species

The  $^{31}\text{P}\{^1\text{H}\}$  NMR spectra of  $\text{SO}_2$  adducts 10b and 10c are consistent with one phosphine environment in each case and are similar to that obtained for  $[\text{Rh}_2(\text{CO})_2(\mu\text{-SO}_2)(\mu\text{-Cl})-$



$(\text{DPM})_2]^+ 10a^{96}$  (see Chapter IV) (Cl, Br, I;  $\delta = 24.6, 27.0, 26.0$ ;  $|^1J_{\text{Rh-P}} + ^xJ_{\text{Rh-P}}| = 91.6, 90.6, 90.3$  Hz, respectively). In addition the infrared spectra of  $10b$  and  $10c$  are comparable to that of  $10a$  leading to the formulation of these species as shown previously. Preliminary studies with *trans*- $[\text{RhX}(\text{CO})(\text{DAM})]_2$  ( $X = \text{Cl}, \text{Br}$ ), indicate that these complexes react in a manner similar to *trans*- $[\text{RhCl}(\text{CO})(\text{DPM})]_2$  yielding initially  $[\text{Rh}_2(\text{CO})_2(\mu\text{-SO}_2)(\mu\text{-X})(\text{DAM})_2][\text{X}]$  and eventually undergoing CO loss yielding  $[\text{Rh}_2\text{X}_2(\mu\text{-SO}_2)(\text{DAM})_2]$ . Similarly the iodo complexes  $6$  and  $7$  react with  $\text{SO}_2$  to yield an  $\text{SO}_2$  adduct  $[\text{Rh}_2(\text{CO})_2(\mu\text{-SO}_2)(\mu\text{-I})(\text{DAM})_2][\text{I}] 12$  analogous to the DPM complexes.

The bromo species,  $[\text{Rh}_2(\text{CO})_2(\mu\text{-SO}_2)(\mu\text{-Br})(\text{DPM})_2][\text{Br}]$  ( $10b$ ), on prolonged  $\text{SO}_2$  treatment, undergoes a decarbonylation reaction yielding  $[\text{Rh}_2\text{Br}_2(\mu\text{-SO}_2)(\text{DPM})_2] 13b$ , paralleling the chemistry of the chloro analogue.<sup>96b</sup> In contrast, the iodo species  $10c$  does not undergo this reaction. Studies on the conversion of  $[\text{Rh}_2(\text{CO})_2(\mu\text{-SO}_2)(\mu\text{-Cl})(\text{DPM})_2]$  to  $[\text{Rh}_2\text{Cl}_2(\mu\text{-SO}_2)(\text{DPM})_2]$  indicated that chloride ion coordination was required before CO loss was observed (Chapter IV), so we assume that although  $\text{Br}^-$  coordination occurs in  $10b$  the increased steric bulk of the iodo ligand prevents coordination of a second  $\text{I}^-$  ion in  $10c$  and therefore prevents CO loss.

Although  $\text{SO}_2$  can be readily removed from species  $10a$  it is not removed from complexes  $10b$  and  $10c$ . The bromo





species  $10b$  instead undergoes CO loss in solution under an  $N_2$  flush to yield  $13b$ , whereas  $10c$  loses neither CO nor  $SO_2$ .

### ii) Monocarbonyl Species

The reaction of  $[Rh_2X_2(\mu-CO)(DPM)_2]$  ( $X = Cl, 4a$ ;  $X = Br, 4b$ ) with  $SO_2$  yields as the final products  $[Rh_2X_2(\mu-SO_2)(DPM)_2]$  ( $13a$  and  $13b$ ) and  $[Rh_2(CO)_2(\mu-SO_2)(\mu-X)(DPM)_2][X]$  ( $10a$  and  $10b$ ) for the chloro and bromo complexes, respectively. When these reactions are monitored, during the slow stepwise addition of  $SO_2$ , utilizing  $^{31}P\{^1H\}$  NMR spectroscopy, several unexpected products are observed. The spectra of the reaction of  $4b$  with  $SO_2$  show the presence of two asymmetric species ( $3$  and  $14b$ ) and four symmetric species ( $4b, 9b, 10b$  and  $13b$ ) at different times during the experiment (see Figure 18). Of these species only  $14b$  has not been previously characterized by us. This species we tentatively assign as a monocarbonylmonosulfur dioxide species, possibly having the structure shown. This asymmetric structure is consistent with the  $^{31}P\{^1H\}$  NMR pattern observed and the infrared data which show an  $SO_2$  species with a terminal carbonyl ligand as one of the first products. Of course,  $14b$  is not an unreasonable initial product in the reaction. All other species can be explained by facile CO transfer from this species to others present in solution. Although Figure 18 is not meant to represent unambiguously the sequence of events, it does present some plausible steps in the production of the ob-



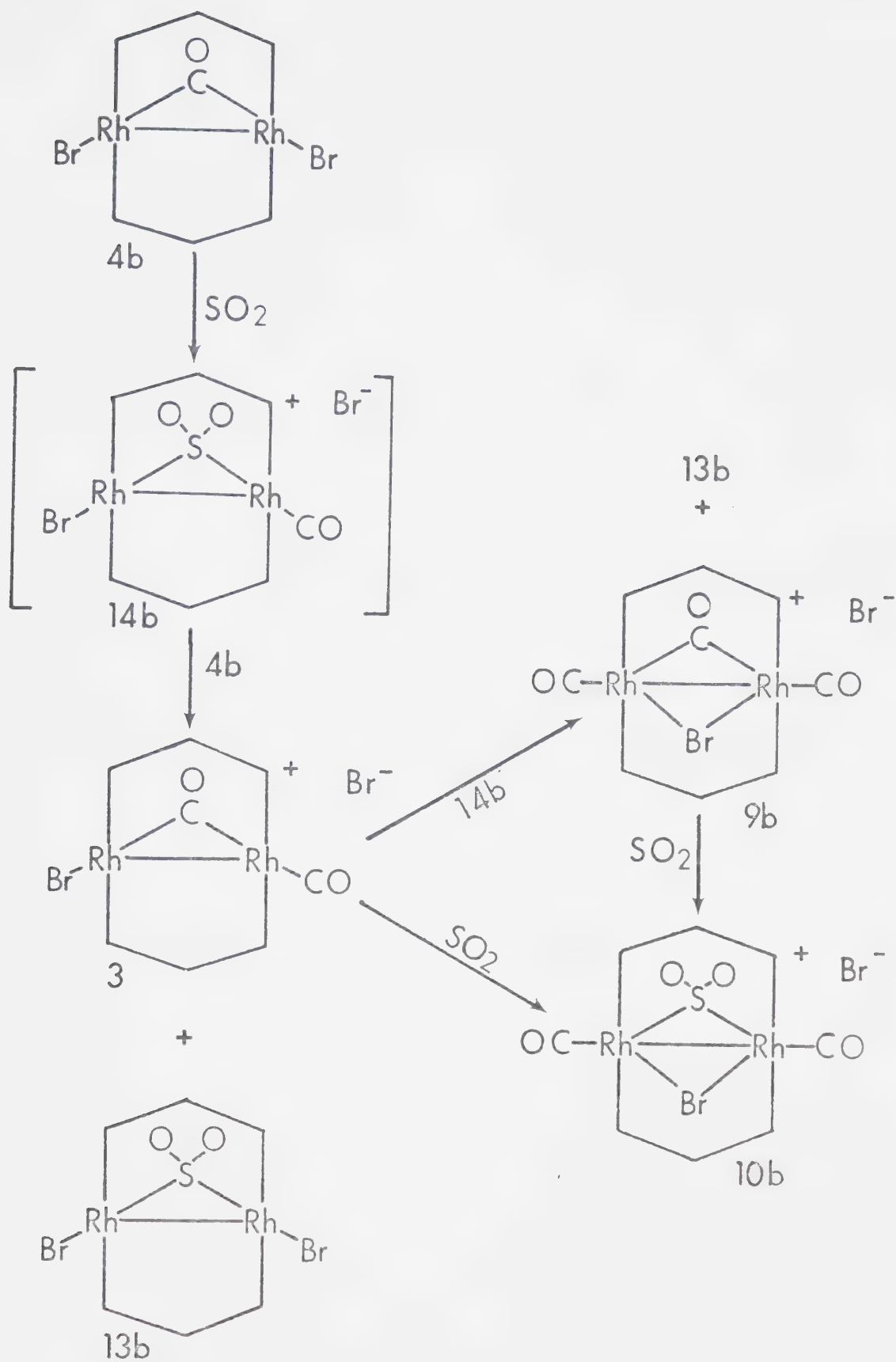


Figure 18. A Possible Reaction Sequence for the Reaction of  $[\text{Rh}_2\text{Br}_2(\mu\text{-CO})(\text{DPM})_2]$  with  $\text{SO}_2$ .



served species, and in particular offers some rationale for the production of di- and tricarbonyl products from a monocarbonyl reactant. For example, CO transfer from  $14b$  to  $4b$  would yield  $3$  and one of the final products,  $13b$ . The other final product in the reaction,  $10b$ , can be obtained by the reaction of  $3$  with  $SO_2$ . Complex  $3$  can also react with  $14b$  yielding more of  $13b$  and the tricarbonyl species  $9b$  which can subsequently react with  $SO_2$  giving  $10b$ .

The analogous reaction of  $4a$  with  $SO_2$  seems to proceed by a simpler route. Again an asymmetric species  $14a$  tentatively assigned as being analogous to the bromo species  $14b$ , is observed in the NMR experiment. However only two other species  $10a$  and  $13a$  are observed, resulting from CO transfer from one molecule of  $14a$  to another. There may be other intermediates in this reaction but none is observed.

### Summary

We have seen in these halide complexes an interesting structural trend which is dependent on halide size and on the relative dimensions of the DPM and DAM ligands. The chemistries of these halide species with CO and  $SO_2$  also show interesting trends which again can be attributed, at least in part, to steric interaction between the ligands. Also notable in this chemistry is the strong tendency toward symmetric species. Only in the two iodo species  $5$  and  $7$ , where steric bulk of the iodo ligand inhibits the chemistry favoured by the other halide species, are the asym-



metric species stable. Therefore the asymmetric complex  $[\text{Rh}_2\text{Br}(\text{CO})(\mu\text{-CO})(\text{DPM})_2][\text{Br}]$  either loses CO yielding the symmetric species  $[\text{Rh}_2\text{Br}_2(\mu\text{-CO})(\text{DPM})_2]$  or gains CO to give another symmetric species  $[\text{Rh}_2(\text{CO})_2(\mu\text{-CO})(\mu\text{-Br})(\text{DPM})_2][\text{Br}]$ . This tendency toward symmetric species is commonly observed throughout our binuclear chemistry with the DPM and DAM ligands (Chapter IV) but is in contrast to analogous complexes with the related methoxydiphenylazane ligand,  $(\text{MeO})_2\text{PN}(\text{Et})\text{P}(\text{OMe})_2$ , which show a tendency toward asymmetric species.<sup>145</sup>





## CHAPTER VI.

### The Structure of $[\text{Rh}_2\text{Br}_2(\mu\text{-CO})(\text{DPM})_2]$ :

#### A Binuclear Rhodium Carbonyl Complex Having an Unusually Low Carbonyl Stretching Frequency

### INTRODUCTION

The reaction of *trans*- $[\text{RhCl}(\text{CO})(\text{DPM})]_2$  with NaBr initially yields an asymmetric species  $[\text{Rh}_2\text{Br}(\text{CO})(\mu\text{-CO})(\text{DPM})_2][\text{Br}]$  which undergoes a rearrangement in solution to give a symmetric species having an unusually low value for  $\nu(\text{CO})$  of  $1745\text{ cm}^{-1}$  (see Chapter V).<sup>126</sup> Based on spectral data, elemental analyses, and its chemistry with  $\text{SO}_2$  this symmetric product can be equally well formulated as  $[\text{RhBr}(\mu\text{-CO})(\text{DPM})]_2$ , containing two "ketonic" carbonyl ligands, or as  $[\text{Rh}_2\text{Br}_2(\mu\text{-CO})(\text{DPM})_2]$ , having one carbonyl ligand and a formal Rh-Rh bond. The low value of the carbonyl vibration is consistent with a "ketonic" carbonyl formulation, being comparable to the value observed in  $[\text{Pd}_2\text{Cl}_2(\mu\text{-CO})(\text{DAM})_2]$ <sup>32</sup> and  $[\text{Rh}_2\text{Cl}_2(\mu\text{-CO})(\mu\text{-DMA})(\text{DPM})_2]$ <sup>42</sup> which contain "ketonic" carbonyl ligands and the  $^{31}\text{P}\{^1\text{H}\}$  NMR is very similar to other symmetric dirhodium species which have no metal-metal bond.<sup>120,146,147</sup> Furthermore, its reaction with  $\text{SO}_2$  yields the dicarbonyl species  $[\text{Rh}_2(\text{CO})_2(\mu\text{-SO}_2)(\mu\text{-Br})(\text{DPM})_2][\text{Br}]$  as one of the final products. However, this data can also be interpreted in terms of a monocarbonyl formulation. The analogous  $\text{SO}_2$ -bridged compound<sup>96</sup>



$[\text{Rh}_2\text{Cl}_2(\mu\text{-SO}_2)(\text{DPM})_2]$  (Chapter IV), has a low value for  $\nu(\text{SO})$  and has  $^{31}\text{P}\{^1\text{H}\}$  NMR parameters very similar to those in the present carbonyl compound, although it has a formal Rh-Rh bond. In addition, the formation of a dicarbonyl product in the reaction with  $\text{SO}_2$  can be explained by CO transfer from one molecule to another (see Chapter V) since a carbonyl-free species,  $[\text{Rh}_2\text{Br}_2(\mu\text{-SO}_2)(\text{DPM})_2]$  is also observed.

The structure determination was therefore undertaken in order to unambiguously establish the mode of carbonyl bonding.

### EXPERIMENTAL

#### Crystallization of $[\text{Rh}_2\text{Br}_2(\mu\text{-CO})(\text{DPM})_2]$

A (50 mg) sample of  $[\text{Rh}_2\text{Br}_2(\mu\text{-CO})_x(\text{DPM})_2]$  ( $x = 1, 2$ ), prepared as described in Chapter V, was dissolved in 3 mL of  $\text{CH}_2\text{Cl}_2$  from which well formed crystals were obtained by slow diethyl ether diffusion. The crystals were analyzed spectrally as either  $[\text{Rh}_2\text{Br}_2(\mu\text{-CO})(\text{DPM})_2]$  or  $[\text{Rh}_2\text{Br}_2(\mu\text{-CO})_2(\text{DPM})_2]$ .

#### Data Collection

A clear red plate of the title complex was mounted on a glass fibre. Preliminary film data showed that the crystal belonged to the monoclinic system with extinctions ( $h0l$ ,  $h+l$  odd;  $0k0$ ,  $k$  odd) characteristic of the centrosymmetric space group  $\text{P}2_1/\text{n}$ , a non standard setting of  $\text{P}2_1/\text{c}$ .



Data collection was as previously described in Chapter II and pertinent crystal and intensity collection data are presented in Table 27.

### Structure Solution and Refinement

The positions of the Rh, Br and P atoms were obtained by direct methods using MULTAN.<sup>148</sup> The remaining atoms were located from subsequent least-squares refinements and electron density difference maps. Anomalous dispersion terms for Rh, Br and P<sup>108</sup> were included in  $F_c$ . All carbon atoms of the phenyl rings were refined as rigid groups having  $D_{6h}$  symmetry and C-C distance of 1.392 Å. The hydrogen atoms were included as fixed contributions and were not refined. All non group atoms were refined individually with anisotropic thermal parameters (see Chapter II for a more detailed discussion).

The final model with 205 parameters varied converged to  $R = 0.045$  and  $R_w = 0.055$ .<sup>121</sup> In the final electron density difference map the highest 20 peaks were in the vicinities of either the phenyl groups or the Rh and Br atoms (0.45 - 0.25 e/Å<sup>3</sup>). A typical carbon atom on earlier syntheses had an electron density of about 3.5 e/Å<sup>3</sup>.

### Results

The positional and thermal parameters for the individual anisotropic atoms, rigid group atoms and idealized hydrogen parameters are given in Tables 28, 29 and 30 respectively. Least-squares plane calculations are pre-



Table 27. Summary of Crystal Data and Intensity Collection  
for  $[\text{Rh}_2\text{Br}_2(\mu\text{-CO})(\text{DPM})_2]$

Compound	[Rh <sub>2</sub> Br <sub>2</sub> (μ-CO) (DPM) <sub>2</sub> ]																																												
Formula	C <sub>51</sub> H <sub>44</sub> Br <sub>2</sub> O <sub>1</sub> P <sub>4</sub> Rh <sub>2</sub>																																												
Formula Weight	1162.4 amu																																												
Cell Parameters																																													
a	20.429 (2) Å																																												
b	11.895 (1) Å																																												
c	18.865 (2) Å																																												
β	100.275 (9) °																																												
V	4510.7 Å <sup>3</sup>																																												
Z	4																																												
Density	1.711 (calc'd.)																																												
Space Group	C <sub>2h</sub> <sup>5</sup> -P2 <sub>1</sub> /n (non-standard setting of P2 <sub>1</sub> /c)																																												
Crystal Dimensions	0.240 x 0.088 x 0.301 mm																																												
Crystal Volume	0.00442 mm <sup>3</sup>																																												
Crystal Faces (and distances from an arbitrary origin within the crystal (mm))	<table><tr><td>0</td><td>1</td><td>0</td><td>(0.044)</td></tr><tr><td>0</td><td><math>\bar{1}</math></td><td>0</td><td>(0.044)</td></tr><tr><td>1</td><td>0</td><td>0</td><td>(0.138)</td></tr><tr><td><math>\bar{1}</math></td><td>0</td><td>0</td><td>(0.098)</td></tr><tr><td>0</td><td>0</td><td><math>\bar{1}</math></td><td>(0.156)</td></tr><tr><td><math>\bar{1}</math></td><td>0</td><td>2</td><td>(0.131)</td></tr><tr><td><math>\bar{2}</math></td><td>0</td><td><math>\bar{1}</math></td><td>(0.120)</td></tr><tr><td>2</td><td><math>\bar{1}</math></td><td><math>\bar{1}</math></td><td>(0.094)</td></tr><tr><td>1</td><td><math>\bar{1}</math></td><td>0</td><td>(0.082)</td></tr><tr><td>1</td><td><math>\bar{1}</math></td><td>0</td><td>(0.059)</td></tr><tr><td>1</td><td>0</td><td>1</td><td>(1.103)</td></tr></table>	0	1	0	(0.044)	0	$\bar{1}$	0	(0.044)	1	0	0	(0.138)	$\bar{1}$	0	0	(0.098)	0	0	$\bar{1}$	(0.156)	$\bar{1}$	0	2	(0.131)	$\bar{2}$	0	$\bar{1}$	(0.120)	2	$\bar{1}$	$\bar{1}$	(0.094)	1	$\bar{1}$	0	(0.082)	1	$\bar{1}$	0	(0.059)	1	0	1	(1.103)
0	1	0	(0.044)																																										
0	$\bar{1}$	0	(0.044)																																										
1	0	0	(0.138)																																										
$\bar{1}$	0	0	(0.098)																																										
0	0	$\bar{1}$	(0.156)																																										
$\bar{1}$	0	2	(0.131)																																										
$\bar{2}$	0	$\bar{1}$	(0.120)																																										
2	$\bar{1}$	$\bar{1}$	(0.094)																																										
1	$\bar{1}$	0	(0.082)																																										
1	$\bar{1}$	0	(0.059)																																										
1	0	1	(1.103)																																										
Temperature	20°C																																												
Radiation	CuKα (λ=1.540562 Å) filtered with 0.5mil thick nickel foil)																																												
μ	98.229 cm <sup>-1</sup>																																												
Range in Absorption	0.190 - 0.476																																												
Correction Factors																																													
Receiving Aperture	6x6 mm, 30 cm from the crystal																																												





Table 27, continued

Takeoff Angle	3.9°
Scan Speed	2° in 20/min
Scan Range	1.00° below $K\alpha_1$ to 1.00° above $K\alpha_2$
Background Counting Time	10s ( $3^\circ \leq 2\theta < 45^\circ$ ) 20s ( $45^\circ \leq 2\theta < 96^\circ$ ) 40s ( $96^\circ \leq 2\theta \leq 120^\circ$ )
2 $\theta$ limits	$3^\circ \leq 2\theta \leq 120^\circ$
2 $\theta$ units for centred reflections	$(60^\circ \leq 2\theta \leq 70^\circ)$
Final number of variables	205
Unique Data Collected	7071
Unique Data Used ( $F_O^2 \geq 3\sigma(F_O^2)$ )	4718
Error in observation of unit weight	1.392
R	0.045
$R_w$	0.055



sented in Table 31 and selected bond length and angles are shown in Tables 32 and 33, respectively. A listing of observed and calculated structure amplitudes is available.<sup>110</sup>

A stereoview of the unit cell of  $[\text{Rh}_2\text{Br}_2(\mu\text{-CO})(\text{DPM})_2]$  is shown in Figure 19. The crystallographic *a* axis is horizontal to the right, the *c* axis runs from the bottom to the top and the *b* axis goes into the page. Figure 20 presents a perspective view of the compound including the numbering scheme, 50% thermal ellipsoids are drawn. The inner coordination sphere is shown in Figure 21 along with some relevant bond lengths, 50% thermal ellipsoids are drawn.



TABLE 28. Positional and Thermal Parameters For The Nongroup Atoms of [Rh<sub>2</sub>Br<sub>2</sub>( $\mu$ -CO)(DPM)<sub>2</sub>].

Atom	a			b			U11	U12	U13	U22	U23	U33	U12	U13	U23
	x	y	z	x	y	z									
Rh(1)	0.58004(3)	0.09336(5)	0.32748(3)	2.10(3)			2.10(3)	2.26(3)	2.89(3)	0.06(2)		0.98(2)			-0.06(3)
Rh(2)	0.44867(3)	0.15824(5)	0.31124(3)	1.99(3)			1.99(3)	2.13(3)	3.44(4)	-0.01(2)		0.61(2)			0.25(3)
Br(1)	0.69272(4)	0.03208(8)	0.31204(6)	3.03(4)			3.03(4)	3.94(5)	5.79(6)	0.57(4)		1.96(4)			-0.37(5)
Br(2)	0.33105(5)	0.20589(9)	0.26417(8)	2.60(5)			2.60(5)	3.90(5)	13.0(1)	0.10(4)		-0.32(5)			1.93(7)
P(1)	0.61619(9)	0.2724(2)	0.3085(1)	2.35(9)			2.35(9)	2.56(9)	2.7(1)	-0.21(8)		1.02(8)			-0.01(8)
P(2)	0.47370(9)	0.3473(2)	0.3022(1)	2.36(9)			2.36(9)	2.32(9)	3.2(1)	0.10(8)		0.67(8)			-0.06(9)
P(3)	0.55003(9)	-0.0946(2)	0.3208(1)	2.5(1)			2.5(1)	2.31(9)	3.8(1)	0.14(8)		1.02(8)			0.15(9)
P(4)	0.40793(9)	-0.0248(2)	0.3104(1)	2.31(9)			2.31(9)	2.37(9)	3.3(1)	-0.26(8)		0.57(8)			0.45(9)
O	0.5269(3)	0.1498(6)	0.4559(3)	4.0(3)			4.0(3)	6.5(4)	2.7(4)	0.9(3)		1.3(3)			-0.9(3)
C(1)	0.5210(4)	0.1375(6)	0.3938(5)	2.5(4)			2.5(4)	2.2(4)	4.6(6)	-0.5(3)		1.3(4)			-0.3(4)
C(2)	0.5613(4)	0.3818(6)	0.3346(4)	2.4(4)			2.4(4)	2.7(4)	3.0(5)	-0.2(3)		0.5(3)			-0.6(3)
C(3)	0.4716(4)	-0.1243(6)	0.3513(4)	3.0(4)			3.0(4)	2.5(4)	3.1(5)	0.4(3)		1.2(3)			0.3(3)

a

b

Estimated standard deviations in the least significant figure(s) are given in parentheses in this and all subsequent tables.

The form of the thermal ellipsoid is:  $\exp[-2\pi^2(a^*U_{11}h^2 + b^*U_{22}k^2 + c^*U_{33}l^2 + 2a^*b^*U_{12}hk + 2a^*c^*U_{13}hl + 2b^*c^*U_{23}kl)]$ . The quantities given in the table are the thermal coefficients  $\times 10^3$ .



TABLE 29. Derived Parameters For the Rigid Group Atoms of [Rh2Br2(mu-CO)(DPM)2].

Atom	X	Y	Z	B(A <sup>2</sup> )	Atom	X	Y	Z	B(A <sup>2</sup> )
C(11)	0.6232(3)	0.3053(5)	0.2153(2)	2.5(1)	C(51)	0.6042(3)	-0.2070(4)	0.3643(5)	3.1(2)
C(12)	0.6298(3)	0.4160(4)	0.1937(3)	3.8(2)	C(52)	0.5958(5)	-0.2493(5)	0.4308(3)	3.8(2)
C(13)	0.6387(3)	0.4391(4)	0.1238(3)	4.3(2)	C(53)	0.6360(5)	-0.3367(5)	0.4626(4)	5.2(2)
C(14)	0.6412(3)	0.3515(5)	0.0754(2)	4.6(2)	C(54)	0.6846(3)	-0.3817(4)	0.4278(5)	5.0(2)
C(15)	0.6347(3)	0.2407(4)	0.0970(3)	4.8(2)	C(55)	0.6931(5)	-0.3393(5)	0.3612(3)	5.4(3)
C(16)	0.6257(3)	0.2176(4)	0.1670(3)	3.5(2)	C(56)	0.6529(5)	-0.2520(5)	0.3295(4)	4.3(2)
C(21)	0.6969(3)	0.3113(5)	0.3614(3)	2.3(1)	C(61)	0.5346(3)	-0.1274(6)	0.2240(3)	3.0(2)
C(22)	0.7070(4)	0.2903(4)	0.4352(8)	3.1(2)	C(62)	0.5191(4)	-0.0366(4)	0.1774(4)	3.6(2)
C(23)	0.7674(5)	0.3183(5)	0.4783(6)	3.6(2)	C(63)	0.5057(4)	-0.0540(5)	0.1033(3)	5.1(2)
C(24)	0.8177(3)	0.3672(5)	0.4478(3)	3.4(2)	C(64)	0.5078(3)	-0.1622(6)	0.0757(3)	5.8(3)
C(25)	0.8076(4)	0.3882(4)	0.3740(8)	3.4(2)	C(65)	0.5233(4)	-0.2530(4)	0.1222(4)	6.1(3)
C(26)	0.7472(6)	0.3603(5)	0.3308(6)	2.9(2)	C(66)	0.5367(4)	-0.2356(5)	0.1963(3)	4.7(2)
C(31)	0.4569(3)	0.3856(5)	0.2071(3)	2.4(1)	C(71)	0.3700(3)	-0.0935(5)	0.2259(2)	2.4(1)
C(32)	0.4441(3)	0.4956(4)	0.1836(3)	3.5(2)	C(72)	0.3549(3)	-0.2076(5)	0.2272(3)	3.7(2)
C(33)	0.4321(3)	0.5198(4)	0.1103(3)	4.7(2)	C(73)	0.3229(3)	-0.2606(4)	0.1648(3)	4.0(2)
C(34)	0.4329(3)	0.4338(5)	0.0603(3)	5.0(2)	C(74)	0.3059(3)	-0.1997(5)	0.1011(2)	4.3(2)
C(35)	0.4458(3)	0.3238(4)	0.0838(3)	4.7(2)	C(75)	0.3211(3)	-0.0857(5)	0.0999(3)	5.0(2)
C(36)	0.4578(3)	0.2996(4)	0.1572(3)	3.7(2)	C(76)	0.3531(3)	-0.0326(4)	0.1623(3)	3.9(2)
C(41)	0.4304(3)	0.4574(4)	0.3449(3)	2.4(1)	C(81)	0.3454(4)	-0.0352(5)	0.3681(5)	2.1(1)
C(42)	0.3636(3)	0.4783(5)	0.3176(4)	3.9(2)	C(82)	0.3619(2)	0.0074(4)	0.4378(5)	3.3(2)
C(43)	0.3301(2)	0.5628(5)	0.3475(3)	4.5(2)	C(83)	0.3157(5)	0.0042(4)	0.4837(7)	4.2(2)
C(44)	0.3633(3)	0.6264(4)	0.4048(3)	4.1(2)	C(84)	0.2529(4)	-0.0415(5)	0.4601(5)	3.8(2)
C(45)	0.4301(3)	0.6054(5)	0.4321(4)	3.9(2)	C(85)	0.2363(2)	-0.0840(4)	0.3904(5)	3.8(2)
C(46)	0.4636(2)	0.5209(5)	0.4021(3)	3.3(2)	C(86)	0.2825(5)	-0.0809(4)	0.3445(7)	2.9(2)

## Rigid Group Parameters

	a		b	
	Xc	Yc	Zc	
Ring1	0.6322(2)	0.3284(4)	0.1454(2)	Delta
Ring2	0.7573(2)	0.3393(3)	0.4046(2)	Epsilon
Ring3	0.4449(2)	0.4097(4)	0.1337(2)	Eta
Ring4	0.3968(2)	0.5419(3)	0.3748(2)	
Ring5	0.6444(2)	-0.2943(4)	-0.720(4)	
Ring6	0.5212(2)	-0.1448(4)	0.3960(2)	
Ring7	0.3380(2)	-0.1466(4)	0.1498(3)	
Ring8	0.2991(2)	-0.0383(3)	0.1635(2)	
a			0.4141(2)	
b			1.119(4)	

Xc, Yc and Zc are the fractional coordinates of the centroid of the rigid group.

The rigid group orientation angles Delta, Epsilon and Eta (radians) are the angles by which the rigid body is rotated with respect to a set of axes X, Y and Z. The origin is the centre of the ring; X is parallel to a\*, Z is parallel to c and Y is parallel to the line defined by the intersection of the plane containing a\* and b\* with the plane containing b and c.





TABLE 30. Idealized Positional and Thermal Parameters For the Hydrogen Atoms of [Rh<sub>2</sub>Br<sub>2</sub>( $\mu$ -CO)(DPM)<sub>2</sub>].

Atom	x	y	z	B(A <sup>2</sup> )	Atom	x	y	z	B(A <sup>2</sup> )
H(1C2)	0.5714	0.4512	0.3121	3.10	H(45)	0.4522	0.6483	0.4717	4.90
H(2C2)	0.5698	0.3905	0.3843	3.10	H(46)	0.5090	0.5068	0.4211	4.26
H(1C3)	0.4784	-0.1174	0.4025	3.29	H(52)	0.5629	-0.2178	0.4549	4.92
H(2C3)	0.4580	-0.1985	0.3383	3.29	H(53)	0.6304	-0.3650	0.5082	5.97
H(12)	0.6285	0.4758	0.2267	4.57	H(54)	0.7117	-0.4416	0.4493	6.04
H(13)	0.6430	0.5146	0.1088	5.25	H(55)	0.7255	-0.3709	0.3370	6.17
H(14)	0.6469	0.3672	0.0274	5.38	H(56)	0.6580	-0.2237	0.2837	5.37
H(15)	0.6363	0.1809	0.0639	5.78	H(62)	0.5184	0.0373	0.1964	4.62
H(16)	0.6217	0.1421	0.1818	4.26	H(63)	0.4946	0.0082	0.0716	6.06
H(22)	0.6726	0.2562	0.4558	3.97	H(64)	0.4971	-0.1739	0.0250	6.74
H(23)	0.7740	0.3039	0.5286	4.46	H(65)	0.5233	-0.3269	0.1030	6.67
H(24)	0.8586	0.3866	0.4773	4.33	H(66)	0.5471	-0.2977	0.2278	5.45
H(25)	0.8418	0.4216	0.3533	4.34	H(72)	0.3668	-0.2495	0.2702	4.54
H(26)	0.7404	0.3739	0.2804	4.08	H(73)	0.3130	-0.3383	0.1650	5.14
H(32)	0.4438	0.5541	0.2176	4.17	H(74)	0.2842	-0.2351	0.0583	5.10
H(33)	0.4241	0.5947	0.0941	5.60	H(75)	0.3093	-0.0431	0.0567	5.72
H(34)	0.4256	0.4501	0.0102	5.71	H(76)	0.3631	0.0457	0.1619	4.81
H(35)	0.4469	0.2648	0.0497	5.49	H(82)	0.4046	0.0396	0.4532	4.27
H(36)	0.4665	0.2242	0.1732	4.58	H(83)	0.3271	0.0341	0.5309	5.24
H(42)	0.3413	0.4357	0.2780	4.91	H(84)	0.2215	-0.0435	0.4916	4.86
H(43)	0.2845	0.5771	0.3286	5.48	H(85)	0.1934	-0.1156	0.3746	4.70
H(44)	0.3399	0.6834	0.4255	4.95	H(86)	0.2709	-0.1101	0.2969	3.95



Table 31. Least-Squares Plane Calculations

Plane no.	Equation <sup>a</sup>											
1	$0.0657X - 0.1380Y - 0.9883Z + 5.4452 = 0.0$											
2	$0.1037X - 0.0040Y - 0.9941Z + 4.8736 = 0.0$											
3	$0.2867X + 0.9530Y - 0.0975Z = 3.5520 = 0.0$											

deviation from planes, Å											
Plane no.	Rh(1)	Rh(2)	Br(1)	Br(2)	P(1)	P(2)	P(3)	P(4)	C(1)	C(2)	C(3)
1	-0.0091(6)	0.0097(6)									0
2	-0.0053(6)	0.0056(6)			0.098(2)	0.100(2)				-0.639(8) <sup>b</sup>	
3	-0.0044(5)	0.0066(5)	0.0037(9)	-0.012(1)			0.063(2)	-0.060(2)	-0.034(7)		-0.683(8) <sup>b</sup>
											-0.032(7)

<sup>a</sup>X, Y, Z are orthogonal coordinates (Å) with X along the a axis, Y in the a-b plane and Z along the c\* axis.

<sup>b</sup>Not included in least squares plane calculations.



Table 32. Selected Distances ( $\text{\AA}$ ) in  $[\text{Rh}_2\text{Br}_2(\mu\text{-CO})(\text{DPM})_2]$ 

Rh(1)-Rh(2)	2.7566(8)		P(1)-C(2)	1.841(8)	} 1.832(8)
Rh(1)-Br(1)	2.481 (1)		P(2)-C(2)	1.832(7)	
Rh(2)-Br(2)	2.474 (1)		P(3)-C(3)	1.830(8)	
Rh(1)-C(1)	1.958 (8)		P(4)-C(3)	1.825(7)	
Rh(2)-C(1)	1.961 (8)		P(1)-C(11)	1.831(5)	
Rh(1)-P(1)	2.303 (2)	} 2.317(11) <sup>a</sup>	P(1)-C(21)	1.828(4)	} 1.833(7)
Rh(1)-P(3)	2.316 (2)		P(2)-C(31)	1.824(5)	
Rh(2)-P(2)	2.319 (2)		P(2)-C(41)	1.844(4)	
Rh(2)-P(4)	2.330 (2)		P(3)-C(51)	1.833(5)	
C(1)-O	1.167 (9)		P(3)-C(61)	1.840(5)	
C(1)-O <sup>b</sup>	1.192 (9)		P(4)-C(71)	1.835(4)	
			P(4)-C(81)	1.826(4)	

## Nonbonded Distances

P(1)-P(2)	3.026(3)	Br(2)-H(42)	2.75
P(3)-P(4)	2.992(3)	H1C2-H(12)	2.17
Rh(1)-H(62)	2.65	H2C2-H(46)	2.06
Rh(2)-H(36)	2.81	H1C3-H(52)	2.19
C(12)-H(26)	2.59	H2C3-H(72)	2.15
C(56)-H(66)	2.68	H(33)-H(65) <sup>c</sup>	2.21
C(72)-H(86)	2.61	H(35)-H(65) <sup>d</sup>	2.25
Br(1)-H(56)	3.15		

<sup>a</sup>For averaged quantities, the estimated standard deviation is the larger of an individual standard deviation or the standard deviation of a single observation as calculated from the mean.

<sup>b</sup>Riding Motion Corrected; Atom O riding on atom C(1).

<sup>c</sup>Atom located at  $x, 1+y, z$ .

<sup>d</sup>Atom located at  $1-x, \bar{y}, \bar{z}$ .



Table 33. Selected Angles (deg) in  $[\text{Rh}_2\text{Br}_2(\mu\text{-CO})(\text{DPM})_2]$ 

Rh(2)-Rh(1)-Br(1)	167.06(4)	Rh(1)-P(3)-C(51)	123.1(2)
Rh(2)-Rh(1)-P(1)	93.24(5)	Rh(1)-P(3)-C(61)	104.8(2)
Rh(2)-Rh(1)-P(3)	91.22(5)	Rh(2)-P(4)-C(71)	121.2(2)
Rh(2)-Rh(1)-C(1)	45.3 (2)	Rh(2)-P(4)-C(81)	110.3(2)
Br(1)-Rh(1)-C(1)	147.6 (2)	C(2)-P(1)-C(11)	105.2(3)
Br(1)-Rh(1)-P(1)	85.62(5)	C(2)-P(1)-C(21)	102.0(3)
Br(1)-Rh(1)-P(3)	87.25(5)	C(2)-P(2)-C(31)	105.8(3)
P(1)-Rh(1)-P(3)	166.78(8)	C(2)-P(2)-C(41)	102.2(3)
P(1)-Rh(1)-C(1)	95.9 (2)	C(3)-P(3)-C(51)	102.2(3)
P(3)-Rh(1)-C(1)	96.1 (2)	C(3)-P(3)-C(61)	105.5(3)
Rh(1)-Rh(2)-Br(2)	165.45(5)	C(3)-P(4)-C(71)	103.7(3)
Rh(1)-Rh(2)-P(2)	93.24(5)	C(3)-P(4)-C(81)	103.1(3)
Rh(1)-Rh(2)-P(4)	94.51(5)	C(11)-P(1)-C(21)	104.6(3)
Rh(1)-Rh(2)-C(1)	45.2 (2)	C(31)-P(2)-C(41)	103.4(3)
Br(2)-Rh(2)-C(1)	149.2 (2)	C(51)-P(3)-C(61)	105.8(3)
Br(2)-Rh(2)-P(2)	87.96(5)	C(71)-P(4)-C(81)	104.8(3)
Br(2)-Rh(2)-P(4)	83.61(5)	P(1)-C(11)-C(12)	120.7(3)
P(2)-Rh(2)-P(4)	171.41(7)	P(1)-C(11)-C(16)	119.2(3)
P(2)-Rh(2)-C(1)	92.0 (2)	P(1)-C(21)-C(22)	117.3(3)
P(4)-Rh(2)-C(1)	96.1 (2)	P(1)-C(21)-C(26)	122.7(3)
Rh(1)-C(1)-Rh(2)	89.4 (4)	P(2)-C(31)-C(32)	122.7(3)
Rh(1)-C(1)-O	135.3 (6)	P(2)-C(31)-C(36)	117.3(3)
Rh(2)-C(1)-O	135.3 (6)	P(2)-C(41)-C(42)	118.7(3)
P(1)-C(2)-P(2)	111.0 (4)	P(2)-C(41)-C(46)	121.2(3)
P(3)-C(3)-P(4)	109.9 (4)	P(3)-C(51)-C(52)	120.4(4)
Rh(1)-P(1)-C(2)	112.6 (3)	P(3)-C(51)-C(56)	119.6(4)
Rh(2)-P(2)-C(2)	114.1 (2)	P(3)-C(61)-C(62)	116.2(4)
Rh(1)-P(3)-C(3)	114.0 (2)	P(3)-C(61)-C(66)	123.8(4)
Rh(1)-P(4)-C(3)	112.1 (2)	P(4)-C(71)-C(72)	118.7(3)
Rh(1)-P(1)-C(11)	115.4 (2)	P(4)-C(71)-C(76)	121.2(3)
Rh(1)-P(1)-C(21)	115.6 (2)	P(4)-C(81)-C(82)	117.4(3)
Rh(2)-P(2)-C(31)	108.0 (2)	P(4)-C(81)-C(86)	122.6(3)
Rh(2)-P(2)-C(41)	121.8 (2)		

## Torsion Angles

P(1)-Rh(1)-Rh(2)-P(2)	- 5.42(7)	C(2)-P(1)-Rh(1)-C(1)	- 17.9 (4)
P(1)-Rh(1)-Rh(2)-P(4)	170.87(7)	C(2)-P(2)-Rh(2)-C(1)	28.3 (4)
P(2)-Rh(2)-Rh(1)-P(3)	-172.97(7)	C(3)-P(3)-Rh(1)-C(1)	17.6 (4)
P(3)-Rh(1)-Rh(2)-P(4)	3.32(8)	C(3)-P(4)-Rh(2)-C(1)	- 24.8 (4)
C(11)-P(1)-Rh(1)-Br(1)	73.8 (2)	C(11)-P(1)-P(2)-C(31)	2.6 (3)
C(21)-P(1)-Rh(1)-Br(1)	- 48.7 (2)	C(11)-P(1)-P(3)-C(61)	- 6.5 (3)
C(31)-P(2)-Rh(2)-Br(2)	- 65.2 (2)	C(21)-P(1)-P(2)-C(41)	5.2 (4)
C(41)-P(2)-Rh(2)-Br(2)	54.1 (2)	C(21)-P(1)-P(3)-C(51)	- 9.3 (3)
C(51)-P(3)-Rh(1)-Br(1)	40.7 (3)	C(31)-P(2)-P(4)-C(71)	- 3.0 (3)
C(61)-P(3)-Rh(1)-Br(1)	- 80.0 (2)	C(41)-P(2)-P(4)-C(81)	- 6.6 (3)
C(71)-P(4)-Rh(2)-Br(2)	63.1 (2)	C(51)-P(3)-P(4)-C(81)	30.1 (4)
C(81)-P(4)-Rh(2)-Br(2)	- 59.7 (2)	C(61)-P(3)-P(4)-C(71)	19.1 (3)





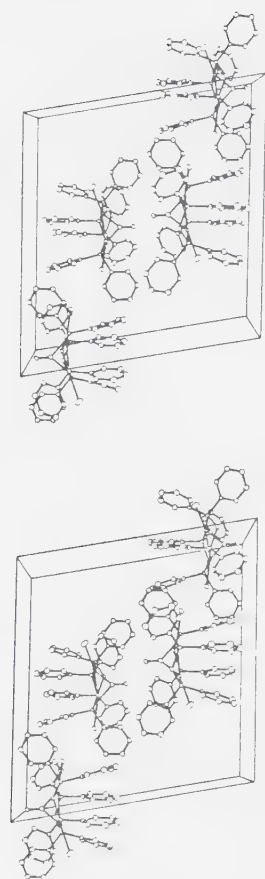


Figure 19. Cell Packing Diagram of  $[\text{Rh}_2\text{Br}_2(\mu\text{-CO})(\text{DPM})_2]\cdot$ .



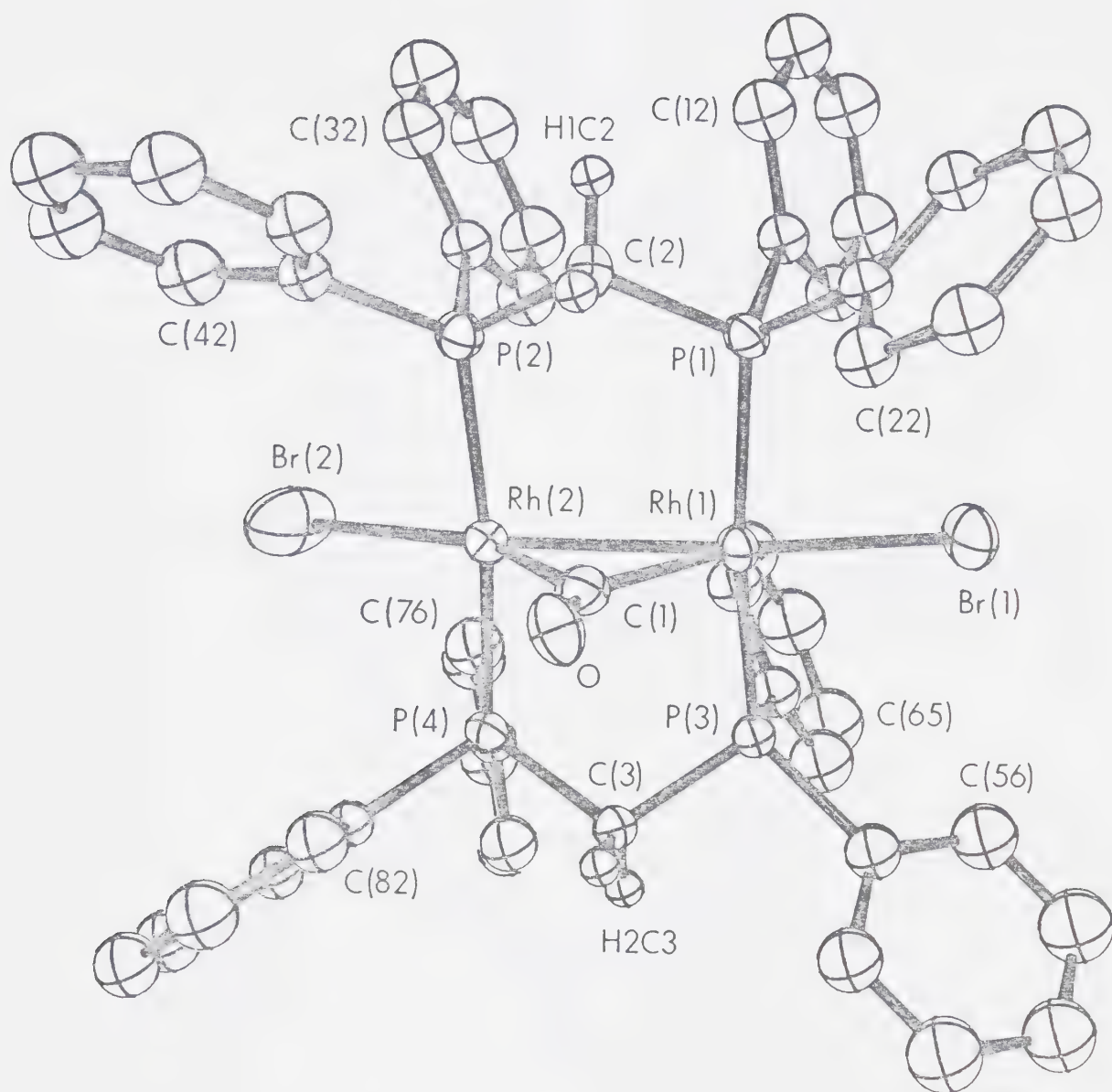


Figure 20. A Perspective View of  $[\text{Rh}_2\text{Br}_2(\mu\text{-CO})(\text{DPM})_2]$ .



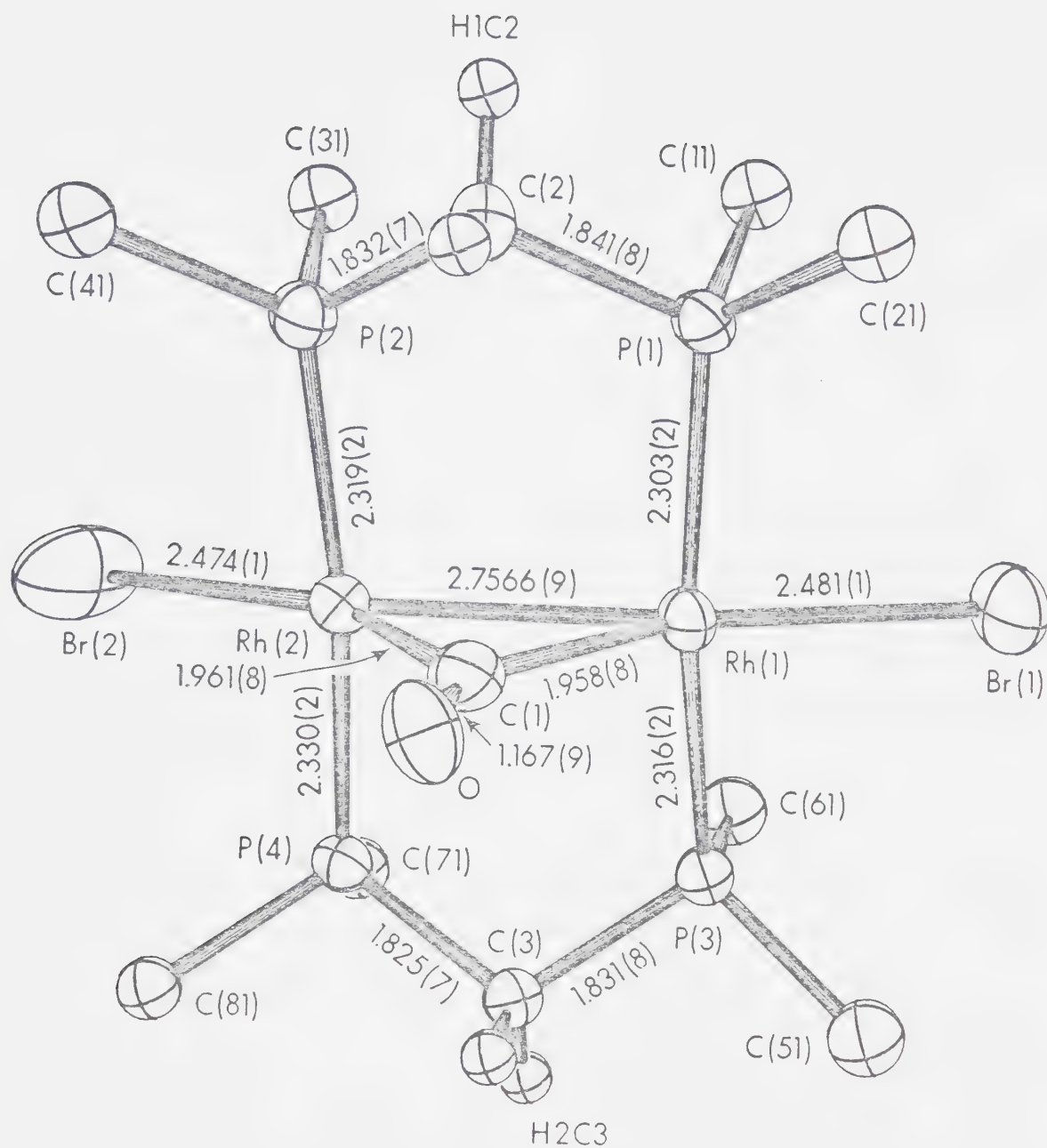


Figure 21. The Inner Coordination Sphere of  $[\text{Rh}_2\text{Br}_2(\mu\text{-CO})(\text{DPM})_2]$ .



## DESCRIPTION OF STRUCTURE

The coordination about each rhodium atom is quasi-trigonal bipyramidal. Two transoid DPM ligands bridge the Rh atoms in the axial positions with the bridging carbonyl ligand, a terminal bromo ligand on each Rh atom and a formal Rh-Rh bond completing coordination in the equatorial plane. The resulting distorted "A-frame" geometry is similar to that observed in  $[\text{Rh}_2\text{Cl}_2(\mu\text{-SO}_2)(\text{DPM})_2]^{96}$  (Chapter IV). The distortions in the "A-frame" geometry arise due to steric interactions between the terminal bromo ligands and the phenyl rings of the DPM ligands (Table 32) and because of the presence of a metal-metal bond, both resulting in a flattening of the "A" configuration. Angles about each Rh atom in the equatorial plane clearly show the distortions from trigonal bipyramidal coordination (Rh-Rh-Br, Rh-Rh-C(1), and Br-Rh-C(1);  $167.06(4)$ ,  $45.3(2)$  and  $147.6(2)^\circ$ , respectively).

The Rh-Br distances of  $2.481(1)$  and  $2.474(1)\text{\AA}$  are not unusual and compare well with other determinations.<sup>149,150</sup> Within the Rh-DPM framework most parameters are as expected. The Rh-P distances (average  $2.317(11)\text{\AA}$ ) and the P-C distances both methylene and phenyl (average,  $1.833(7)$  and  $1.832(8)\text{\AA}$ , respectively) compare well with other determinations.<sup>35,89,96,120,126,142</sup> The Rh-P vectors as viewed down the Rh-Rh axis are slightly staggered (see P-Rh-Rh-P torsion angles in Table 33 and least-squares planes in





Table 31). This skewing of the Rh-DPM framework results in phenyl rings 3 and 6 being forced into the open coordination site opposite the carbonyl ligand giving rise to close contacts between Rh and the ortho hydrogen atoms (2.65 and 2.81 Å). An almost identical skewing was observed in the chloro/SO<sub>2</sub> analogue, [Rh<sub>2</sub>Cl<sub>2</sub>(μ-SO<sub>2</sub>)(DPM)<sub>2</sub>]<sup>96</sup> (Chapter IV). The Rh-P-C angles with the exceptions of those for rings 4 and 5 are close to the expected tetrahedral values. In contrast, the Rh-P-C angles involving ring 4 and 5 (121.8(2)° and 123.1(2)°, respectively) are significantly larger than the expected tetrahedral values. These distortions seem to arise from steric interactions between the bromo ligand and the phenyl rings, as evidenced by the short Br-H distances involving these rings (Br(1) - H(56) = 3.15 Å and Br(1) - H(42) = 2.75 Å) which are less than the sums of the van der Waal's radii.<sup>112</sup> In the structure of [Rh<sub>2</sub>Cl<sub>2</sub>(μ-SO<sub>2</sub>)(DPM)<sub>2</sub>]<sup>96</sup> where the bromo ligand is replaced by the less bulky chloro ligand these distortions are somewhat less pronounced, with a maximum value for the Rh-P-C angle of 118.9(2)°. The bromo ligands in the present compound, are staggered with respect to the DPM phenyl groups, in order to minimize nonbonded contacts between these groups. This staggering is evident in the phenyl-P-Rh-Br torsion angles which range from 40.7(3)° to 80.0(2)° (Table 33).

Formally the present compound contains a Rh-Rh single bond as suggested by several structural parameters:



i) the Rh-Rh distance of  $2.7566(9)\text{\AA}$  falls within the range previously reported for similar Rh-Rh bond species  $(2.617(3) - 2.8415(7)\text{\AA})$ <sup>35,129-133</sup> and can be contrasted to the distances of  $3.1520(8)$  and  $3.155(4)\text{\AA}$ , observed in the "A-frame" species  $[\text{Rh}_2(\text{CO})_2(\mu\text{-Cl})(\text{DPM})_2]^+$  (Chapter II) and  $[\text{Rh}_2(\text{CO})_2(\mu\text{-S})(\text{DPM})_2]$ ,<sup>89</sup> respectively, where no formal metal-metal bond is present; ii) the Rh-C-Rh bond angle of  $89.4(4)^\circ$  compares well with other determinations in which a carbonyl ligand bridges a metal-metal bond,<sup>35,130-133</sup> and is significantly smaller than the values of  $119(3)^\circ$ ,  $106(3)^\circ$  and  $116.4(6)^\circ$  observed in  $[\text{Pd}_2\text{Cl}_2(\mu\text{-CO})(\text{DPM})_2]$ ,<sup>32</sup>  $[\text{Pt}_2\text{Cl}_2(\mu\text{-CO})(\text{DPM})_2]$ <sup>41</sup> and  $[\text{Rh}_2\text{Cl}_2(\mu\text{-CO})(\mu\text{-DMA})(\text{DPM})_2]$ ,<sup>42</sup> respectively, where no metal-metal bond is present; iii) the Rh-Rh separation is significantly less than the P...P intraligand separations of  $3.026(3)$  and  $2.992(3)\text{\AA}$  as is usually observed in these systems when a Rh-Rh bond is present.<sup>35</sup>

Although the above parameters suggest a direct metal-metal bond, this formulation is by no means unambiguous. Recent molecular orbital calculations<sup>151</sup> on carbonyl bridged species with short metal-metal distances have shown that in some cases no metal-metal bond is actually present even though the structural parameters suggest otherwise. Furthermore, these calculations have been substantiated by experimental differential electron density determinations<sup>152</sup> on the compounds in question showing no significant build-up of electron density along the metal-metal axis.



The carbonyl ligand bridges the two Rh atoms symmetrically as evidenced by the Rh-C distances of 1.958(8) and 1.961(8) Å. These distances are significantly shorter than those observed in other Rh systems containing bridging carbonyl ligands where the values of 2.104(7) and 2.034(7) Å, observed in  $[\text{Rh}_2(\text{CO})_2(\mu\text{-CO})(\mu\text{-Cl})(\text{DPM})_2][\text{BPh}_4]$ ,<sup>35</sup> are more typical. Instead, the observed distances are comparable to the values of 1.90(6) and 1.97(9) Å obtained in the  $\text{Pd}$ <sup>32</sup> and  $\text{Pt}$ <sup>41</sup> analogues  $[\text{M}_2\text{Cl}_2(\mu\text{-CO})(\text{DAM})_2]$ , ( $\text{M} = \text{Pd}, \text{Pt}$ ) and that of 1.974(7) observed in  $[\text{Rh}_2\text{Cl}_2(\mu\text{-CO})(\mu\text{-DMA})(\text{DPM})_2]$ .<sup>42</sup> It is notable that these distances correspond to "ketonic" carbonyl species which show low values for  $\nu(\text{CO})$  in the infrared spectrum similar to that observed for the present compound. It is also relevant that the analogous  $\text{SO}_2$  species  $[\text{Rh}_2\text{Cl}_2(\mu\text{-SO}_2)(\text{DPM})_2]$  has short Rh-S bonds and a low value for  $\nu(\text{SO})$  in the infrared spectrum (Chapter IV).

In the title compound the C(1)-O distance is not as long as one might expect based on the low  $\nu(\text{CO})$ , but rather is comparable to that observed in "normal" bridging carbonyls which have  $\nu(\text{CO})$  ca.  $100 \text{ cm}^{-1}$  higher. However, carbonyl C-O distances are not overly sensitive to such changes owing to the relatively large uncertainty in the atomic positions. Therefore the present distance is, within experimental error, comparable to the analogous distances in the "ketonic" carbonyl species of  $[\text{Rh}_2\text{Cl}_2(\mu\text{-CO})(\mu\text{-DMA})(\text{DPM})_2]$ <sup>42</sup> and  $[\text{Pd}_2\text{Cl}_2(\mu\text{-CO})(\text{DPM})_2]$ <sup>32</sup> where the  $\nu(\text{CO})$  values of 1700 and  $1720 \text{ cm}^{-1}$ , respectively are ob-



served. Applying a riding motion correction the present C(1)-O distance (atom O riding on C(1)) yields a corrected value of 1.192(9) Å which is closer to the value we had expected based on spectral parameters.

### DISCUSSION

The structural determination of  $[\text{Rh}_2\text{Br}_2(\mu\text{-CO})(\text{DPM})_2]$  has unambiguously established it to be a monocarbonyl species having a formal Rh-Rh bond and not the alternate dicarbonyl species. The spectral parameters are consistent with both formulations (mono and dicarbonyl species), but the reaction of the compound with  $\text{SO}_2$ , yielding a dicarbonyl product, at first glance actually favours the dicarbonyl formulation. Prompted by the present structural characterization however, a reinvestigation of the  $^{31}\text{P}\{^1\text{H}\}$  NMR spectra during the slow stepwise addition of  $\text{SO}_2$  indicates the dicarbonyl species results from CO transfer from one monocarbonyl species to another (see Chapter V). A somewhat analogous, facile CO transfer has been reported<sup>35a,91</sup> between  $[\text{Rh}_2(\text{CO})_2(\mu\text{-Cl})(\text{DPM})_2]^+$  and  $[\text{Rh}_2(\text{CO})_2(\mu\text{-CO})(\mu\text{-Cl})(\text{DPM})_2]^+$ . These results clearly indicate the need for further structural and spectral characterizations of related complexes in order to yield the needed correlations between their structural and spectral parameters.

The complex,  $[\text{Rh}_2\text{Br}_2(\mu\text{-CO})(\text{DPM})_2]$  is only the second structurally characterized example with rhodium<sup>145</sup> in which a carbonyl ligand occupies the bridging site in





preference to the halide ligand. Generally the reverse is true,<sup>153</sup> yet in binuclear DPM-,<sup>42,125</sup> DAM-<sup>32,41</sup> and analogous diphosphazane-bridged<sup>145</sup> complexes of the Group VIII metals several complexes have now been characterized with bridging CO and terminal halide ligands. The closely related, SO<sub>2</sub> bridged species, [Rh<sub>2</sub>Cl<sub>2</sub>(μ-SO<sub>2</sub>)(DPM)<sub>2</sub>] is also anomalous in this regard having bridging SO<sub>2</sub> and terminal chloro groups (Chapter IV). It seems that in these complexes there is a strong tendency for the better π-acceptor ligand to enter the bridging site, even when initial attack by this ligand is terminal. In the bridging site the π-acceptor ligand can accept electron density from both electron rich metals, which in the present complex would account for the low value of ν(CO) and the short rhodium carbonyl distances. In addition the build-up of electron density on the carbonyl ligand, resulting from the large degree of back donation from the metal is also reflected in the low field chemical shift (227.5 ppm) of the <sup>13</sup>C carbonyl resonance. The trend in spectral parameters with increasing metal carbonyl back bonding is seen clearly in the series of closely related complexes [Rh<sub>2</sub>(CO)<sub>2</sub>(μ-CO)(μ-Cl)(DPM)<sub>2</sub>]<sup>+</sup>, [Rh<sub>2</sub>I(CO)(μ-CO)(DPM)<sub>2</sub>][I] and [Rh<sub>2</sub>Br<sub>2</sub>(μ-CO)(DPM)<sub>2</sub>], where the observed <sup>13</sup>C chemical shifts for the bridging carbonyl ligands (203.2,<sup>154</sup> 212.8<sup>154</sup> and 227.5 ppm, respectively) directly parallel the corresponding ν(CO) values (1850, 1810 and 1745 cm<sup>-1</sup>,



respectively).<sup>155</sup> In contrast however, the "ketonic" carbonyl complexes,  $[\text{Rh}_2\text{X}_2(\mu\text{-CO})(\mu\text{-acetylene})(\text{DPM})_2]$  ( $\text{X} = \text{Cl}, \text{Br}, \text{I}$ ), which have even lower values of  $\nu(\text{CO})$  of *ca.*  $1700\text{ cm}^{-1}$  have relatively high field  $^{13}\text{C}$  shifts of *ca.*  $190\text{ ppm}$ .<sup>42</sup> It is unclear at this time why the "ketonic" carbonyl species have such different  $^{13}\text{C}$  chemical shifts from the present compound when the carbonyl stretching frequencies are comparable, but it is clear that the use of spectral parameters to assign the mode of carbonyl bonding is fraught with difficulties, at least until more complete spectral and structural correlations are available.



## CHAPTER VII.

### Carbon Disulfide Chemistry and the the Structure of $[\text{Rh}_2\text{Cl}_2(\text{CO})(\text{C}_2\text{S}_4)(\text{DPM})_2]$

#### INTRODUCTION

Much of the recent interest in carbon disulfide chemistry stems from the close similarity of this molecule to the less reactive carbon dioxide molecule. Few species, however containing either of these ligands have been structurally characterized.<sup>45-47,156-160</sup> For the  $\text{CS}_2$  molecule, the commonest coordination mode, and one of the bonding modes also observed for the analogous  $\text{CO}_2$  molecule,<sup>160</sup> has the  $\text{CS}_2$  molecule bound to the metal in a side-on manner, through the carbon atom and one of the sulfur atoms (see Chapter I).<sup>45,156-159</sup>

For rhodium and iridium several  $\text{CS}_2$  containing complexes have been prepared<sup>48,161</sup> but until recently none had been structurally characterized.<sup>162</sup> In several of these complexes the  $\text{C},\text{S}-\eta^2$  bonding mode of the  $\text{CS}_2$  molecules had been inferred based on analogies with other transition metal complexes<sup>48,161</sup> even though the C-S stretching frequencies observed were typically *ca.*  $100\text{ cm}^{-1}$  lower than those observed in structurally confirmed complexes. These low values of  $\nu(\text{CS})$  suggest that the  $\text{CS}_2$  molecule may adopt another coordination geometry in these rhodium and iridium complexes. One possibility which must be considered in-



volves the condensation of the  $\text{CS}_2$  molecules. Certainly rhodium has previously displayed a tendency of condensing sulfur containing ligands, for example in  $[\text{RhCl}(\text{PPh}_3)_2(\text{PhCONCS})_2]^{163}$  and  $[\text{RhCl}(\text{PPh}_3)_2(\text{C}_2\text{H}_5\text{OCONCS})_3]^{164}$  where two molecules of  $\text{PhCONCS}$  and three molecules of  $\text{C}_2\text{H}_5\text{OCONCS}$ , respectively, are condensed at the metal centres. Significantly, one of the few structurally characterized " $\text{CO}_2$  complexes" actually contains a  $\text{C}_2\text{O}_4$  fragment resulting from the condensation of two  $\text{CO}_2$  molecules.<sup>50</sup> The  $\text{CO}$  stretching frequencies for this species are  $25\text{--}75\text{ cm}^{-1}$  lower than those in a typical  $\text{C},\text{O}-\eta^2$  bond species.<sup>160</sup> Furthermore, while this work was in progress the structural determination of  $[\text{Rh}(\text{C}_2\text{S}_4)(\eta^5\text{-C}_5\text{H}_5)(\text{PMe}_3)]^{162}$  indicated that the  $\text{C}_2\text{S}_4$  fragment was bound in an analogous manner to the above  $\text{C}_2\text{O}_4$  moiety and again the values of  $\nu(\text{CS})$  for this species were low.

In view of the obvious lack of structural information available on  $\text{CS}_2$  complexes, the present study was undertaken in order to form a much needed basis for spectral and structural correlations in these complexes and to gain a better understanding of transition metal activation of  $\text{CS}_2$  and related molecules.

### EXPERIMENTAL

All reactions were performed under a dinitrogen atmosphere using degassed solvents.





### Preparation of $[\text{Rh}_2\text{Cl}_2(\text{CO})(\text{C}_2\text{S}_4)(\text{DPM})_2]$

A suspension of 0.200 g (0.182 mmol) of *trans*- $[\text{RhCl}(\text{CO})(\text{DPM})]_2$ <sup>66</sup> (1) in 25 mL of  $\text{CH}_2\text{Cl}_2$  was treated with 10 mL of  $\text{CS}_2$  and allowed to react for 24 h. To the resulting red solution was added 25 mL of diethyl ether to induce crystallization. This complex may also be prepared in a manner analogous to that shown above, from the reaction of  $\text{CS}_2$  with  $[\text{Rh}_2\text{Cl}_2(\mu\text{-CO})(\text{DPM})_2]$ .

### Spectroscopic Studies

A solution was prepared by dissolving 0.100 g (0.072 mmol) of  $[\text{Rh}_2\text{Cl}_2(\mu\text{-CO})(\text{DPM})_2]$  (2) in 4 mL of  $\text{CD}_2\text{Cl}_2$  in a 10 mm NMR tube. The  $^{31}\text{P}\{^1\text{H}\}$  NMR spectrum was recorded at 233 K. Subsequent  $^{31}\text{P}\{^1\text{H}\}$  NMR spectra were then recorded after each 1.5  $\mu\text{L}$  (0.035 mmol) addition of  $\text{CS}_2$  until all of 2 had been converted to  $[\text{Rh}_2\text{Cl}_2(\text{CO})(\text{C}_2\text{S}_4)(\text{DPM})_2]$  (3). In addition to resonances assignable to 2 ( $\delta = 19.7$  ppm:  $|^1J_{\text{Rh-P}} + ^xJ_{\text{Rh-P}}| = 115.9$  Hz)<sup>101</sup> and 3 ( $\delta = 7.5$  ppm; AA'BB'XY multiplet), two additional resonances due to symmetric species at  $\delta = 15.7$  ppm ( $|^1J_{\text{Rh-P}} + ^xJ_{\text{Rh-P}}| = 116.5$  Hz) and  $\delta = 14.3$  ppm ( $|^1J_{\text{Rh-P}} + ^xJ_{\text{Rh-P}}| = 98.2$  Hz) were also observed at intermediate times in the reaction. Similarly the  $^{13}\text{C}\{^{31}\text{P}\{^1\text{H}\}\}$  NMR spectra were monitored using exactly the same technique and starting with  $[\text{Rh}_2\text{Cl}_2(\mu\text{-}^{13}\text{CO})(\text{DPM})_2]$ . Carbonyl resonances assignable to 2 ( $\delta = 229.0$  ppm; triplet;  $|J_{\text{Rh-C}}| = 44.9$  Hz), 3 ( $\delta = 191.5$  ppm; doublet;  $|J_{\text{Rh-C}}| = 69.1$  Hz) and a third species ( $\delta = 186.5$  ppm; doublet;



$|J_{\text{Rh-C}}| = 80.1 \text{ Hz})$  were observed.

Infrared spectra were obtained in an analogous manner, by recording the solution spectrum after each stepwise addition of 7  $\mu\text{L}$  (0.116 mmol) of  $\text{CS}_2$  to a  $\text{CH}_2\text{Cl}_2$  solution of 2 (0.500 g, 0.465 mmol) in 30 mL). Unfortunately the  $\text{CS}_2$  stretching region was obscured by DPM and free  $\text{CS}_2$  bands. In the bridging carbonyl region only one band was observed, which was assignable to 2 ( $\nu(\text{CO}) = 1750 \text{ cm}^{-1}$ ). In addition, two vibrations were observed in the terminal carbonyl region; the one at  $2030 \text{ cm}^{-1}$  increased in intensity throughout the experiment and was assigned to species 3, and the second at  $1990 \text{ cm}^{-1}$  was observed at intermediate times in the experiment.

#### Crystallization of $[\text{Rh}_2\text{Cl}_2(\text{CO})(\text{C}_2\text{S}_4)(\text{DPM})_2]$

To a solution of 0.100 g (0.0798 mmol) of 3 in 10 mL of  $\text{CH}_2\text{Cl}_2$  was added 2 mL of  $\text{CS}_2$  and 7 mL of diethyl ether. Crystallization was induced from this solution by slow cooling, yielding red crystals. An infrared spectrum ( $\nu(\text{CO}) = 2040(\text{sh}), 2020(\text{s}) \text{ cm}^{-1}$ ;  $\nu(\text{C-S}) = 1050(\text{m}), 995(\text{sh}), 980(\text{s}) \text{ cm}^{-1}$ ) verified that it was species 3.

#### X-Ray Data Collection

Red crystals of  $[\text{Rh}_2\text{Cl}_2(\text{CO})(\text{C}_2\text{S}_4)(\text{DPM})_2]$  were mounted in glass capillaries. Preliminary film data showed that these crystals were of only mediocre quality, however repeated attempts to obtain crystals of better quality failed.



The structural investigation was therefore continued on the original crystals. These crystals belong to the monoclinic system with extinctions ( $h0l$ ,  $l$  odd;  $0k0$ ,  $k$  odd) characteristic of the centrosymmetric space group  $P2_1/c$ . The density calculation, and the cell parameters, indicated that  $Z = 8$ , revealing that two independent dimers per asymmetric unit were present. Therefore, a cell reduction<sup>102</sup> was performed to rule out the possibility that the crystals might belong to a system of higher symmetry. The cell reduction confirmed the  $P2_1/c$  cell as the reduced cell and the solution of the structure verified this, showing that the two independent dimers in the asymmetric unit have slight but significant differences in their geometries (vide infra).

Data collection was carried out as previously described in Chapter II. Pertinent crystal and intensity collection data are presented in Table 34. Data collection was suspended at  $2\theta = 100^\circ$ , owing to the lack of diffracted intensity beyond this point. During data collection a clear colorless liquid was observed condensing on the inside of the capillary. However, by the time data collection had finished this liquid had disappeared (presumably through a pinhole in the capillary) so no identification of this liquid was possible.

### Solution of Structure

Since species 3 crystallized with two independent dimers per asymmetric unit, and therefore has four inde-



Table 34. Summary of Crystal Data and Intensity Collection  
for  $[\text{Rh}_2\text{Cl}_2(\text{CO})(\text{C}_2\text{S}_4)(\text{DPM})_2]$

Compound	[Rh <sub>2</sub> Cl <sub>2</sub> (CO)(C <sub>2</sub> S <sub>4</sub> )(DPM) <sub>2</sub> ]			
Formula	C <sub>53</sub> H <sub>44</sub> Cl <sub>2</sub> O <sub>1</sub> P <sub>4</sub> Rh <sub>2</sub> S <sub>4</sub>			
Formula Weight				
Cell Parameters				
a	22.311(3)	Å		
b	22.843(3)	Å		
c	22.828(3)	Å		
β	115.21(1)	°		
V	10526	Å <sup>3</sup>		
Z	8			
Density	1.547 g·cm <sup>-3</sup>	(calc'd.)		
	1.56(2) g·cm <sup>-3</sup>	(expt'l. by flotation)		
Space Group	C <sub>2h</sub> <sup>5</sup> - P2 <sub>1</sub> /c			
Crystal Dimensions	0.586 x 0.211 x 0.629			
Crystal Volume	0.0458 mm <sup>3</sup>			
Crystal Faces (and distances from an arbitrary origin within the crystal (mm))	1	0	0	(0.256)
	$\bar{1}$	0	$\bar{1}$	(0.203)
	5	0	2	(0.252)
	$\bar{1}$	0	1	(0.182)
	0	$\bar{1}$	0	(0.105)
	0	$\bar{1}$	0	(0.105)
Temperature	20°C			
Radiation	CuKα (λ=1.540562 Å) filtered with 0.5 mil thick nickel foil			
μ	90.85			
Range in Absorption Correction Factors	0.081 - 0.230			
Receiving Aperture	6 x 6 mm, 30 cm from the crystal			





Table 34, continued

Takeoff Angle	6.2°
Scan Speed	2° in 2θ/min
Scan Range	1.00° below $K_{\alpha 1}$ to 1.00° above $K_{\alpha 2}$
Background Counting Time	10s ( $2^\circ < 2\theta < 80^\circ$ ) 20s ( $80^\circ < 2\theta \leq 100^\circ$ )
2θ limits	$2^\circ \leq 2\theta \leq 100^\circ$
2θ limits for centered reflections	$50^\circ \leq 2\theta \leq 60^\circ$
Final number of variables	337
Unique Data Collected	11195
Unique Data Used ( $F_O^2 \geq 3\sigma(F_O^2)$ )	5929
Error in observation of unit weight	2.472
R	0.114
$R_w$	0.145



pendent rhodium atoms, structure solution was initially attempted using the direct methods program MULTAN.<sup>148</sup> However, efforts at solving the structure using MULTAN failed after repeated attempts, using between 500 and 700 reflections having the highest E's and generating between 2000 to 5000 unique phase relationships. In all solutions generated by MULTAN the same molecular orientations (for Rh and P) kept recurring, only with different relative positions of the dimers. This problem (of finding the molecular framework but failing to fix the origin) is not uncommon with MULTAN and is not unexpected given that in this structure we were attempting to push MULTAN far beyond its recommended limits. It is generally recommended to use about seven phase relationships per reflection and seven reflections per atom, whereas we were using at maximum 5.3 reflections per atom and generating 7.1 phase relationships per reflection. In addition, structures that require more than 500 reflections are generally too difficult for MULTAN to solve.

Our previous experience with these systems suggested that the Patterson map would be extremely difficult to interpret owing to vector build-up, especially considering that two molecules per asymmetric unit were present. This suspicion was confirmed by the calculated Patterson map, which showed severe Rh-Rh and Rh-P vector build-up. The top weighted vector, for example, at (0.44, 0.50, 0.44) was equal to approximately eleven times a singly weighted Rh-Rh



vector. As a result of this vector build-up in the Patterson map even using the Rh-P frameworks found in MULTAN, again the origin could not be uniquely defined. Therefore, one of the dimers, obtained from MULTAN, was arbitrarily chosen and its Rh-P framework was shifted to all possible positions consistent with the Patterson map, maintaining the orientation given by MULTAN. Subsequent full matrix least-squares and electron density difference maps on each possible solution established that the solution having Rh(A1) at (0.77, 0.14, 0.02) and Rh(A2) at (0.78, 0.02, 0.02) was considerably better than the others. In this solution, including the four associated P atoms,  $R = 0.49$  and  $R_w = 0.61$ <sup>121</sup> compared to values of near 0.53 and 0.63 for  $R$  and  $R_w$ , respectively, for other solutions. Furthermore, with this solution the Rh-P framework of the second dimer was observed at a position consistent with the Patterson map (other possible solutions did not yield this framework). The remaining atoms were located from subsequent least-squares calculations and electron density difference maps. Anomalous dispersion terms<sup>108</sup> for Rh, P, Cl and S were included in  $F_c$ . The phenyl carbon atoms were refined as rigid groups and hydrogen atoms were included as fixed contributions and not refined. All other nongroup atoms except hydrogens were refined with isotropic thermal parameters. An anisotropic refinement of, at least the heavy atoms (Rh, Cl, S and P), would have been appropriate on the



basis of the residual electron density observed around these atoms (range  $-3.11$  to  $2.69 \text{ e}/\text{\AA}^3$ ). However, this was not attempted due to the extremely high cost associated with refining these atoms anisotropically.

At this point an electron density difference map revealed the presence of an unresolved tunnel of electron density in the area enclosed by the phenyl ring of P(A3), P(A4), P(B2), and P(B4). Attempts to fit this area to  $\text{CS}_2$ ,  $\text{CH}_2\text{Cl}_2$  or  $(\text{C}_2\text{H}_5)_2\text{O}$  molecules were unsuccessful, however. Unreasonable geometries and thermal parameters resulted and no significant improvement in the crystallographic residuals was observed. The poorly resolved nature of this electron density probably results in part from the loss in solvent of crystallization which was observed during data collection (vide supra) and explains the poor diffraction quality of the crystals and the slight decrease in intensities of the standard reflections during data collection.

The final model with 337 parameters varied converged to  $R = 0.114$  and  $R_w = 0.145$ .<sup>121</sup> At this point an electron density difference map showed the highest 20 peaks ( $2.69 - 1.00 \text{ e}/\text{\AA}^3$ ) were in the vicinities of the heavy atoms and the tunnel of electron density. A typical carbon atom of an earlier syntheses had an electron density of  $3.2 \text{ e}/\text{\AA}^3$ .

## Results

The positional and thermal parameters for the individual isotropic atoms, rigid group atoms and idealized hydro-





gen atoms are given in Tables 35, 36 and 37, respectively. Least squares plane calculations are presented in Table 38 and selected bond lengths and angles are shown in Tables 39 and 40, respectively. A listing of observed and calculated structure amplitudes is available.<sup>110</sup>

A stereoview of both dimers is shown in Figure 22. Figure 23 shows a perspective view of dimers A and B. Phenyl carbon atoms are labelled sequentially around the ring starting at the carbon bound to phosphorus. The equatorial planes for  $[\text{Rh}_2\text{Cl}_2(\text{CO})(\text{C}_2\text{S}_4)(\text{DPM})_2]$  are shown in Figure 24 and include relevant bond lengths.



TABLE 35. Positional and Thermal Parameters For The Nongroup Atoms of [Rh2C12(CO)(C2S4)(DPM)2].

Atom	a			B(A <sup>2</sup> )	Atom	x			B(A <sup>2</sup> )
	x	y	z			x	y	z	
Rh(A1)	0.76980(9)	0.14301(8)	0.01950(9)	3.93(5)	P(A3)	0.8667(4)	0.1538(3)	0.1173(4)	4.8(2)
Rh(A2)	0.7819(1)	0.02064(8)	0.0180(1)	4.06(5)	P(A4)	0.8686(3)	0.0216(3)	0.1226(3)	4.5(2)
Rh(B1)	0.32896(9)	0.10029(8)	0.59006(9)	4.03(5)	P(B1)	0.3452(4)	0.2008(3)	0.5886(3)	4.6(2)
Rh(B2)	0.2210(1)	0.09592(9)	0.4676(1)	4.65(5)	P(B2)	0.2181(4)	0.1984(3)	0.4604(4)	5.4(2)
Cl(A1)	0.7146(3)	0.1599(3)	0.0895(3)	5.1(1)	P(B3)	0.3242(3)	-0.0010(3)	0.6054(3)	4.3(1)
Cl(A2)	0.8062(4)	-0.0864(3)	0.0166(4)	6.5(2)	P(B4)	0.2072(4)	-0.0069(3)	0.4692(4)	4.9(2)
Cl(B1)	0.2562(3)	0.1228(3)	0.6429(3)	5.3(2)	O(A1)	0.6919(9)	-0.0050(8)	0.0811(9)	6.8(5)
Cl(B2)	0.1467(4)	0.0905(3)	0.3476(4)	6.7(2)	O(B1)	0.118(1)	0.101(1)	0.516(1)	11.3(8)
S(A1)	0.7775(3)	0.2436(3)	0.0021(3)	4.9(2)	C(A1)	0.725(1)	0.010(1)	0.058(1)	4.8(6)
S(A2)	0.8120(5)	0.3064(4)	-0.0926(5)	8.3(2)	C(B1)	0.147(1)	0.102(1)	0.492(1)	5.8(7)
S(A3)	0.8279(4)	0.1810(3)	-0.0821(4)	5.3(2)	C(A2)	0.670(1)	0.081(1)	-0.130(1)	4.6(5)
S(A4)	0.8439(3)	0.0611(3)	-0.0354(3)	4.6(2)	C(A3)	0.875(1)	0.089(1)	0.169(1)	3.8(5)
S(B1)	0.4355(3)	0.0967(3)	0.6764(3)	4.7(1)	C(B2)	0.266(1)	0.238(1)	0.537(1)	6.2(7)
S(B2)	0.5694(4)	0.0879(4)	0.6791(4)	7.3(2)	C(B3)	0.248(1)	-0.036(1)	0.554(1)	5.5(6)
S(B3)	0.4554(3)	0.0835(3)	0.5558(3)	5.2(2)	C(A4)	0.802(1)	0.247(1)	-0.058(1)	5.1(6)
S(B4)	0.3210(3)	0.0869(3)	0.4536(3)	5.1(2)	C(A5)	0.816(1)	0.128(1)	-0.032(1)	4.9(6)
P(A1)	0.6672(3)	0.1356(3)	-0.0715(3)	4.3(1)	C(B4)	0.488(1)	0.089(1)	0.639(1)	5.1(6)
P(A2)	0.7001(3)	0.0106(3)	-0.0892(3)	4.1(1)	C(B5)	0.370(1)	0.090(1)	0.531(1)	4.0(5)

<sup>a</sup>

Estimated standard deviations in the least significant figure(s) are given in parentheses in this and all subsequent tables.



TABLE 36. Derived Parameters For the Rigid Group Atoms of [Rh2C12(CO)(C2S4)(DPM)2].

Atom	x	y	z	B(A')	Atom	x	y	z	B(A')
C(A11)	0.6399(9)	0.2021(7)	-0.121(1)	3.9(5)	C(B11)	0.3670(8)	0.2404(8)	0.6641(7)	4.2(5)
C(A12)	0.637(1)	0.2082(7)	-0.183(1)	6.6(7)	C(B12)	0.3828(9)	0.2127(5)	0.7231(9)	5.5(6)
C(A13)	0.610(1)	0.2586(9)	-0.2187(7)	7.8(9)	C(B13)	0.4022(8)	0.2456(8)	0.7796(7)	6.3(7)
C(A14)	0.5861(9)	0.3030(7)	-0.193(1)	7.5(8)	C(B14)	0.4057(8)	0.3063(8)	0.7770(7)	5.4(6)
C(A15)	0.589(1)	0.2969(7)	-0.131(1)	7.6(8)	C(B15)	0.3899(9)	0.3341(5)	0.7179(9)	9.0(9)
C(A16)	0.616(1)	0.2465(9)	-0.0949(7)	4.6(6)	C(B16)	0.3706(8)	0.3012(8)	0.6615(7)	6.3(7)
C(A21)	0.588(2)	0.1139(8)	-0.0710(7)	4.1(5)	C(B21)	0.410(2)	0.2249(8)	0.566(4)	4.1(5)
C(A22)	0.588(2)	0.0893(8)	-0.015(2)	5.5(7)	C(B22)	0.398(4)	0.2307(8)	0.501(2)	6.6(7)
C(A23)	0.528(2)	0.0721(8)	-0.015(2)	6.4(7)	C(B23)	0.449(5)	0.2450(8)	0.484(3)	4.7(6)
C(A24)	0.459(2)	0.0795(8)	-0.0695(7)	6.8(7)	C(B24)	0.513(2)	0.2534(8)	0.532(4)	6.7(7)
C(A25)	0.469(2)	0.1041(8)	-0.125(2)	7.6(8)	C(B25)	0.525(4)	0.2476(8)	0.597(2)	7.6(8)
C(A26)	0.528(2)	0.1213(8)	-0.126(2)	5.2(6)	C(B26)	0.474(5)	0.2334(8)	0.614(3)	5.1(6)
C(A31)	0.6253(8)	-0.0310(7)	-0.1010(6)	3.4(5)	C(B31)	0.2404(9)	0.2368(8)	0.4035(7)	4.7(6)
C(A32)	0.564(1)	-0.0191(6)	-0.1521(9)	5.3(6)	C(B32)	0.2494(9)	0.2972(8)	0.4078(7)	5.8(7)
C(A33)	0.5088(7)	-0.0521(7)	-0.1598(8)	5.0(6)	C(B33)	0.2666(9)	0.3263(6)	0.3636(9)	7.9(9)
C(A34)	0.5145(8)	-0.0970(7)	-0.1165(6)	5.6(6)	C(B34)	0.2748(9)	0.2951(8)	0.3152(7)	6.5(7)
C(A35)	0.576(1)	-0.1088(6)	-0.0654(9)	5.3(6)	C(B35)	0.2658(9)	0.2347(8)	0.3109(7)	6.1(7)
C(A36)	0.5310(7)	-0.0759(7)	-0.0576(8)	5.1(6)	C(B36)	0.2485(9)	0.2055(6)	0.3551(9)	6.0(7)
C(A41)	0.722(2)	-0.0274(9)	-0.149(2)	4.5(5)	C(B41)	0.136(1)	0.233(2)	0.437(1)	8.7(9)
C(A42)	0.681(1)	-0.0208(9)	-0.215(2)	8.7(9)	C(B42)	0.086(2)	0.220(1)	0.376(2)	10(1)
C(A43)	0.698(2)	-0.045(1)	-0.2612(9)	10(1)	C(B43)	0.024(2)	0.246(2)	0.355(2)	18(2)
C(A44)	0.758(2)	-0.0753(9)	-0.242(2)	6.5(7)	C(B44)	0.012(1)	0.287(2)	0.394(1)	13(1)
C(A45)	0.799(1)	-0.0819(9)	-0.176(2)	11(1)	C(B45)	0.062(2)	0.300(1)	0.455(2)	21(2)
C(A46)	0.781(2)	-0.053(1)	-0.1300(9)	8.9(9)	C(B46)	0.124(2)	0.274(2)	0.477(2)	18(2)
C(A51)	0.864(1)	0.2183(9)	0.167(1)	6.3(7)	C(B51)	0.3301(9)	-0.0263(7)	0.6843(6)	4.1(5)
C(A52)	0.848(1)	0.273(1)	0.1628(8)	9(1)	C(B52)	0.3401(8)	0.0128(5)	0.7344(8)	4.8(6)
C(A53)	0.883(1)	0.3179(8)	0.205(1)	10(1)	C(B53)	0.3378(8)	-0.0069(7)	0.7911(7)	6.9(7)
C(A54)	0.865(1)	0.3071(9)	0.252(1)	7.7(8)	C(B54)	0.3256(9)	-0.0657(7)	0.7978(6)	5.3(7)
C(A55)	0.841(1)	0.252(1)	0.2562(8)	9.5(9)	C(B55)	0.3156(8)	-0.1048(5)	0.7477(8)	5.0(6)
C(A56)	0.840(1)	0.2075(8)	0.214(1)	7.9(8)	C(B56)	0.3178(8)	-0.0851(7)	0.6909(7)	5.5(6)
C(A61)	0.953(2)	0.169(1)	0.128(1)	7.3(8)	C(B61)	0.392(1)	-0.0412(8)	0.598(2)	5.2(6)
C(A62)	1.006(3)	0.165(1)	0.189(3)	7.3(8)	C(B62)	0.452(2)	-0.0458(8)	0.653(2)	5.1(6)
C(A63)	1.069(2)	0.182(1)	0.197(2)	8.3(9)	C(B63)	0.508(1)	-0.0670(8)	0.6478(7)	6.6(7)
C(A64)	1.079(2)	0.203(1)	0.144(1)	15(2)	C(B64)	0.504(1)	-0.0836(8)	0.588(2)	7.5(7)
C(A65)	1.025(3)	0.207(1)	0.084(3)	18(2)	C(B65)	0.444(2)	-0.0789(8)	0.533(2)	4.7(6)
C(A66)	0.962(2)	0.190(1)	0.076(2)	14(2)	C(B66)	0.388(1)	-0.0577(8)	0.5378(7)	4.8(6)
C(A71)	0.8532(9)	-0.0343(7)	0.1789(8)	4.5(5)	C(B71)	0.2355(9)	-0.0542(7)	0.4222(7)	5.5(6)
C(A72)	0.8945(8)	-0.0881(8)	0.1851(7)	6.4(7)	C(B72)	0.2444(9)	-0.1134(8)	0.4378(7)	5.8(7)
C(A73)	0.8909(9)	-0.1299(6)	0.2279(9)	7.4(8)	C(B73)	0.2656(9)	-0.1511(5)	0.4026(9)	6.6(7)
C(A74)	0.8500(9)	-0.1178(7)	0.2645(8)	6.5(7)	C(B74)	0.2780(9)	-0.1296(7)	0.3518(7)	6.2(7)
C(A75)	0.8246(8)	-0.0640(8)	0.2583(7)	5.5(6)	C(B75)	0.2691(9)	-0.0703(8)	0.3361(7)	6.1(7)
C(A76)	0.8282(9)	-0.0222(6)	0.2155(9)	4.9(6)	C(B76)	0.2478(9)	-0.0326(5)	0.3713(9)	4.3(6)
C(A81)	0.953(2)	0.0071(9)	0.1294(7)	5.1(6)	C(B81)	0.122(1)	-0.033(1)	0.447(4)	5.9(7)
C(A82)	0.963(3)	-0.0185(9)	0.079(2)	5.6(6)	C(B82)	0.082(4)	-0.035(1)	0.380(5)	10(1)
C(A83)	1.026(2)	-0.0359(8)	0.088(2)	4.9(6)	C(B83)	0.017(3)	-0.053(1)	0.357(2)	13(1)
C(A84)	1.079(2)	-0.0277(9)	0.1482(7)	7.5(8)	C(B84)	-0.009(1)	-0.070(1)	0.401(4)	14(1)
C(A85)	1.069(3)	-0.0021(9)	0.199(2)	7.9(9)	C(B85)	0.031(4)	-0.069(1)	0.467(5)	21(2)
C(A86)	1.006(2)	0.0153(8)	0.189(2)	6.3(7)	C(B86)	0.097(3)	-0.050(1)	0.490(2)	23(3)



TABLE 36. (Continued)

## Rigid Group Parameters

	a			b		
	Xc	Yc	Zc	Delta	Epsilon	Eta
Ring1	0.5130(5)	0.2526(6)	-0.1568(6)	-0.44(1)	1.57(1)	4.30(1)
Ring2	0.5282(6)	0.0967(5)	-0.0703(6)	1.14(1)	2.89(3)	2.39(3)
Ring3	0.5699(6)	-0.0640(5)	-0.1087(5)	3.84(1)	2.87(1)	3.93(1)
Ring4	0.7400(7)	-0.0513(6)	-0.1956(7)	2.13(1)	2.04(2)	3.98(3)
Ring5	0.8643(6)	0.2627(7)	0.2095(7)	0.28(1)	1.27(1)	5.42(2)
Ring6	1.0157(9)	0.1860(7)	0.1363(9)	4.34(2)	2.64(4)	0.86(5)
Ring7	0.8596(5)	-0.0761(5)	0.2217(5)	2.76(1)	1.11(1)	5.45(1)
Ring8	1.0160(6)	-0.0103(5)	0.1388(6)	2.01(1)	2.76(3)	5.56(3)
Ring9	0.3854(5)	0.2734(5)	0.7205(6)	3.21(1)	1.87(1)	0.57(1)
Ring10	0.4616(6)	0.2392(5)	0.5489(6)	1.33(1)	2.16(5)	4.61(5)
Ring11	0.2576(5)	0.2659(6)	0.3594(6)	3.27(1)	1.35(1)	2.64(1)
Ring12	0.074(1)	0.2600(8)	0.416(1)	-0.83(2)	2.65(3)	3.85(3)
Ring13	0.3278(5)	-0.0460(5)	0.7410(5)	0.19(1)	1.60(1)	0.34(1)
Ring14	0.4431(6)	-0.0624(5)	0.5928(6)	-1.20(1)	2.43(3)	1.26(3)
Ring15	0.2567(5)	-0.0919(5)	0.3870(6)	-0.18(1)	1.31(1)	2.46(1)
Ring16	0.0569(9)	-0.0517(7)	0.424(1)	4.37(2)	2.13(6)	4.25(6)

a

Xc, Yc and Zc are the fractional coordinates of the centroid of the rigid group.

b

The rigid group orientation angles Delta, Epsilon and Eta (radians) are the angles by which the rigid body is rotated with respect to a set of axes X, Y and Z. The origin is the centre of the ring; X is parallel to a\*, Z is parallel to c and Y is parallel to the line defined by the intersection of the plane containing a\* and b\* with the plane containing b and c.





TABLE 37. Idealized Positional and Thermal Parameters For the Hydrogen Atoms of [Rh2C12(CO)(C2S4)(DPM)2].

Atom	x	y	z	B(A <sup>2</sup> )	Atom	x	y	z	B(A <sup>2</sup> )
H(A1)	0.7019	0.0928	-0.1492	5.58	H(A83)	1.0331	-0.0532	0.0542	5.85
H(A2)	0.6293	0.0749	-0.1675	5.58	H(A84)	1.1227	-0.0405	0.1554	8.49
H(A3)	0.8353	0.0931	0.1805	4.85	H(A85)	1.1059	0.0017	0.2407	8.93
H(A4)	0.9122	0.0933	0.2067	4.85	H(A86)	0.9995	0.0312	0.2248	7.31
H(B1)	0.2787	0.2769	0.5263	7.21	H(B12)	0.3804	0.1722	0.7240	6.49
H(B2)	0.2425	0.2441	0.5616	7.21	H(B13)	0.4152	0.2264	0.8199	7.32
H(B3)	0.2153	-0.0281	0.5708	6.45	H(B14)	0.4220	0.3286	0.8163	6.37
H(B4)	0.2527	-0.0751	0.5506	6.45	H(B15)	0.3940	0.3765	0.7179	9.98
H(A12)	0.6519	0.1783	-0.2020	7.61	H(B16)	0.3592	0.3222	0.6220	7.29
H(A13)	0.6073	0.2640	-0.2606	8.80	H(B22)	0.3537	0.2243	0.4661	7.59
H(A14)	0.5885	0.3384	-0.2150	8.46	H(B23)	0.4406	0.2486	0.4389	5.68
H(A15)	0.5742	0.3269	-0.1108	8.60	H(B24)	0.5475	0.2633	0.5206	7.71
H(A16)	0.6187	0.2411	-0.0522	5.61	H(B25)	0.5673	0.2537	0.6295	8.60
H(A21)	0.6377	0.0821	0.0237	6.55	H(B26)	0.4803	0.2293	0.6567	6.11
H(A23)	0.5265	0.0511	0.0211	7.44	H(B32)	0.2449	0.3186	0.4424	6.83
H(A24)	0.4282	0.0651	-0.0723	7.73	H(B33)	0.2749	0.3686	0.3694	8.92
H(A25)	0.4399	0.1103	-0.1633	8.56	H(B34)	0.2873	0.3174	0.2863	7.50
H(A26)	0.5320	0.1413	-0.1638	6.24	H(B35)	0.2697	0.2161	0.2764	7.14
H(A32)	0.5535	0.0137	-0.1800	6.32	H(B36)	0.2397	0.1660	0.3494	6.96
H(A33)	0.4650	-0.0429	-0.1937	5.99	H(B42)	0.0958	0.1907	0.3523	11.30
H(A34)	0.4769	-0.1207	-0.1230	6.64	H(B43)	-0.0092	0.2339	0.3147	19.15
H(A35)	0.5804	-0.1419	-0.0387	6.28	H(B44)	-0.0316	0.3028	0.3787	14.26
H(A36)	0.6729	-0.0852	-0.0249	6.07	H(B45)	0.0510	0.3285	0.4804	21.90
H(A42)	0.6406	0.0001	-0.2308	9.67	H(B46)	0.1560	0.2853	0.5180	19.20
H(A43)	0.6720	-0.0437	-0.3062	10.88	H(B52)	0.3476	0.0522	0.7308	5.81
H(A44)	0.7712	-0.0965	-0.2707	7.46	H(B53)	0.3456	0.0182	0.8267	7.92
H(A45)	0.8391	-0.1054	-0.1597	11.56	H(B54)	0.3259	-0.0810	0.8378	6.35
H(A46)	0.8077	-0.0616	-0.0843	9.86	H(B55)	0.3082	-0.1462	0.7528	5.99
H(A52)	0.9015	0.2779	0.1291	9.86	H(B56)	0.3101	-0.1123	0.6568	6.51
H(A53)	0.9032	0.3543	0.1981	11.26	H(B62)	0.4521	-0.0341	0.6927	6.12
H(A54)	0.8656	0.3382	0.2782	8.69	H(B63)	0.5467	-0.0705	0.6851	7.61
H(A55)	0.8264	0.2457	0.2893	10.54	H(B64)	0.5411	-0.0993	0.5844	8.54
H(A56)	0.8247	0.1693	0.2202	8.86	H(B65)	0.4410	-0.0917	0.4915	5.68
H(A62)	0.9977	0.1492	0.2253	8.28	H(B66)	0.3465	-0.0554	0.4991	5.80
H(A63)	1.1032	0.1796	0.2393	9.27	H(B72)	0.2379	-0.1269	0.4732	6.78
H(A64)	1.1198	0.2135	0.1504	15.99	H(B73)	0.2741	-0.1905	0.4145	7.62
H(A65)	1.0308	0.2169	0.0476	18.62	H(B74)	0.2940	-0.1547	0.3283	7.22
H(A66)	0.9254	0.1864	0.0336	15.41	H(B75)	0.2776	-0.0553	0.3008	7.15
H(A72)	0.9146	-0.0969	0.1560	7.45	H(B76)	0.2414	0.0083	0.3595	5.33
H(A73)	0.9093	-0.1677	0.2278	8.40	H(B82)	-0.0953	-0.0238	0.3476	10.51
H(A74)	0.8540	-0.1470	0.2926	7.49	H(B83)	-0.0132	-0.0583	0.3137	14.36
H(A75)	0.8040	-0.0555	0.2855	6.46	H(B84)	-0.0509	-0.0877	0.3905	14.65
H(A76)	0.8093	0.0153	0.2136	5.92	H(B85)	0.0199	-0.0826	0.5011	21.72
H(A82)	0.9267	-0.0237	0.0382	6.55	H(B86)	0.1284	-0.0481	0.5349	24.40



Table 38. Least Squares Plane Calculations

Plane No.	Dimer	Equation <sup>a</sup>				
1	A	0.8729X+0.1141Y-0.4743Z-14.9811 = 0.0				
	B	0.8952X-0.0956Y-0.4353Z+4.0804 = 0.0				
2	A	0.8862X+0.0856Y-0.4553Z-15.1615 = 0.0				
	B	0.8948X-0.1440Y-0.4227Z+4.0503 = 0.0				
3	A	-0.6211X-0.0716Y-0.7804Z+11.0834 = 0.0				
	B	0.0947X+0.9925Y-0.0779Z-1.4659 = 0.0				
deviation from planes, Å						
Plane no.						
Atom	1-A	1-B	2-A	2-B	3-A	3-B
Rh(1)	0.027(2)	-0.010(2)	-0.012(2)	0.002(2)	-0.015(2)	0.010(2)
Rh(2)	-0.030(2)	0.012(2)	0.013(2)	-0.003(2)	0.033(2)	-0.007(2)
P(1)	-0.326(8)	0.121(8)				
P(2)	0.312(8)	-0.143(9)				
P(3)			0.163(8)	-0.027(8)		
P(4)			-0.154(8)	0.030(8)		
S(1)					-0.110(7)	-0.065(7)
S(2)					0.26(1)	0.012(9)
S(3)					0.141(8)	-0.018(7)
S(4)					-0.355(7)	0.035(7)
C(2)	0.67(3) <sup>b</sup>	-0.63(3) <sup>b</sup>				
C(3)			-0.74(3) <sup>b</sup>	-0.54(3)	0.14(3)	-0.03(3)
C(4)					-0.11(3)	0.01(2)
C(5)						

<sup>a</sup>X, Y, and Z are orthogonal coordinates (Å) with X along the a axis, Y in the a-b plane and Z along the c\* axis.

<sup>b</sup>Not included in least-squares plane calculations.



Table 39: Select Distances ( $\text{\AA}$ ) in  $[\text{Rh}_2\text{Cl}_2(\text{CO})(\text{C}_2\text{S}_4)(\text{DPM})_2]$ 

Bond Distance			
	Dimer A	Dimer B	
Rh(1) - Rh(2)	2.810 (3)	2.809 (3)	
Rh(1) - Cl(1)	2.427 (6)	2.454 (6)	
Rh(2) - Cl(2)	2.507 (8)	2.529 (8)	
Rh(1) - P(1)	2.353 (7)	2.326 (7)	
Rh(2) - P(2)	2.359 (7)	2.345 (8)	
Rh(1) - P(3)	2.367 (8)	2.349 (7)	
Rh(2) - P(4)	2.346 (8)	2.371 (7)	
Rh(1) - S(1)	2.351 (7)	2.356 (7)	
Rh(1) - C(5)	1.89 (2)	1.95 (2)	
Rh(2) - S(4)	2.388 (7)	2.392 (7)	
Rh(2) - C(1)	1.86 (2)	1.97 (3)	
S(1) - C(4)	1.67 (2)	1.73 (2)	
S(2) - C(4)	1.63 (3)	1.64 (3)	
S(3) - C(4)	1.79 (2)	1.73 (3)	
S(3) - C(5)	1.76 (2)	1.74 (2)	
S(4) - C(5)	1.68 (3)	1.63 (2)	
C(1) - O(1)	1.13 (2)	1.01 (3)	
P(1) - C(2)	1.85 (2)	1.86 (2)	
P(2) - C(2)	1.84 (2)	1.86 (2)	
P(3) - C(3)	1.85 (2)	1.78 (3)	
P(4) - C(3)	1.84 (2)	1.88 (3)	
P(1) - C(11)	1.84 (1)	1.82 (1)	
P(1) - C(21)	1.85 (1)	1.83 (1)	
P(2) - C(31)	1.84 (1)	1.80 (1)	
P(2) - C(41)	1.86 (1)	1.86 (2)	
P(3) - C(51)	1.89 (2)	1.84 (1)	
P(3) - C(61)	1.86 (2)	1.84 (1)	
P(4) - C(71)	1.85 (1)	1.82 (1)	
P(4) - C(81)	1.85 (1)	1.84 (2)	

## Nonbonded Contacts

P(A1) - P(A2)	3.018 (9)
P(B1) - P(B2)	3.088 (10)
P(A3) - P(A4)	3.022 (10)
P(B3) - P(B4)	3.096 (10)
Cl(A2) - H(A46)	2.39
Cl(B2) - H(B42)	2.58
O(A1) - H(A22)	2.48
C(B3) - H(B22)	2.33
H(A76) - H(A3)	2.11
H(A86) - H(A4)	2.30
H(A13) - H(B25) <sup>a</sup>	2.29
H(A65) - H(B45) <sup>b</sup>	2.05

<sup>a</sup>Atom located at x,y,-1+3.<sup>b</sup>Atom located at 1+x,  $\frac{1}{2}$ -y,  $-\frac{1}{2}$ +z.



Table 40. Selected Angles (deg) in  $[\text{Rh}_2\text{Cl}_2(\text{CO})(\text{C}_2\text{S}_4)(\text{DPM})_2]$ 

	<u>Bond Angles</u>	
	Dimer A	Dimer B
Rh(2)-Rh(1)-S(1)	163.0(2)	164.4(2)
Rh(2)-Rh(1)-Cl(1)	104.1(2)	91.7(2)
Rh(2)-Rh(1)-C(5)	74.7(8)	76.3(7)
Rh(2)-Rh(1)-P(1)	88.9(2)	95.3(2)
Rh(2)-Rh(1)-P(3)	93.5(2)	92.3(2)
Rh(1)-Rh(2)-Cl(2)	172.9(2)	165.5(2)
Rh(1)-Rh(2)-S(4)	72.6(2)	71.5(2)
Rh(1)-Rh(2)-C(1)	91.9(8)	100.4(8)
Rh(1)-Rh(2)-P(2)	94.2(2)	91.2(2)
Rh(1)-Rh(2)-P(4)	91.2(2)	94.7(2)
Cl(1)-Rh(1)-S(1)	92.9(2)	103.8(2)
Cl(1)-Rh(1)-C(5)	177.5(8)	166.9(7)
Cl(1)-Rh(1)-P(1)	91.0(2)	86.6(2)
Cl(1)-Rh(1)-P(3)	83.0(2)	93.0(2)
Cl(2)-Rh(2)-S(4)	101.2(2)	94.0(2)
Cl(2)-Rh(2)-C(1)	94.4(8)	94.1(8)
Cl(2)-Rh(2)-P(2)	88.2(2)	89.2(3)
Cl(2)-Rh(2)-P(4)	86.1(3)	86.5(3)
S(1)-Rh(1)-C(5)	88.3(8)	88.3(7)
S(1)-Rh(1)-P(1)	92.0(2)	86.5(3)
S(1)-Rh(1)-P(3)	87.4(2)	86.3(2)
S(4)-Rh(2)-C(1)	164.3(8)	171.8(8)
S(4)-Rh(2)-P(2)	82.4(2)	94.4(2)
S(4)-Rh(2)-P(4)	96.3(2)	93.0(2)
C(5)-Rh(1)-P(1)	91.2(8)	89.3(7)
C(5)-Rh(1)-P(3)	94.8(8)	92.8(7)
C(1)-Rh(2)-P(2)	96.4(8)	87.2(8)
C(1)-Rh(2)-P(4)	86.4(8)	86.0(8)
P(1)-Rh(1)-P(3)	173.9(2)	172.4(3)
P(2)-Rh(2)-P(4)	173.8(2)	171.7(3)
Rh(1)-S(1)-C(4)	105.1(9)	104.5(9)
S(1)-C(4)-S(2)	127(2)	123(1)
S(1)-C(4)-S(3)	118(1)	119(2)
S(2)-C(4)-S(3)	115(1)	117(1)
C(4)-S(3)-C(5)	102(1)	104(1)
Rh(1)-C(5)-S(3)	124(1)	124(1)
Rh(1)-C(5)-S(4)	120(1)	117(1)
S(3)-C(5)-S(4)	116(1)	119(1)
Rh(2)-S(4)-C(5)	91.1(8)	95.1(8)
Rh(2)-C(1)-O(1)	169(3)	165(3)





Table 40, continued

<u>Bond Angles</u>		
	Dimer A	Dimer B
Rh(1)-P(1)-C(2)	114.4(8)	110.7(9)
Rh(2)-P(2)-C(2)	113.2(8)	116 (1)
Rh(1)-P(3)-C(3)	108.5(8)	115.4(9)
Rh(2)-P(4)-C(3)	114.7(8)	110.7(8)
Rh(1)-P(1)-C(11)	115.3(6)	117.2(7)
Rh(1)-P(1)-C(21)	126.1(6)	116.7(6)
Rh(2)-P(2)-C(31)	117.1(6)	121.9(9)
Rh(2)-P(2)-C(41)	118.8(8)	116 (1)
Rh(1)-P(3)-C(51)	113.5(7)	117.8(6)
Rh(1)-P(3)-C(61)	128 (1)	112.8(6)
Rh(2)-P(4)-C(71)	115.5(6)	120.0(6)
Rh(2)-P(4)-C(81)	116.9(7)	116.6(8)
P(1)-C(2)-P(2)	110 (1)	112 (1)
P(3)-C(3)-P(4)	110 (1)	115 (1)
C(2)-P(1)-C(11)	102 (1)	100 (1)
C(2)-P(1)-C(21)	99.1(9)	110 (1)
C(2)-P(2)-C(31)	105.8(9)	102 (1)
C(2)-P(2)-C(41)	101 (1)	99 (1)
C(3)-P(3)-C(51)	105 (1)	99 (1)
C(3)-P(3)-C(61)	104 (1)	108 (1)
C(3)-P(4)-C(71)	100.9(9)	105 (1)
C(3)-P(4)-C(81)	106 (1)	99 (1)
C(11)-P(1)-C(21)	99.1(8)	101.4(8)
C(31)-P(2)-C(41)	99.1(8)	97 (1)
C(51)-P(3)-C(61)	94 (1)	102.4(8)
C(71)-P(4)-C(81)	100.5(9)	102 (1)

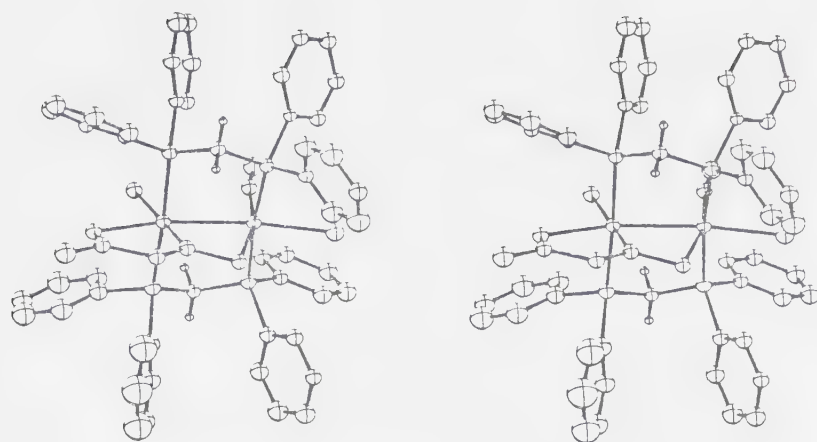
<u>Torsion Angles</u>		
	Dimer A	Dimer B
P(1)-Rh(1)-Rh(2)-P(2)	17.0(2)	7.1(2)
P(3)-Rh(1)-Rh(2)-P(4)	8.4(2)	1.5(2)
Cl(1)-Rh(1)-P(1)-C(11)	98.8(7)	49.5(7)
Cl(1)-Rh(1)-P(1)-C(21)	25.5(8)	170.0(7)
Cl(1)-Rh(1)-P(3)-C(51)	45.6(8)	42.4(7)
Cl(1)-Rh(1)-P(3)-C(61)	162 (1)	161.4(7)
Cl(2)-Rh(2)-P(2)-C(31)	70.1(6)	54.4(8)
Cl(2)-Rh(2)-P(2)-C(41)	48.9(7)	64 (1)
Cl(2)-Rh(2)-P(4)-C(71)	51.9(7)	62.0(8)
Cl(2)-Rh(2)-P(4)-C(81)	66.0(7)	62 (1)
S(1)-Rh(1)-P(1)-C(11)	5.9(7)	54.6(7)
S(1)-Rh(1)-P(1)-C(21)	118.4(7)	65.9(7)
S(1)-Rh(1)-P(3)-C(51)	47.6(8)	61.3(7)



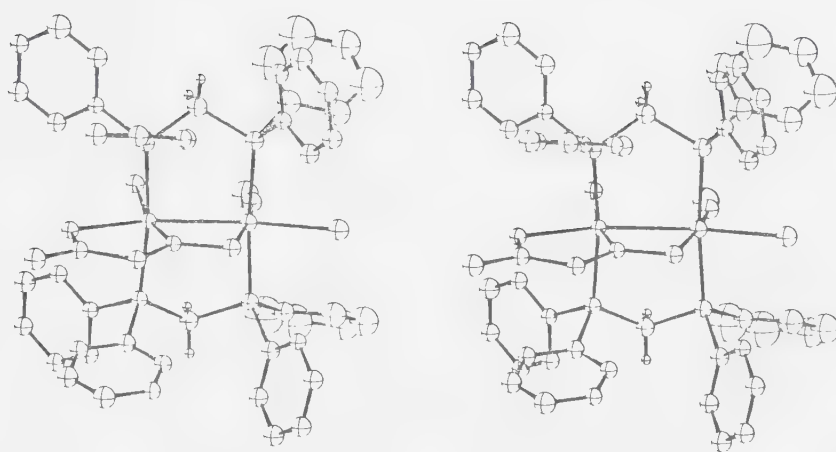
Table 40, continued

<u>Torsion Angles</u>		
	Dimer A	Dimer B
S(1)-Rh(1)-P(3)-C(61)	69 (1)	57.7(7)
S(4)-Rh(2)-P(2)-C(31)	171.6(6)	39.6(8)
S(4)-Rh(2)-P(2)-C(41)	52.7(7)	158 (1)
S(4)-Rh(2)-P(4)-C(71)	152.8(7)	31.8(8)
S(4)-Rh(2)-P(4)-C(81)	34.9(7)	156 (1)
C(5)-Rh(1)-P(1)-C(11)	82 (1)	142.9(9)
C(5)-Rh(1)-P(1)-C(21)	153 (1)	22 (1)
C(5)-Rh(1)-P(3)-C(51)	136 (1)	149.4(9)
C(5)-Rh(1)-P(3)-C(61)	19 (1)	30 (1)
C(1)-Rh(2)-P(2)-C(31)	24 (1)	148 (1)
C(1)-Rh(2)-C(41)	143 (1)	30 (1)
C(1)-Rh(2)-P(4)-C(71)	43 (1)	156 (1)
C(1)-Rh(2)-P(4)-C(81)	161 (1)	32 (1)





(A)



(B)

Figure 22. Stereoviews for Molecules A and B of  $[\text{Rh}_2\text{Cl}_2(\text{CO})(\text{C}_2\text{S}_4)(\text{DPM})_2]$ .



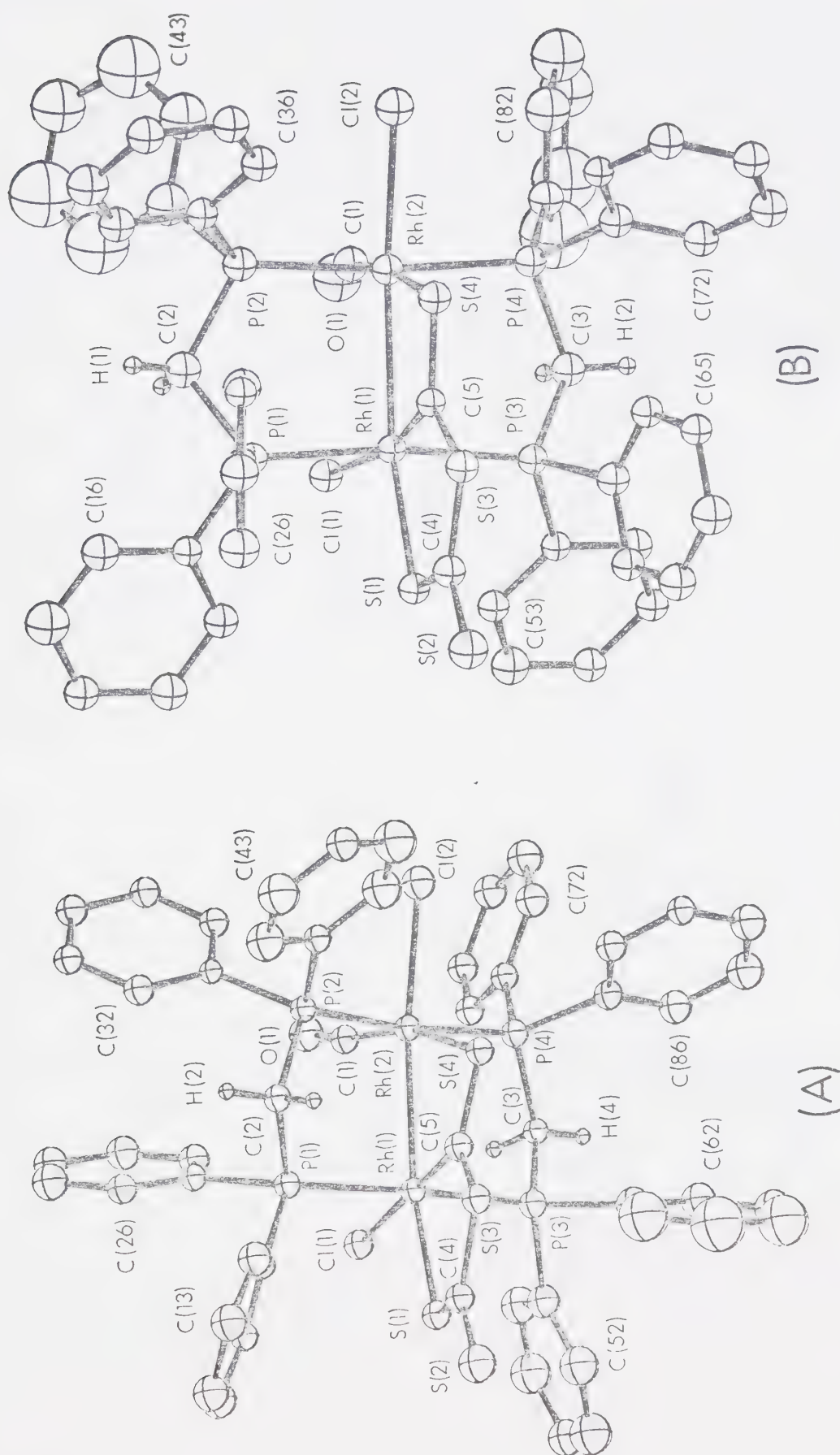


Figure 23. A Perspective View for Dimers A and B of  $[\text{Rh}_2\text{Cl}_2(\text{CO})(\text{C}_2\text{S}_4)(\text{DPM})_2]$ .





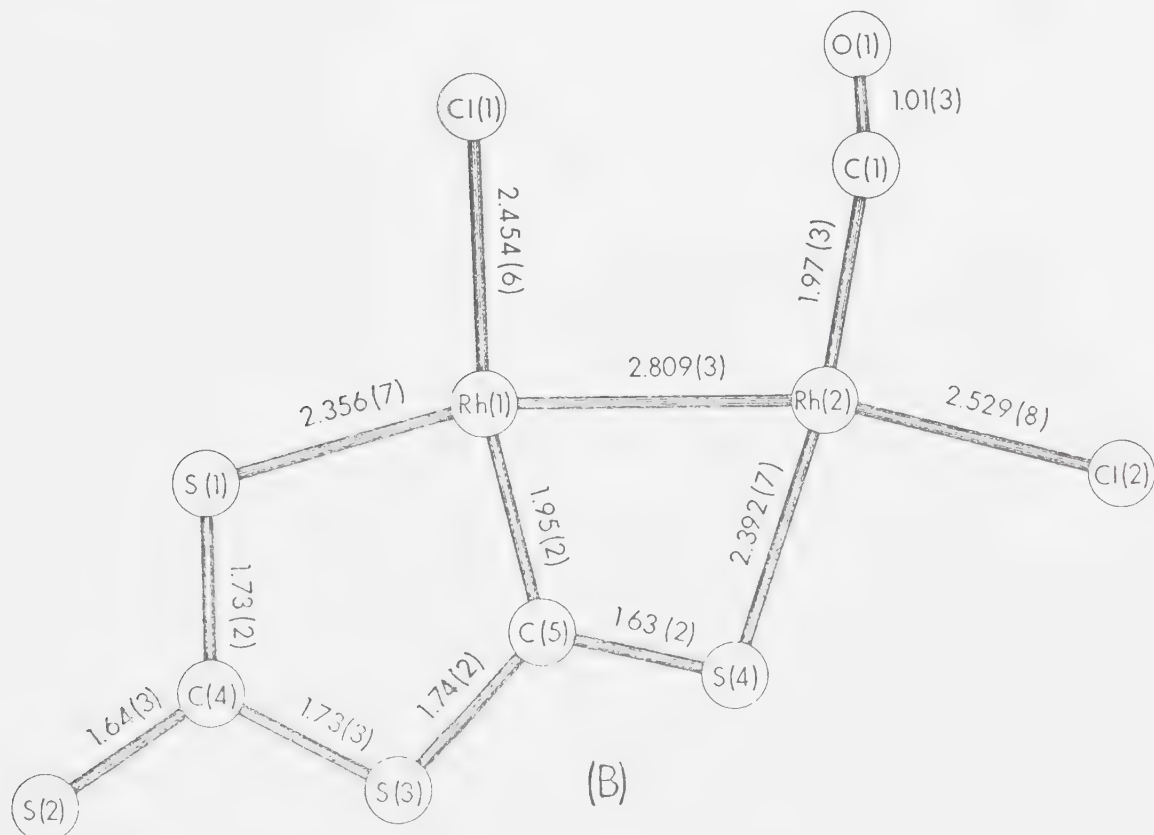
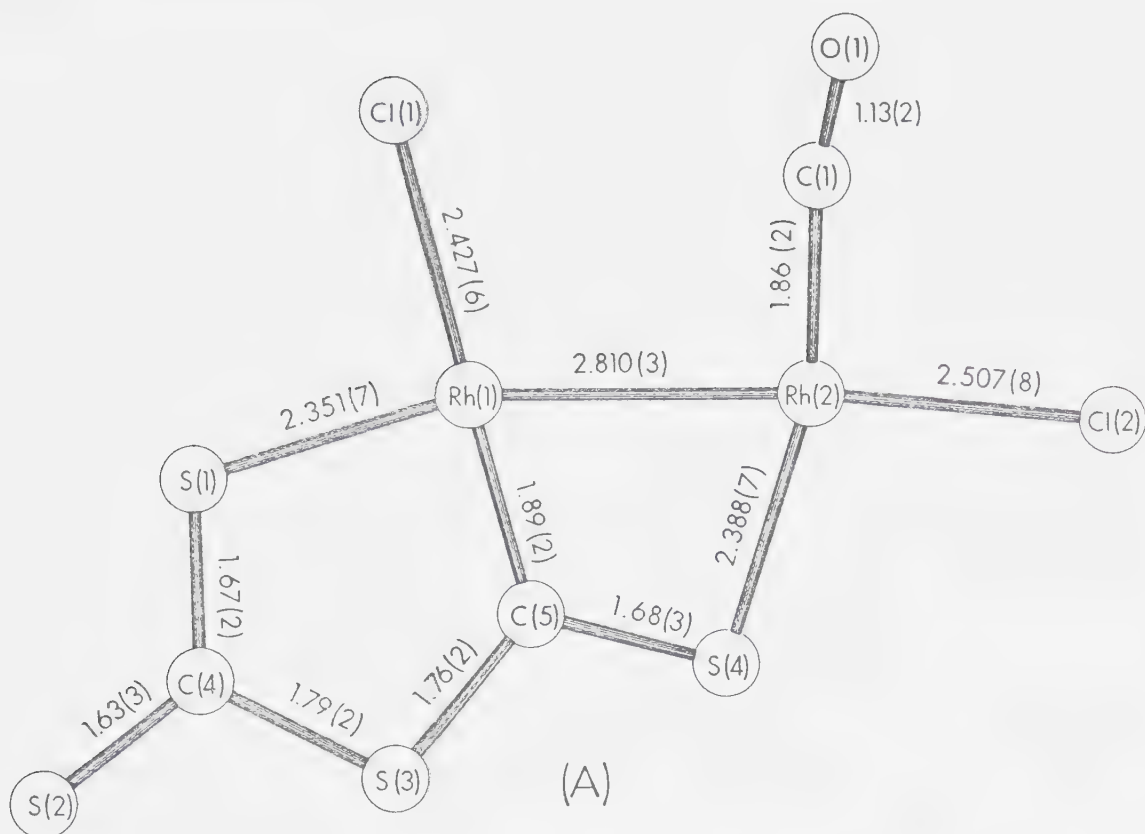


Figure 24. The Equatorial Planes of Dimers A and B of  $[\text{Rh}_2\text{Cl}_2(\text{CO})(\text{C}_2\text{S}_4)(\text{DPM})_2]$ .



## DISCUSSION

### Description of Structure

The complex,  $[\text{Rh}_2\text{Cl}_2(\text{CO})(\text{C}_2\text{S}_4)(\text{DPM})_2]$  (3), crystallizes with two independent molecules per asymmetric unit. Both dimers have the same overall geometry, with the Rh centres bridged by two transoid DPM ligands, but differ slightly in the orientations of the ligands (vide infra). Within each dimer the Rh atoms display distorted octahedral coordinations. One rhodium atom of each dimer (Rh(A1),Rh(B1)) has two mutually trans P atoms in the axial sites with the equatorial positions occupied by a sulfur and a carbon atom of the  $\text{C}_2\text{S}_4$  fragment, a chloro ligand and the other Rh atom. The second Rh atom (Rh(A2),Rh(B2)) also has mutually trans axial P atoms, with a sulfur atom of the  $\text{C}_2\text{S}_4$  moiety, a chloro ligand, a carbonyl ligand and the other Rh atom occupying its equatorial sites.

The Rh-Rh distances of  $2.810(3)\text{\AA}$  and  $2.809(3)\text{\AA}$ , for dimers A and B, respectively, compare well with each other and are consistent with a normal Rh-Rh single bond, falling within the range previously reported for such distances ( $2.617(3)$  to  $2.8415(7)\text{\AA}$ ).<sup>129-133</sup>

The Rh-C and C-O distances of the carbonyl ligands are not unusual, comparing acceptably with other determinations.<sup>35,120,126</sup> However, both carbonyl groups are significantly bent ( $\text{Rh(A2)-C(A1)-O(A1)} = 169(3)^\circ$ ,  $\text{Rh(B2)-C(B1)-O(B1)} = 165(3)^\circ$ ). A consideration of the nonbonded contacts indi-



cates that in both dimers the carbonyl ligands bend in such a way as to minimize the contacts with the phenyl rings suggesting that the bending of these ligands is steric in origin.

The rhodium-chlorine distances ( $\text{Rh(A1)}-\text{Cl(A1)} = 2.427(6)\overset{\circ}{\text{\AA}}$ ;  $\text{Rh(B1)}-\text{Cl(B1)} = 2.454(6)\overset{\circ}{\text{\AA}}$ ) which are trans to  $\text{C(A5)}$  and  $\text{C(B5)}$ , respectively, are quite long but compare well with other determinations, where the chloro ligand is trans to a  $\sigma$ -bound alkyl group or carbene ligand.<sup>163-165</sup> On the other hand, the  $\text{Rh(2)}-\text{Cl(2)}$  bond distances ( $2.507(8)\overset{\circ}{\text{\AA}}$  and  $2.529(8)\overset{\circ}{\text{\AA}}$  for molecules A and B, respectively), which are opposite the rhodium atoms,  $\text{Rh(A1)}$  and  $\text{Rh(B1)}$ , are significantly longer than those typically observed in these systems;<sup>96,125,126</sup> in fact they are even longer than those observed when a chloro ligand is opposite a ligand of high trans influence such as a carbene. These long rhodium-chloro distances probably arise as a result of steric crowding about the  $\text{Rh(2)}$  centre. Support for this comes from the short nonbonded phenyl hydrogen-chloro contacts observed for these two chloro ligands ( $\text{Cl(A2)}-\text{H(A46)} = 2.39\overset{\circ}{\text{\AA}}$ ;  $\text{Cl(B2)}-\text{H(B42)} = 2.58\overset{\circ}{\text{\AA}}$ ). Further, these interactions are such that they tend to force these chloro ligands away from the metal centres (see Figures 22 and 23).

The  $\text{C}_2\text{S}_4$  fragment contains two intact  $\text{CS}_2$  molecules ( $\text{S(1)C(4)S(2)}$  and  $\text{S(3)C(5)S(4)}$ ) fused at  $\text{C(4)}-\text{S(3)}$ . This fragment is then bound to one rhodium atom ( $\text{Rh(1)}$ ) via  $\text{S(1)}$  and  $\text{C(5)}$  and to the other rhodium atom through  $\text{S(4)}$ .



Within the resulting  $\text{Rh}_2\text{C}_2\text{S}_4$  metallocycles the C-S distances ( $1.63(2)$ - $1.79(2)\text{\AA}$ ) and angles (see Table 40) compare favourably with those reported for  $[\text{Rh}(\eta^5\text{-C}_5\text{H}_5)(\text{C}_2\text{S}_4)(\text{PMe}_3)]$ ,<sup>162</sup> where an analogous  $\text{C}_2\text{S}_4$  fragment was observed. These distances suggest delocalization over the carbon-sulfur framework and range from values comparable to the C-S double bond distance observed in ethylene thiourea ( $1.71\text{\AA}$ )<sup>166</sup> to single bond values ( $1.81\text{\AA}$ ).<sup>166</sup> The Rh(1)-S(1) and Rh(2)-S(4) distances (average  $2.354(7)\text{\AA}$  and  $2.390(7)\text{\AA}$ , respectively), although significantly different compare favourably with other determinations.<sup>163,164,167,168</sup>

The  $\text{C}_2\text{S}_4$  ligand can be considered as a carbene ligand,  $\text{C}_2\text{S}_4^{2-}$ , with each of the coordinated sulfur atoms functioning as a two electron donor to the rhodium atoms, leaving the carbene carbon atom as a two electron donor. Therefore the rhodium atoms are formally Rh(II). The unusually short Rh(1)-C(5) distances ( $1.89(2)$  and  $1.95(2)$ , for dimers A and B respectively) are comparable to the rhodium carbonyl distances indicating significant multiple bond character. These rhodium-carbene distances are comparable to other such distances and are especially close to those observed in  $[\text{RhCl}(\text{PPh}_3)_2(\text{PhCONCS})_2]$ <sup>163</sup> and  $[\text{RhCl}(\text{PPh}_3)_2(\text{EtOCONCS})_3]$ .<sup>164</sup> In these complexes five membered metallocycle rings again resulted as a consequence of condensation of sulfur-containing molecules on rhodium.

Within the DPM framework the parameters are, on the whole, not unusual and compare well with other determin-





ations.<sup>35,89,96,120,126</sup> The P-C-C angles, for example, (range 125(2) to 115(2)°) do not deviate significantly from the expected value of 120° and compare favourably with other similar compounds. However it is significant that the methylene orientations in the two dimers are different. In dimer A a trans methylene arrangement is observed whereas these groups are cis in dimer B. Based on previous work it was anticipated that the methylene groups of the DPM ligands would fold in a cis manner towards the C<sub>2</sub>S<sub>4</sub> fragment (i.e. towards the site of the bulkier ligand). In dimer B, where the expected cis methylene arrangement is observed the phenyl rings avoid unusually short contacts with the C<sub>2</sub>S<sub>4</sub> fragment and as a result this fragment is quite planar. Here, phenyl rings 2 and 6 are parallel to the C<sub>2</sub>S<sub>4</sub> moiety, instead of perpendicular to it as is typically observed for the endo phenyl groups of cis oriented methylene groups. This phenyl ring orientation minimizes interactions with the C<sub>2</sub>S<sub>4</sub> moiety but tends to force the two other endo phenyl rings 3 and 7 away from their normal orientation (see Chapter VI, for example). However, in dimer A the trans methylene arrangement thrusts ring 6 close to the C<sub>2</sub>S<sub>4</sub> fragment resulting in a significant puckering of this fragment (see Figure 22 and Table 38). Therefore, despite comparable bond angle and distance within the Rh<sub>2</sub>C<sub>2</sub>S<sub>4</sub> metallocycles, significant differences in their overall geometries are present as a result of these phenyl ring interactions.



The differences noted above between the phenyl ring orientations in dimers A and B also lead to differences in the equatorial chloro and carbonyl ligands (see Figure 24) with these ligands tending to stagger themselves with respect to the phenyl rings (see Torsion Angles, Table 40) to again minimize nonbonded contacts. This staggering of the phenyl rings with respect to the equatorial ligands is further assisted in dimer A by a skewing of the Rh-P framework. Without this skewing of the Rh-P framework the phenyl rings of P(A2) would be essentially eclipsed with the chloro and carbonyl ligands of Rh(A2). Whereas, in dimer B because of the *cis* methylene orientation and the subsequent phenyl group orientations no skewing is necessary to maintain normal nonbonded contacts. Therefore, most differences observed between the two dimers are a direct result of the differing methylene orientations.

Reaction of *trans*-[RhCl(CO)(DPM)]<sub>2</sub> and [Rh<sub>2</sub>Cl<sub>2</sub>(μ-CO)-(DPM)<sub>2</sub>] with CS<sub>2</sub>

The reaction of either *trans*-[RhCl(CO)(DPM)]<sub>2</sub> (1) or [Rh<sub>2</sub>Cl<sub>2</sub>(μ-CO)(DPM)<sub>2</sub>] with CS<sub>2</sub> results in the isolation of the final product, [Rh<sub>2</sub>Cl<sub>2</sub>(CO)(C<sub>2</sub>S<sub>4</sub>)(DPM)<sub>2</sub>] (3). Based on analogies with the previous studies involving SO<sub>2</sub><sup>96</sup> (Chapters IV and V) and acetylene<sup>42</sup> molecules we can postulate a scheme for the reaction of 1 with CS<sub>2</sub>. Initial attack is probably terminal, since this is the only site open (see Chapter III). The resulting species [Rh<sub>2</sub>Cl(CO)-(CS<sub>2</sub>)(μ-Cl)(μ-CO)(DPM)<sub>2</sub>] (4), (see Figure 25) although not



observed is analogous to that proposed for  $\text{SO}_2$  (Chapter IV). This species we believe then rearranges to  $[\text{Rh}_2(\text{CO})_2(\mu\text{-Cl})(\mu\text{-CS}_2)(\text{DPM})_2][\text{Cl}]$  (5), which is a 1:1 electrolyte in acetone and dichloromethane, and has a very similar infrared spectrum ( $\nu(\text{CO}) = 1990 \text{ cm}^{-1}$ , the  $\text{CS}_2$  region is obscured by bands due to the DPM ligands) and similar  $^{31}\text{P}\{^1\text{H}\}$  NMR spectral parameters ( $\delta = 14.3 \text{ ppm}$ ;  $|^1J_{\text{Rh-P}} + ^xJ_{\text{Rh-P}}| = 98.2 \text{ Hz}$ )<sup>101</sup> to the well characterized  $\text{SO}_2$  analogue<sup>96</sup> (Chapter IV). Chloride recoordination, loss of one carbonyl ligand and a facile rearrangement would then yield  $[\text{Rh}_2\text{Cl}_2(\mu\text{-CO})(\mu\text{-CS}_2)(\text{DPM})_2]$  (6), which although not observed is exactly analogous to an acetylene complex,<sup>42</sup> which has been prepared in our laboratory by the same route and structurally characterized. Electrophilic attack at S(3) of the bound  $\text{CS}_2$  molecule (see Figure 24) by a second  $\text{CS}_2$  molecule would then readily yield the final product 3.

Since the monocarbonyl species 2 is soluble, its reaction during the stepwise addition of  $\text{CS}_2$  was carefully monitored by infrared,  $^{31}\text{P}\{^1\text{H}\}$  and  $^{13}\text{C}\{^{31}\text{P}\{^1\text{H}\}\}$  NMR spectroscopy. For the  $^{13}\text{C}$  NMR experiment  $^{13}\text{CO}$  enriched  $[\text{Rh}_2\text{Cl}_2(\mu\text{-}^{13}\text{CO})(\text{DPM})_2]$  was used. Initially in the  $^{31}\text{P}\{^1\text{H}\}$  NMR spectrum resonances assignable to unreacted 2 and two other symmetric species are observed. One resonance can be assigned to compound 5 which was previously characterized and the other is believed to be due to  $[\text{Rh}_2\text{Cl}_2(\mu\text{-CS}_2)(\text{DPM})_2]$  (7) ( $\delta = 15.7 \text{ ppm}$ ;  $|^1J_{\text{Rh-P}} - ^xJ_{\text{Rh-P}}| = 116.5 \text{ Hz}$ ) (vide supra).



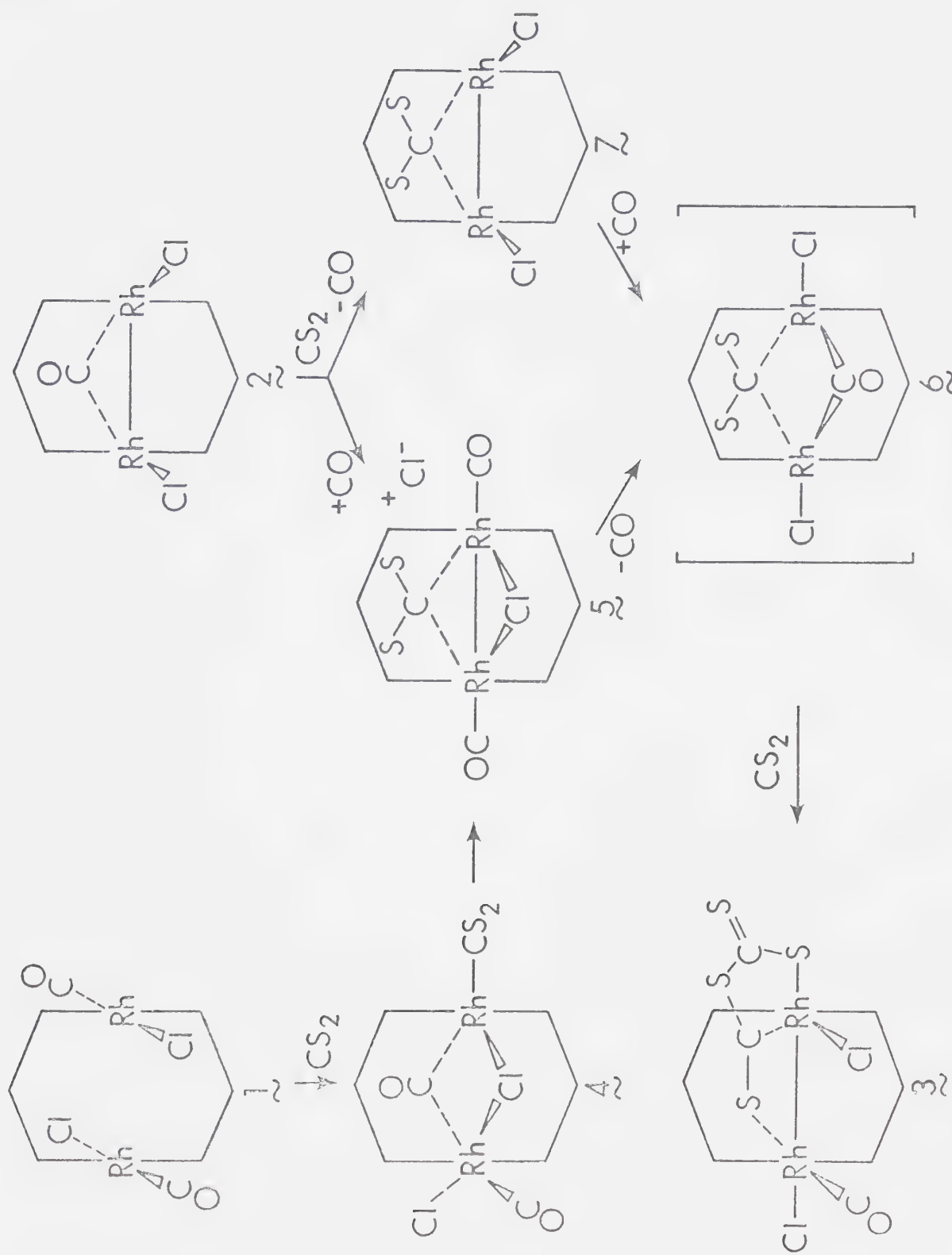


Figure 25. Proposed Scheme for the Reactions of  $\text{trans-}[\text{RhCl}(\text{CO})(\text{DPM})]_2$  and  $[\text{RhCl}_2(\mu\text{-CO})(\text{DPM})_2]$  with  $\text{CS}_2$ .





These observations are consistent with species  $\tilde{5}$  and  $\tilde{7}$ , shown in Figure 25, resulting from  $\text{CS}_2$  attack on  $\tilde{2}$  and CO transfer. Analogous species have been observed in the reaction of  $\tilde{2}$  with  $\text{SO}_2$  (Chapter V). In these  $\text{SO}_2$  studies we observed that these Rh dimers act as efficient CO scavengers. Therefore when  $\tilde{5}$  loses CO yielding  $\tilde{6}$ , compound  $\tilde{7}$  picks up CO also giving  $\tilde{6}$ , which subsequently yields the final product  $\tilde{3}$  by condensation of the second  $\text{CS}_2$  molecule (vide supra). Complex  $\tilde{3}$  shows a complex multiplet ( $\delta = 7.5$  ppm) pattern in the  $^{31}\text{P}\{^1\text{H}\}$  NMR spectrum, arising from its AA'BB'XY spin system. No resonance assignable to  $\tilde{6}$  was observed.

Since in compounds  $\tilde{5}$  and  $\tilde{7}$  the four phosphorus atoms are equivalent at  $-50^\circ\text{C}$ , it is suggested that the  $\text{CS}_2$  ligand in species  $\tilde{5}$ ,  $\tilde{6}$  and  $\tilde{7}$  is coordinated solely through the carbon atom, as has been proposed for  $\text{CO}_2$  in some of its compounds.<sup>51</sup> A C-S bound species would give rise to a more complex  $^{31}\text{P}$  NMR owing to the resulting chemical inequivalence of the phosphorus atoms unless the  $\text{CS}_2$  molecule were fluxional at this temperature. No evidence suggesting fluxionality of these species was observed.

The  $^{13}\text{C}$  NMR spectra of the same reaction initially shows the resonance assignable to  $\tilde{2}$ , as well as one additional species at  $\delta = 186.5$  ppm (doublet,  $|^1J_{\text{Rh-C}}| = 80.1$  Hz), characteristic of a terminal carbonyl ligand and consistent with species  $\tilde{5}$ . The only other carbonyl resonance observed



later in the experiment is assignable to species  $\tilde{3}$  at  $\delta = 191.5$  ppm (doublet,  $|J_{\text{Rh-C}}| = 69.1$  Hz). Similarly the infrared spectrum shows only bands assignable to  $\tilde{2}$ ,  $\tilde{3}$  and a band at  $1990\text{ cm}^{-1}$  which is again consistent with species  $\tilde{5}$ . Therefore, all the spectral parameters and the analogies to the  $\text{SO}_2$ <sup>96</sup> and acetylene<sup>42</sup> chemistry appear to support this scheme.

### CONCLUSIONS

This study presents only the second structural characterization<sup>162</sup> of a rhodium-carbon disulfide complex and is the first such binuclear species. Based on its infrared spectrum, which is similar to other  $\text{Rh-CS}_2$  complexes, which are believed to contain  $\text{C,S-}\eta^2$  side-on bound  $\text{CS}_2$ , this work suggests that these compounds should probably be reformulated as  $\text{C}_2\text{S}_4$  species. Certainly it is becoming apparent that rhodium has a marked tendency for activating and condensing sulfur containing molecules as has now been demonstrated by several structural determinations.<sup>162-164</sup> The similarities in the mode of  $\text{CS}_2$  condensation to that of  $\text{CO}_2$  in an iridium complex,  $[\text{IrCl}(\text{C}_2\text{O}_4)(\text{PPh}_3)_3]$ ,<sup>50</sup> supports the argument that  $\text{CS}_2$  is a useful model for studying  $\text{CO}_2$  binding in metal complexes and suggests the possibility of analogous  $\text{CO}_2$  binuclear chemistry.



## CHAPTER VIII.

### Summary and Conclusions

One reason for undertaking the present study was to obtain a better understanding of the coordination and activation of CO, CS<sub>2</sub> and SO<sub>2</sub> utilizing binuclear diphosphine and diarsine bridged complexes. Additionally, the effect of metal proximity on the chemistries of these small molecules was of interest, as well as the potential relevance of such studies to homogeneous catalysis. Although, not all these goals were met, this study was successful in extending our understanding of the chemistry of this class of binuclear complexes.

With regard to the effect of metal proximity on the chemistry of these dirhodium species, one obvious difference, compared to the analogous mononuclear species, is the possibility of bridging coordination modes for these small molecules. This possibility was realized in almost every study, and in fact, the small molecules of interest show a remarkable tendency to finally reside in the bridging site. It is believed that this site is favoured for these Lewis acids since here they are able to accept electron density from both low valent metals. Another related consequence of the metal proximity is the facile ligand rearrangements which occur in these dirhodium complexes. In almost all cases these rearrangements are preceded by halide dissociation and result in a symmetrical arrangement of the



ligands with the better  $\pi$ -acceptor ligand coordinated in the bridging site. The few exceptions, where a symmetric species does not result, are believed to favour their observed geometries as a consequence of the high steric bulk of the ligands involved, as for example in  $[\text{Rh}_2\text{I}(\text{CO})(\mu\text{-CO})(\text{DPM})_2][\text{I}]$  (1) where the large iodo ligands are not both readily coordinated in the same compound.

The site of attack by small molecules in these species is not altogether straight forward. In *trans*- $[\text{RhCl}(\text{CO})(\text{DPM})]_2$  (2), there is probably only one site of attack at the open fifth coordination site on one of the metal centres opposite the second metal atom. However, in the "A-frame" type species attack can be either at the bridging site or at the terminal site, remote from the bridging site. In  $[\text{Rh}_2(\text{CO})_2(\mu\text{-Cl})(\text{DPM})_2]^+$  (3), we (Chapter IV) and others have shown,<sup>35a,91</sup> that  $\text{SO}_2$  attacks the bridging site, whereas CO attacks terminally. In the distorted "A-frame" species  $[\text{Rh}_2\text{Cl}_2(\mu\text{-SO}_2)(\text{DPM})_2]$  (4) and  $[\text{Rh}_2\text{Br}_2(\mu\text{-CO})(\text{DPM})_2]$  (5) we have observed that the bridging site is blocked in the solid state by four phenyl groups. Consistent with this, much of our chemistry indicates terminal attack. However, this is certainly not unambiguous and recent work with acetylenes seems to indicate that direct attack and insertion of the acetylenes into the Rh-Rh bond occurs.<sup>169</sup> The above  $\text{SO}_2$  (4) and monocarbonyl (5) complexes are significantly different from the dicarbonyl "A-frame" species 3 however in that they have a metal-metal bond, which may serve





as a site of attack for the Lewis acids. The reactivity of the metal-metal bond in these systems is shown by the facile reaction of  $[\text{Rh}_2\text{Cl}_2(\mu\text{-CO})(\text{DPM})_2]$  (6) with  $\text{CS}_2$ , whereas the dicarbonyl "A-frame" species 3 shows no reaction. Corroborating this finding, other work in our group has shown that the metal-metal bond species 1, 5 and 6 react instantly with acetylenes, whereas species such as 3, in which no metal bond is present, do not react.<sup>169</sup>

Other aspects of the study regarding the activation of the small molecules and the relevance of these studies to catalysis are still in their infancy. In the carbonyl and sulfur dioxide complexes, these small molecules were certainly activated in the molecular orbital and spectroscopic sense (i.e. we noted a large drop in bond order due to a redistribution of electron density in these molecules). However these small molecules were not activated in a catalytic sense, at least not in the very limited context in which we observed them. The two species which had, spectroscopically, the largest activation of CO and  $\text{SO}_2$  were 6 and 4, respectively. In the first species the carbonyl ligand behaved quite normally and attempts to oxidize the coordinated  $\text{SO}_2$  ligand to  $\text{SO}_4^{2-}$  under mildly forcing conditions were unsuccessful. In contrast the  $\text{CS}_2$  molecule is readily activated and undergoes a subsequent condensation reaction yielding the  $\text{C}_2\text{S}_4$  moiety. In this area of activation further work is underway in our group. One notable success in this regard, concerns the reaction of 6 with acetylenes



yielding complexes of the type  $[\text{Rh}_2\text{Cl}_2(\mu\text{-CO})(\mu\text{-acetylene})\text{-(DPM)}_2]$  (8),<sup>42</sup> in which the acetylene molecule is activated, as seen by its structural parameters which resemble those of a cis dimetallated olefin molecule. Furthermore, as a result of the reaction of 6 with acetylenes a catalytic study using complex 6 was initiated<sup>169</sup> and preliminary results show that this complex catalyzes the cyclotrimerization of dimethylacetylenedicarboxylate, whereas with phenylacetylene, catalytic hydrogenation is observed.



## REFERENCES AND FOOTNOTES

1. M.M. Taqui Khan and A.E. Martell, "Homogeneous Catalysis by Metal Complexes", Academic Press, New York, 1974.
2. B.R. James, "Homogeneous Hydrogenation", Wiley, New York, 1973.
3. "Homogeneous Catalysis", Adv. Chem. Ser. No. 70, Chapters 1, 2, 4-7 and 10. A.C.S., Washington, D.C., 1968; D. Forster and J.F. Roth, eds., "Homogeneous Catalysis. II", Adv. Chem. Ser. No 132, A.C.S., Washington, D.C., 1974.
4. G.N. Schrauzer, "Transition Metals in Homogeneous Catalysis", Marcel Dekker, Inc., New York, 1971.
5. P.M. Henry, Adv. Organometal. Chem. (1975), 13, 363.
6. P.M. Henry, J. Am. Chem. Soc. (1972), 94, 4437 and references therein.
7. G. Yagupsky, C.K. Brown and G. Wilkinson, J. Chem. Soc. A. (1970), 1392; (1970), 2753, and references therein.
8. J.F. Roth, J.H. Craddock, A. Hershman and F.E. Paulick, Chem. Tech. (1971), 600.
9. D. Forster, J. Am. Chem. Soc. (1976), 98, 846.
10. R. Eisenberg and D.E. Hendricksen, Adv. Catal. (1979), 28, 79, and references therein.
11. E.L. Muettertieties, Bull. Soc. Chim. Belg. (1975), 84, 959.



12. S.D. Ittel and J.A. Ibers, Adv. Organometal. Chem. (1976), 14, 33.
13. M.J.S. Dewar, Bull. Soc. Chim. (1951), 18, 79.
14. J. Chatt and L.A. Duncanson, J. Chem. Soc. (1953), 2939.
15. J.A.J. Jarvis, B.T. Kilbourn and P.G. Owston, Acta Crystallogr., Sect. B (1971), 27, 366.
16. F.R. Hartley, Agnew. Chem. Internat. Edit. (1972), 11, 596, and references therein.
17. W.P. Hayes and A.J. Forney, "High BTU Gas from Coal: Status and Prospects", Tech. Rep. PERC/IC-76-1 U.S.E.R.D.A., Office of Public Affairs, 1976.
18. R.E. Kirk and Othmer, eds., "Encyclopedia of Chemical Technology", 2nd ed., Wiley (Interscience), New York, 1963-1970. For CO/H<sub>2</sub> reaction, see Vol. 4, p. 446 for methanation, see Vol. 13, p. 364.
19. H. Pichler and H. Schulz, Chem. Ing. Tech. (1970), 42, 1162.
20. H.H. Storch, H. Golumbic and R.B. Anderson, "The Fischer-Tropsch and Related Syntheses", Wiley, New York, 1951.
21. F. Fischer and H. Tropsch, Chem. Ber. (1923), 56, 2428; (1926), 59, 830, 832, 923.
22. D.A. Edge and J.S. Adams, J.S. Afr. Inst. Min. Metall. (1975), 76, 145.





23. F.C. Palilla, U.S. Patent 3931393.
24. J. Freiberg, Atmos. Environ. (1976), 10, 121.
25. D.G. Jones and K.S. Campbell, AICHE Symp. Ser. (1975) 71, 306.
26. P.T. Roberts and S. Friedlander, Environ. Health Perspect. (1975), 103.
27. A.J. Chalk and R.F. Harrod, Adv. Organometal. Chem. (1968), 6, 119.
28. I. Wender and P. Pino, eds., "Organic Synthesis via Metal Carbonyls," Vol. 1, Wiley (Interscience), 1968.
29. R. Colton and M.J. McCormick, Coord. Chem. Rev. (1980), 31, 1, and references therein.
30. a) L. Vaska, Science (1966), 152, 769.  
b) N. Payne and J.A. Ibers, Inorg. Chem. (1969), 8, 2714.
31. J.T. Mague, Inorg. Chem. (1969), 8, 1975.
32. R. Colton, M.J. McCormick and C.D. Pannan, J. Chem. Soc. Chem. Comm. (1977), 823; Aust. J. Chem. (1978), 31, 1425.
33. F.A. Cotton and J.M. Troup, J. Am. Chem. Soc. (1974), 16, 4422.
34. P. Singh, C.B. Damman and D.J. Hodgson, Inorg. Chem. (1972), 12, 1335.
35. a) M. Cowie, J.T. Mague and A.R. Sanger, J. Am. Chem. Soc. (1978), 100, 3628.  
b) M. Cowie, Inorg. Chem. (1979), 18, 286, and references therein.



36. Y. Degreve, J. Meunier-Piret, M. van Meerssche and P. Piret, Acta Crystallogr., Sect. B. (1969), 25, 519.
37. C.J. Commons and B.F. Hoskins, Aust. J. Chem. (1975), 28, 1663.
38. V.G. Albano, P.L. Bellon, P. Chini and V. Scatturin, J. Organometal. Chem. (1969), 16, 461.
39. F.A. Cotton and D.L. Hunter, Inorg. Chem. (1974) 13, 2044.
40. P.S. Batterman, Strut. Bonding (Berlin) (1972), 10, 1.
41. M.P. Brown, A.N. Keith, Lj. Manojlovic-Muir, K.W. Muir, R.J. Puddephatt and K.R. Seddon, Inorg. Chim. Acta (1979), 34, L223.
42. M. Cowie and T.G. Southern, J. Organometal. Chem., in press.
43. I.S. Butler and A.E. Fenster, J. Organometal. Chem. (1977), 66, 161.
44. P.V. Yaneff, Coord. Chem. Rev. (1977), 23, 183.
45. M.C. Baird, G. Hartwell, R. Mason, A.I.M. Rae and G. Wilkinson, Chem. Comm. (1967), 92.
46. J.M. Lisey, E.D. Dobrzynski, R.J. Angelici and J. Clardy, J. Am. Chem. Soc. (1975), 97, 656.
47. T.G. Southern, D.Sc. Thesis, L'Université de Rennes, 1979.
48. M.C. Baird and G. Wilkinson, J. Chem. Soc. A (1967), 865.



49. M. Kubota and C.R. Carey, J. Organometal. Chem., (1970), 24, 491.
50. T. Herskovitz and L.J. Guggenberger, J. Am. Chem. Soc. (1976), 98, 1615.
51. M. Aresta and G.F. Nobile, J. Chem. Soc. Dalton (1977), 708.
52. D.M.P. Mingos, Transition Met. Chem. (1978) 3, 1.
53. G.J. Kubas, Inorg. Chem. (1979), 18, 182.
54. D.C. Moody and R.R. Ryan, Inorg. Chem. (1979), 18, 223.
55. R.R. Ryan, P.G. Eller and G.J. Kubas, Inorg. Chem. (1976), 15, 797.
56. S.J. LaPlaca and J.A. Ibers, Inorg. Chem. (1966), 5, 405.
57. G.J. Kubas and R.R. Ryan, Cryst. Strut. Comm. (1977), 6, 295.
58. D.C. Moody and R.R. Ryan, J. Chem. Soc., Chem. Comm. (1976), 503; Inorg. Chem. (1977), 16, 2473.
59. R.D. Wilson and J.A. Ibers, Inorg. Chem. (1978), 17, 2134.
60. M. Angoletta, P.L. Bellon, M. Manssero and M. Sansoni, J. Organometal. Chem. (1974), 81, C40.
61. M. Angoletta, L. Malatesta and G. Caglio, J. Chem. Soc., Dalton (1977), 2131.
62. J.W. Moore, H.W. Baird and H.B. Miller, J. Am. Chem. Soc. (1968), 90, 1358.



63. a) B.L. Haymore and J.A. Ibers, Inorg. Chem. (1975), 14, 2610.  
b) B.A. Frenz and J.A. Ibers, M.T.P. Int. Rev. Sci., Phys. Chem. Ser. One (1973), 11, 33.
64. M.R. Churchill, B.G. DeBoer and K.L. Karla, Inorg. Chem. (1973), 12, 1650.
65. M.R. Snow and J.A. Ibers, Inorg. Chem. (1973), 12, 224.
66. J.T. Mague and J.P. Mitchner, Inorg. Chem. (1969), 8, 119.
67. L. Vallarino, J. Chem. Soc. (1957), 2287.
68. L. Vaska and J.W. Diluzio, J. Am. Chem. Soc. (1961), 83, 2784.
69. L. Vaska, Acc. Chem. Res. (1968), 1, 335.
70. J.P. Collman and W.R. Roper, Adv. Organometal. Chem. (1968), 7, 53.
71. A.L. Balch and B. Tulyathan, Inorg. Chem. (1977), 16, 2840.
72. M. Brockhaus, F. Standacher and H. Vahrenkamp, Chem. Ber. (1972), 105, 3716; L.R. Nassimbeni, Inorg. Nucl. Chem. Lett. (1971), 7, 187.
73. E.W. Ainscough, A.M. Brodie and G. Leng-Ward, J. Chem. Soc., Dalton (1974), 2437.
74. H. Vahrenkamp, Chem. Ber. (1972), 105, 3574.
75. a) J.A. Connor and G.A. Hudson, J. Organometal. Chem. (1974), 73, 351.





- b) J.A. Connor, G.K. McEwan and C.J. Rix, J. Less Common Metals (1974), 36, 207; J. Chem. Soc., Dalton (1974), 589.
76. J.A. Connor, J.P. Day, E.M. Jones and G.K. McEwan, J. Chem. Soc., Dalton (1973), 347; S.C. Tripathi, S.C. Srivastava and A.K. Shrimal, J. Organometal. Chem. (1976), 73, 343.
77. A.J. Pryde, B.L. Shaw and B. Weeks, J. Chem. Soc., Dalton (1976), 322.
78. J.P. Crow, W.R. Cullen, F.L. Hou, L.Y.Y. Chan and F.W.B. Einstein, J. Chem. Soc., Chem. Comm. (1971) 1229.
79. J.P. Crow, W.R. Cullen and F.L. Hou, Inorg. Chem. (1972), 11, 2125.
80. R. Colton and C.J. Commons, Aust. J. Chem. (1975), 28, 1673.
81. a) A.L. Balch and L.S. Benner, J. Organometal. Chem. (1977), 135, 339.
- b) L.S. Benner, M.M. Olmstead and A.L. Balch, J. Organometal. Chem. (1978), 159, 289.
82. A.R. Sanger, J. Chem. Soc., Dalton (1977), 1971.
83. a) M.P. Brown, R.J. Puddephatt, M. Rashidi and K.R. Seddon, J. Chem. Soc., Dalton (1977), 951.
- b) M.P. Brown, R.J. Puddephatt, M. Rashidi, Lj. Manojlović-Muir, K.W. Muir, T. Solomun and K.R. Shedden, Inorg. Chim. Acta (1977), 23, L33.



84. A.L. Balch and L.S. Benner, J. Am. Chem. Soc. (1978) 100, 6099.
85. a) L.S. Benner, M.M. Olmstead, H. Hope and A.L. Balch, J. Organometal. Chem. (1978), 153, C31.  
b) A.L. Balch, L.S. Benner and M.M. Olmstead, Inorg. Chem. (1979), 18, 2996.
86. A.D. Rattray and D. Sutton, Inorg. Chim. Acta (1978), 27, L85.
87. A.L. Balch, C.L. Lee, C.H. Lindsay and M.M. Olmstead, J. Organometal. Chem. (1979), 177, C22.
88. a) M.P. Brown, J.R. Fisher, S.J. Franklin and R.J. Puddephatt, J. Chem. Soc., Chem. Comm. (1978), 749.  
b) M.P. Brown, J.R. Fisher, R.J. Puddephatt and K.R. Seddon, Inorg. Chem. (1979), 18, 2808.
89. C.P. Kubiak and R. Eisenberg, J. Am. Chem. Soc. (1978), 100, 3628.
90. M.M. Olmstead, L.S. Benner, H. Hope and A.L. Balch, Inorg. Chim. Acta (1979), 32, 193.
91. J.T. Mague and A.R. Sanger, Inorg. Chem. (1979), 18, 2060.
92. G.H. Stout and L.H. Jensen, "X-ray Structure Determination", 3rd ed., The MacMillan Company, Toronto, Canada, 1970.
93. M.J. Burger, "Crystal Structure Analysis", Wiley, New York, 1960.
94. M.J. Burger, "Vector Space", Wiley, New York, 1959.



95. "International Tables for X-ray Crystallography", 3rd Ed., The Kynoch Press, Birmingham, England, Vol. I, II, III and IV, 1974.
96. a) M. Cowie, S.K. Dwight and A.R. Sanger, Inorg. Chim. Acta (1978), 31, L407.  
b) M. Cowie and S.K. Dwight, Inorg. Chem. (1980), 19, 209.
97. M. Cowie and S.K. Dwight, unpublished results.
98. A.R. Sanger, private communication.
99. J. Chatt and L.M. Venazzi, J. Chem. Soc. (1957), 4735.
100. Positive  $^{19}\text{F}$  NMR shifts are upfield from  $\text{CFCl}_3$ .
101. Positive  $^{31}\text{P}$  NMR shifts are downfield from  $\text{H}_3\text{PO}_4$ .
102. The cell reduction was performed using a modification of TRACER II by S.L. Lawson. See: S.L. Lawson, R.A. Jacobson, "The Reduced Cell and Its Crystallographic Applications", Ames Laboratory Report IS-1141; USEAC: Iowa State University, Ames, Iowa, April, 1965.
103. R.J. Doedens and J.A. Ibers, Inorg. Chem. (1967) 6, 204.
104. A.L. Patterson, Phys. Rev. (1934), 46, 372.
105. A.L. Patterson, Z. Kristallogr., Sect. A. (1935), 90, 517.
106. D.T. Cromer, J.T. Waber, "International Tables for X-ray Crystallography", The Kynoch Press, Birmingham, England (1974), Vol. IV, Table 2.2A.



107. R.F. Stewart, E.R. Davidson and W.T. Simpson, J. Chem. Phys. (1965), 42, 3175.
108. D.T. Cromer and D.J. Liberman, J. Chem. Phys. (1970), 53, 1891.
109.  $f_{\text{O}}^{\text{anom}} = f_{\text{O}} + \Delta f' + i\Delta f''$ , where  $f_{\text{O}}$  is the normal scattering factor,  $\Delta f'$  is the real correction term and  $\Delta f''$  is the imaginary component.
110. Supplementary material is available from the National Library of Canada, 395 Wellington St., Ottawa, Ontario, K1A 0N4.
111. B.L. Haymore and J.A. Ibers, Inorg. Chem. (1975), 14, 1369; S.D. Ittel and J.A. Ibers, ibid. (1975), 14, 636; P.H. Davis, L.K. White and R.L. Belford, ibid. (1975), 14, 1753; R.E. Crommer, W. Van Doorne and R. Dubois, ibid. (1975), 14, 2462; D.S. Milbraith, J.P. Springer, J.C. Cardy and J.G. Verkade, ibid. (1975), 14, 2665.
112. F.A. Cotton and G. Wilkinson, "Advanced Inorganic Chemistry", 3rd Ed., Wiley (Interscience), New York, (1972), pg. 120.
113. L.F. Dahl, C. Martell and D.L. Wampler, J. Am. Chem. Soc. (1961), 83, 1761.
114. J.A. Ibers and R.G. Snyder, Acta Crystallogr., Sect. B. (1962), 15, 923.
115. J.J. Bonnet, Y. Jeanin, P. Kalck, A. Maisonnnet and R. Poilblanc, Inorg. Chem. (1975), 14, 743.





116. J. Coetzer and G. Gafner, Acta Crystallogr., Sect. B (1970), 26, 985.
117. M.J. Bennett and P. Donaldson, Inorg. Chem. (1977), 16, 655.
118. G. Holloway, B.R. Penfold, R. Colton and M.J. McCormick, J. Chem. Soc., Chem. Comm. (1976), 485.
119. J.T. Mague and A.R. Sanger, private communication.
120. M. Cowie and S.K. Dwight, Inorg. Chem. (1979), 18, 2700.
121.  $R = \Sigma ||F_O| - |F_C|| / \Sigma |F_O|$  ;  
 $R_W = [\Sigma (|F_O| - |F_C|)^2 / \Sigma F_O^2]^{1/2}$
122. J.L. DeBoer, D. Rogers, A.C. Shapski and P.G.H. Troughton, Chem. Comm. (1966), 756.
123. M.J. Bennett, P.B. Donaldson, P.B. Hitchcock and R. Mason, Inorg. Chim. Acta. (1975), 12, L9.
124. For average quantities the estimated standard deviation shown is the larger of an individual standard deviation or the standard deviation of a single observation from the mean.
125. M. Cowie and S.K. Dwight, to be submitted for publication.
126. M. Cowie and S.K. Dwight, Inorg. Chem. (1980), in press.
127. P. Singh, C.B. Dammann and D.J. Hodgson, Inorg. Chem. (1973), 12, 1335.
128. J. Donohue, "The Structures of the Elements", Wiley, New York, (1974), p. 216.



129. E.R. Corey, L.F. Dahl and W.J. Beck, J. Am. Chem. Soc. (1963), 85, 1202.
130. O.S. Mills and J.P. Nice, J. Organometal. Chem. (1967), 10, 337.
131. O.S. Mills and E.F. Paulus, J. Organometal. Chem. (1967), 10, 331.
132. E.F. Paulus, Acta Crystallogr., Sect. B (1969), 25, 2206.
133. C.H. Wei, Inorg. Chem. (1969), 8, 2384.
134. M. Meunier-Piret, P. Piret and M. Van Meerssche, Bull. Soc. Chim. Belg. (1967), 76, 374.
135. M.R. Churchill and K.L. Karla, Inorg. Chem. (1973), 12, 1650.
136. R.R. Ryan and D.C. Moody, Inorg. Chem. (1977), 16, 1052.
137. M.R. Churchill, B.G. DeBoer, K.L. Karla, P. Reich-Rohrwig and A. Wojcicki, J. Chem. Soc., Chem. Comm. (1972), 981.
138. S. Otsuka, Y. Tatsuno, M. Miki, T. Aoki, M. Matsumoto, H. Yoshioka and K. Nakatsu, J. Chem. Soc., Chem. Comm. (1973), 445.
139. B. Post, R.S. Schewrtz and I. Rankuchen, Acta Crystallogr. (1952), 5, 372.
140. K.W. Muir and J.A. Ibers, Inorg. Chem. (1969), 8, 1921.



141. M. Cowie and S.K. Dwight, Inorg. Chem. (1979), 18, 1209.
142. M.M. Olmstead, C.H. Lindsay, L.S. Benner and A.L. Balch, J. Organometal. Chem. (1979), 179, 289.
143. A.L. Balch, private communication.
144. M. Cowie and S.K. Dwight, Inorg. Chem. (1980), in press.
145. R.J. Haines, private communication.
146. A.R. Sanger, J. Chem. Soc., Chem. Comm. (1975), 893.
147. A.R. Sanger, J. Chem. Soc., Dalton (1977), 122.
148. G. Germain, P. Main and M.M. Woolfson, Acta Crystallogr., Sect. A. (1971), 27, 368.
149. M.R. Churchill and S.A. Julis, Inorg. Chem. (1978), 17, 3011.
150. C. Nave and M.J. Trutter, J. Chem. Soc., Dalton (1973), 2202.
151. M. Benard, Inorg. Chem. (1979), 18, 2782.
152. A. Mitschler, B. Rees and M.S. Lehman, J. Am. Chem. Soc. (1978), 100, 3390.
153. F.A. Cotton and G. Wilkinson, "Advanced Inorganic Chemistry", 3rd Ed., Wiley (Interscience), New York, (1972), pg. 707.
154. M. Cowie, R.S. Dickson and T.G. Southern, unpublished results.
155. All carbonyl vibrations are quoted for natural abundance CO.



156. R. Mason and A.I.M. Rae, J. Chem. Soc. A (1970), 1767.
157. T. Kushiwagi, N. Yasuoka, T. Ueki, N. Kasai, M. Kakuda, S. Takahashi and N. Hagihara, Bull. Chem. Soc. Jap. (1968), 41, 296.
158. H. Werner, K. Leonhard and Ch. Burschka, J. Organometal Chem. (1978), 160, 291.
159. H. LeBozec, P.H. Dixneuf, A.J. Carty and N.J. Taylor, Inorg. Chem. (1978), 17, 2568.
160. M. Aresta, C.F. Nobile, V.G. Albano, E. Forni and M. Manassero, J. Chem. Soc., Chem. Comm. (1975), 636.
161. D. Commereuc, I. Douek and G. Wilkinson, J. Chem. Soc. A (1970), 1771.
162. a) H. Werner, O. Kolb, R. Feser and U. Schubert, J. Organometal. Chem. (1980), 191, 283.  
b) H. Werner, private communication
163. M. Cowie and J.A. Ibers, Inorg. Chem. (1976), 15, 552.
164. K. Itoh, I. Matsuda, F. Ueda, Y. Ishii and J.A. Ibers, J. Am. Chem. Soc. (1978), 99, 2118.
165. B. Cetinkaya, M.F. Lappert, G.M. McLaughlin and K. Turner, J. Chem. Soc., Dalton (1974), 1591.
166. "International Tables for X-ray Crystallography", 3rd Ed., The Kynoch Press, Birmingham, England, Vol. III, (1972), pg. 276.
167. R. Beckett, and B.F. Hopskin, Inorg. Nuc. Chem. Lett. (1972), 8, 683.





168. V.R. Richter, J. Kaiser, J. Sieler and L. Kutschabsky,  
Acta Crystallogr., Sect. B (1975), 31, 1642.
169. M. Cowie and T.G. Southern, unpublished results.



Appendix 1: Programs Used in Crystal Structure Solution,  
Refinement and Analysis.

<u>Author</u>	<u>Program</u>	<u>Description</u>
Northwestern University Version	AGNOST	Absorption correction program using Gaussian integration.
J.A. Ibers A.P. Gaughan	CELREF	Refines crystal alignment and cell parameters.
S.K. Dwight	DATABL	Outputs tables of posi- tion and thermal para- meters for publication.
A. Zalkin	FORDAP	Fourier summation for Patterson or Fourier maps.
P.D. Cradwick	HATOM	Calculates positions of hydrogen atoms attached to atoms which are $sp^3$ or $sp^2$ hybridized.
M.J. Bennett B. Foxman	MMMR	Calculates starting para- meters for rigid bodies and hindered rotors.
G. Germain P. Main M.M. Woolfson	MULTAN	General direct methods program.
P. Main C.T. Grainger	NORMAL	Calculates E's, does Wilson statistics. For input to MULTAN.
M.E. Pippy F.R. Ahmed	NRC-22	Calculates least-squares planes.



## Appendix 1, continued

<u>Author</u>	<u>Program</u>	<u>Description</u>
W. Busing H.A. Levy	ORFFE	Calculates bond lengths, angles and associated standard deviations. Modified by W.L. Brooks and M. Elder for hindered rotors and rigid bodies.
C. Johnson	ORTEP	Thermal ellipsoids plotting program.
M.J. Bennett	PMMO	Transforms raw data to intensities, applying corrections.
A.P. Gaughan	PRCNTA	Molecular weight, % composition, density, absorption coefficient calculations from formula and cell.
M. Cowie	PUBE	Sorts data according to any desired sequence of h, k or l.
R.C. Elder	PUBTAB	Prints structure factor amplitude tables, modified by S.K. Dwight for use on the page printer.
S.K. Dwight	RIGIDH	Calculated rigid body parameters for hydrogen atoms.



## Appendix 1, continued

<u>Author</u>	<u>Program</u>	<u>Description</u>
C.T. Prewitt	SFLS5	Structure factor calculation and least-squares refinement of parameters. Modified by B.M. Foxman and M.J. Bennett for rigid body routine, and by W.L. Hutcheon and M.J. Bennett for the hindered rotor.
S.L. Lawton	TRACERA	General Cell Reduction Program.





Appendix 2: Structure Factor Amplitudes for  
 $[\text{Rh}_2(\text{CO})_2(\mu\text{-Cl})(\text{DPM})_2][\text{BF}_4]$ , *trans*- $[\text{RhCl}(\text{CO})\text{-(DPM)}]_2$ ,  $[\text{Rh}_2\text{Cl}_2(\mu\text{-SO}_2)(\text{DPM})_2]$ ,  $[\text{Rh}_2\text{Br}_2(\mu\text{-CO})\text{-(DPM)}]_2$  and  $[\text{Rh}_2\text{Cl}_2(\text{CO})(\text{C}_2\text{S}_4)(\text{DPM})_2]$ .

(On Microfiche in Back Pocket).



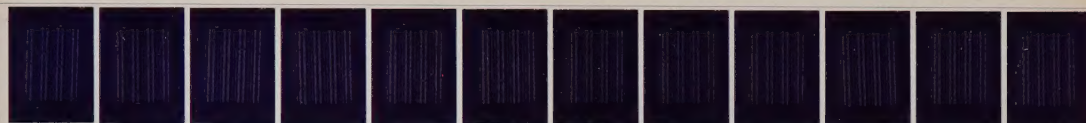




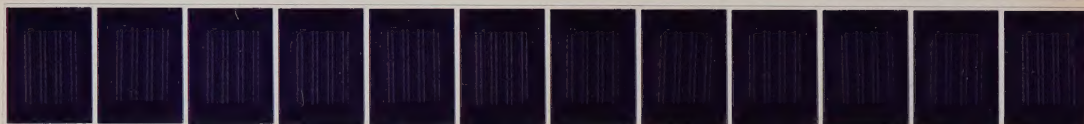


Tables 43 and 44

S.K. Dwight Ph.D. Thesis



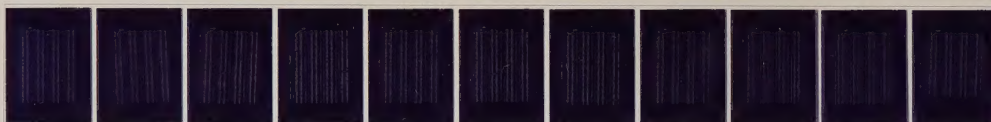
A horizontal strip of 12 microfilm frames, each containing a table of data.



A horizontal strip of 12 microfilm frames, each containing a table of data.



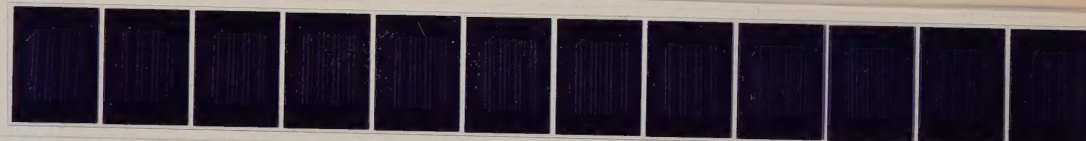
A horizontal strip of 10 microfilm frames, each containing a table of data.



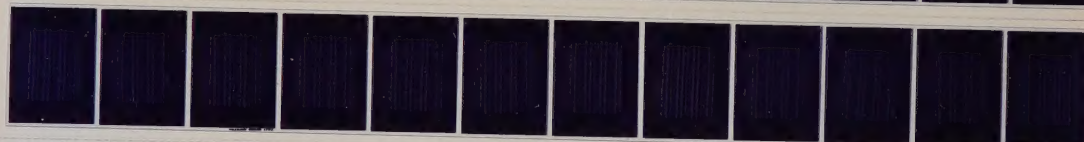
A horizontal strip of 10 microfilm frames, each containing a table of data.

Table 45


S.K. Dwight Ph.D. Thesis



A horizontal strip of 12 microfilm frames, each containing a table of data.












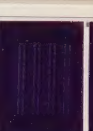
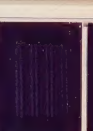







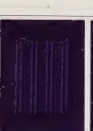
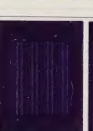
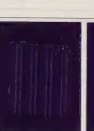
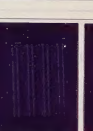
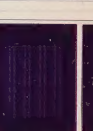



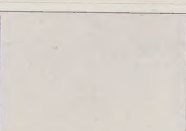



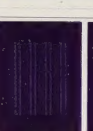
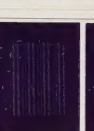
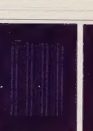










A horizontal strip of 12 microfilm frames, each containing a table of data.



A horizontal strip of 3 microfilm frames, each containing a table of data.

Tables 41 and 42

S.K. Dwight Ph.D. Thesis



**B30290**